

Structure and Dynamics of Charged Colloid-Polymer Mixtures



Miguel Alberto Peláez Fernández

Biocolloid and Fluid Physics Group

University of Granada

A thesis submitted for the degree of

Doctor of the University of Granada and Doctor Europeus

Granada, October 2011

Editor: Editorial de la Universidad de Granada
Autor: Miguel Alberto Peláez Fernández
D.L.: GR 1077-2012
ISBN: 978-84-695-1050-6

A PhD dissertation supervised by:

Dr. D. José Callejas Fernández
Catedrático de Física Aplicada
Dpto. Física Aplicada
Universidad de Granada

Dr. D Arturo Moncho Jordá
Profesor Titular
Dpto. Física Aplicada
Universidad de Granada

A mis padres y mi hermano,
por su **Q** amor incondicional

Acknowledgements

El agradecimiento es un ritual a la altura del amor; al amor que siento hacia el ser humano. Durante el transcurso de esta tesis, he estado bien arropado por el calor de muchas personas. ¡¡Se lo comunico al viento, al agua, al fuego y a la tierra para que mi infinita gratitud se esparza por todo el universo!!... Invocados a los Dioses, mis palabras de seguro serán certeras.

En primer lugar a mis directores les agradezco su dedicación para que este trabajo llegase a buen puerto. Gracias, Pepe, por ponerme la ciencia en la bandeja. Me has ayudado muchísimo a crecer como científico y como persona. A ti Arturo, te considero, más que un director, mi *alma mater* en los últimos años. Ha sido hermoso descubrirte y perseguirte como ser humano.

A mi lado también he percibido el calor humano que desprende toda la buena gente del grupo i8. Entre todos ellos, quisiera destacar a Delfi, Juan Luis, Migue, María, Juan de Vicente, Roque, Paco, Conrado, Alicia y José Antonio, por ofrecerme en determinados momentos su ayuda desinteresada.

Fue algo absolutamente idílico compartir despacho en los primeros momentos de mi tesis con gente como Juan Carlos, Roberto, Manolo, Luis, Javier, ... (siempre me quedaré con las ganas de haber jugado una última partida a los *gusanos*). En especial, me siento tremendamente agradecido a dos personas en concreto: Moro, gracias por abrirme los ojos a hostias y a ti, Fernando Martínez, gracias por abrimelos con caricias. Siempre llevaré un puñado de cada en los bolsillos. Con la nueva era de la Sala de Becarios, la cual se me antoja pequeña

por la cantidad de recuerdos que almacena, he disfrutado también muy buenos momentos. Os agradezco vuestra infinita paciencia si mis “poesías” o mi “prosa” no han estado a la altura. En particular, a Pablo Moreno, gracias por mostrarme tu entereza en las momentos más difíciles, se aprende mucho a tu vera. A mi tocayo Wulff, gracias por tu saque a 200 km/h, con el que he aprendido a profundizar en el mundo de la risa donde siempre seré un profano. César, gracias por ser tan ordenado.

Quiero destacar especialmente a dos grandes seres humanos, a los que agradezco su irrupción en mi vida: Sándalo, sinceramente el mejor resultado de esta tesis ha sido conocerte. Eres un maravilloso *sensei*, y tu recuerdo está grabado a fuego en mi alma. Fernando Vereda, todos los que te conocemos solo vemos luz en ti.

Durante estos años de ciencia día sí y día también, he tenido la enorme fortuna de conocer a gente de otros “mundos” que han querido ayudarme en mi trabajo. En San Sebastian, a Jaqueline y a su grupo, en especial a Josetxo, Ainara, Andoni y Luis, les agradezco ser tan cariñosos y tan bien dispuestos conmigo. También a mi amigo Yanko, por ser un mago que hace que la quimifobia se convierta en quimifilia. In Konstanz (Germany), I have spent fantastic days surrounded by great scientists. Thanks Matthias for give me the opportunity to live an experience that I will never forgive.

Quiero también agradecerle a mis amigos de Granada (Cauchy, Toni, Guille, los Edus, Fran, Aixa, Paco, Clara, Mark, Yuka-san, ...) el quererme como soy y a mis amigos de Almería (Juanjo, Bejamín, Esteban, Mariángeles, Lucas, Miguel Angel, ...) seguir queriéndome en la distancia. También quiero extender mis agradecimientos a los miembros de La Rosa de los Vientos por haber participado durante estos 3 últimos años en mi aprendizaje; nunca olvidaré mi vigésimo octavo cumpleaños. Y por supuesto, a ti Henar, ser tan distintos nos hace ser únicos. Quiero que sepas que te admiro tanto que me resulta imposible encontrar una manera adecuada para expresar cuánto, cómo, dónde y

por qué te quiero.

Por último, agradezco a toda mi familia los buenos momentos que me hacen pasar en las fechas marcadas en el calendario. En particular, a ti abuela Rosa, gracias por mostrarme la chispa de vida que llevas dentro. Pablo, te agradezco que no me dejes alejarme de la niñez de manera precipitada. Y, por último, mi padre y mi madre, quiero daos las gracias por concederme el don de ser vuestro hijo . . .

Lucainena de las Torres, 2 Octubre 2011.

Capítulo 11

Treinta radios se unen en un eje;
Precisamente donde no hay nada,
hallamos la utilidad de la rueda.
Horneamos arcillas y hacemos vasijas;
Precisamente donde no hay sustancia,
hallamos la utilidad de los pucheros.
Con el escoplo hacemos puertas y ventanas;
Precisamente en esos espacios vacíos,
hallamos la utilidad de la sala.
Así pues, consideramos que la posesión es beneficiosa,
Pero no tener nada es útil.

Capítulo 24

Quien se jacta no está establecido;
Quien se pavonea no llega a ser importante;
Quien se exhibe carece de intenso brillo;
A quien alardea de sí mismo no le conceden crédito;
Quien se alaba a sí mismo resiste poco.
Exceso de alimento y acción redundante
Se llama en el Camino a tales cosas.
Y hay quienes odian esas cosas.
Así pues, quien está con el Camino
no insiste en ellas.
Lao-Tse, *Tao Te Ching*

Contents

1	Introduction	1
2	Interactions in Colloidal Suspensions	7
2.1	Particle-solvent interaction: <i>Brownian Motion</i>	7
2.2	Electrostatic interaction	12
2.3	Depletion interaction	15
3	Structural Description of a Colloidal Suspension	19
3.1	One-component system	19
3.1.1	Radial distribution function	19
3.1.2	The Ornstein-Zernike Equation	25
3.2	Generalization to binary mixtures	28
4	Polymer Reference Interaction-Site Model	33
4.1	Polymer Reference Interaction-Site Model: Basic aspects	33
4.2	Generalization to colloid-polymer mixtures	38
4.2.1	<i>Intramolecular</i> correlations	40
4.2.2	Electrostatic depletion mechanism	43
4.3	Deformation of the polymer close to the colloidal surface	45
5	Experimental details	51
5.1	Light Scattering methods	51
5.1.1	Basic concepts	52
5.1.2	Static Light Scattering (SLS)	54
5.1.3	Dynamic Light Scattering (DLS)	56
5.2	3D-DLS device	58
5.2.1	3D-DLS description	58

CONTENTS

5.2.2	Suppression of the multiple scattering	61
5.3	Experimental systems	67
5.3.1	Colloidal particles	67
5.3.2	Polymers	74
6	Results	79
6.1	Paper I. <i>Nondiffusive Brownian motion of deformable particles: Breakdownn of the “long-time tail”</i>	81
6.2	Paper II. <i>Structure of charged colloid-polymer mixtures</i>	95
6.3	Paper III. <i>Charged colloid-polymer mixtures: A study on electrostatic depletion attraction</i>	113
6.4	Paper IV. <i>The structure of charged colloid-polymer binary mixtures: From like Wigner glass systems to fluid of clusters</i>	141
6.5	Paper V. <i>Study on the effective potential of an asymmetric charged binary mixture: the non-monotonic behaviour with the big colloid charge</i>	161
6.6	Project in progress. <i>Deformation of the polymer close to the colloidal surface: beyond the “thread limit”</i>	183
7	Conclusions	195
7.1	English	195
7.2	Español	198
	References	203

Chapter 1

Introduction

A colloidal suspension is a system of particles¹ suspended in a solvent medium, formed by molecules that are very small compared to the particle size, in such a way that the continuity of the medium can be assumed. Such particles (colloids) are well defined by their typical size, $1\text{nm} < L < 1\mu\text{m}$, the typical time scale of their motion, $1\mu\text{s} < \tau < 1\text{s}$, and the weak mechanical response comparing with atomic solids. From a physical viewpoint, colloids are used as “model atoms”, since both colloids and atoms can be theoretically described with the same framework² (*Statistical Mechanics*). The main experimental advantages of the colloids (colloidal suspensions) respect to the atoms (atomic systems) are the following ones: visibility (bigger particles), slow motion (easier temporal resolution), softer materials and tunable interactions (leading to a richer phase diagram than the atomic systems). In this sense, many statistical mechanical theories developed for atomic systems have been directly confronted with experimental results using colloidal suspensions. The ubiquitous presence of colloids in everyday life also justify the experimental and theoretical study of such systems with the intention to improve the quality of our life. In this respect, one find the boom of the colloidal applications mainly linked to the *first world* emergence in fields such as health (1), industry (2) and technology (3).

The large number of different colloidal interactions is strongly related with the huge number of different colloidal suspensions that can be synthesized. The modelling of these interactions is a challenge *per se*, although there are accu-

¹Here, the term particle refers to a macromolecule (hundred of glued molecules).

²“*The same equations have the same solutions . . . so what is different?*”, R. Feynman (1918-1988).

1. INTRODUCTION

rate theoretical descriptions for some of them. The experimental control of the colloidal interactions allows the study of many interesting physical phenomena, depending on whether they are attractive or repulsive. Repulsive interactions are mainly found in colloidal suspensions containing sterically coated particles and/or bearing certain superficial charge. The resulting repulsive interaction can be short-range (sterically coated particles) or long-range (charged particles) depending on the ionic conditions of the medium. Repulsive interactions are usually employed to stabilize the suspension and even to establish a microscopic order. Attractive interactions are perhaps more requested by the scientific community, because they generate instability in colloidal suspensions leading to the emergence of non-equilibrium processes: aggregation, gelation, . . . ; the van der Waal's force between colloids at short distances, as well as magnetic forces or the electrostatic attraction are good examples of attractive interactions.

Concerning the experimentally controllable interactions, the mixtures of colloids and polymers in a common medium deserves a special mention. The polymer can be adsorbed to the colloidal surface, or not, depending on properties such as the direct colloid-polymer electrostatic interaction, the chemical affinity, the hydrophobicity of the particles, etc. In consequence, the monomer density close to the colloidal surface differs from the bulk composition. In case of adsorption, the adopted conformation of the polymer along the colloidal surface can provide a steric short-range repulsion or attraction between colloids. This interaction is controlled among others by the degree of adsorbed polymer and/or the molecular mass of the polymer (4). In case of non-adsorption, the depleted polymer from the colloidal surface can lead to an imbalance of osmotic pressure generating attraction between colloids. Usually, the range of this polymer-induced attraction is controlled by its radius of gyration, R_g , while the strength of the attraction is proportional to the polymer concentration, c/c^* , being $c^* = \frac{3}{4\pi R_g^3}$ the overlapping polymer concentration. As a curiosity, the first of this twofold behaviors (adsorbing polymer) was applied by the Ancient Chinese people who found, by mixing suspension of carbon with Arabic gum¹, that the sedimentation of the *Chinese ink* was slowed down (stabilization). Nowadays, an example of the second case (non-adsorbing polymer) is found in the treatment of wine after fer-

¹That is a natural polymer taken from the sap of the *acacia* tree.

mentation, where the so-called in enology *fining agent* (generally bentonite clay) is added to speed up the precipitation process of some undesirable substances, *flocculation* (5, 6).

This memory tries to shed light into the specific problem on the interplay between opposite tunable colloidal interactions. For that propose, we have focused our attention on mixtures of colloids and non-adsorbed polymers. The repulsive interaction is achieved using charged colloids in a low ionic strength medium, where the repulsion is long-ranged. The attractive interaction is induced by the presence of non-adsorbing polymers. From a thermodynamic viewpoint, the interest of this work lies on the understanding of the way how charged colloid-polymer mixtures minimize the free energy of the system to reach the equilibrium state. It is well known that a mixture of colloids and ideal non-adsorbing polymers minimizes the free energy by increasing the entropy, S . Indeed, the polymer tries to be homogeneously distributed along the free space. Since colloids do not allow the polymer homogenization, a gradient of polymer concentration emerges leading to a flux in the opposite sense of the gradient, *i.e.*, the *Fick's law*. Therefore, an imbalance of pressure arises around the colloidal surface pushing colloids at closer distances to each other; this interaction leads to an effective attraction between colloids induced by the polymers. When colloids bear charge, the extra electrostatic repulsive interaction leads to a different route to minimize the free energy. In this case, to approach two colloids also induces an increase of the potential energy, U , which drives to an unfavorable configuration to minimize the free energy, $F = U - TS$. At this point, a non-trivial competition between both routes emerges. Moreover, it is expected that the interplay between repulsion and effective attraction will drive to new phenomena, which are undocumented for atoms and/or monocomponent colloidal suspensions.

Recently, the interest has been focused on the study of charged colloidal suspensions containing two components. Waltz-Sharma *et al.* (7) calculated numerically the depletion force between two charged planar parallel walls in a solution of charged spherical macromolecules. They reported results confirming that the long-range wall-particle electrostatic repulsion induces an enhancement of the induced effective attraction between walls, the so-called *depletion*. Mondain-Monval *et al.* performed measurements of the depletion forces focusing on charged

1. INTRODUCTION

droplets under the presence of smaller charged micelles and concluded that, apart from the electrostatic repulsion, an attractive depletion induced by the charges of the micelles has to be considered too (8). Helden *et al.* presented measurements of the depletion potential generated by charged rods using the Total Internal Reflection Microscopy technique, showing the important role that the depletion plays in this kind of charged colloid-polymer mixtures (9). Campbell *et al.* studied gelation in suspensions of model colloidal particles with short-range attractive and long-range repulsive interactions by means of three-dimensional fluorescence confocal microscopy. They studied the gel formation process by increasing the packing fraction of particles (10, 11). L. Belloni *et al.*, using the Polymer Reference Interaction-Site Model, studied theoretically the structural properties of charged colloid-polymer mixtures and specifically focused on the electrostatic depletion mechanism (12).

In relation with the aim of this thesis, we are also interested in performing an exhaustive documentation of this electrostatically enhanced depletion mechanism. For this reason, charged colloid-polymer mixtures have been studied by means of experimental observations, simulations and theoretical models. Colloids such as polystyrene latex and biocompatible liposomes have been used given their interest in technological and pharmaceutical applications, respectively. The experimental information has been mainly obtained by Light Scattering techniques, which allows to measure the dynamic and structure of the system without disturbing the sample. Then, the Liquid State Theory has been also applied to describe charged colloid-polymer mixtures and to reinforce the discussion of the experimental results. Additionally, Monte-Carlo simulations have been also performed to study the effective potential between two charged colloids induced by the presence of smaller charged ones.

This thesis is divided in 7 chapters. A theoretical, as well as an experimental background supporting our main findings is presented from Chapters 2 to 5. In Chapter 6, the production of this thesis is collected in 6 sections. In section 6.1 (paper I), the motion of deformable/non-deformable particles at short times (transition from ballistic to diffusive motion) is compared. The main result is that the deformability affects to the particle non-diffusive motion, and at longer times (diffusive regime) the vibrational modes affecting to the particle mo-

tion become compensated, so the particle diffusion is recovered. Although in this first work we have not employed colloid-polymer mixtures, the results are useful for the next works, where we study the dynamic of charged vesicle in presence of charged polymers at time scales where the deformational effects can be certainly neglected under the conclusions of this work. In paper II (section 6.2), mixtures of charged colloids and charged polymers in water at low electrolyte concentration are studied. This work represents an experimental evidence of the so-called *electrostatic depletion mechanism*. The experimental measurements are successfully confronted with a theoretical model that is able to capture the monomer connectivity along the polymer as well as the colloid-monomer interaction. The relevant length scales governing the structure of these mixtures are discussed in paper III (section 6.3). We also find that the dynamical properties of the colloids are consistent with the structural ones. In paper IV (section 6.4), we have extended the studies on charged colloid-polymer mixtures to a higher colloidal concentrations using liposome-polymer mixtures. The increase of the liposome packing fraction enhances the competition between entropic and electrostatic depletion mechanisms absent in sections 6.2 and 6.3. In paper V (section 6.5), we present a simulation study of the mixture of charged asymmetric spheres in the “colloidal limit”, *i.e.*, when the big colloid density vanishes. This work highlights the subtle mechanisms that can appear in charged binary systems, as the fact that increasing the charge of the big particles does not necessarily leads to the increase of the repulsion between big colloids. Finally, in section 6.6, the theoretical model used in the physical description of the charged colloid-polymer mixtures is improved to capture the rearrangement of polymer close to the colloidal surface. This section only contains a brief summary of the results developed in this theoretical project, which was carried out in the University of Konstanz (Germany) under the supervision of Prof. M. Fuchs. In Chapter 7, the main conclusions of this thesis are exposed.

1. INTRODUCTION

Chapter 2

Interactions in Colloidal Suspensions

In Colloidal Physics, the knowledge of the interactions between particles is the keystone to solve many physical problems. One of the advantages of the colloidal suspensions respect to the atomic systems lies on the rich variety of interactions, which depends on the physical and chemical details of the colloidal surface, the magnetic character of its core, the temperature, the conductivity of the medium, The interactions in colloidal suspensions arise from experimentally accessible features and, therefore, can be controlled. Against, an accuracy notion of these interactions stand for a problem *per se*, although appropriate approximations exist to model a wide range of different systems.

The aim of this chapter is to review the most important interactions arising in colloidal systems. We start from the interaction between the colloids and the solvent molecules that leads to the emergence of the *Brownian Motion*. Next, as a consequence of the charge on the colloidal surface, the electrostatic interaction between colloids is introduced. Finally, the effective interaction between colloids, induced by the presence of non-adsorbing polymers, is discussed.

2.1 Particle-solvent interaction: *Brownian Motion*

By *Brownian Motion* we understand the random motion that a particle suffers as a consequence of the continuous exchange of momenta with the surrounding

2. INTERACTIONS IN COLLOIDAL SUSPENSIONS

solvent molecules. Despite the some few historical precedents ¹ concerning this phenomenon, it is justified to take the original research of the biologist R. Brown in 1826 (13) as the first scientific treatment of the description of the Brownian motion, observed in suspensions of pollen grains in water with the help of a simply microscopy. About its erratic motion, he pointed out the next: “[...] *I observed many of them very evidently in motion [...] These motions were such as to satisfy me, after frequently repeated observation, that they arose neither from currents in the fluid, nor from its gradual evaporation, but belonged to the particle itself [...]*”. The excellent description given by R. Brown called the attention of A. Einstein, who published in 1905 (14) a physical interpretation in terms of the kinetic theory of heat. After the Einstein’s work, many scientists focused their attention on the study of this phenomenon (15, 16, 17) supporting the origin of this phenomenon on the molecules of the liquid.

Assuming that the solvent molecules are very small compared with the size of the colloidal particles, in 1908 P. Langevin (18) established that a neutral particle with radius R_c and density ρ , which is suspended in a stationary liquid with viscosity η , moves by the imbalance of exchange of momentum following the next equation,

$$m\ddot{\mathbf{r}}(t) = -\zeta\dot{\mathbf{r}}(t) + \mathbf{f}(t) \quad (2.1)$$

where $m = 4\pi R_c^3\rho/3$ is the mass of one spherical particle, $\zeta = 6\pi\eta R_c$ stands for the liquid friction coefficient, and \mathbf{f} is a Gaussian force with null average $\langle \mathbf{f}(t) \rangle = 0$ and time-correlation $\langle \mathbf{f}(t)\mathbf{f}(t') \rangle \propto \delta(t - t')$. The proportionality factor can be determined assuming that the kinetic energy is equally distributed among all the translational modes of each particle at equilibrium. For simplicity, hereinafter eq. (2.1) will be considered in just one dimension.

In eq. (2.1) the force \mathbf{f} , also called *white-noise*, collects the sum of the mechanical collisions coming from the solvent molecules (see fig. (2.1)). Due to the huge number of solvent molecules involved in any colloidal suspension, the deterministic

¹Perhaps the first one is contained in the *De Rerum Nature* where T. Lucretius assumed the existence of atoms based on the erratic movement observed on the Nature. Almost twenty century later, J. Perrin won the Nobel Prize proving the existence of atoms experimentally with the help of the advances done in the *Brownian Motion*.

2.1 Particle-solvent interaction: *Brownian Motion*

calculation of this force is prohibitive. Consequently, a pre-averaged description of the colloid-solvent forces is given by means of this stochastic force, \mathbf{f} . If we neglect both the external forces, like gravity, and interparticle interactions, the time-correlation of the velocity for a Brownian particle is derived from eq. (2.1),

$$\langle \dot{x}(0)\dot{x}(t) \rangle \propto \exp(-t/\tau_B) \quad (2.2)$$

where $\tau_B = \frac{m}{\zeta}$ stands for the relaxation time during which the velocity of a single particle typically remains correlated from an initial time. In a typical colloidal suspension, the value of τ_B is really small (for a colloidal particle with $R_c = 50$ nm, in water at room temperature $\tau_B \approx 0.6$ ns). Due to the experimental limitations concerning the minimum accessible correlation time (in the best case several nanosecond), the description in terms of a time-correlated velocity is prohibitive. Instead, for a larger time-window (the velocity is already decorrelated), the description of the colloidal particle motion is provided by the measurement of the mean-square displacement, or m.s.d. ($\langle \Delta x^2(\tau) \rangle = \sum_i \langle (x(t_i) - \langle x \rangle)^2 \rangle$), since the spatial jumps from the coordinates $\{x(0), y(0), z(0)\}$ to $\{x(t), y(t), z(t)\}$ are experimentally observable. Fig. (2.1) illustrates the latter with several spatial jumps joined by red solid lines. This temporal sequence of positions follows a Gaussian distribution, so the experimental determination of the m.s.d. allows us to know the temporal distribution of positions and so the particle motion. From eq. (2.1), the m.s.d. is given by (16),

$$\langle \Delta x^2(t) \rangle = 2D_0(t - \tau_B + \tau_B \exp(-t/\tau_B)) \quad (2.3)$$

where $D_0 = k_B T / \zeta$ is the particle diffusion coefficient. Here two special limits appear: the so-called *ballistic flight* when $t \ll \tau_B$ ($\langle \Delta x^2(t) \rangle \propto t^2$) and the *diffusive motion* when $t \gg \tau_B$ ($\langle \Delta x^2(t) \rangle \propto t$). The transition from ballistic to diffusive motion in eq. (2.3) was explored by Alder and Wainwright using molecular-dynamics simulations in a hard-sphere system (HS) (19). Their results showed up the existence of an extra delay of the onset of the diffusive motion respect to eq (2.3). This effect was explained in terms of the hydrodynamic interactions, which induce the circulation of the fluid from the front of the particle where is compressed to the rear where a rarefaction wave is developed.

2. INTERACTIONS IN COLLOIDAL SUSPENSIONS

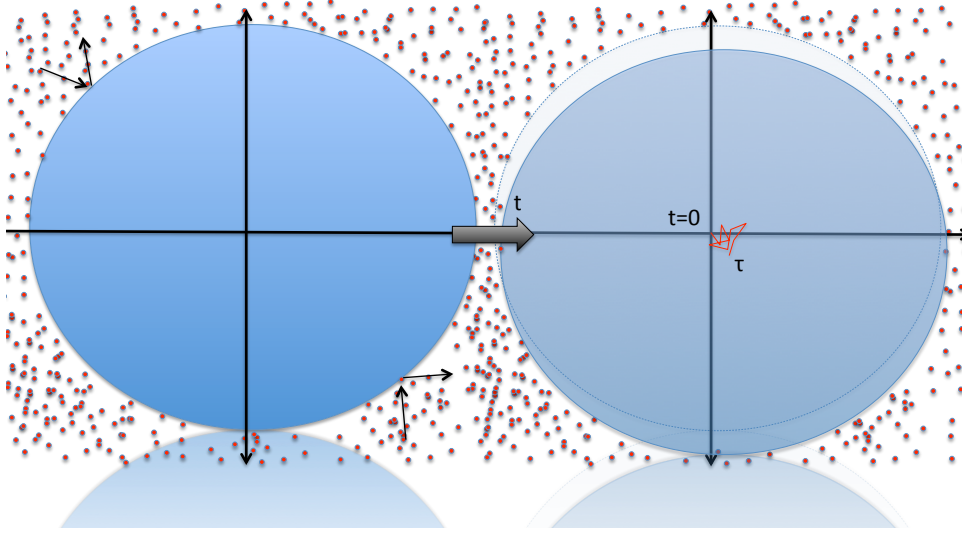


Figure 2.1: 2D scheme of the motion suffered by a colloid. The illustrated time-step t is assumed greater than τ_B . The jumps in the positions, from $t = 0$ to $t = \tau$, are symbolized as points joined by red lines. Within this description, the temporal sequence of the particle positions is the only relevant information.

Introducing the corresponding memory-effect correction in the Langevin equation one can obtain a more accurate equation for the m.s.d. (19),

$$\langle \Delta x^2(t) \rangle = 2D_0 \left[t - 2 \left(\frac{\tau_L}{\pi} t \right)^{1/2} + \frac{\tau_L}{9} \left(8 - \frac{2\rho}{\rho'} \right) - \frac{\tau_L^{3/2}}{9\sqrt{\pi}} \left(7 - 4 \frac{\rho}{\rho'} \right) t^{-1/2} \right]; (t \geq \tau_L) \quad (2.4)$$

where $\tau_L = (9/2)(\rho'/\rho)\tau_B$ is the characteristic time that the hydrodynamic effect introduces and ρ' stands for the fluid density. Effectively, the new version of the m.s.d. presents a softer transition between the two existing regimens, which agrees with the simulation results (19). To corroborate experimentally the transition predicted in eq. (2.4), a good time resolution together with a large τ_L time is necessary. The latter combination provides a wide temporal window where the second term in eq. (2.4) is still relevant respect to the diffusive one (first term in eq. (2.4)) in such a way that the hydrodynamic effect on the transition is indeed observed. Many studies have been devoted to the experimental corroboration of eq. (2.4) for hard-sphere particles using different kind of techniques (20, 21, 22, 23). However, a lack of experiments focused on deformable

2.1 Particle-solvent interaction: *Brownian Motion*

particles still persists. In chapter 6, paper I shows the first experimental evidence against the validity of the transition predicted in eq. (2.4), for deformable Brownian particles.

Until now we have briefly described the consequences of the interaction with the surrounding medium on the motion of the colloidal particles. However the Langevin's equation (eq. (2.1)) can also include external forces and/or interparticle interactions. In this work, the action of an external uniform field (like gravity) is neglected, although an study of the influence of the Earth's gravity on charged colloid-polymer mixtures can also be interesting, as was for neutral colloid-polymer mixtures (24). In absence of an external uniform field, only the presence of an interparticle force $\mathbf{F}_I(t)$ can perturb the free Brownian motion of a test particle. Eq. (2.1) is consequently rewritten as in one-dimension follows,

$$m\ddot{\mathbf{x}}(t) = -\zeta\dot{\mathbf{x}}(t) + f(t) + F_I(t) \quad (2.5)$$

For a short time interval ($\Delta t \geq \tau_B$), the interparticle force can be assumed to be time-independent, since small changes in the particle configuration are expected during times where the particles only undergo short excursions¹. So, taking an interval Δt much larger than τ_B and much smaller than the time taken by the system to reconfigure itself (the so-called *structural relaxation time* τ_R) the integration of eq. (2.5) leads to (25),

$$\Delta x_i(\Delta t) = \Delta x_i^B(\Delta t) + \frac{1}{\zeta} F_{Ii}(0) \Delta t, \quad (\tau_B \ll \Delta t \ll \tau_R) \quad (2.6)$$

where $\Delta x_i^B(\Delta t)$ is the Brownian displacement for a non-interacting particle as was presented before. Eq. (2.6) describes, without hydrodynamic effects, the motion of an interacting colloid, since it includes the *Brownian motion* and the *drift* velocity established by $F_I(t)$. The m.s.d. for short-times can be obtained, as in the non-interacting case, from eq. (2.5) (25),

$$\frac{\langle \Delta x_i(\tau)^2 \rangle}{6} = \tau \frac{k_B T}{\zeta} - \frac{\tau^2}{2!} \frac{k_B T}{\zeta} \langle \left(\frac{\partial U}{\partial r_i} \right)^2 \rangle + O(\tau^3). \quad (2.7)$$

¹Here, by short excursion is understood as $\langle \Delta r^2(\tau) \rangle \ll R_c^2$.

2. INTERACTIONS IN COLLOIDAL SUSPENSIONS

Here, the term $\langle (\frac{\partial U}{\partial r_i})^2 \rangle$ is the average square force per particle. This result confirms that for $t \geq \tau_B$, the diffusive motion of a single colloid is slowed down by the interaction with the nearest neighbor colloids (no matters if the interaction is attractive or repulsive).

Under the presence of longer-range repulsive interactions, or highly concentrated suspensions, the particle motion becomes strongly coupled with the other particles. In such cases, an arrested motion emerges as a consequence of the continuous restriction to the diffusion. In this new framework, the description of these slow-dynamic systems is commonly given by means of a *memory-function* formalism (26) (*e.g.*, Mode Coupling Theory) since such systems keep memory of their initial configurations during long time. In this thesis, both eq. (2.7) (paper III) and the Mode Coupling Theory (27) (paper IV) have been applied to help the discussion on the slow dynamic arising in interacting colloidal systems.

2.2 Electrostatic interaction

The presence of a colloidal particle suspended in a liquid is not free of chemical interactions with the surrounding molecules, which can lead to the partial ionization of its surface (28). Given the electrostatic character on the surface of the particles and the presence of ions suspended in the medium, a spontaneous rearrangement of cations and anions emerges, drawing up an scenario where each colloidal particle is surrounded by an electric double layer composed by a complex mixture of cations and anions (29). Here, we will present the simplest approximation to this problem based on the Poisson equation, which drives to the interaction potential used in this memory to model the electrostatic interaction.

Let us consider that the ions surrounding the colloidal surface are point charges creating a continuous charge density, $\rho(r)$. If the liquid medium is defined by an electric permittivity ϵ , the electrostatic potential ψ created by the colloid is given by the Poisson equation:

$$\Delta\psi(r) = -\frac{\rho(r)}{\epsilon}. \quad (2.8)$$

Given the large size ratio between colloids and ions, the ionic distribution around

2.2 Electrostatic interaction

colloids can be assumed in equilibrium (following the discussion in section 2.1, concerning τ_B and its dependence on R^2 , it is expected that $\tau_B^{col} \gg \tau_B^{ions}$). This allows to take $\rho(r)$ as a Boltzmann distribution (30),

$$\rho(r) = e \sum_{i=0}^M z_i n_i \exp\left(\frac{e^- z_i \psi(r)}{k_B T}\right), \quad (2.9)$$

where e is the elemental charge of an electron, M stands for the number of ionic species, and z_i and n_i represent the valence and density number of the i -th specie. The charge density will only depend on the distance in spherical coordinates, r (ion isotropic distribution), therefore we can rewrite eq. (2.8) as follows,

$$\frac{d^2 \Psi}{dr^2} + \frac{2}{r} \frac{d\Psi}{dr} = \kappa \sinh(\Psi) \quad (2.10)$$

where some terms have been regrouped assuming that ions bear symmetrical valence, $|z_i| = z$. Here, $\Psi = \frac{ze\psi}{k_B T}$, κ is the so-called inverse *Debye length* $\kappa = \sqrt{8\pi L_B N_A I}$ with L_B the Bjerrum length, and I is the ionic strength¹ which contains information about the whole ionic content $I = \frac{1}{2} \sum_{i=1}^n c_i z_i^2$ where c_i is expressed in molar concentration and the sum is performed over all the ionic species (including charged colloids). If eq. (2.10) is linearized (31), it can be analytically solved leading to the following result,

$$\Psi(r) = \Psi_o \frac{\sigma_c}{r} \exp(-\kappa(r - \sigma_c)) \quad (2.11)$$

According to this solution, the electrostatic potential generated by a colloid together with the surrounding ions follows an exponential decay with a tail which is mainly regulated by the *Debye length*. As was shown in the last paragraph, κ depends on the ionic concentration, so that the exponential decay of the generated electrostatic potential is controlled by the ionic content of the electric double layer (29). The resulting electrostatic interaction may be regarded as an interaction between electric double layers.

Using the solution given by eq. (2.11), the potential energy between particles of charges Z_1 and Z_2 and diameters σ_1 and σ_2 , may be calculated as the work involved to approach the particles from the infinite to a distance r through an

¹Note that in paper II and III this magnitude is defined as f_{ion} .

2. INTERACTIONS IN COLLOIDAL SUSPENSIONS

isothermal process. This calculation leads to the interaction potential that has been employed in this dissertation to simulate the electrostatic interaction between two different particles 1 and 2.

$$\beta\phi_{12}^{el}(r) = \frac{Z_1 Z_2}{4\pi\epsilon k_B T} \frac{\exp(0.5\kappa\sigma_1 + 0.5\kappa\sigma_2)}{(1 + 0.5\kappa\sigma_1)(1 + 0.5\kappa\sigma_2)} \frac{\exp(-\kappa r)}{r} \quad (2.12)$$

where $\beta = \frac{1}{k_B T}$ being k_B the Boltzman's constant and T the temperature.

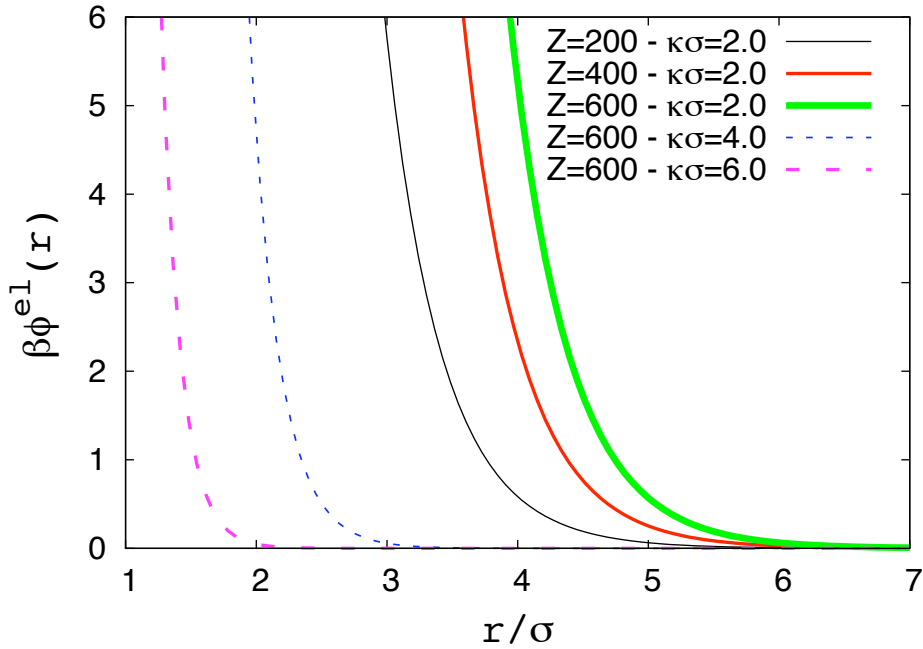


Figure 2.2: Dimensionless electrostatic potential generated between two identical colloids. Each type of line stand for different charges, Z , and dimensionless Debye length, $\kappa\sigma$ (see legend).

Fig. (2.2) shows the dimensionless electrostatic potential between two equal-size colloids as a function of the distance centre-to-centre r derived from eq. (2.12). The interaction is repulsive for equally charged particles (as in fig. (2.2)) and attractive for particles with different sign. The different types of lines and symbols show up the dependence on Z and κ . As was shown before, κ is proportional to $I^{1/2}$, so an increase of the ionic concentration leads to the decrease of the inverse of the Debye length, κ^{-1} . Therefore, the range of the repulsion becomes shorter by the increase of the ion concentration (compare green solid line with dashed and

dotted lines in fig. (2.2)). In this case, it is said that the electrostatic interaction is screened. If we focus now in the Z -dependence, we can find that the increase of the charge in the surface leads to a stronger repulsion with a similar range (compare the solid lines in fig. (2.2)). These results are only consistent with a system where I does not depend strongly on the colloidal concentration, since following its definition, it can be separated in two terms:

$$I = \frac{1}{2}(c_{col}(Z_{col})^2 + \sum c_{ions}(z_{ions})^2), \quad (2.13)$$

where c_{col} and c_{ions} stand for the molar concentration of colloids and rest of ions, respectively, and z_{ion} represents the valance of the ion. For a high colloidal concentration respect to c_{ions} , the Z -dependence will be relevant also for κ as is shown in the definition of the *Debye length*.

2.3 Depletion interaction

In Colloidal Physics, by *depletion* is understood the mechanism by which a colloidal suspension minimizes the free energy under the presence of a non-adsorbing second component. A clear example of this phenomenon is given in colloid-polymer mixtures, which were firstly treated by Asakura and Oosawa more than fifty years ago (32). When a polymer approaches to a colloidal surface, closer than about one coil radius, its conformation becomes altered. The increase of configurational free energy render this process unfavorable, so a layer around any colloidal particle emerges, where the polymer is partially depleted, namely a *depletion layer* (33). If a colloidal particle is isolated, the net osmotic force exercised by the polymer in the entire surface is zero. However, if two colloids overlap their *depletion layer*, there exist an imbalance osmotic pressure driving the colloids together. The so-called *depletion* mechanism is illustrated in fig. (2.3).

In terms of entropy, when two *depletion layers* overlap, the total accessible volume for the polymer increases. This process induces the increase of the entropy of the system and, consequently, a decrease of the free energy. In a one-component model where only colloids are explicitly considered, the increase of entropy implies an attractive interaction between colloids. Both experimental (34, 35, 36) and theoretical (37) works have confirmed the validity of the latter providing a tool to induce, in a controlled way, attractive interactions between colloids, by

2. INTERACTIONS IN COLLOIDAL SUSPENSIONS

adding non-adsorbing polymer chains. Moreover, a colloidal system with this kind of induced attraction generates a richer phase diagram respect to the HS one (38).

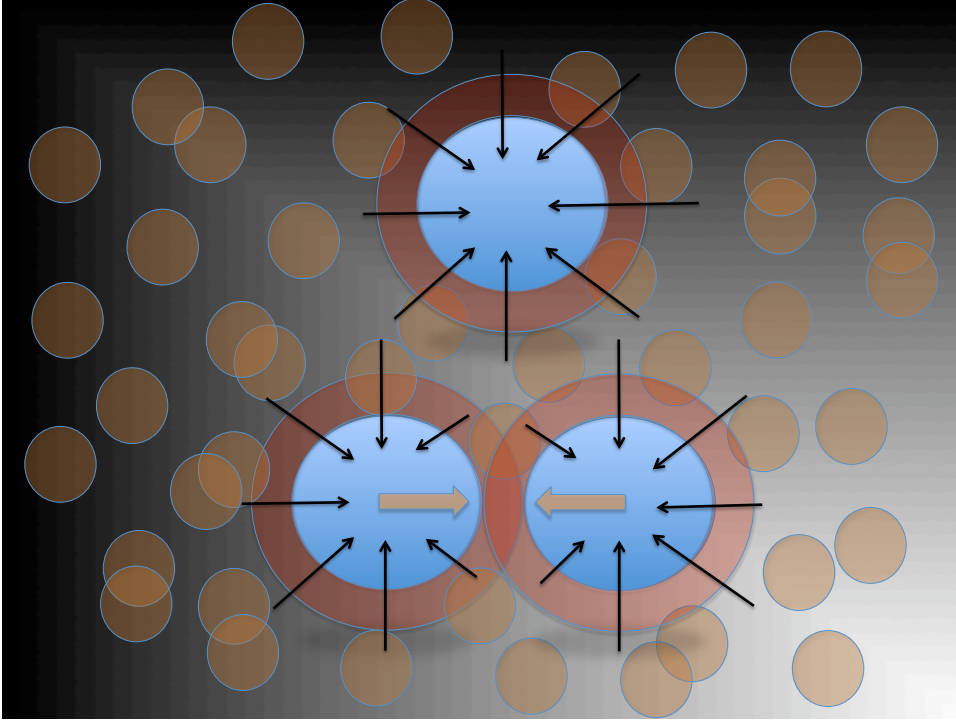


Figure 2.3: Depletion mechanism scheme based on the description of the Asakura-Oosawa model. Orange spheres represent the interpenetrable polymer. Blue spheres, as the colloids, are non-interpenetrable spheres (even for the polymers). Red halos around colloids stand for its *depletion layer*. Arrows indicate the sense of the polymer-exerted pressure.

As was mentioned two paragraphs before, the first analytical result of the induced-polymer attraction was given by the Asakura-Oosawa Model (AO) (32) and generalized by Vrij (36). Here, we will discuss essentially the AO model. To derive it, let us consider a continuous solvent where the interactions (colloid-colloid ϕ_{cc} , colloid-polymer ϕ_{cp} and polymer-polymer ϕ_{pp}) are pairwise additive. In this model, the colloids (with diameter σ_c) are HS-like and the polymers (with radius of gyration R_g) are interpenetrable spheres (*ideal* or non-interacting polymers). However, the cross interaction is again HS-like since the polymers are excluded from the colloids a distance of $\sigma_{cp} \geq (\frac{\sigma_c}{2} + R_g)$. Under these conditions, the

pairwise potentials are mathematically described as follows,

$$\phi_{cc}(r) = \begin{cases} \infty & r \leq \sigma_c \\ 0 & r > \sigma_c \end{cases}, \phi_{cp}(r) = \begin{cases} \infty & r \leq \sigma_{cp} \\ 0 & r > \sigma_{cp} \end{cases}, \phi_{pp}(r) = 0, \quad (2.14)$$

where r is the distance center of mass to center of mass for any combination of components. The force resulting on the imbalance osmotic pressure can be calculated by integrating the pressure over the accessible colloidal surface to the polymers. Equivalently, one can obtain the same result via the geometrical calculation of the overlap volume $V_{overlap}$ between two spheres, of radius σ_{cp} , at distance centre-to-centre $\sigma_c < r < (\sigma_c + \sigma_{cp})$ (39).

$$V_{overlap}(r) = \frac{4\pi}{3} \sigma_{cp}^3 \left(1 - \frac{3r}{4\sigma_{cp}} + \frac{r^3}{16\sigma_{cp}^3}\right) \quad (2.15)$$

The net force is proportional to the osmotic pressure, P , and also proportional to the decrease of excluded volume when they overlap $-V_{overlap}$. Therefore, the normalized Asakura-Oosawa potential that describes the effective interaction between two colloids immersed in a sea of interpenetrable polymers comes from the product $-V_{overlap}P$:

$$\beta\phi_{AO}(r) = \begin{cases} \infty & r < \sigma_{cp} \\ -\frac{4\pi\rho_p^r}{3}\sigma_{cp}^3\left[1 - \frac{3}{4}\frac{r}{\sigma_{cp}} + \frac{1}{16}\left(\frac{r}{\sigma_{cp}}\right)^3\right] & r \leq \sigma_{cp} \\ 0 & r > \sigma_{cp} \end{cases}, \quad (2.16)$$

where ρ_p^r is the polymer number density in the *reservoir*. A *reservoir* is an hypothetical system connected to the real system via a semi-permeable membrane. The polymer goes from the real system to the *reservoir* until the thermodynamic equilibrium is reached. In that situation the polymer concentration at the *reservoir* is ρ_p^r .

Three limitations to this model must be highlighted:

- It is assumed that R_g is the only length scale relevant for the polymer. However for high polymer concentrations this is not true, since the polymer chains overlap each other forming a mesh and so, the polymers lose their initial average conformation. In this respect, theoretical approaches including correlations between the polymer segments are necessary (40).

2. INTERACTIONS IN COLLOIDAL SUSPENSIONS

- The interpenetrability of the polymers loses consistency when the medium is not a Θ -solvent, or the polymer is slightly ionized, so that the repulsion between monomers avoid a clean overlap.
- It is not considered the overlapping between the excluded volume of three or more particles in the calculation of $V_{overlap}$. For the size ratio $\frac{\sigma_p}{\sigma_c} < 0.1547$, the geometrical derivation of the effective interaction potential is exact, but for higher size ratios, triple or higher order overlaps should be considered. The latter leads to weaker attractive potential than the one predicted by the AO potential.

For these reasons, the applicability of this model is very restrictive and more sophisticated derivations of the depletion potential must be taken into account to compare with simulation and experimental results (41, 42).

Chapter 3

Structural Description of a Colloidal Suspension

The previous chapter was devoted to the interactions in the colloidal suspensions. In this chapter, basic concepts of *Statistical Mechanics* are applied to the colloidal dispersions. This allows us to determine the mechanical and thermodynamical properties of any colloidal system in equilibrium from the knowledge of the spatial distribution of the particles. For that reason, in section 3.1, we introduce the radial distribution function, $g(r)$, as the observable magnitude able to describe the structure of interacting colloids in suspension. Then, the *Liquid State Theory* is employed to predict theoretically such structure. Since the aim of this memory is to shed light in the knowledge of binary mixtures, these concepts are generalized for a two-component system in section 3.2.

3.1 One-component system

3.1.1 Radial distribution function

Let us consider an isolated system consisting of N classical spherical particles (with diameter σ), where each particle has three translational degrees of freedom. Then the state of the system at any time will be given by a set of positions $\mathbf{r}^N = \{\mathbf{r}_1, \mathbf{r}_2, \dots, \mathbf{r}_N\}$ and momenta $\mathbf{p}^N = \{\mathbf{p}_1, \mathbf{p}_2, \dots, \mathbf{p}_N\}$. Let $\mathcal{H}_N(\mathbf{r}^N, \mathbf{p}^N)$ be the

3. STRUCTURAL DESCRIPTION OF A COLLOIDAL SUSPENSION

hamiltonian of the system, written as follows (43),

$$\mathcal{H}_N(\mathbf{r}^N, \mathbf{p}^N) = \frac{1}{2m} \sum_{i=1}^N |\mathbf{p}_i|^2 + \Phi_N(\mathbf{r}^N) \quad (3.1)$$

where m denotes the mass of one particle and $\Phi(\mathbf{r}^N)$ represents the total potential energy between the N particles, which will be assumed to be pairwise additive, i.e., $\Phi_N(\mathbf{r}^N) = \frac{1}{2} \sum_{i=1}^N \sum_{j \neq i} \phi(|\mathbf{r}_i - \mathbf{r}_j|)$, being $\phi(\mathbf{r})$ the pair potential. Therefore, knowing the latter interaction potential, the time evolution of the system, from an initial state is given by the canonical Hamilton's equations:

$$\dot{\mathbf{r}}_i = \frac{\partial \mathcal{H}_N}{\partial \mathbf{p}_i} \quad (3.2)$$

$$\dot{\mathbf{p}}_i = -\frac{\partial \mathcal{H}_N}{\partial \mathbf{r}_i} \quad (3.3)$$

Gibbs formulated a method to calculate the macroscopic mechanical properties of the system as a function of the average performed over an ensemble of microscopic systems (44). He showed that any microscopic dynamical function $A(\mathbf{p}^N, \mathbf{r}^N)$ has a macroscopic observable given by,

$$\langle A \rangle = \int d\mathbf{r}^N \int d\mathbf{p}^N A(\mathbf{p}^N, \mathbf{r}^N) f^{(N)}(\mathbf{p}^N, \mathbf{r}^N; t), \quad (3.4)$$

Here, $\langle \dots \rangle$ is the so-called *ensemble-average*. $f^{(N)}(\mathbf{r}^N, \mathbf{p}^N; t)$ is the *phase-space probability density* for a given configuration $\{\mathbf{r}^N, \mathbf{p}^N\}$ of the coordinate system and $d\mathbf{r}^N = d\mathbf{r}_1 d\mathbf{r}_2 \dots d\mathbf{r}_N$. In principal, $\langle A \rangle$ depends implicitly on time. However, in thermodynamic equilibrium, the *phase-space probability density* is not an explicit function of time $f^{(N)}(\mathbf{r}^N, \mathbf{p}^N; t) = f_0^{(N)}(\mathbf{r}^N, \mathbf{p}^N)$, consequently $\langle A \rangle$ is not dependent too. Therefore, the quantity $f_0^{(N)} d\mathbf{r}^N d\mathbf{p}^N$ is the probability, at any time, to find the physical system in a microscopic state represented by a phase point lying in the infinitesimal element $d\mathbf{r}^N d\mathbf{p}^N$. To determine the *phase-space probability density*, we have assumed our system in the *canonical ensemble*, i.e., a system of N identical particles in a volume V , which have been brought into thermal equilibrium with each other by immersing them in a heat bath of temperature T . In that case, the equilibrium probability density is given by (45),

$$f_0^{(N)}(\mathbf{p}^N, \mathbf{r}^N) = \frac{h^{-3N} \exp[-\beta \mathcal{H}_N(\mathbf{p}^N, \mathbf{r}^N)]}{N! Q_N(V, T)} \quad (3.5)$$

where h is the Planck's constant, the factor $\frac{1}{N!}$ takes account that the particles are indistinguishable $Q_N(V, T) = \frac{h^{-3N}}{N!} \int \int \exp[-\beta \mathcal{H}_N(\mathbf{r}^N, \mathbf{p}^N)] d\mathbf{r}^N d\mathbf{p}^N$ is the so-called *canonical partition function*, which normalizes eq. (3.5), $\int \int f_0^{(N)} d\mathbf{r}^N d\mathbf{p}^N = 1$. By factorization of positions and momenta, one can integrate the \mathbf{p}^N momenta leading to a probability density function depending only on the positions,

$$f_0^{(N)}(\mathbf{r}^N) = \frac{\exp[-\beta \Phi_N(\mathbf{r}^N)]}{Z_N(V, T)}. \quad (3.6)$$

where the *configuration integral* $Z_N(V, T) = \int \exp[-\beta \Phi_N(\mathbf{r}^N)] d\mathbf{r}^N$ is now the normalizing factor.

The integration of a subset of $n < N$ particles in eq. (3.6) yields an equilibrium particle density $\rho^{(n)}(\mathbf{r}^n)$, where $\rho^{(n)}(\mathbf{r}^n) d\mathbf{r}^n$ is $\frac{N!}{(N-n)!}$ times the probability of finding n particles of the system with coordinates in the element $d\mathbf{r}^n$, irrespective of the positions of the remaining particles and their momenta. In the *canonical ensemble*, the n -particle density is given by,

$$\rho_N^{(n)}(\mathbf{r}^n) = \frac{N!}{(N-n)!} \frac{\int \exp[-\beta \Phi(\mathbf{r}^N)] d\mathbf{r}^{(N-n)}}{Z_N(V, T)} \quad (3.7)$$

where the prefactor $\frac{N!}{(N-n)!}$ includes the possible combinations of n subset of identical particles in a system formed by N particles. Eq. (3.7) provides a complete description of the structure of a fluid. In particular, in our work the pair distribution function, $n = 2$, have been indirectly used as the observable magnitude to describe the structure of the colloidal dispersions.

Attending to the definition of $Z_N(V, T)$ for a homogeneous system, in the absence of external fields and taking $n = 1$, the normalization factor of eq. (3.7) leads to the next result:

$$\int \rho_N^{(1)}(\mathbf{r}) d\mathbf{r} = N \Rightarrow \rho_N^{(1)}(\mathbf{r}) = N/V = \rho \quad (3.8)$$

3. STRUCTURAL DESCRIPTION OF A COLLOIDAL SUSPENSION

being ρ the bulk particle density. A relevant result is that for an ideal gas the particle distribution function is given by,

$$\rho_N^{(n)}(\mathbf{r}^n) = \rho^n(1 + O(\frac{n}{N})) \quad (3.9)$$

In particular, for $n = 2$, $\rho_N^{(2)}(\mathbf{r}_1, \mathbf{r}_2) = \rho^2(1 - \frac{1}{N})$, which means that in a system containing a fixed number of particles, the probability of finding a particle at \mathbf{r}_2 , while another is at \mathbf{r}_1 , is proportional to $(N-1)/V$ and not to N/V . The so-called *pair distribution function* is commonly defined in terms of the corresponding particle density $\rho_N^{(2)}(\mathbf{r}_1, \mathbf{r}_2)$ by

$$g_N^{(2)}(\mathbf{r}_1, \mathbf{r}_2) = \frac{\rho_N^{(2)}(\mathbf{r}_1, \mathbf{r}_2)}{\rho^2}. \quad (3.10)$$

Therefore, eq. (3.10) reaches the ideal-gas limit (non-interacting particles) when the separation distance, namely \mathbf{r}_{12} , is much larger than the range of the interparticle potential, $g_N^{(2)}(\mathbf{r}_{12} \rightarrow \infty) \sim 1 - \frac{1}{N}$. At typical distances where the interparticle potential does not vanish, the pair distribution function measures the extent to which the structure of the fluid deviates from complete randomness due to the particle-particle interactions. Hereinafter, we will consider homogeneous and isotropic systems, so that for simplicity, $g_N^{(2)}(\mathbf{r}_1, \mathbf{r}_2) = g(r)$, where $r = |\mathbf{r}_1 - \mathbf{r}_2|$ is the distance between a pair of particles. Additionally, the knowledge of the *2nd-order* particle distribution function defined in eq. (3.10) is often sufficient to calculate the *equation of state* and other thermodynamic properties of the system. As an example, the excess internal energy can be obtained applying eq. (3.4) to the result in eq. (3.10) and assuming that the total potential energy $\Phi_N(r)$ is pairwise additive,

$$\frac{U^{ex}}{N} = \frac{4\pi}{NZ_N(V, T)} \int r^2 \Phi_N(r) \exp[-\beta\Phi_N(r)] dr = 2\pi\rho \int_0^\infty \phi(r)g(r)r^2 dr \quad (3.11)$$

The $g(r)$ function defined in eq. (3.10) is also useful to know the phase state of a system attending to its shape, or r -dependence. Studying the shape of $g(r)$ illustrated in fig. (3.1), we can distinguish between a solid (a), a liquid (b) and a gas phase (c). Panel (a) shows that for a crystalline order structure $g(r)$ is characterized by very thin peaks corresponding with the typical lattice parameters defined in a crystal. Instead, panel (b) represents the liquid-order given by $g(r)$, where a

persistence of a main peak is consequence of the well-defined coordination layer around one particle (see illustration on panel (b)). Secondary peaks stand for the seconds and next coordination layers but the correlation of this liquid-order becomes generally lost at far distances. The broad width of this peak compared with the solid one comes directly from the configurational differences between both phase states: in the liquid state particles has more mobility and, so can break up the close solid-order. Panel (c) shows the position randomness of the particles of a gas state. Indeed, we find that $g(r) \sim 1$ for distances greater than the contact ($r = 1$) meaning that all typical distances are equally likely.

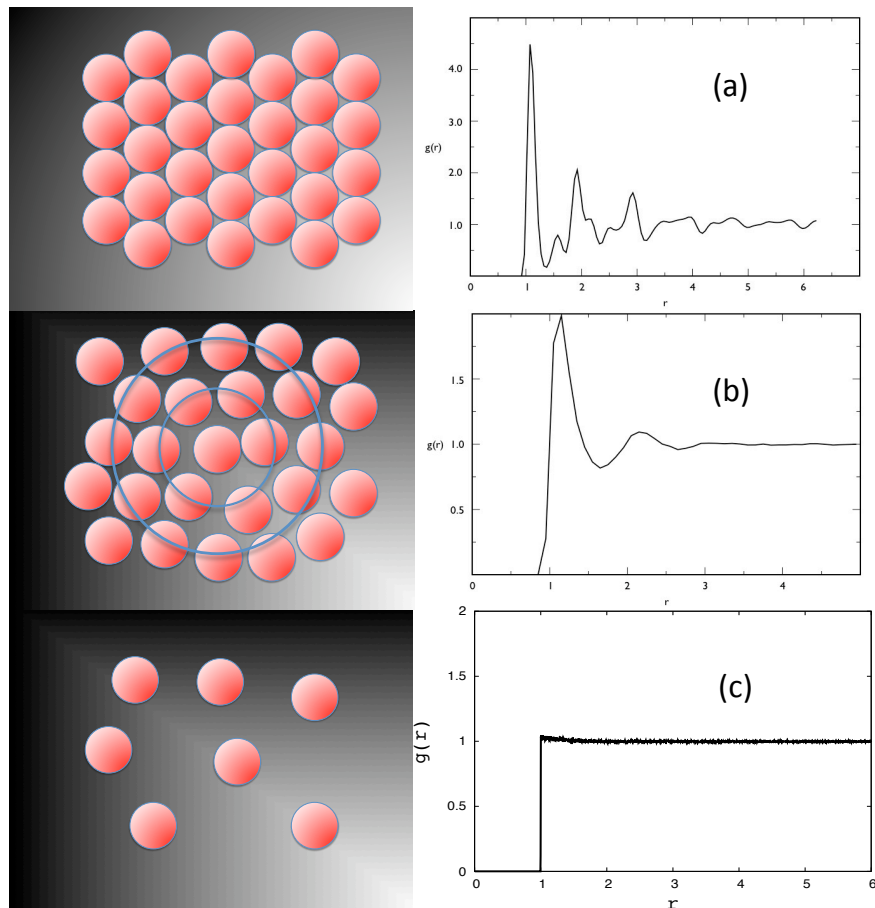


Figure 3.1: Solid (a), liquid (b) and gas (c) phases represented by their characteristic $g(r)$. Left panels illustrate the typical microscopic arrangement of each phase, while right panels show its corresponding $g(r)$.

3. STRUCTURAL DESCRIPTION OF A COLLOIDAL SUSPENSION

Despite to the importance of $g(r)$ describing the structure and thermodynamic of a colloidal system, in some cases it is more useful to work with the corresponding Fourier transform, called *static structure factor*, which is given by

$$S(q) = 1 + 4\pi\rho \int_0^\infty r^2 \frac{\sin(qr)}{qr} (g(r) - 1) dr. \quad (3.12)$$

If we consider $\rho(q)$ as the Fourier component of the number density $\rho(r)$ (pair particle density defined by eq. (3.7)), the *static structure factor* in eq. (3.12) can be calculated by means of the autocorrelation function of $\rho(q)$, $S(q) = \frac{1}{N} \langle \rho(\mathbf{q})\rho(-\mathbf{q}) \rangle$. This autocorrelation function provides information about the fluctuation of density particles in the system.

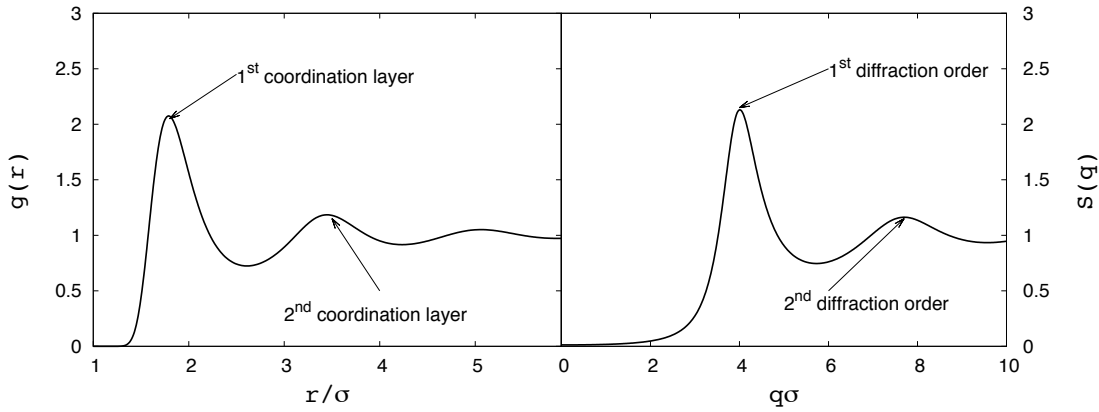


Figure 3.2: Correspondence between $g(r)$ (left panel) and $S(q)$ (right panel) for a liquid of charged colloids.

One of the major advances of using $S(q)$ is the fact that it can be experimentally determined by means of light scattering techniques and similar (neutron, x-rays scattering, ...). On the contrary, $g(r)$ can only be measured with the help of sophisticated microscopy techniques (47). The visual shape of $S(q)$ is similar to the $g(r)$ one. Fig. (3.2), shows an example of both functions (panel (a) $g(r)$ and panel (b) $S(q)$) for the same charged colloidal suspension. The first peak in $S(q)$ stands for the typical length of the system, in this particular case, typical distance between colloids. The first peak in $g(r)$, as was mention before, corresponds with the first coordination layer of particles around one central particle. So, the height and position of the main-peak is directly related with the one on $S(q)$. In fact, if

r_{peak} is the preference distance in $g(r)$, then $q_{peak} \sim \frac{2\pi}{r_{peak}}$, under the relationship established in eq. (3.12). However, the secondary and higher order maximums in $S(q)$ come from the secondary and further constructive interference orders (46), similar to the one defined by the Bragg's law for the solid state. Therefore, the secondary peak of $S(q)$ does not correspond to the secondary coordination layer in the $g(r)$.

3.1.2 The Ornstein-Zernike Equation

A theory that establishes a relationship between the structural information, the correlations and the pair interaction potential is the Ornstein-Zernike Equation (OZE) (48), in such a way that one can predict $g(r)$, or $S(q)$, for a given interaction and so extract any thermodynamic information. Despite it was formulated in 1914, the OZE still persists as a powerful approach to study homogeneous liquids. This equation sets that the correlation between two particles in an isotropic and homogeneous monocomponent system can be separated into two contributions: the direct correlation between these two particles and the indirect correlation through the rest of particles. Mathematically, it is expressed as follows,

$$h(\mathbf{r}) = c(\mathbf{r}) + \rho \int c(|\mathbf{r} - \mathbf{r}'|)h(\mathbf{r}')d\mathbf{r}'. \quad (3.13)$$

where $h(\mathbf{r}) = g(\mathbf{r}) - 1$, $c(\mathbf{r})$ stands for the direct correlation and the convolution term covers the rest of correlations through the other particles. In the Fourier space, eq. (3.13) may be expressed as an algebraic equation,

$$\hat{h}(q) = \hat{c}(q) + \rho \hat{c}(q)\hat{h}(q). \quad (3.14)$$

To solve eq (3.13), an additional equation relating $c(r)$, $g(r)$ and $\phi(r)$ is needed: the so-called closure equation. The theoretical explanation of this closure is somewhat artificial, although a physical interpretation can be provided using a diagrammatic expansion (48). In general, there are many possible closure equations attending to the diagrammatic expansion formalism. In this memory, we have used only a pair of theirs: HNC¹, which is given by

$$c(r) = -\beta\phi(r) + h(r) - \ln [h(r) + 1], \quad (3.15)$$

¹Acronyms of Hyppernetted Chain.

3. STRUCTURAL DESCRIPTION OF A COLLOIDAL SUSPENSION

used with good results for long-range repulsive potentials like the electrostatic one, and PY¹,

$$c(r) = (1 - \exp[\beta\phi(r)])(h(r) + 1), \quad (3.16)$$

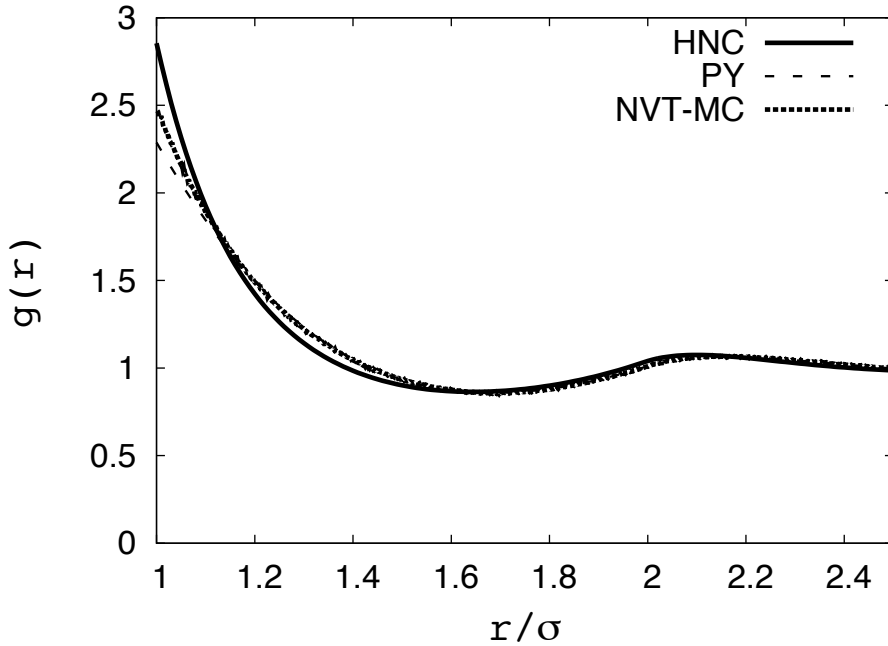


Figure 3.3: The radial distribution functions of a hard-sphere colloidal suspension predicted from OZE with HNC (solid line) and PY (dashed line) closure equations are compared with the one resulting from a Monte Carlo simulation (dotted line) at $\phi = 0.35$.

commonly employed in systems with short-range interactions (*e.g.* HS-like systems). Both are always applied under repulsive interactions, since attractions may lead to inhomogeneities that are not contemplated by OZE. A lack of accuracy is also found in the description of polydisperse systems.

Fig. (3.3) shows an example of the accuracy of this theory for a monodisperse colloidal suspension of hard-spheres. It includes the predictions from OZE with the HNC (solid line) and the PY (dashed line) equations (45) together with a Monte-Carlo simulation for a system of hard spheres (49) (dotted line) at the

¹Acronyms of Percus-Yevick.

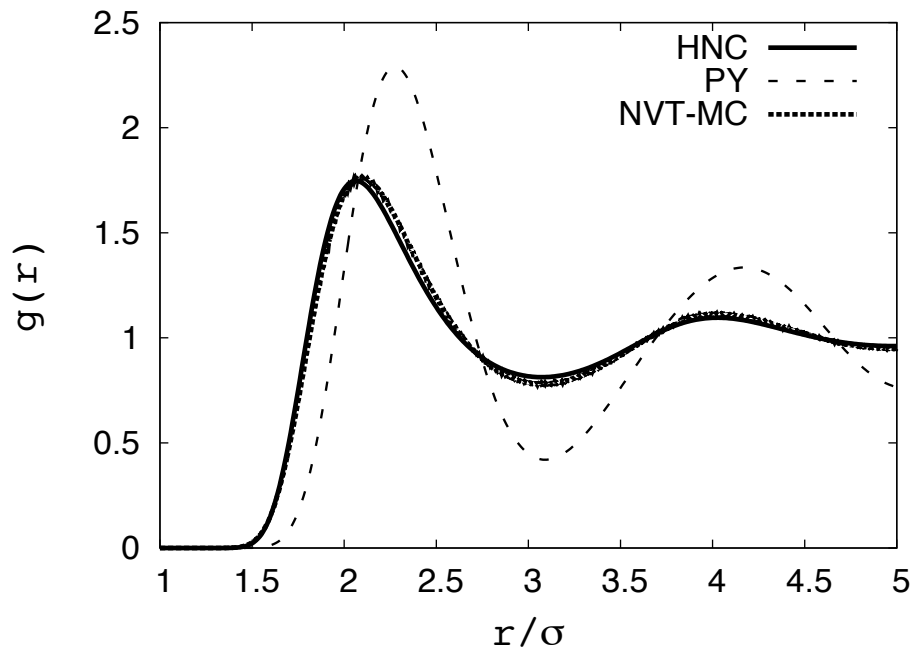


Figure 3.4: The radial distribution functions of a charged colloidal suspension predicted from OZE with HNC (solid line) and PY (dashed line) closure equations are compared with the one resulting from a Monte Carlo simulation (dotted line). Parameters: $\phi = 0.1$, $\kappa =$ and $Z = 25$.

volume packing fraction $\phi(= \frac{\pi}{6} \frac{\sigma^3 N}{V}) = 0.35$. For HS-like colloids, the PY closure is more accurate than the HNC one, although both throw acceptable results. If we compare fig. (3.3) with fig. (3.4), a different conclusion is derived. Following the same notation that in fig. (3.3), fig. (3.4) shows the radial distribution function for a charged colloidal suspension with packing fraction $\phi = 0.06$, charge $Z = 25$ and repulsive range $\kappa^{-1} = 2.5\sigma$. Now, the HNC closure provides a quite good description of the particle structure, while PY predicts a result far from the simulated one. Both figs. (3.3) and (3.4) highlight the relevance of the closure equation under the framework of the OZE to describe faithfully the structure of a real colloidal suspension, that in last term depends on the particle interactions.

3.2 Generalization to binary mixtures

A formal generalization of the section 3.1 to binary mixtures is fully justified since in this memory we have dealt with two-component system (mainly with colloid-polymer mixtures, but this will be particularly treated in chapter 4). Let us consider again an isolated, homogeneous and isotropic system consisting on N_1 particles of the specie 1 and N_2 of the specie 2 in a volume V at temperature T . The new hamiltonian is given by the sum of kinetic energy of the two species $\mathcal{K} = \sum_{i=1}^{N_1} \frac{p_i^2}{2m_1} + \sum_{i=1}^{N_2} \frac{p_i^2}{2m_2}$ and the total potential energy $\Phi = \Phi_{11} + \Phi_{12} + \Phi_{22}$ where

$$\Phi_{11} = \sum_{i<j}^{N_1} \phi_{11}(r_{ij}); \quad \Phi_{12} = \sum_{i=1}^{N_1} \sum_{j=1}^{N_2} \phi_{12}(r_{ij}); \quad \Phi_{22} = \sum_{i<j}^{N_2} \phi_{22}(r_{ij}). \quad (3.17)$$

Again pairwise additive potentials have been assumed. The subscripts indicate any combination between particles.

To simplify, it is convenient to substitute the two-component description by a one-component system (50, 51), where the potential energy is decomposed into two terms: Φ_{11} and an effective one Ω . For that, the ensemble used is not (N_1, N_2, V, T) as before, but (N_1, μ_2, V, T) , *i.e.* the chemical potential of the specie 2 is keep fixed instead of the corresponding number of particles 2. Here, $\Omega = \Omega(N_1, \mu_2, V; r_i^1)$ is the grand potential of a fluid of small particles at fugacity $z_2 = \Lambda_2^{-3} \exp(\beta\mu_2)$ with Λ_2 the corresponding *de Broglie's wavelength* of the specie 2, subjected to the external potential of the fixed configuration $\{r_i^1\}$ of the particles type 1. This grand potential can be further expanded as a sum of n -body terms in order to calculate it explicitly,

$$\Omega = \sum_{n=0}^{N_1} \Omega_n. \quad (3.18)$$

Once Ω , and thus $\mathcal{H} = \mathcal{K} + \Phi_{11} + \Omega$, is known for all values of z_2 , the thermodynamics and the phase behavior of the mixture can be determined from the standard procedures discussed for a one-component system in section 3.1.

In this work, the mapping onto an effective one-component system has been used specially in paper V. There, an asymmetric binary mixture ($\sigma_1 > \sigma_2$) is studied

in the “colloidal limit” (where $\rho_1 \rightarrow 0$), in such a way that just a pair of big particles are considered. In this case, eq. (3.18) is only expanded until $n=2$, since higher order terms are not expected to be very important, as long as the ranges of ϕ_{22} and ϕ_{12} are small compared to the range of ϕ_{11} (51, 52). For a calculation of the mean-field potential in the “colloidal limit”, a simulation in the *canonical* ensemble can be carried out, keeping in mind that the $\phi_{11}^{Total}(r)$ (sum of the direct interaction $\phi_{11}(r)$ and the effective one) will depend on ρ_2 , the density of small particles at the *reservoir*. Another example where the expansion to $n = 2$ eq. (3.18) is enough, is the Asakura-Oosawa potential mentioned in chapter 2. Here, the 2-order expansion of Ω leads to the exact result that the one obtained by Asakura and Oosawa (32) being $\frac{R_2}{R_1} < 0.157$.

Turning back to the description of the structure of a colloidal suspension, it is easy to define the partial structure factor, by generalization of the structure factor in section 3.1.1,

$$S_{\nu\mu}(q) = \frac{1}{N} \langle \rho_\nu(\mathbf{q})\rho_\mu(-\mathbf{q}) \rangle . \quad (3.19)$$

ν and μ stand for the different combination of species. The relationship between $S_{\nu\mu}(q)$ and $g_{\nu\mu}(r)$ follows directly from the eq. (3.12) taking into account that the contribution to the structure factor will depend on the fraction of particles of each $\nu\mu$ -pair of species. So we can rewrite eq. (3.12) as,

$$S_{\nu\mu}(q) = x_\nu\delta_{\nu\mu} + 4\pi\rho_{\nu\mu} \int r^2 \frac{\sin(qr)}{qr} (g_{\nu\mu}(r) - 1) dr \quad (3.20)$$

where $\rho_{\nu\mu} = \sqrt{\rho_\nu\rho_\mu}$, $\delta_{\nu\mu}$ is the Kronecker’s delta and $x_\nu = \frac{\rho_\nu}{\rho_\nu + \rho_\mu}$. Now, the function $g_{\nu\mu}(r)$ is the pair distribution function of particles of type μ around a central particle (at $r = 0$) of type ν and satisfy $g_{\nu\mu}(r) = g_{\mu\nu}(r)$

Following section 3.1, the generalization of the OZE will be given by a system of 4-equations. Again, the total correlation between any $\nu\mu$ -pair of particles not only depends on the correlation through the direct correlations of all the $\nu\mu$ -pairs but also through the direct correlations of all the $\nu\nu$ -pairs and $\mu\mu$ -pairs. In the

3. STRUCTURAL DESCRIPTION OF A COLLOIDAL SUSPENSION

real space, eq. (3.13) is generalized for binary mixtures as follows,

$$\begin{aligned}
 h_{11}(\mathbf{r}) &= c_{11}(\mathbf{r}) + \rho_1 \int c_{11}(|\mathbf{r} - \mathbf{r}'|) h_{11}(\mathbf{r}') d\mathbf{r}' + \sqrt{\rho_1 \rho_2} \int c_{12}(|\mathbf{r} - \mathbf{r}'|) h_{12}(\mathbf{r}') d\mathbf{r}' \\
 h_{12}(\mathbf{r}) &= c_{12}(\mathbf{r}) + \sqrt{\rho_1 \rho_2} \int c_{11}(|\mathbf{r} - \mathbf{r}'|) h_{12}(\mathbf{r}') d\mathbf{r}' + \sqrt{\rho_1 \rho_2} \int c_{12}(|\mathbf{r} - \mathbf{r}'|) h_{22}(\mathbf{r}') d\mathbf{r}' \\
 h_{22}(\mathbf{r}) &= c_{22}(\mathbf{r}) + \sqrt{\rho_1 \rho_2} \int c_{12}(|\mathbf{r} - \mathbf{r}'|) h_{12}(\mathbf{r}') d\mathbf{r}' + \rho_2 \int c_{22}(|\mathbf{r} - \mathbf{r}'|) h_{22}(\mathbf{r}') d\mathbf{r}',
 \end{aligned} \tag{3.21}$$

and in the Fourier space, eq. (3.21) leads to an algebraic system as in the mono-component case,

$$\begin{aligned}
 \hat{h}_{11}(q) &= \hat{c}_{11}(q) + \rho_1 \hat{c}_{11}(q) \hat{h}_{11}(q) + \sqrt{\rho_1 \rho_2} \hat{c}_{12}(q) \hat{h}_{12}(q) \\
 \hat{h}_{12}(q) &= \hat{c}_{12}(q) + \sqrt{\rho_1 \rho_2} \hat{c}_{11}(q) \hat{h}_{12}(q) + \sqrt{\rho_1 \rho_2} \hat{c}_{12}(q) \hat{h}_{22}(q) \\
 \hat{h}_{22}(q) &= \hat{c}_{22}(q) + \sqrt{\rho_1 \rho_2} \hat{c}_{12}(q) \hat{h}_{12}(q) + \rho_2 \hat{c}_{22}(q) \hat{h}_{22}(q).
 \end{aligned} \tag{3.22}$$

Hereinafter, eq. (3.22) will be considered in its matrix version to simplify the discussion,

$$\begin{aligned}
 \begin{bmatrix} \hat{h}_{11}(q) & \hat{h}_{12}(q) \\ \hat{h}_{21}(q) & \hat{h}_{22}(q) \end{bmatrix} &= \begin{bmatrix} \hat{c}_{11}(q) & \hat{c}_{12}(q) \\ \hat{c}_{21}(q) & \hat{c}_{22}(q) \end{bmatrix} \\
 \left\{ \begin{bmatrix} 1 & 0 \\ 0 & 1 \end{bmatrix} + \begin{bmatrix} \rho_1 & \sqrt{\rho_1 \rho_2} \\ \sqrt{\rho_2 \rho_1} & \rho_2 \end{bmatrix} \begin{bmatrix} \hat{h}_{11}(q) & \hat{h}_{12}(q) \\ \hat{h}_{21}(q) & \hat{h}_{22}(q) \end{bmatrix} \right\} &
 \end{aligned} \tag{3.23}$$

$\hat{f}_{\nu\mu}(q)$ stands for the Fourier component of the function $f_{\nu\mu}(r)$. Note that the system of equations (3.23) is reduced to three coupled equations since $\hat{f}_{ij}(q) = \hat{f}_{ji}(q)$. Therefore, three closure equations are needed to solve (3.23). Here, the selection of a suitable closure for each pair of interactions emerges as a delicate point. In fact, for binary mixtures the diagrammatic expansion developed for one-component system becomes a hard task (40). Hence, the closure must be based on *heuristic* reasons (*e.g.*, in paper V, the HNC closure equation has been used to complete the system (3.23), since the interaction between each pair of particles is long-ranged).

Fig. (3.5) shows an example of the pair distribution functions for a binary mixture of charged spheres ($\phi_1 = 0.10$, $\phi_2 = 0.001$, $\sigma_1 = 10$ nm, $\sigma_2 = 1$ nm, $\kappa^{-1} = 1.5\sigma_1$, $Z_1 = 250$ and $Z_2 = 6$). Relevant information about the configuration of each

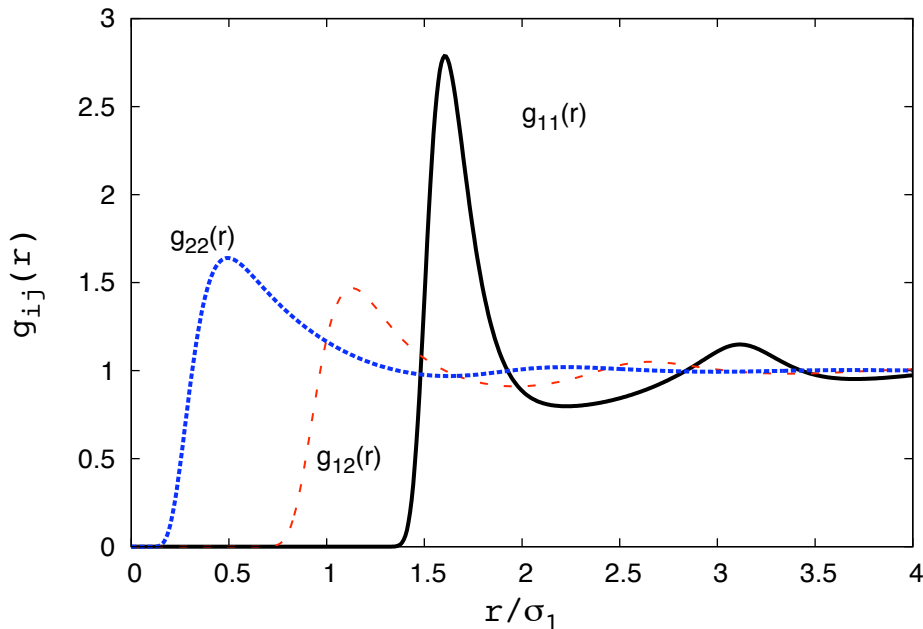


Figure 3.5: Example of the radial distribution function for each kind of pair in a binary mixture of charged colloids. The results come from the solution of eq. (3.23) with HNC closures. The label 1 indicates the biggest particle while 2 stands for the smallest one.

component respect to the other and itself can be obtained from these functions, *i.e.*, a complete information about the structure. On one hand, $g_{11}(r)$ and $g_{22}(r)$ show that both components remains in a liquid-order. On the other hand, from the peak of $g_{12}(r)$ is deduced that the small particles form a coordination layer around the big ones. It is important to highlight that the height of the peak of $g_{12}(r)$ and the broad width of the $g_{22}(r)$ peak are related: the layering of small particles around the big ones breaks up the liquid-order for the small particles leading to the spread of the typical distance, defined by the peak of $g_{22}(r)$.

The validity of the OZE to hard-spheres or slightly charged colloidal suspension in a low concentration regimen has been tested, finding that eq. (3.15) is a good approximation (53, 54). Even for colloid-polymer mixtures in the “colloidal limit” (vanishing colloidal concentration) eq. (3.23) together with HNC is a suitable theory to describe system under Θ -solvent conditions (55). In this memory, an explicit comparison between OZE and simulations has been carried out for highly

3. STRUCTURAL DESCRIPTION OF A COLLOIDAL SUSPENSION

charged asymmetric spheres (paper V). Our results will show that as much as the repulsion becomes more important the agreement between OZE and simulation is lost.

Chapter 4

Polymer Reference Interaction-Site Model

In Chapter 3, we have shown that the OZE represents a powerful theoretical technique to predict the structure of a binary colloidal suspension. Here, we will improve this model to study the structure of a charged colloid-polymer mixture. Real colloid-polymer mixtures demand a model able to capture their fundamental aspects such as the connectivity between monomers along the polymer chain and the rigidity of the polymer as well as the polymer-polymer and polymer-colloid interactions. The latter draws a non-trivial scenario from a theoretical point of view, since many restrictions must be imposed. In this chapter, we will introduce the *Polymer Reference Interaction-Site Model* (section 4.1) that will be applied to deduce the structure of like-charged colloid-polymer mixtures (section 4.2). In section 4.3, a brief exposition of the PRISM improvements to take into account the polymer deformability close to the colloidal surface is presented.

4.1 Polymer Reference Interaction-Site Model: Basic aspects

As was exposed in Chapter 3, the OZE is a theoretical description suitable to model an isotropic and homogeneous system of interacting spherical particles, *i.e.*, atomic or colloidal liquids. In 1982, D. Chandler (56) presented an equilibrium theory of polyatomic fluids, or molecular fluids, where the OZE was gen-

4. POLYMER REFERENCE INTERACTION-SITE MODEL

eralized from atomic to molecular liquids: the *Reference Interaction-Site Model*, also called RISM. It establishes that each particle (molecule) is subdivided into bonded symmetric entities called interaction-sites simulating the chemical bonds inherent in a molecule. To do that, the *intramolecular* distribution of atoms in the molecule is introduced through the *intramolecular* pair distribution:

$$w(r) = \frac{1}{N_m} \sum_{\alpha\gamma} w_{\alpha\gamma}(r), \quad (4.1)$$

Here, $w_{\alpha\gamma}(r)$ is defined, following eq (3.7), as the probability density of finding two sites, α and γ , in the same molecule separated by a distance r , being N_m the number of atoms per molecule.

Following the correlation scheme drawn by the OZE (eq. (3.13)), the correlations between atoms (sites) of the same molecule, *intramolecular* correlations, must be in principle linked up together with the *intermolecular* correlations. For a one component system, the RISM equation is given by (56),

$$\mathbf{H}(r) = \int d\mathbf{r}' \int d\mathbf{r}'' w(|\mathbf{r} - \mathbf{r}'|) \mathbf{C}(|\mathbf{r}' - \mathbf{r}''|) (w(r'') + \rho \mathbf{H}(r'')) \quad (4.2)$$

where ρ stands for the molecule number density and $\mathbf{H}(r)$ and $\mathbf{C}(r)$ are $N_m \times N_m$ matrices with element $h_{\alpha\gamma}(r)$ and $c_{\alpha\gamma}(r)$, respectively. Assuming a linear molecule, where all the links are equals, eq. (4.2) can be formulated in an simple manner where $h_{\alpha\gamma}(r) = h(r)$ and $c_{\alpha\gamma}(r) = c(r)$ for any α and γ pair of sites. In such case, eq. (4.2) is rewritten as follows,

$$h(r) = \int d\mathbf{r}' \int d\mathbf{r}'' w(|\mathbf{r} - \mathbf{r}'|) c(|\mathbf{r}' - \mathbf{r}''|) (w(r'') + \rho_a h(r'')) \quad (4.3)$$

where $\rho_a = N_m \rho$ stands for the atom (or site) density. As in chapter 2, in the Fourier space eq. (4.3) becomes algebraic,

$$\hat{h}(q) = \hat{w}(q) \hat{c}(q) (\hat{w}(q) + \rho_a \hat{h}(q)). \quad (4.4)$$

Here, $\hat{w}(q)$ is the Fourier transform of $w(r)$, also called *form factor* of the molecule. Note that for a molecule containing just one spherical atom (spherical colloid) $\hat{w}(q) \equiv 1$, therefore eq. (4.4) is immediately reduced to the OZE (eq. (3.14)).

An expansion in geometric series, using ρ_a as the ordering parameter, is demanded to understand the physics behind eq. (4.2) after introducing the $w(r)$ function

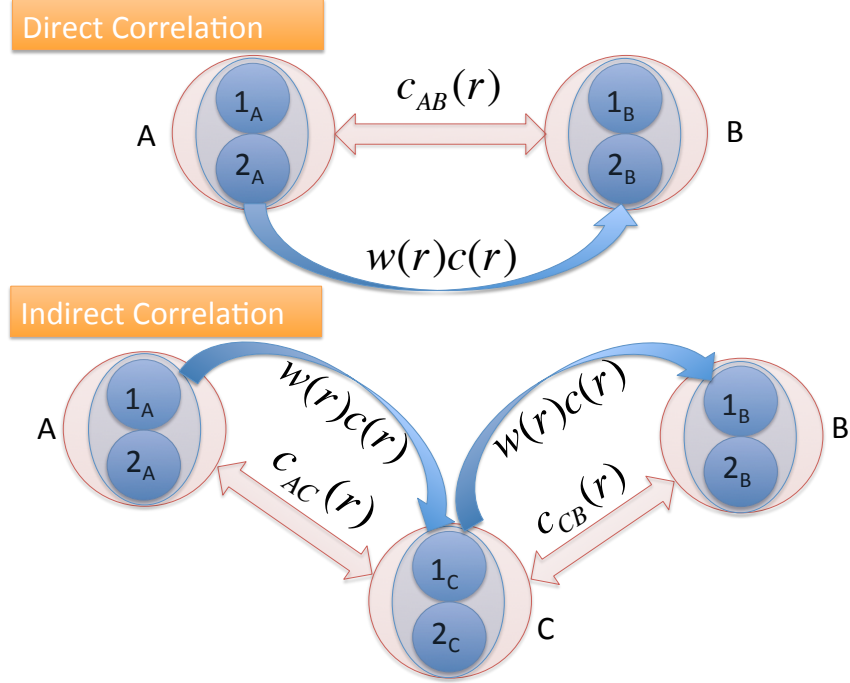


Figure 4.1: Scheme for the correlation decomposition in a diatomic liquid under the RISM approximation (eq. (4.2)) (blue symbols). It is schematically compared to the atomic liquid (red symbols) defined in eq. (3.13).

(this can be formally consulted in ref (56)). For simplicity, the meaning of eq. (4.2) is schematically illustrated in fig. (4.1) for a diatomic liquid. The total correlation is decomposed into direct and indirect correlations (first and second terms in eq. (4.2), respectively). In general, the direct correlation between an atom of the molecule A , labelled 1_A , and another of the molecule B , labelled 1_B , arises in the following way: the site 1_A is connected to the site 2_A of the same molecule ($w_{1_A 2_A}(r)$), the site 2_A is directly correlated with the site 2_B ($c_{2_A 2_B}(r)$) and it is in turn connected with the site 1_B ($w_{1_B 2_B}(r)$). So that, the *intramolecular* information is “propagated ” along the direct correlation between any two sites. The indirect correlation can be also understood following the scheme in fig. (4.1): the site 1_A is connected to the site 2_A , which is correlated to the site 2_C in an intermediate molecule. The site 2_C is connected with the site 1_C and it is correlated to the site 2_B , which in turn is connected with the site 1_B . Eq. (4.2) also includes indirect correlations through 2-intermediate molecules, 3-intermediate molecules

4. POLYMER REFERENCE INTERACTION-SITE MODEL

and so on. The latter description is shown in fig. (4.1) using blue symbols to help and to compare with the simple framework for atomic liquids, which is illustrated as well (red symbols).

As it is schematically proved, eq. (4.2) couples the *intracorrelations* with the *intercorrelations* and vice versa. It must be noted that under this integral equation theory, a *configurational pre-averaging* of the molecule conformations is imposed. For small molecules, *e.g.*, $N_m = 3$ or 4, a real static configuration can be assumed and, therefore $w(r)$ is equal to the real one (57).

The application of RISM to polymer systems, the so-called *Polymer Reference Interaction-Site Model* (PRISM), was suggested and studied by K. S. Schweizer *et al.* in 1990 (40). The idea consisted in expanding the RISM formalism to molecules with a high N_m value. It is equivalent to speak about polymers, replacing atoms by spherical monomers with diameter σ_m . At the most fundamental level, the applicability rests on the assumption that the site-site direct correlation function does not depend on where the monomers are located along the chain. Such simplification would be exact for cycling ring homopolymers (57). In spite of the loss of details due to the “pre-averaging of end-effects” (58), PRISM agrees with simulations and experiments for $N_m \sim 1000$, or even higher, using a suitable *conformational pre-averaging* (59), where the end-effects are not really important due to the extension of the polymer chain. Under the “pre-averaging of end-effects” applied to the polymers, the use of eq. (4.3) instead of eq. (4.2) becomes valid, since a polymer is in fact a well-defined linear molecule. So, it is the version of the PRISM equation that we will refer onwards.

In order to solve eq. (4.3), a “closure equation” is required again. In RISM, or PRISM, it has become a question of enduring interest, since a proper diagrammatic expansion, like for atomic liquids (48), cannot be derived. Therefore, the use of a closure is argued to be useful based on analogies with atomic liquids and *heuristic* physical concepts (60). For example, the use of PY is based on exploiting the standard idea that the atom-atom (site-site) direct correlation function is spatially short-ranged for HS-like atoms. Following the same reasoning, another closures (*e.g.*, the HNC-equation for long-ranged repulsive forces) have been also applied in PRISM (12, 61). So, in this memory an *heuristic* sense is also taken

into account to decide which kind of closure should be employed.

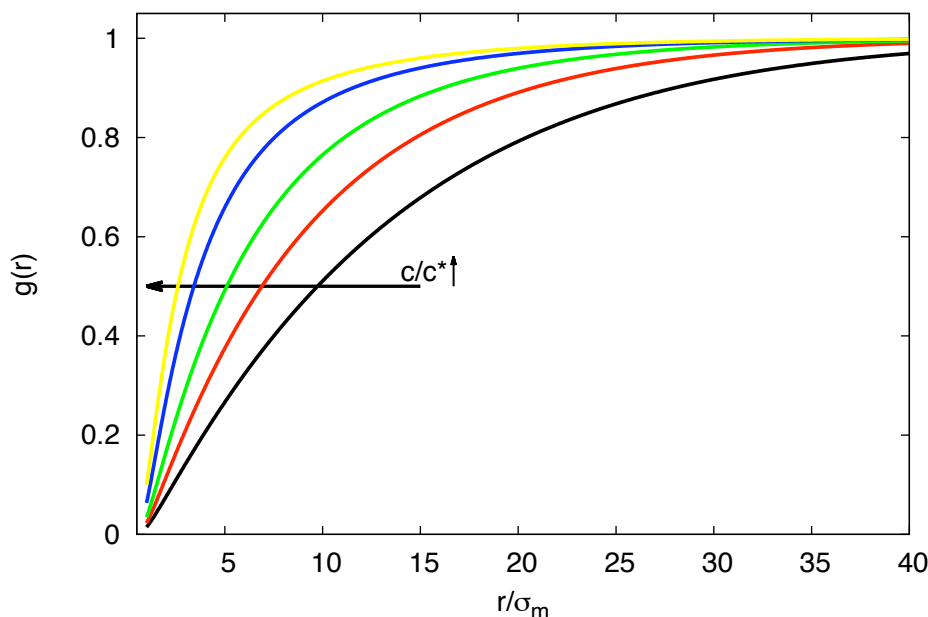


Figure 4.2: Monomer-monomer radial distribution function predicted by solving numerically the PRISM equation at different polymer concentrations, $c/c^* = 0.01, 0.05, 0.1, 0.2$ and 0.3 . For that, we have employed a HS-like monomer-monomer potential, the gaussian polymer chain and the PY closure. Dimensionless distance has been used in the x-axis, being σ_m the monomer diameter.

As an example, the monomer-monomer radial distribution function of a polymer derived from PRISM is shown in fig. (4.2). It is calculated for a polymer gaussian chain (a brief description of this model will be given on the next section) with $N_m = 2000$, a HS-like monomer-monomer interaction, a PY closure and for different polymer concentrations, $c/c^* = 0.01, 0.05, 0.1, 0.2$ and 0.3 , where c^* is the overlap polymer concentration. Two main features must be noted: there is not a defined typical distance (a main peak) and the monomer-monomer radial distribution function at the contact, $g(r = \sigma_m)$, increases with the polymer concentration. On the one hand, the absence of a monomer coordination layer is explained as a consequence of the connectivity of monomers along the chain, whose restrictions break the simple arrangement shown in fig. (3.1) for the atomic liquids. On the

4. POLYMER REFERENCE INTERACTION-SITE MODEL

other hand, the monomer connectivity gives rise to a monomer depletion hole at short distances. Increasing the polymer concentration, the packing leads to shorter monomer depletion holes (see the arrow in fig. (4.2)). For HS-like atoms, the contact value of $g(r)$ is not zero (see fig. (3.3)) as is for long-ranged repulsive atoms, or colloids, (results shown in figs. (3.2), (3.4) and (3.5)). The absence of repulsion until the contact between particles, allows the arrangement of particles very close to the surface, therefore, at the contact, $g(r)$ rises up. The increase of the polymer concentration in fig. (4.2) shows that the polymer packing leads to an increase of the monomer concentration at contact.

In this memory (paper II and III), as well as in other works (62, 63), PRISM has been employed to predict the monomer rearrangement (equivalently, the polymer rearrangement) in the presence of big colloids and vice versa. Therefore, the next section is mainly devoted to the generalization of PRISM to colloid-polymer mixtures.

4.2 Generalization to colloid-polymer mixtures

In this theory, colloid-polymer mixtures have been modelled by means of eq. (4.3), generalized to two-component systems. In the Fourier space and using matrix notation, we find the following PRISM equations,

$$\begin{aligned} \begin{bmatrix} \hat{h}_{cc}(q) & \hat{h}_{cm}(q) \\ \hat{h}_{mc}(q) & \hat{h}_{mm}(q) \end{bmatrix} &= \begin{bmatrix} \hat{w}_c(q) & 0 \\ 0 & \hat{w}_m(q) \end{bmatrix} \begin{bmatrix} \hat{c}_{cc}(q) & \hat{c}_{cm}(q) \\ \hat{c}_{mc}(q) & \hat{c}_{mm}(q) \end{bmatrix} \\ \left\{ \begin{bmatrix} \hat{w}_c(q) & 0 \\ 0 & \hat{w}_m(q) \end{bmatrix} + \begin{bmatrix} \rho_c & \sqrt{\rho_c \rho_m} \\ \sqrt{\rho_c \rho_m} & \rho_m \end{bmatrix} \begin{bmatrix} \hat{h}_{cc}(q) & \hat{h}_{cm}(q) \\ \hat{h}_{mc}(q) & \hat{h}_{mm}(q) \end{bmatrix} \right\} & \end{aligned} \quad (4.5)$$

where the subscripts “c” and “m” stand for colloid and monomer, respectively. Two points in eq. (4.5) must be highlighted: the matrix containing the *intra*molecular information is diagonal by definition and all the cross-terms are equal, $\hat{f}_{ij}(q) = \hat{f}_{ji}(q)$, so the system of equations is reduced again to three equations.

The first application of PRISM to mixtures of nanoparticles immersed in a polymer solution was performed by A. Yethiraj *et al.* (64). Their study proved that the PRISM agrees with the simulations and the experimental results (65). One

of the goals of PRISM theory compared to other approaches is the fact that includes the polymer correlations (66). Another advantage of PRISM is the easy implementation and its adaptability to a large number of real systems by playing with the $w(r)$ function and the combination of interaction-sites (12, 67).

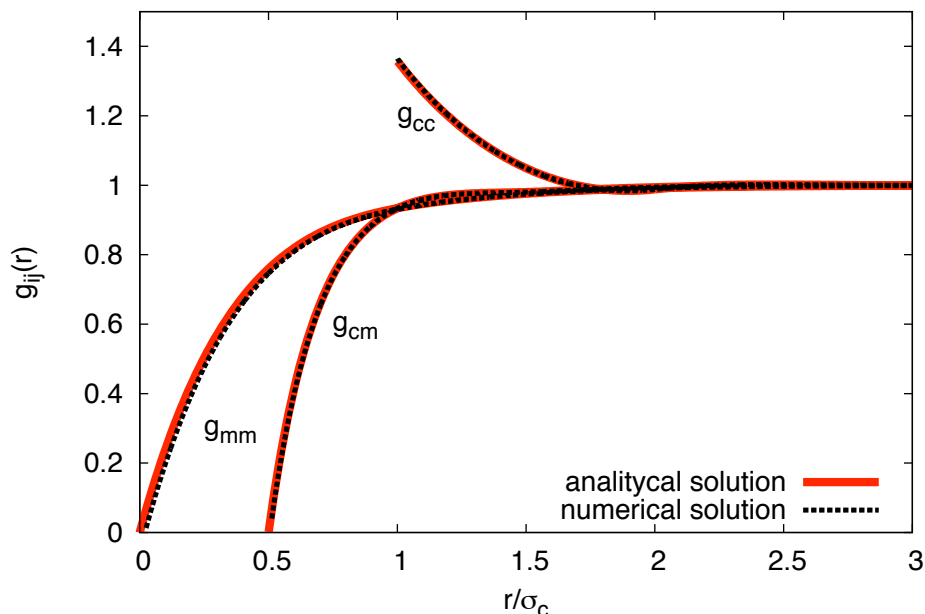


Figure 4.3: PRISM prediction of the radial distribution functions for a neutral colloid-polymer mixtures. Solid lines stand for the analytical solution in the so-called “thread limit” (courtesy of Prof. M. Fuchs) while dashed lines correspond with the numerical solution for $N_m = 8000$, polymer gaussian chain and HS-like interaction-sites. The calculation were performed with the next set of parameters: $\phi_c = 0.10$, $c/c^* = 0.001$ and $R_g = 0.7\sigma_c$, where σ_c stands for the colloidal diameter.

In this thesis, we have specially focus on the applicability of PRISM to charged colloid-polymer mixtures. For this propose, eq. (4.5) must be numerically solved. Before applying the PRISM, we have checked our numerical algorithm (based on the standard Picard’s method (68) to solve integral equations) with the analytical solution of eq. (4.5) for a particular case: neutral colloid-polymer mixtures with the polymer in the so-called “thread limit”. By “thread limit” is understood that $\sigma_m \rightarrow 0$, while $N_m \rightarrow \infty$, in such a way that the polymer radius of gyration,

4. POLYMER REFERENCE INTERACTION-SITE MODEL

R_g , remains finite. In this case, eq. (4.5) is analytically solvable for a gaussian polymer chain, HS-like interaction-sites and PY closures (69). Since such limit is not numerically reachable, we have studied the convergence of our numerical results to the analytical one. Fig. (4.3) proves that for large enough N_m (in that case $N_m = 8000$), our numerical solution (dashed lines) successfully converges to the analytical one (solid lines).

4.2.1 Intramolecular correlations

As was pointed out, the results shown in figs. (4.2) and (4.3) correspond to a gaussian model for the polymer pre-averaged conformation. In a gaussian polymer, the monomers follow a random walk along the chain, in such a way that given two joined monomers, the third one posses a random three dimensional orientation. The explicit expression of this model in the Fourier space is given by,

$$\hat{w}^{(G)}(q) = \frac{1 - f^2 - 2f/N_m + 2f^{N_m+1}/N_m}{(1 - f)^2} \quad (4.6)$$

where $f = e^{-q^2\sigma_m^2/6}$. Actually, in fig. (4.3), a Padé interpolation of eq. (4.6) is employed in substitution of the gaussian model. The Padé interpolation is another function that reproduces the asymptotic behavior, in this case, of the gaussian model. The expression satisfying the latter condition is,

$$w^{(G)}(q) = 1 + \frac{N_m}{1 + \frac{\sigma_m^2 q^2}{\sqrt{6}}}. \quad (4.7)$$

It is particularly a necessary condition to solve analytically eq. (4.5) in the “thread limit” (69). Therefore, we have used the same expression (eq. (4.7)) in our numerical calculations with the intention to reproduce the same conditions within the two cases shown in fig. (4.3) (analytical and numerical solution).

Nevertheless, a real polymer conformation is consequence of the coupling of several effects: the polymer-specific chemical bond, the presence of long-range interactions, the deformation caused by a physical wall, or a colloid, Accordingly to these restrictions, an improvement respect to the randomly gaussian chain considering some of the latter effects is well demanded for the *intramolecular*

4.2 Generalization to colloid-polymer mixtures

correlations. In this respect, in 1980, R. Koyama proposed a model alluding to the semi-flexibility properties that a polymer manifests in solution (70). Based on the *worm*-like chain model (71), the so-called Koyama's form factor is a semi-empirical model, since it takes into account the interpolation between two limit cases, the gaussian and the rigid chain (72). The interpolating parameter is called the *persistence length*, l_p , and describes the local rigidity (rod-like shape) that is transmitted along the chain. If $l_p \approx L_c (= N_m \sigma_m)$ we can consider the polymer as a rigid chain, while if $l_p \approx \sigma_m$ the polymer is similar to the one defined by the gaussian model (an explicit expression of the Koyama's model may be found in ref. (73)). To check the advantages of the semi-flexible model respect to the gaussian one, we show in fig. (4.4) the form factor for three different cases: a gaussian chain from eq. (4.6) (dashed line), a Koyama's chain in the gaussian limit $l_p = \sigma_m$ (solid blue line) and a Koyama's chain with a higher stiffness, $l_p = 10\sigma_m$ (red symbol-line).

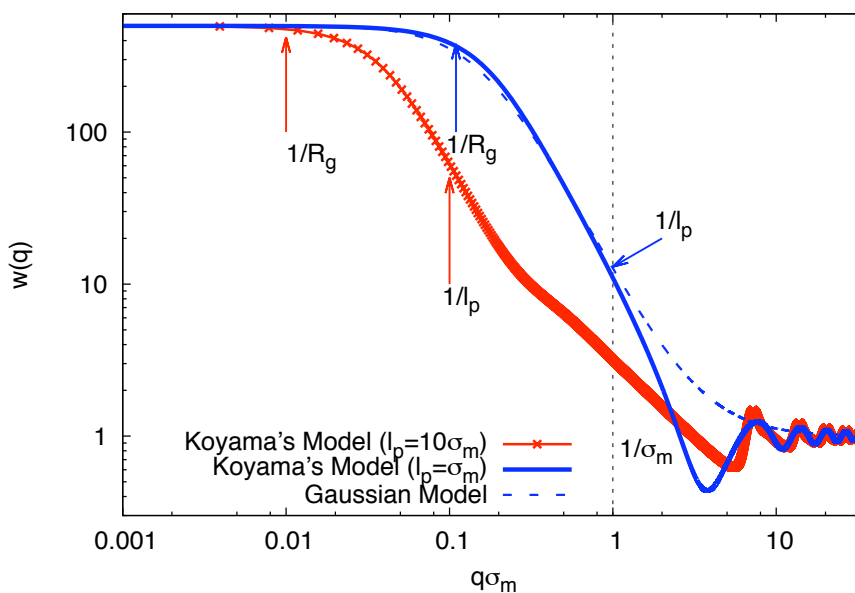


Figure 4.4: Theoretical polymer form factors. Dashed line stands for the gaussian model (eq. (4.6)), while solid and symbol-line correspond with the Koyama's model for $l_p = \sigma_m$ and $l_p = 10\sigma_m$, respectively. Labels of the relevant lengths are included.

In the limit $l_p \approx \sigma_m$, the Koyama's model effectively looks like the gaussian form

4. POLYMER REFERENCE INTERACTION-SITE MODEL

factor (compare blue lines) at least until $q^{-1} \approx \sigma_m$. However, for $q^{-1} > \sigma_m$ both models are markedly different. To understand the latter, it must be distinguished three different ranges in the Koyama's form factor. For $R_g < q^{-1} < l_p$, $w(q) \propto q^{-2}$, like a gaussian chain dependence, for $l_p < q^{-1} < \sigma_m$, $w(q) \propto q^{-1}$ like a rigid chain dependence (72), and for $q^{-1} > \sigma_m$ the asymptotic behavior is reached by oscillations around 1, where the period of the oscillations can be related with σ_m . In the above discussion, we have assumed that two neighboring monomers are connected at a distance given by $b = \sigma_m$ (monomers connected at the contact). However, it can be larger, $b > \sigma_m$, being b the so-called *Kunh length* (74). In the case of $b > \sigma_m$ the period of the oscillation for $q^{-1} > \sigma_m$ is related with b instead of σ_m .

For a charged polymer, it is important to taking into account the extra-rigidity introduced by the repulsive interaction between neighbor monomers. In this respect, l_p represents an excellent parameter to model charged polymers respect to the gaussian chain, since it allows us to vary the local-rigidity of the polymer. There exist some models that separate the *persistence length* into two contributions, of a different physical meaning (75): the intrinsic one, l_o , originated by the specific properties of the polymer and the electrostatic one, l_e , due to the electrostatic repulsion between the charged monomers. Assuming a Debye-Hückel potential and considering that cationic condensation occurs (76), Odijk, Skolnick and Fixman found,

$$l_e = \frac{L_B}{4\kappa^2 b^2}, \quad \text{for } L_B < b, \quad (4.8)$$

where the *Debye length*, κ^{-1} , introduces the ionic concentration dependence (additional information about this model can be found in refs. (77, 78, 79)).

The assumption of the cation condensation in the monomers along the linear polymer chain makes also valid the use of the Manning's expression to predict the monomer charge, $Z_m = b/L_B$. A previous study on polyelectrolyte using PRISM proofs that this expression remains correct in the presence of flexible linear polymers as in our case (62). For that reason, in this thesis we have used the Manning's expression to document the monomer charge alluding to the condensation of ions, since the experimental knowledge of this magnitude is only known for some specific polymers.

4.2.2 Electrostatic depletion mechanism

An example of how far we can go with PRISM lies on the applicability to charged colloid-polymer mixtures. In this mixtures, the depletion interaction between colloids has an electrostatic contribution, that is mainly caused by the electrostatic repulsion between colloids and polymers. This electrostatic enhanced depletion attraction is the key to understand the equilibrium distribution of charged colloid-polymer mixtures. To separate the *electrostatic depletion mechanism* respect to the entropic depletion (section 2.3), the radial distribution functions predicted by the PRISM for a mixture of like-charged colloids and charged/uncharged polymers are presented in fig. (4.5) (charged polymers at the top and uncharged polymers at the bottom). A couple of polymer concentrations are given in both cases, $c/c^* = 0.001$ and 1. As fig. (4.5) shows, two relevant features emerge:

- For neutral polymers (panel at the bottom), the increase of polymer concentration leads to weak changes based on just the packing of polymer. In particular, g_{cc} does not show any important changes by increasing of the polymer concentration even in three order of magnitudes.
- For charged polymers (panel at the top), we observe an important polymer rearrangement in g_{mm} and g_{cm} as a consequence of the monomer-monomer and colloid-monomer electrostatic repulsion, respectively. However, the colloid-colloid radial distribution remains equal for the diluted case that the one for neutral polymers. By increasing the charged polymer concentration, again in three order of magnitude, the packing of polymer is really important and, now, the colloid distribution is strongly affected. Colloids become typically closer (shift of the main peak to small r values) and the number of colloids at such distance markedly increases (higher main peak).

In fig. (4.5), like-charged colloids at $\phi_c = 0.05$ are typically at distances centre-to-centre of $r_{cc} = 1.6\sigma_c (\sim 65\sigma_m)$. Under the depletion interaction discussed on section 2.3 for neutral polymers, the range of the induced attraction is $2R_g$ ($\sim 80\sigma_m$ in fig. (4.5)), so that the colloids are separated at a distance where the polymer-induced attraction can be neglected. As a consequence of that, the increase of the neutral polymer concentration in three order of magnitude only induces a very slightly change respect to the colloidal structure for $c/c^* = 0.001$ (panel at the bottom).

4. POLYMER REFERENCE INTERACTION-SITE MODEL

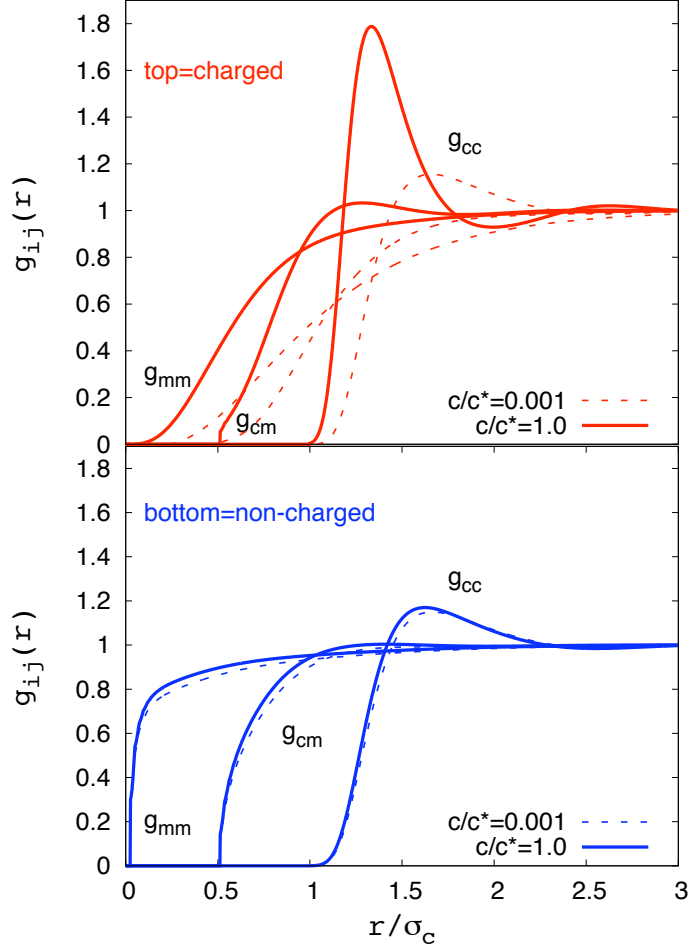


Figure 4.5: PRISM prediction of the radial distribution functions for colloid-polymer mixtures. The polymer was modelled with the Koyama’s form factor: $N_m = 500$ and $l_p = 10\sigma_m$ leading to $R_g = 40\sigma_m$. Site-site interactions were modelled with the Debye-Hückel potential using the following set of parameters: $Z_c = 50$, $Z_m = 0.347$, $\kappa^{-1} = 6\sigma_m$ and $\sigma_c = 40\sigma_m$. HNC for the colloid-colloid correlation and PY for the rest of correlations were employed to close the system of equations. For $\phi_c = 0.05$, two polymer concentrations have been included: $c/c^* = 0.001$ and 1.0 .

However, for charged polymers the arrangement of both components strongly vary with the polymer concentration. The monomers are depleted from the colloidal surface and from each other by means of electrostatic repulsion (see red lines g_{cm} and g_{mm}). At $c/c^* = 0.001$, $g_{cc}(r)$ is similar to the one for neutral polymers,

4.3 Deformation of the polymer close to the colloidal surface

since the polymer concentration is really small and the electrostatically repelled polymer can move away from the colloidal surface without packing restrictions. By increasing the polymer concentration until $c/c^* = 1$, the polymer is forced to be close to the colloidal surface. At such separation distances the colloid-polymer repulsion becomes stronger. In a simple view, if two charged colloids are close enough to typically prevent the charged polymer to fit inside the volume between them, an imbalance of electrostatic repulsion will generate an effective attraction between them. This effect does not only depend on the size of the polymer, R_g , but also on the range of the electrostatic colloid-polymer repulsion. Therefore, the resulting effective depletion attraction can have a range much longer than $2R_g$. The latter mechanism, was properly analyzed by L. Belloni under the PRISM formalism (12) and then corroborated by simulations (80, 81) and experiments (paper II and III of this memory).

4.3 Deformation of the polymer close to the colloidal surface

The model discussed in section 4.2 is able to describe a huge variety of colloid-polymer mixtures. As it was commented, PRISM takes the monomer correlations and the finite size of the monomers into account. These effects are important and wrong predictions are obtained with theories that do not include them (82, 83, 84). We have already mentioned that PRISM relies on two relevant assumptions that in real systems are not always valid: to neglect *end-effects* and *pre-average* the *intra*molecular correlation. However, when a real polymer approaches to a colloidal surface, the number of possible conformations diminishes due to the restrictions that the hard-surface (colloid) offers (see fig. (4.6)). In principle, this effect represents an important inconvenient as the PRISM formalism needs to pre-average the polymer conformation. In order to include the polymer deformation close to a colloidal surface, Fuchs *et al.* proposed a new strategy to include this physical mechanism within the PRISM formalism (63, 85, 86).

The PY equation states that the direct correlation, $c(r)$, is a short range function that at long distances than the contact one rapidly tends to zero. For hard-sphere suspensions, this is an acceptable hypothesis. However for the colloid-monomer correlation, given the connectivity of one monomer along the chain, the validity

4. POLYMER REFERENCE INTERACTION-SITE MODEL

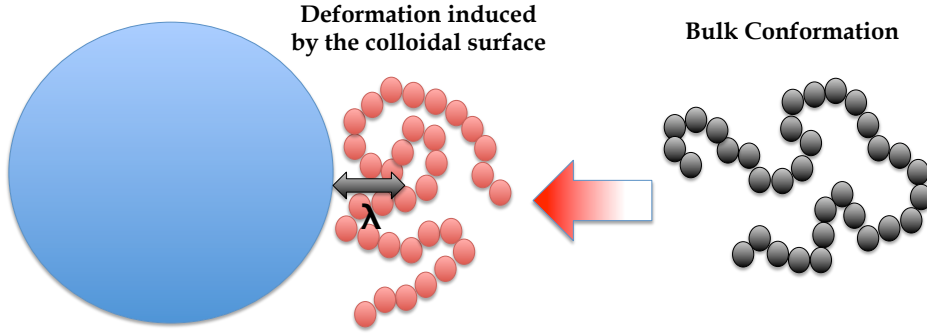


Figure 4.6: The scheme illustrates how a colloid avoids that the polymer develops its natural conformations in solution. The λ parameter represents the distance from which the polymer feels the colloidal surface as a non-negligible obstacle to adopt some conformations.

of the PY-assumption at longer distances than $\sigma_{cm}(= \frac{\sigma_c + \sigma_m}{2})$ is not strictly justified. Since the monomer connectivity leads to the emergence of the polymer rearrangement close to the colloidal surface, Fuchs *et al.* proposed that $c(r)$ should be extended at distances longer than σ_{cm} . In this respect, a new length parameter, λ , was defined to take into account the distance at which the polymer *feels* the colloidal surface as a non-negligible obstacle. In consequence, λ should extend the colloid-monomer direct correlation beyond the overlap. These premises are satisfied under the so-called modified PY (or m-PY) equation, given by (63),

$$\hat{c}_{cm}(q) = \frac{\hat{c}_{cm}^{PY}(q)}{1 + q^2 \lambda^2}, \quad (4.9)$$

where $\hat{c}_{cm}^{PY}(q)$ stands for the direct correlation defined by the PY equation already defined in Chapter 3 (eq (3.16)). In the real space, eq. (4.9) is equivalent to,

$$c_{cm}(r) = \int \frac{1}{4\pi\lambda} \frac{1}{|\mathbf{r} - \mathbf{s}|} e^{|\mathbf{r} - \mathbf{s}|/\lambda} c_{cm}^{PY}(\mathbf{s}) d\mathbf{s}, \quad (4.10)$$

that clearly shows that the colloid-monomer correlation does not vanish immediately beyond the overlap but decays to zero smoothly along a distance of the order of λ . An example is given in fig. (4.7) calculated for a neutral colloid-polymer

4.3 Deformation of the polymer close to the colloidal surface

mixtures with a gaussian polymer chain ($N_m = 50000$, $R_g = 1.4$, with $\sigma_c = 1$), $c/c^* = 0.0001$ and $\phi_c = 0.01$. In the figure, the analytical solution as well as the numerical solution for PY and m-PY ($\lambda = 0.3$) are included (see legend). In the “thread limit”, the direct colloid-monomer correlation is a constant value that depends on the parameters of the system (solid line). However, comparing with the numerical solution (PY closure), the direct correlation shows a strong deviation from the constant value close to the contact point $r = \sigma_{cm}$ as a consequence of the monomer finite-size (dashed line). In contrast, the m-PY closure result for $\lambda = 0.3$ shows the emergence of a smooth decay of the direct correlation at the range $\sigma_{cm} < r < (\sigma_{cm} + \lambda)$, as is desired. In other words, the spatial convolution that introduces eq. (4.10), captures the non-local changes in the polymer conformation close to the colloidal particles not included in the PY description.

It is expected that λ varies non-trivially with the physical system parameters and its magnitude should be smaller than R_g and/or σ_c . For that reason, it is necessary the implementation of a *thermodynamic consistency* to enforce the determination of λ uniquely for each system, or set of parameters. The *thermodynamic consistency* philosophy lies on the fact that the solution of PRISM must provide the same thermodynamic results calculated by different routes (87). In particular, the polymer excess chemical potential, $\delta\mu_p$, is calculated by means of two routes. The λ value is then chosen as the one which forces that both $\delta\mu_p$ values are the same. The routes proposed to reach the consistency were (63):

- The compressibility route (45),

$$\beta\delta\mu_p^{(1)}|_{\rho_m \rightarrow 0} = - \int_0^{\rho_c} d\rho_c \hat{c}_{cm}(q=0, \rho_c)|_{\rho_m \rightarrow 0}, \quad (4.11)$$

where the excess chemical potential, $\delta\mu_p^{(1)}|_{\rho_m \rightarrow 0}$, for inserting polymers into a colloidal suspension at density ρ_c is calculated, in the limit $\rho_m \rightarrow 0$.

- The second route is based on the calculation of $\delta\mu_p^{(2)}|_{\rho_m \rightarrow 0}$ in a process where the colloid size is continuously increased from geometrical points ($\sigma_c^{(\zeta)} (= \zeta\sigma_c) = 0$, with $\zeta = 0$) to their real sizes ($\sigma_c^{(\zeta)} = \sigma_c$, with $\zeta = 1$) (56). Therefore, it formally consists on an integration over the colloidal size being ζ the parameter that controls the colloidal size. During the growing process,

4. POLYMER REFERENCE INTERACTION-SITE MODEL

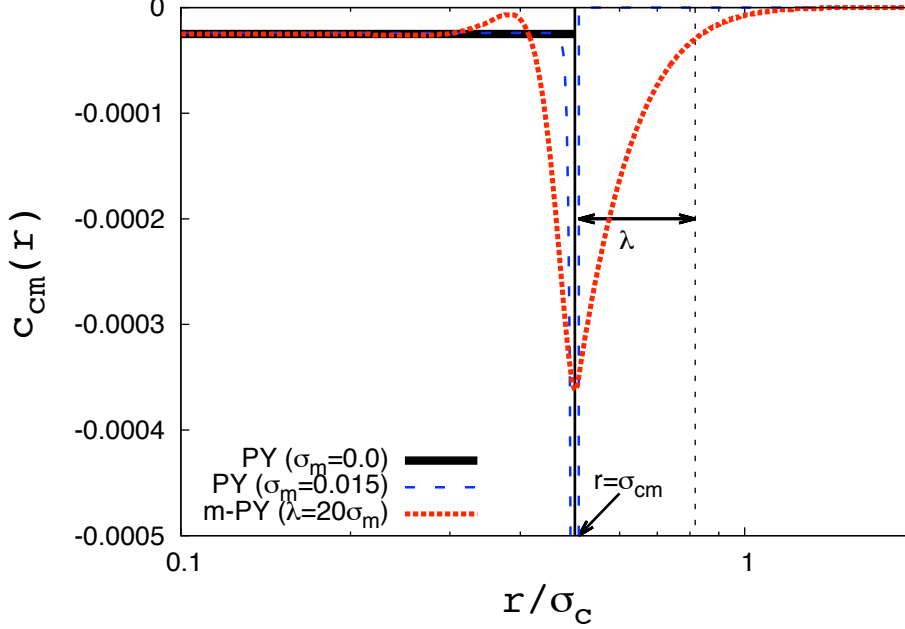


Figure 4.7: The direct colloid-monomer correlation for a gaussian polymer with $N_m = 50000$, $R_g = 1.4$, $c/c^* = 0.0001$ and $\phi_c = 0.01$. Three different cases are shown: the analytical solution ($\sigma_m = 0.0$) for the PY closure ($\lambda = 0$) with solid line, the numerical solution ($\sigma_m = 0.015$) also for the PY closure with dashed line and the numerical solution for the m-PY closure ($\lambda = 0.3$) with dotted line. Additionally, two vertical lines have been included to remark the colloid-monomer contact distance and the range of λ . As in previous calculations, all spatial lengths are reduced to $\sigma_c = 1$.

the colloids have to push against the pressure of the surrounding polymers. Then, calculating the excess chemical potential from the free energy of this process finally leads to the following expression,

$$\beta\delta\mu_p^{(2)}|_{\rho_m \rightarrow 0} = \frac{\pi\rho_c\sigma_c}{2} \int_0^1 d\zeta (\sigma_m + \zeta\sigma_c)^2 g_{cm}^{(\zeta)}(\sigma_{cm})|_{\rho_m \rightarrow 0} + 2\pi\rho_c^2\sigma_c^3 \int_0^1 d\zeta \zeta^2 \frac{\partial g_{cc}^{(\zeta)}(\zeta\sigma_c)}{\partial \rho_m}|_{\rho_m \rightarrow 0}. \quad (4.12)$$

It must be noted that $g_{ij}^{(\zeta)}(r)$ stands for the corresponding radial distribution of a mixture with colloidal particles with diameter $\sigma_c^{(\zeta)}$.

Comparing both routes, it is easy to understand that both calculations in prin-

4.3 Deformation of the polymer close to the colloidal surface

ciple will lead to different results. On the one hand, the compressibility route takes the large spatial scales into account ($q = 0$, being q the scattering vector) to obtain the excess chemical potential. Usually, the result is rather insensitive to λ . On the other hand, the “growing” route depends on $g_{cm}(r)$ at the contact, which is strongly dependent on λ . In summary, the method consists on reaching the λ value, which makes equal both routes, looking for the thermodynamic consistency of the PRISM theoretical predictions.

At the end of Chapter 6, we have briefly exposed the first results on this topic for mixtures of hard spheres and neutral polymers as well as mixtures of charged colloids and polymers with finite-size monomers. This theoretical project has been carried out in collaboration with Prof. Matthias Fuchs from the University of Konstanz (Germany).

4. POLYMER REFERENCE INTERACTION-SITE MODEL

Chapter 5

Experimental details

In this chapter, all experimental details of this dissertation are presented ¹. Firstly, a wide description of the light scattering methods has been provided in section 5.1. It has been the main experimental technique used for the particle characterization and the study of the structural and dynamics properties of our experimental systems. A special treatment has been given to the device (3D-DLS Spectrometer) in section 5.2, since it has allowed us to work with turbid systems eluding the multiple scattering from the analysis. In section 5.3, the particles employed in our experiments are described. Moreover, the previous light scattering knowledge are applied in the characterization of such particles.

5.1 Light Scattering methods

When a monochromatic and polarized light beam passes through a colloidal suspension, the interaction of the light with the colloidal particles scatters the light in all directions. The scattered light is collected by a photon-detector placed at a fix position, which forms an imaginary plane with the incident light beam, *i.e.*, the so-called *scattering plane*. Under this geometry, the *scattering vector* is defined as the vector difference between the wave propagation vectors of the incident, \vec{k}_i , and the scattered beam, \vec{k}_s , $\vec{q} = \vec{k}_i - \vec{k}_s$. In a quasi-elastic light scattering experiment, the *scattering vector* can be expressed with its modulus, $q = \frac{4\pi n \sin(\theta/2)}{\lambda_o}$, where λ_o is the wave length of the light in the vacuum, n is

¹In chapter 6, they are scarcely given due to the format of the result chapter as individual publications.

5. EXPERIMENTAL DETAILS

the refractive index of the medium and θ is the angle between vectors \vec{k}_s and \vec{k}_i . The *scattering volume* V_s is defined as the intersection between the incident beam and the optic field of the detector. This intersection defines the control volume, from where the experimental information is registered, and it should contain a large enough number of particles to be a representative sub-sample of the whole system. All this parameters are illustrated in fig. (5.1).

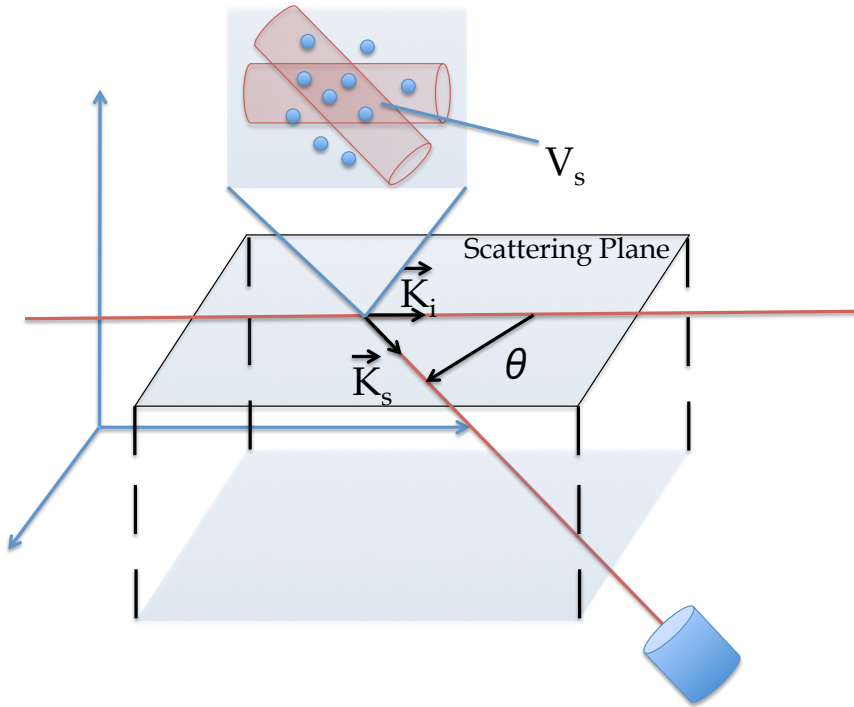


Figure 5.1: Illustration of a light scattering experiment.

5.1.1 Basic concepts

An electromagnetic field propagated through a material medium can induce, by means of its oscillatory electric component, dipoles on the colloidal particles. These dipoles also oscillate generating new isotropic radiation. This physical phenomenon leads to the so-called light scattering (88). The resolution of the Maxwell's equations for the conditions, where the light scattering phenomenon is defined, leads to the following expression for the scattered electric field, $E_s(\vec{R}, t)$,

in a far-field point¹, \vec{R} , and at a given time t ,

$$E_s(\vec{R}, t) = -\frac{k_s^2 E_0 \exp[i(\vec{k}_s \cdot \vec{R} - \omega t)]}{4\pi R} \int_V \left[\frac{\epsilon(\vec{r}, t) - \epsilon_0}{\epsilon_0} \right] \exp[-i\vec{q} \cdot \vec{r}] d\vec{r}. \quad (5.1)$$

Here, ω is the frequency of the incident scattered light, respectively, E_0 stands for the amplitude of the incident beam, $\epsilon(\vec{r}, t)$ is the dielectric constant at the position \vec{r} on the suspension and ϵ_0 is the average dielectric constant of the suspension. In eq. (5.1), the term $\frac{\epsilon(\vec{r}, t) - \epsilon_0}{\epsilon_0}$ represents the relative fluctuation of the dielectric constant on the medium, which is essentially the origin of the scattering phenomenon. The term $\exp[-i\vec{q} \cdot \vec{r}]$ describes the phase factor between the scattering radiation of two points separated a distance \vec{r} .

The colloidal suspension contained in the *scattering volume* can be decomposed into *subvolumes*, since the system is constituted by discrete spots (colloids) where the dielectric constant is different to the solvent, ϵ_{medium} . Under this idea, eq. (5.1) can be rewritten as follows,

$$E_s(\vec{R}, t) = -E_0(R) \sum_{j=1}^N \int_{V_j} \frac{k^2}{4\pi} \left[\frac{\epsilon_p(\vec{r}_j, t) - \epsilon_{medium}}{\epsilon_0} \right] \exp[-i\vec{q} \cdot \vec{r}_j] \exp[-i\vec{q} \cdot \vec{R}_j(t)] d\vec{r}_j \quad (5.2)$$

where N is the number of scattering particles, $\epsilon_p(\vec{r}_j, t)$ stands for the dielectric constant of the j -th particle at \vec{r}_j and the factor $E_0(R) = E_0 \frac{\exp[i(\vec{k}_s \cdot \vec{R} - \omega t)]}{R}$. $\vec{R}_j(t)$ denotes the centre of mass position of the particle j , being V_j its volume.

Hereinafter, let us consider just the term that modulates the scattered electric field regardless the term $E_0(R)$. This will be noted as $E(q, t)$,

$$E(q, t) = \sum_{j=1}^N b_j(q, t) \exp[-i\vec{q} \cdot \vec{R}_j(t)] \quad (5.3)$$

¹By far-field assumption, we mean that the electromagnetic radiation is collected far away from the scattering object, so that the scattering electric field is a planar wave perpendicular to the propagation direction and the amplitude decays inversely with the distance to the object.

5. EXPERIMENTAL DETAILS

where $b_j(q, t) = \int_{V_j} \frac{k^2}{4\pi} \left[\frac{\epsilon_p(\vec{r}_j, t) - \epsilon_{medium}}{\epsilon_0} \right] \exp[-i\vec{q} \cdot \vec{r}_j] d\vec{r}_j$. Since in a light scattering experiment the scattered photons are detected per unit of area and time, the relevant physical magnitude will be the instantaneous scattered intensity. It is given by,

$$I(q, t) = |E(q, t)E^*(q, t)| = \sum_{i=1}^N \sum_{j=1}^N |b_i(q, t)b_j^*(q, t)| \exp(-i\vec{q} \cdot (\vec{R}_i(t) - \vec{R}_j(t))). \quad (5.4)$$

Eq. (5.4) represents a fluctuant observable, since it comes from a system of moving scattering particles. Thus, it should be considered in terms of time-average, $\langle I(q) \rangle$. In this respect, the time during the intensity is collected must be longer than the typical time where the system explores a representative set of points in the phase-space. This allows us to assume that the intensity time-average is equal to the intensity ensemble-average: the *ergodicity* condition. There are systems where this typical time is much longer than the time taken for a standard light scattering experiment, the so-called arrested systems. In such cases, the intensity ensemble-average is measured by means of more sophisticated methods (89, 90).

5.1.2 Static Light Scattering (SLS)

This technique is based on the detection of the average intensity per angle within a wide angular range. Depending on the ratio between the laser wave length, λ_o , and the size of the scattering particle, a ¹, several scattering regimes can be distinguished: Rayleigh, if $\lambda_o \gg a$, Rayleigh-Gans-Debye (RGD), if $\lambda_o \sim a$, and Mie², if $\lambda_o \ll a$. In this research, we have worked with different spherical particles³ but always satisfying $\lambda_o \approx R_c$, the radius of the particle, so the RGD model is good enough to describe the scattering pattern of the average intensity per angle (88).

¹For homogeneous spherical particles, a corresponds with its radius, R_c .

²The Mie's regime requires a special treatment, since the scattered photons at far-field points can interfere depending on the geometry of the particles. In this sense, the particles act as a set of scattering centers.

³Note that in paper I, we have used particles with $R_c \sim 0.7 \mu\text{m}$, therefore the Mie's regime could be applied for SLS measurements. However, this work was focused only on the colloidal dynamics at a fixed angle, so that the SLS technique is not required and also the Mie's treatment.

From eq. (5.4), the intensity average can be easily decomposed into the product of two q functions assuming identical particles ($b_i(q, t) = b(q)$ for all the particles). So, eq. (5.4) can be rewritten as follows,

$$\langle I(q) \rangle = AP(q)S(q). \quad (5.5)$$

where $A = N\langle |b(0)|^2 \rangle$ depends mainly on the particle number density, the size of the particle and the refractive index. $P(q)$ is the form factor, already defined in section 4.1. Although for the RISM formalism, the form factor is usually noted as $\hat{w}(q)$, in light scattering the $P(q)$ notation is more common. $P(q) (\equiv \frac{\langle |b(q)|^2 \rangle}{\langle |b(0)|^2 \rangle})$ contains the interference of the photons scattered from individual particles. Instead, $S(q)$ stands for the structure factor (already defined in section 3.1) and takes into account the interference of the scattered light from different particles.

For a homogeneous spherical particle of radius $R_c (\sim \lambda_0)$, the RGD form factor is given by,

$$P(q) = \left[\frac{3}{(qR_c)^3} (\sin(qR_c) - qR_c \cos(qR_c)) \right]^2. \quad (5.6)$$

Eq. (5.6) may be used to obtain an accurate prediction of R_c by measuring the $\langle I(q) \rangle$ in a very diluted colloidal suspension (where $S(q) \sim 1$). In section 5.3 will be shown that the predictions obtained by means of eq. (5.6) are quite similar to the one obtained with other techniques (91).

From eq. (5.4), the exponential term is identified with the structure factor that was already defined in section 3.1.1,

$$S(q) = \frac{1}{N} \left\langle \sum_{i=1}^N \sum_{j=1}^N \exp(-i\vec{q} \cdot (\vec{R}_i(t) - \vec{R}_j(t))) \right\rangle. \quad (5.7)$$

The scattering vector q takes here an important role. In an ensemble-average, all relative distances between particles for all the possible configurations of the phase-space are considered. If there is not a preferential separation distance between particles (non-structured system), the average in eq. (5.7) will be equal to N . In case of correlated particles, leading to the emergence of a typical separation distance each other, we can look for the q value satisfying the relationship $\vec{q} \cdot (\vec{R}_i - \vec{R}_j) \propto 2\pi$, since it relates the typical distance with its Fourier component

5. EXPERIMENTAL DETAILS

(position of the main peak of $S(q)$, see section 3.2). Experimentally, the information concerning the spatial distribution of the particles in equilibrium, $S(q)$, can be derived from the interference pattern in a range of q using eq. (5.6):

$$\begin{aligned} \langle I_{con}(q) \rangle \propto P(q)S(q) \\ \langle I_{dil}(q) \rangle \propto P(q) \end{aligned} \Rightarrow S(q) = \frac{\rho_{dil} T_{dil} \langle I_{con}(q) \rangle}{\rho_{con} T_{con} \langle I_{dil}(q) \rangle} \quad (5.8)$$

Here, labels “*dil*” and “*con*” stand for a diluted and a concentrated sample, respectively. The prefactor ρ is the number density of particles and T is the transmission factor. A typical cylindrical cell possesses a thickness of 1 cm, while the thickness of the *scattering volume* is much smaller, therefore the photons go through several millimeters before they leave the sample. During such optic path, the energy of some photons can be absorbed by the medium and these photons does not reach the photon-detector. The ratio between the real number of scattering photons at q in the *scattering volume* and the photons at the same q that reach the detector defines the latter transmission factor. In a scattering experiment, the transmission parameter is elusive. However, using the fact that the $S(q)$ approaches asymptotically to the unity¹ for $q \rightarrow \infty$, the transmission parameter can be indirectly known.

5.1.3 Dynamic Light Scattering (DLS)

A DLS experiment consists on the measurement of the scattered intensity time-correlation at a fixed scattering vector, q ,

$$G^{(2)}(q, \tau) = \langle I(q, t)I(q, t + \tau) \rangle. \quad (5.9)$$

At $\tau \rightarrow 0$, $G^{(2)}(q, 0) = \langle I(q, t)^2 \rangle$, while at $\tau \rightarrow \infty$, $G^{(2)}(q, \infty) = \langle I(q, t) \rangle^2$. Therefore, eq. (5.9) is commonly normalized with $\langle I(q, t) \rangle^2$,

$$g^{(2)}(q, \tau) = \frac{G^{(2)}(q, \tau)}{\langle I(q, t) \rangle^2}. \quad (5.10)$$

Since $I(q, t)$ is a fluctuant signal, the temporal dependence in eq. (5.10) between the two limit cases ($\tau \rightarrow 0$ and ∞) provides information about the temporal decorrelation of the signal. This decorrelation must be related with the motion

¹ $S(q)$ goes to 1 for $q \rightarrow \infty$, since at such spatial scales ($r \rightarrow 0$) there is not interaction between particles.

of the dispersed particles in the medium. As was pointed out in the chapter 2, the particles move following specific statistical properties. Extrapolating these statistical properties to the scattered intensity, it can be demonstrated (92) that the scattering electric field, $E(q, t)$, is a complex gaussian variable with null average. From eq. (5.9), the relationship between the intensity time-correlation and the electric field time-correlation can be established as follows,

$$G^{(2)}(q, \tau) = \langle I(q) \rangle^2 + \beta_{inter}^2 |G^{(1)}(q, \tau)|^2, \quad (5.11)$$

where $G^{(1)}(q, \tau) = \langle E(q, t)E^*(q, t + \tau) \rangle$ is the electric field time-correlation. This is the so-called *Siegert relationship*¹. The coefficient β_{inter} , commonly called *intercept*, is the ratio between the coherence area of the scattered light beam and the surface area where the signal is detected.

The most important magnitude in a DLS experiment is the function $G^{(1)}(q, \tau)$. This is clearly shown on the following expression, constructed from eq. (5.4) and normalized by $\langle I(q) \rangle$,

$$g^{(1)}(q, \tau) = \frac{\sum_{i=1}^N \sum_{j=1}^N \langle b_i(q, t)b_j^*(q, t + \tau) \exp[-i\vec{q}[\vec{R}_i(t) - \vec{R}_j(t + \tau)]] \rangle}{\sum_{i=1}^N \sum_{j=1}^N \langle b_i(q, t)b_j^*(q, t + \tau) \exp[-i\vec{q}[\vec{R}_i(t) - \vec{R}_j(t)]] \rangle}. \quad (5.12)$$

In eq. (5.12), the so-called *normalized dynamic structure factor*, $g^{(1)}(q, \tau) = \frac{G^{(1)}(q, \tau)}{\langle I(q) \rangle}$, contains explicit information about the relative motion between any two interacting particles, $\vec{R}_i(t) - \vec{R}_j(t + \tau)$. Therefore, the measure of eq. (5.12) by means of eqs (5.10) and (5.11) allows us to follow the particles motion of an interacting particle system. For a colloidal suspension without structure (non-interacting particles), eq. (5.12) is reduced to,

$$g^{(1)}(q, \tau) = \frac{1}{Nb^2(q)} \sum_{j=1}^N b_j^2(q) \langle \exp[-i\vec{q}[\vec{R}_j(t) - \vec{R}_j(t + \tau)]] \rangle. \quad (5.13)$$

The cross terms $i \neq j$ that correlate different particles have been removed. In this case, the displacement $\vec{R}_j(t) - \vec{R}_j(t + \tau)$ can be expressed by means of the

¹This is a statistical relationship established between the fourth and second moment of a gaussian distribution.

5. EXPERIMENTAL DETAILS

free-diffusion coefficient, D_0 (eq. (2.3)), giving,

$$g^{(1)}(q, \tau) = \frac{1}{N b^2(q)} \sum_{j=1}^N b_j^2(q) \exp[-D_{0,j} q^2 \tau]. \quad (5.14)$$

where $D_{0,j} = \frac{1}{6} \langle |\vec{R}_j(t) - \vec{R}_j(t+\tau)|^2 \rangle$ is the diffusion coefficient of the j -th particle. In the trivial case of identical particles, eq. (5.14) leads to,

$$g^{(1)}(q, \tau) = \exp[-D_0 q^2 \tau]. \quad (5.15)$$

Therefore, the hydrodynamic radius, R_h , of the colloidal particle in suspension can be calculated by fitting eq. (5.15) with an exponential function.

As was pointed out some paragraphs before, an exponential decay similar to the one obtained in eq. (5.15) can be also found on the dynamic analysis of interactive particle suspensions. In such cases, an effective diffusion coefficient, D_{eff} , is incorporated to eq. (5.15) in substitution of D_0 . It is usually distinguished between different temporal ranges (short and long times coefficients) and different spatial scales q , alluding to a regimes where the motion is *autodiffusive* ($q > 1/R_c$) or the diffusion is cooperative between an ensemble of particles. ($0 < q < 1/R_c$) (a wide theoretical treatment of the latter is given in refs. (25, 93)).

5.2 3D-DLS device

The main laser light scattering device used within this dissertation is the 3D-DLS Spectrometer, from LS Instrument (Fribourg, Switzerland). This apparatus was designed with the intention of avoiding the multiple scattering effects. The multiple scattering becomes a serious inconvenient in highly concentrated colloidal systems or even at low concentrations, if the refractive indexes particle-solvent do not match (turbid sample). In these cases, the use of techniques to eliminate the multiple scattering contribution becomes essential.

5.2.1 3D-DLS description

Next, we list the main components of the 3D-DLS Spectrometer giving a brief description of each one. Fig. (5.2) shows a picture of the apparatus with labels

identifying the different components:

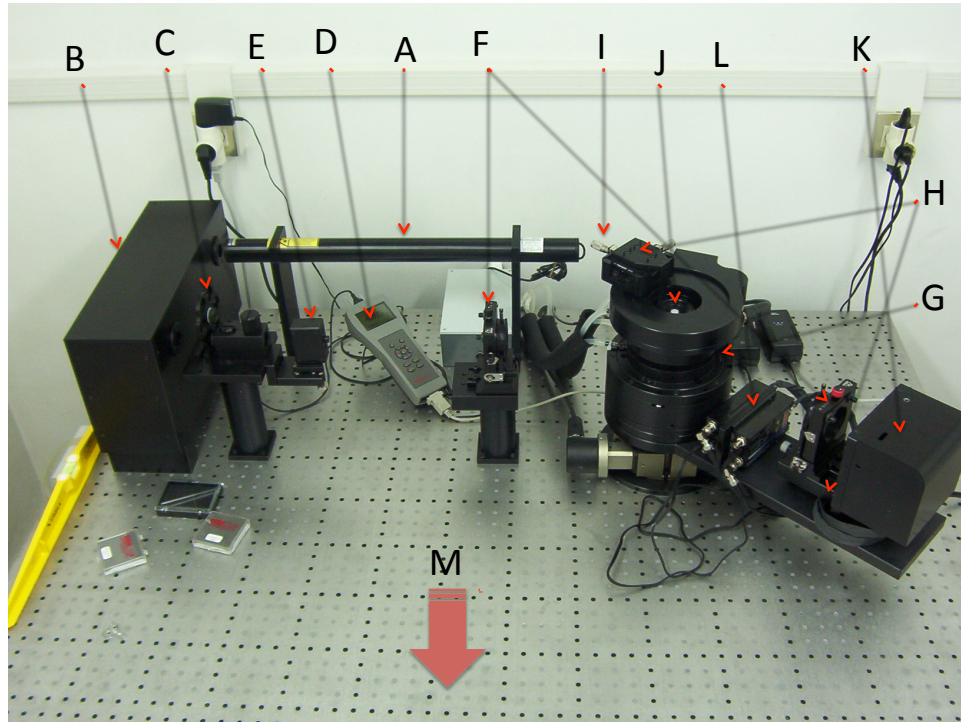


Figure 5.2: Picture of the 3D-DLS Spectrometer device. Labels indicate the different components (see text).

- **A - Helium-Neon Laser beam.** A coherent and polarized beam with a wave length $\lambda_o = 632.8$ nm and maximum power 35 mW. The fluctuation of the power does not change in more than 1% during the stable phase of the laser¹.
- **B - Mirrors.** A set of two mirrors placed in a black box guiding the light beam to the sample. This reduces the extension of the device, since the optical arrangement can take a long distance in straight-line.
- **C - Light Filters.** The beam passes through a filter to reduce its power. A set of seven filters are settled in a rotatory wheel to carry on the experiments in optimal photon-counting conditions.

¹The stable phase of a laser is reached around 30 min after to turn on. Then, it can be stable during 5-6 hours.

5. EXPERIMENTAL DETAILS

- **D - Potentiometer.** This device instantaneously registers the power of the main beam after crossing the filter. The potentiometer is connected to the computer to provide the average power during any light scattering experiment.
- **E - Beam Splitter.** Optical device to split the main beam into two parallel and incoherent beams.
- **F - Converging Lenses.** They are focused on the center of the bath, where the sample is placed. This allows to cross the parallel incident beams in the centre of the sample and register the scattered light again as two parallel beams.
- **G - Bath.** The centre of a thermal bath is placed just in the image focus of the latter lenses. A water closed circuit covers the bath to keep a constant temperature. The circuit is connected to a thermostat (Thermostat HAAKE K10) and to the computer, where the temperature is registered at any time. The bath is filled with decahydronaphtalene (cis+trans) with the aim to match the refractive index of the sample cell.
- **H - Double Goniometer.** The thermal bath is assisted by two independent motors moving the nest, where the sample is placed, and the light detector arm. The first goniometer is useful for samples with slow dynamics like glassy systems (89, 90), since the rotation of the sample allow us to perform a fast ensemble-average. The second goniometer selects the angle θ , where the photons are collected by the detectors placed on it.
- **I - Micrometer Screws.** Suitable for squares sample cells, since the optical path of the light can be reduced changing the x-y position of the cell from an overhead view. This application is specially indicated for turbid samples.
- **J - Cells.** We can use either quartz or glass cells. They can be geometrically different (square or cylindrical with diameter 5 or 10 mm). The quality of the cell material does not affect the angular distribution of intensity, but improves the photon transmission.
- **K - Fiber Optic.** After crossing the second lens, the photons are collected by two detectors consisting on two fiber optic “eyes”, which drive the collected light to an electronic device where both beams are treated.

- **L - Photodiode Receivers (EG and G)**. Avalanche photodiodes are settled during the fiber optic circuit to multiply the input signal. The confidence range of this device is $(1-50) \cdot 10^5$ photon per second.
- **M - Correlator Multi-tau (ALV)**. In this electronic device the correlation of the signal is calculated. One can chose between auto and cross time-correlation to obtain the correlation between the two beams (cross) or only one (auto). The resulting information is finally transmitted to the computer.

5.2.2 Suppression of the multiple scattering

During a light scattering experiment, the incident light beam is scattered from the sample and collected by a detector placed at the scattering angle θ . When the photons are inside the sample, they can interact with several particles, or scattering centres, and so the collected photons do not always come from a *single scattering*. Let us consider now the scheme illustrated in fig. (5.3). In a single scattering, the incident light beam is scattered by the scattering centre A and collected by the detector. In a double scattering, the incident light is scattered from the centre B and, before leaving the sample, is again scattered from the scattering centre C in such a way that the photons ends up in the detector. Considering both examples, the registered intensity is not only the one coming from particle A, but also from the *double scattering*, (optical path B-C). As the scattering vector q contains specific information from the $2\pi/q$ spatial scale, under the situation illustrated in fig. (5.3), the latter ceases to be valid, since $\langle I(q) \rangle$ becomes contaminated by other q vectors.

In this work, we have treated with different kind of particles at several concentrations (section 5.3) and almost always exceeding the limit where the multiple scattering can be neglected. Fortunately, using the 3D-DLS Spectrometer, we are able to eliminate the multiple scattering effect in all our experiments from the analysis. On the next paragraphs, the theoretical fundamentals to understand how the single scattering information is isolated from the multiple scattering are exposed.

In 1980, G. D. J. Phillies proposed an idea (94, 95) to elude the multiple scatter-

5. EXPERIMENTAL DETAILS

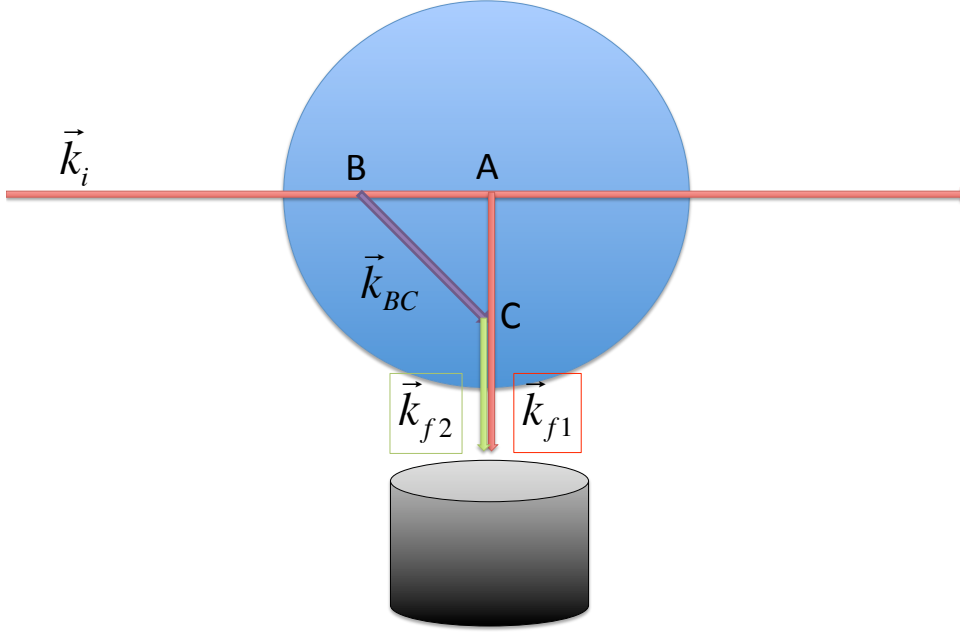


Figure 5.3: Single and double scattering scheme.

ing contamination in a quasi-elastic light scattering experiment keeping the basic structure of a standard scattering device. This pioneering idea was widely developed and applied to more sophisticated apparatus on the next twenty years (96, 97). The new scheme was based on the cross-correlation of the scattered electric field of two simultaneous experiments coming from the same scattering volume, but for two different scattering vectors: \vec{q} and $-\vec{q}$. Let us consider the field amplitude as a sum of two contributions: single plus double and higher-order scattering,

$$E(\vec{q}, t) = E^s(\vec{q}, t) + E^m(\vec{q}, t). \quad (5.16)$$

The superscripts s and m stand for the single and multiple scattering, respectively. Both are complex gaussian variables for a large enough scattering volume. Let us also consider the signal coming from another scattering vector $-\vec{q}$. The average

intensity at any scattering vector will be given by,

$$\langle I(q) \rangle = \langle I^s(q) \rangle + \langle I^m(q) \rangle \quad (5.17)$$

and the auto-correlation of $I(q, t)$ by,

$$\begin{aligned} \langle I(q, 0)I(q, \tau) \rangle &= \langle I^s(q, 0)I^s(q, \tau) \rangle + \langle E^s(q, 0)E^{s*}(q, \tau) \rangle \langle E^{m*}(q, 0)E^m(q, \tau) \rangle \\ &\quad + \langle E^{s*}(q, 0)E^s(q, \tau) \rangle \langle E^m(q, 0)E^{m*}(q, \tau) \rangle \\ &\quad + \langle I^m(q, 0)I^m(q, \tau) \rangle + 2\langle I^s(q) \rangle \langle I^m(q) \rangle \end{aligned} \quad (5.18)$$

By auto-correlation is understood the time-correlation between the scattering intensity coming from the same scattering vector. Eq. (5.18) explicitly contains the contributions from both single and multiple scattering. Given the statistical independence between the single-multiple and multiple-multiple¹ scattering contributions to the electric field, only the $E^s(\vec{q}, t)$ and $E^s(-\vec{q}, t)$ will show correlated fluctuations in the cross-correlation function of the intensity (the time-correlation between \vec{q} and $-\vec{q}$), since in a single scattering only the modulus of the scattering vector, q , is relevant and is equal for both simultaneous experiments. Following the latter expression, the cross-correlation of the intensity can be calculated as follows,

$$\begin{aligned} \langle I(\vec{q}, 0)I(-\vec{q}, \tau) \rangle &= \langle I^s(\vec{q}, 0)I^s(-\vec{q}, \tau) \rangle + \langle I^m(\vec{q}, 0)I^m(-\vec{q}, \tau) \rangle \\ &\quad + \langle I^s(\vec{q}) \rangle \langle I^m(-\vec{q}) \rangle + \langle I^m(\vec{q}) \rangle \langle I^s(-\vec{q}) \rangle. \end{aligned} \quad (5.19)$$

where the vectorial notation for q , has been explicitly shown to distinguish between both simultaneous scattering experiments. The statistical independence of the electric field from \vec{q} and $-\vec{q}$ has been applied to suppress the cross-correlated terms. Using eq. (5.17) on eq. (5.19) and simplifying, the normalized cross-correlation function can be written as follows

$$g_c^{(2)}(q, \tau) = 1 + \frac{\langle I^s(\vec{q}) \rangle \langle I^s(-\vec{q}) \rangle}{\langle I(\vec{q}) \rangle \langle I(-\vec{q}) \rangle} \left[\frac{\langle I^s(\vec{q}, 0)I^s(-\vec{q}, \tau) \rangle}{\langle I^s(\vec{q})I^s(-\vec{q}) \rangle} - 1 \right] \quad (5.20)$$

where the subscript in $g_c(q, \tau)$ notes that is a cross-correlation function. The main consequence of this results is that the time-dependent factor in eq. (5.20)

¹The higher order scattering involves different Fourier components, which are statistically independent and undergo uncorrelated temporal fluctuations (see ref. (95))

5. EXPERIMENTAL DETAILS

only involves the single scattering. In fact, using eq. (5.12) on eq. (5.20), it is easy to show that the time-dependent term $\frac{\langle I^s(\vec{q}, 0)I^s(-\vec{q}, \tau) \rangle}{\langle I^s(\vec{q})I^s(-\vec{q}) \rangle} - 1$ is equal to $(\beta g^{(1)}(q, \tau))^2$. The ratio between single and total intensities enters here as an amplitude modulating the temporal information contained in the cross-correlation function. Following the notation for the intercept, β_{inter} , the new static pre-factor is commonly rewritten as $\beta_{MS}^2(q)$. Additionally, any misalignment in the overlap of the scattering volumes must be taken into account on the pre-factor term (β_{OV}), since it also modulates the electric field cross-correlation (more information about this can be found in ref. (97)). Thus, the final expression follows the same aspect than eq. (5.12) but with $\beta_{cross}(q) = \beta_{MS}(q)\beta_{OV}\beta_{inter}$.

Special care should be taken during a cross-correlation experiment concerning the duration of the measurement. In case of a strong multiple scattering contribution, the collected photons coming from single scattering can be scarce, even though the ensemble-average of the total intensity, $\langle I(q) \rangle$, is rapidly reached. So that, the expended time to measure the cross-correlation of the single scattering electric field (in particular, the second term in eq. (5.20)) will be insufficient to reach an ensemble-average of this magnitude. There is not a rule to know *a priori* the extra-time necessary to measure the ensemble-average of the latter. In our experiments, we focused on the β_{MS} value at the end of each $g^{(1)}(q, \tau)$ measurement, since it contains the rate of average single photons registered respect to the total intensity, to decide if a long-time measurement is required.

In fig. (5.4), the normalized electric field time-correlation calculated by means of the auto and cross techniques are compared. The results correspond to a diluted colloidal suspension of polystyrene latex (see section 5.3). At low colloidal concentration (as in this example), the sample is transparent and, so the multiple scattering contribution should be totally negligible. However, this is not the case, as there is still a small difference between the cross and the auto correlation functions. As the particle concentration increase, the small disagreement becomes more significant.

We have not yet mentioned the advantages of this multiple scattering suppression method applied to the SLS technique. As was presented in section 5.1.2, we have to measure the total average intensity as a function of q to obtain the shape

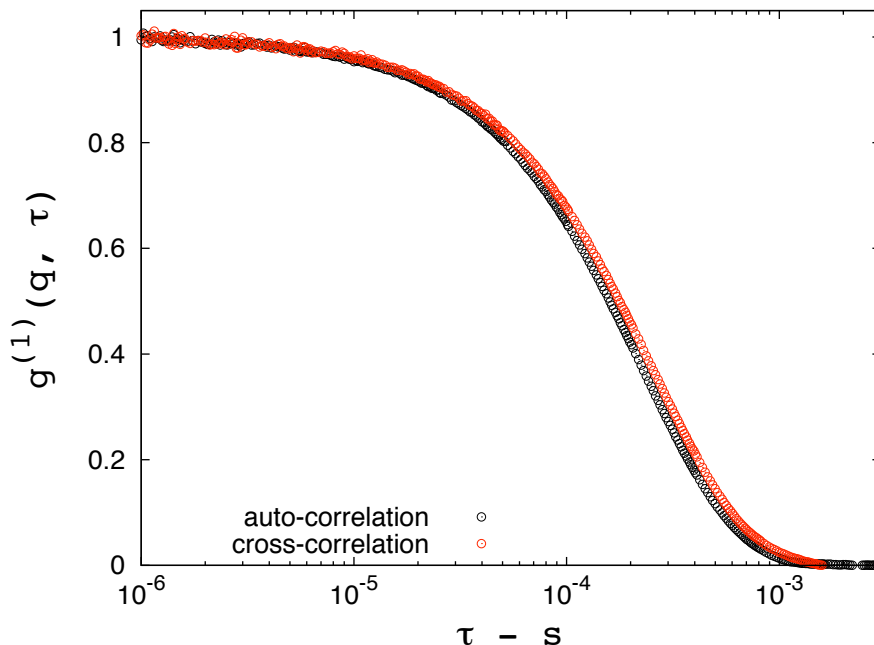


Figure 5.4: Auto and cross normalized electric field time-correlation for polystyrene particles in free-diffusion at $\phi_c = 0.02\%$ and $[\text{KNO}_3]=2$ mM. Under this conditions the sample is transparent.

and spatial order of the particles. However, following eq. (5.17), the multiple scattering is not removed from that measurements, since it contains the $\langle I(q) \rangle (= \langle I^s(q) \rangle + \langle I^m(q) \rangle)$ average magnitude. To perform an analysis based on the single scattering scheme, one can derive the corresponding structure factor, $S(q)$, taking into account only the single contribution (98). From eq. (5.19), the total average intensity as a function of the single scattering is derived as follows,

$$\langle I_s^A(q) \rangle \langle I_s^B(q) \rangle = \beta_{MS}(q) \langle I^A(q) \rangle \langle I^B(q) \rangle. \quad (5.21)$$

$\beta_{MS}(q) = \sqrt{g^{(2)}(q, 0) - 1}$ is directly deduced from eq. (5.20). The superscripts A and B denote each detector (to distinguish between \vec{q} and $-\vec{q}$) and the notation of the single scattering is taken now in the subscript. Since the modulus of the \vec{q} vector of both light beams is the same, in a single scattering both intensities share a common spatial scale information and therefore the vectorial notation is removed. So, if we insert eq. (5.21) into eq. (5.8) for the structure factor, we

5. EXPERIMENTAL DETAILS

finally obtain the next expression,

$$S(q) = \frac{\rho_{dil} T_{con}}{\rho_{con} T_{dil}} \sqrt{\frac{\langle I_{con}^A(q) \rangle \langle I_{con}^B(q) \rangle \beta_{MS}^{con}(q)}{\langle I_{dil}^A(q) \rangle \langle I_{dil}^B(q) \rangle \beta_{MS}^{dil}(q)}} \quad (5.22)$$

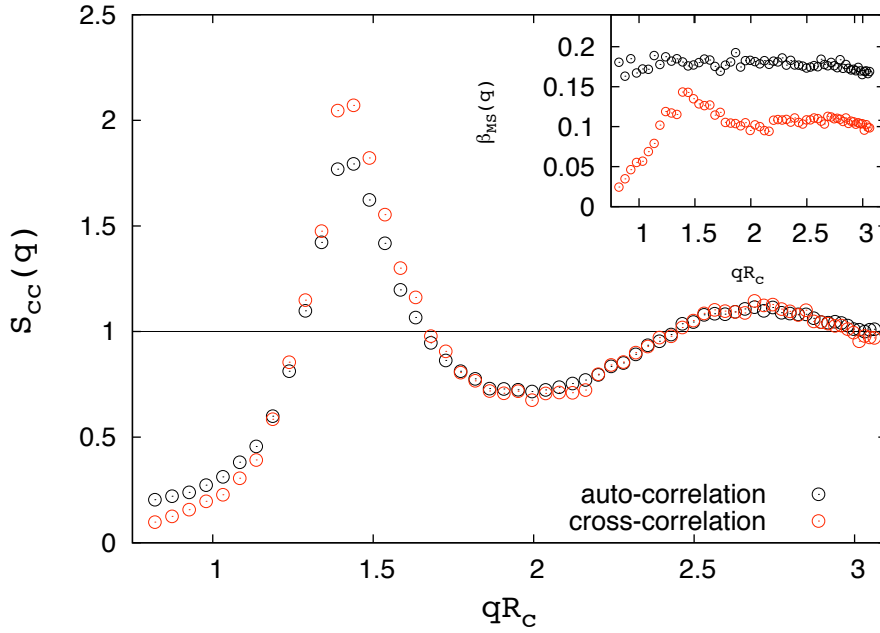


Figure 5.5: Comparison of the colloidal structure factor measured with (red) and without (black) the multiple scattering corrections. The inset shows the dependence of β_{MS} on q when the multiple scattering is considered.

Here, we assume that the transmission factors are equal for both beams along the sample. Note that in the latter expression the angular dependence does not only lies on the explicit intensity but also in the $\beta_{MS}(q)$ function.

Fig. (5.5) compares the colloidal structure factor obtained using the technique of the cross-correlation with the one without the multiple scattering suppression, auto-correlation. It should be noted that the colloidal packing fraction is here more than 10 times greater respect to the one studied in fig. (5.4), therefore it is expected a more presence of multiple scattering than in the sample of fig. (5.4). With the multiple scattering corrections, a result quite different to the one obtained without corrections is documented for $qR_c < 1.75$. This discrepancy comes

from the $\beta_{MS}(q)$ function (see inset of fig. (5.5)), which for low q values shows an important q -dependence respect to the diluted case. At $q \rightarrow 0$, the single scattering respect to the total one drastically decreases, since the photons are collected from a large spatial scale where the multiple scattering is more likely respect to the single one.

5.3 Experimental systems

In section 5.1, we have presented the fundamental observables, $\langle I(q, t)I(q, t + \tau) \rangle$ and $\langle I(q) \rangle$, that were measured by light scattering techniques in our experimental studies. These were also useful to perform the individual characterization of the particles employed in this thesis. Here, the information about the systematic characterization of each kind of particles is presented.

5.3.1 Colloidal particles

We have employed polystyrene latex (PS) as colloids, which are generally presented as highly monodisperse particles (99). The PS particles were synthesized by the POLYMAT group using the standard synthesis procedures described in ref. (100). During the particle preparation, nanometric spheres of polystyrene are formed and grow, until the chemical reaction is interrupted. At the last stage of the chemical reaction, an ionic surfactant is added covering some of the surface of the polystyrene nucleus to give them an ionic character. After the synthesis, residual amounts of chemical components can be still found in dissolution. To remove the latter, the original sample was purified by means of the commonly known Serum Replacement procedure (68). Figure (5.6) shows the resulting particles after the synthesis. This picture was taken using Transmission Electron Microscopy (TEM). From the picture, the average diameter is around 100 – 110 nm and the polydispersity was found to be smaller than 5% (in particular, the width of the size distribution is 2%).

The PS colloidal particles were characterized using light scattering techniques. In particular, fig. (5.7) shows the experimental form factor (via SLS) together with the prediction given by eq. (5.6) (RGD model). This measurement was carried out at very low particle concentration in order to guarantee that $S(q) = 1$. To ensure the absence of particle-particle electrostatic repulsive interactions, we have

5. EXPERIMENTAL DETAILS

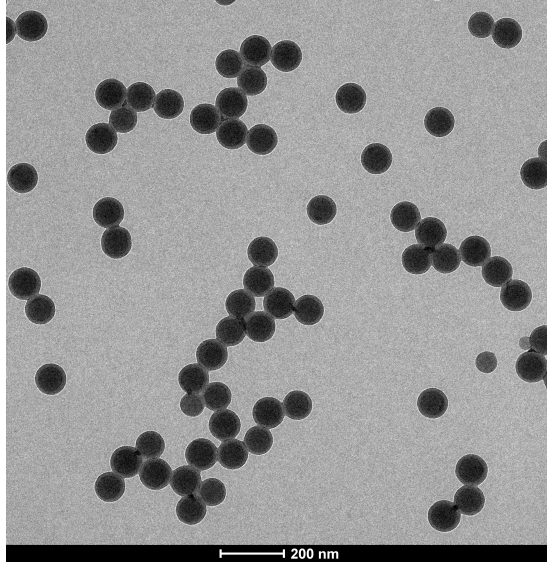


Figure 5.6: TEM image of the polystyrene latex courtesy of J. Ramos and I. Iranburu (POLYMAT Institute).

also added a small amount of salt ($[\text{KNO}_3] = 2 \text{ mM}$). As observed, the experiments fit well to a monodisperse suspension of hard-spheres with hydrodynamic radius $R_c = 55 \text{ nm}$, which is quite similar to the one obtained with TEM.

To confirm the radius estimated using the SLS technique, we performed a second measurement using DLS. The experimental result and the best theoretical prediction is given in fig. (5.8). Here, the exponential decay for $g^{(1)}(q, \tau)$ (eq. (5.14)) is employed to model the free diffusion of the PS particles. The best fit was reached at $R_h = 58.5 \text{ nm}$ that agrees quite well with the previous result. The small difference between the DLS and the SLS predictions for R_c lies on differences in the theoretical fundamentals of both techniques (SLS measures the radius of a sphere, while DLS measures the hydrodynamic radius).

For the wavelength of our laser ($\lambda_o = 632.8 \text{ nm}$), the polystyrene has a refractive index of 1.587, while the water one is 1.33. This difference is large enough to have strong multiple scattering effects, even at low colloidal concentrations (see fig. (5.4)). Notwithstanding, the latter characterization procedure is performed using the cross-correlation technique to assure that only single scattering enters

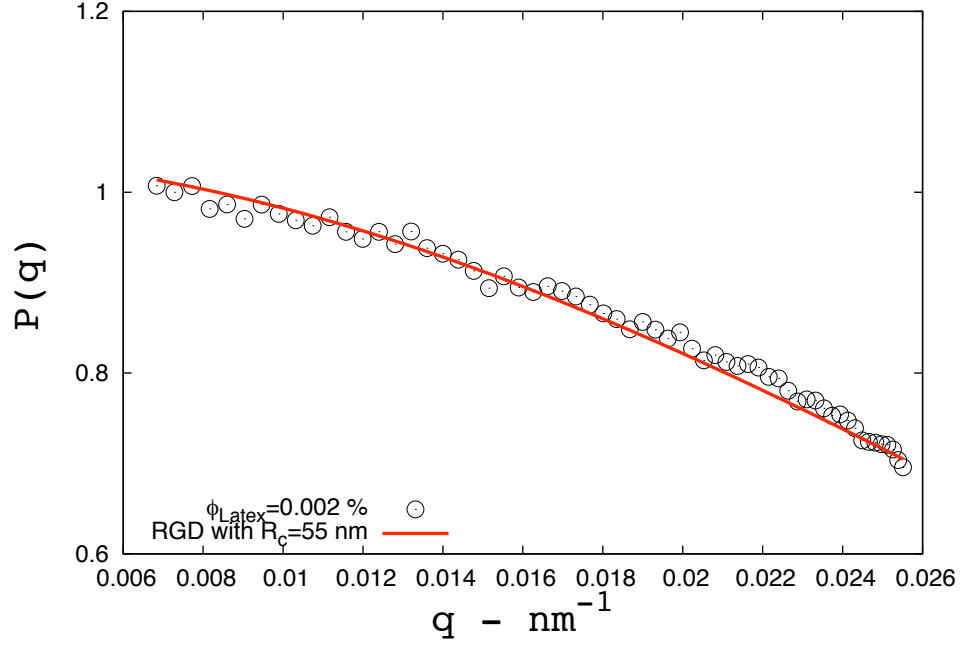


Figure 5.7: Experimental form factor for the polystyrene latex measured with the 3D-DLS Spectrometer (hollow circles). The solid line represents the best fit found respect to the experimental data using eq. (5.6).

in the analysis. At larger particle concentrations, not only the multiple scattering becomes extremely important, but also another trouble emerges. For a colloidal packing fraction of 1%, the PS latex suspension is so turbid that the maximum laser power (35 mW) is insufficient and so, the photons are not able to leave the sample. Therefore, there is no detected signal to analyze.

The latter limitation concerning the high colloidal concentration may be avoided using another kind of particles with a better index matching. In order to extend our experimental studies to larger colloidal particle concentrations, phosphatidyl-serine liposomes have been used. From a geometric viewpoint, a liposome is a sphere constituted by a water core and a phospholipid shell. The shell of a phosphatidyl-serine liposome is a bilayer with a thickness given by 4.5 nm. Using the synthesis process described in ref. (101), a polydisperse liposome suspension with an average diameter smaller than $0.5 \mu\text{m}$ is obtained. The large size of these particles and the narrow thickness of the shell makes the phosphatidyl-serine li-

5. EXPERIMENTAL DETAILS

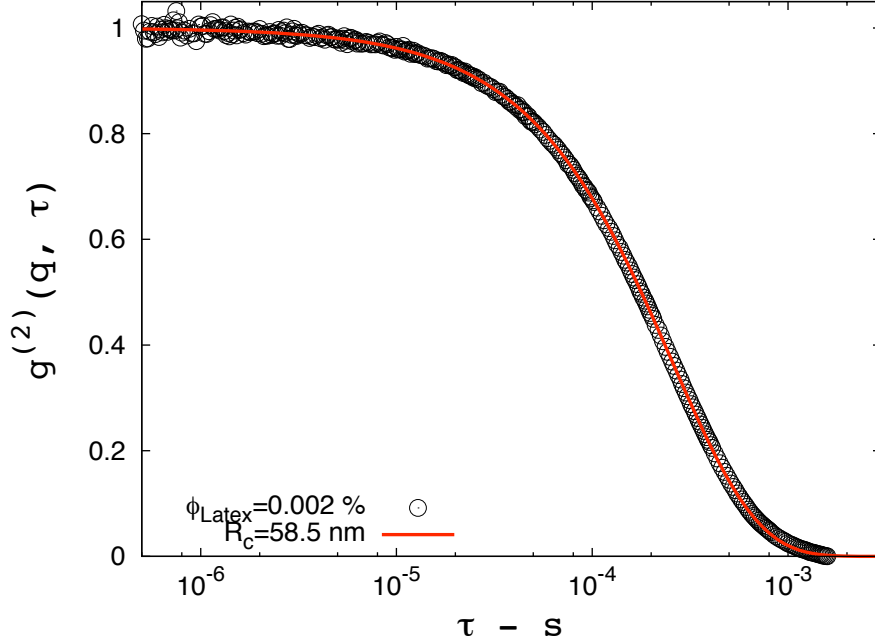


Figure 5.8: Normalized electric field cross-correlation for the PS latex (hollow circles) taken at $\theta = 90^\circ$ ($q = 0.019 \text{ nm}^{-1}$). The solid line stands for the best fit of the experimental data using the exponential decay predicted for non-interacting Brownian particles.

posomes extremely deformable. In this respect, after typically 1-2 weeks after the synthesis, it is not recommended to use these colloidal suspensions, since a large fraction of liposomes can be blown up by thermal agitation leading to a notably different system.

Fig. 5.9 shows an example of the form factor of the phosphatidyl-serine liposomes (hollow circles). The strong dependence with q respect to the result shown in fig. (5.7) indicates that a large variety of sizes exist in the liposome suspension, *i.e.*, the polydispersity. The RGD model can be modified to the case of hollow spheres with core refractive index equal to the medium one and polydispersity. From eq. (5.6), the liposome form factor can be rewritten as follows,

$$P(q) = \left[\frac{3}{(1-t^3)(qR_c^{(int)})^3} (\sin(qR_c^{(int)}) - qR_c^{(int)} \cos(qR_c^{(int)})) + qtR_c^{(int)} \cos(qtR_c^{(int)}) - \sin(qtR_c^{(int)}) \right]^2. \quad (5.23)$$

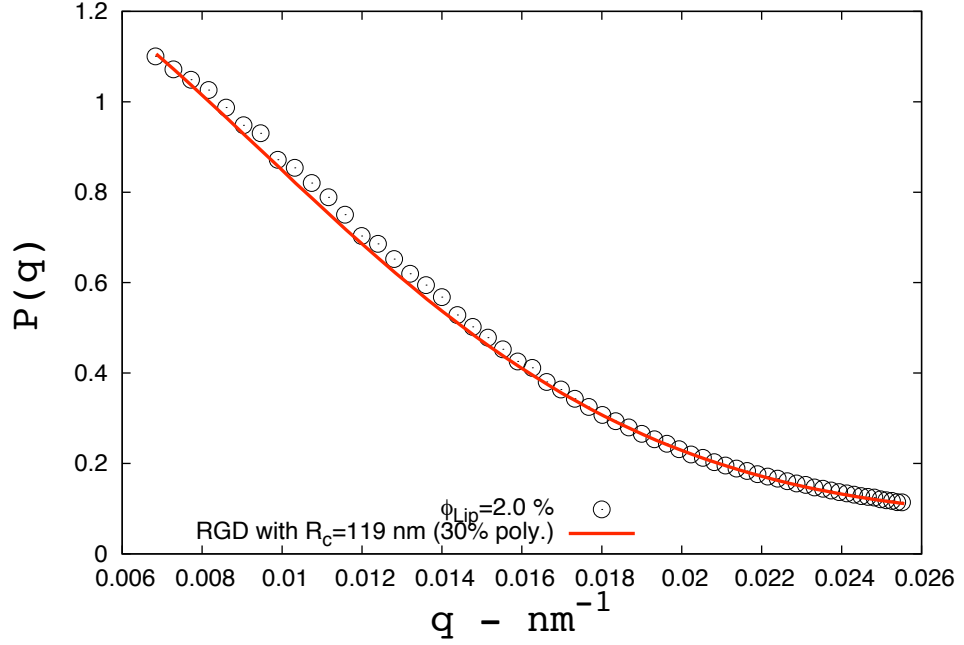


Figure 5.9: Form factor of liposomes (hollow circles). Solid line stands for the best fit of the experimental data with a polydisperse vesicle model derived from eq. (5.23) (courtesy of Dr. S. Roldán-Vargas).

where $R_c^{(int)}$ stand for the internal radius of the liposome and the external radius $R_c^{(ext)}$ is t times $R_c^{(int)}$. The polydispersity is introduced by means of a tri-modal pseudo-Shultz distribution. The theoretical prediction (solid line) was calculated using a code provided by Dr. S. Roldán-Vargas. The best fit (solid line) was found for an average diameter of 240 nm and polydispersity 30%. A DLS analysis performed for different q values throws different results as a consequence of the polydispersity. Setting different spatial windows, the diffusion in a predetermined length scale, of a liposome size, is captured. So that, the results are strongly dependent on the angular position of the detector and, thus the characterization of the average particle size and polydispersity is only recommended to carry out using the SLS technique.

In this thesis, we have also employed a PS latex with a larger size ($\sim 1 \mu\text{m}$) and liposomes with phospholipid bilayer of PC (Phosphatidyl Coline) and DMPC (Dimiristoil Phosphatidyl Coline) all in paper I. The first phospholipid is similar

5. EXPERIMENTAL DETAILS

Table 5.1: Table with the relevant parameters of the particles used in this thesis and the papers where they appear. σ_c stands for the size diameter, μ_e is the electrophoretic mobility and Z_{eff} corresponds with the colloidal effective charge measured by the fit of $S(q)$.

Particle	σ_c (nm)	Polydispersity	μ_e ($\times 10^{-8} \frac{m^2}{Vs}$)	Z_{eff} ($\frac{e}{particle}$)	Paper
PS-micro	1300	4%	–	–	I
PC-lipo	488	15%	–	–	I
DMPC-lipo	484	15%	–	–	I
PS-nano	110	2%	–3.2	600	II & III
PS-lipo	240	30%	–2.1	180	IV

to the phosphatidyl-serine, but uncharged in water. The second one was particularly chosen because it is able to modify the elastic constant of the liposome shell with the temperature (102). A systematic characterization, following the same procedure as before, was carried out for these particles (the results are given in table (5.1)).

The sign of the charged colloidal surfaces were determined using electrophoretic mobility measurements. It consists in a oscillatory electric field that is applied to the colloidal suspension. By means of a laser, the induced motion by the electric field is measured. The electrophoretic mobility, μ_e , is defined as the ratio between induced velocity and electric field. Following the standard procedure given in ref. (68), a value of $\mu_e = -3.2 \cdot 10^{-8} \text{ m}^2\text{V}^{-1}\text{s}^{-1}$ was obtained for the PS latex (the one with $\sigma_c = 110 \text{ nm}$), while for the PS liposomes, an average value of $\mu_e = -2.1 \cdot 10^{-8} \text{ m}^2\text{V}^{-1}\text{s}^{-1}$ was registered. In both cases, these particles shown a negative charge in water. As is shown in table (5.1), the electrophoresis was not performed for the particles of paper I. In this work, we focused on the study of the dynamic in absence of interactions, for what we screened the electrostatic repulsion by the addition of KNO_3 .

The determination of the effective charge that a colloid bear in suspension is a hard task, since it strongly depends on the kind of measurements used to reach such information. The electrophoretic measurements can indirectly provide a prediction of the electrokinetic effective charge Z_{eff}^{elec} . This method requires a suitable model including information of the colloidal shape, the ionic size, etc, connect-

ing μ_e with Z_{eff}^{elec} (103). Another way to determine the colloidal effective charge in suspension is by means of the experimental static structure factor, $S(q)$. We can predict a theoretical $S(q)$ using the Ornstein-Zernike equation (section 3.1.2) and an interaction model that includes Z_{eff}^{struc} as a parameter (*e.g.*, Debye-Hückel potential given in section 2.2). Knowing the rest of system parameters, we can consider Z_{eff}^{struc} as the free parameter that fits the theoretical $S(q)$ with the experimental one. As an example of the methodology to predict Z_{eff}^{struc} , in fig. (5.10), we show the measurement of the PS latex effective charge, $Z_{eff}^{struc} = 600$, by means of $S(q)$ at a low ionic concentration. The symbols stand for the experimental structure factor while the solid lines correspond with the theoretical predictions for several Z_{eff}^{struc} (the rest of parameters are given in the figure legend). To reach a low ionic strength condition ($\sim 1 \mu\text{M}$), we put the colloidal suspension in contact with the ion-exchanger Amberlite NRM-150 resins (more details can be found in ref. (104, 105, 106)).

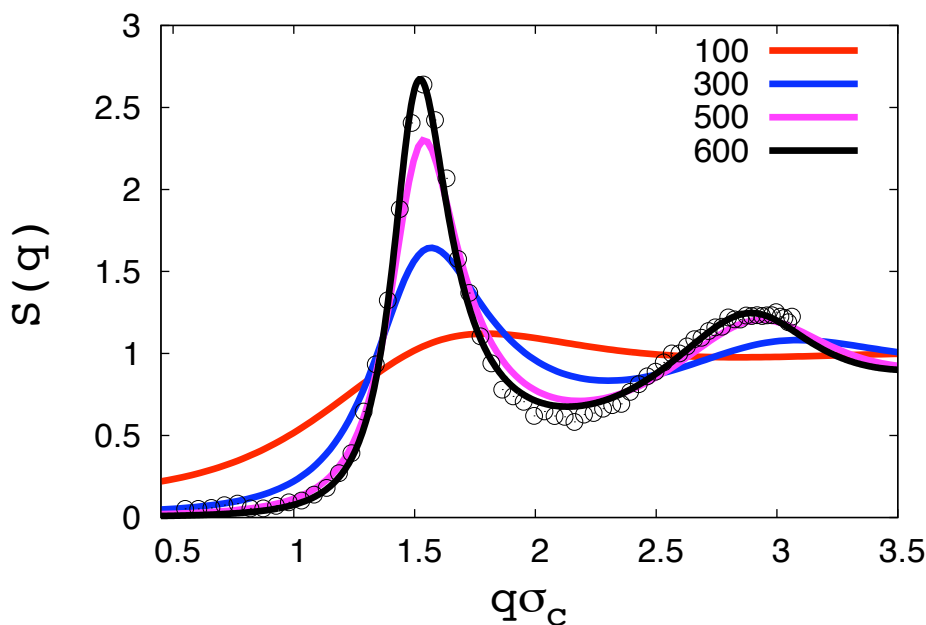


Figure 5.10: Static structure factor of a PS latex in water at low ionic conditions. Symbols stand for the experimental measurement while solid lines correspond with the theoretical prediction (OZE-HNC) for several Z_{eff}^{struc} values, giving in the legend. The experimental parameters also used in the calculations are the following: the $\phi_c = 0.56\%$ and the ionic concentration $c_{ion} = 1 \mu\text{M}$.

5. EXPERIMENTAL DETAILS

5.3.2 Polymers

We have used polyacrylamide from Polyscience Inc., as the polymeric specie in the colloid-polymer mixtures. An important advantage of choosing this linear polymer is its high hydrosolubility. Indeed, the use of a hydrophobic polymer would introduce an additional problem to the mixture as the possible adsorption of the polymer on the colloidal surface.

Two different polymers with molecular masses $5.0 \cdot 10^6$ g/mol and $1.0 \cdot 10^6$ g/mol have been employed in this thesis. To characterize both polymers, a standard procedure denominated Zimm-Plot diagram was carried out (107). This kind of representation is based on the dependency of the scattered intensity with the polymer concentration and the angular position of the detector. This provides relevant information of the polymer, as is its radius of gyration, R_g , the second virial coefficient, B_2 , and the molecular mass of the polymer, M_w . In figure (5.11), the results for the two linear polymers (solid circles) are shown divided in two panels. The corresponding analysis leads to the next information about the polymers: $R_g = 33$ nm, $M_w = 2 \cdot 10^5$ g/mol for the smaller polymer (panel (a)) and $R_g = 54$ nm, $M_w = 2 \cdot 10^6$ g/mol for the longer polymer (panel (b)). The latter information was extracted from the linear fits, also shown in fig. (5.11), as solid and dashed lines with the following equation:

$$\frac{Kc}{R_\theta} = \frac{1}{M_w} \left(1 + \frac{q^2 R_g^2}{3} \right) + 2B_2c, \quad (5.24)$$

where $K = 4\pi^2 n^2 (dn/dc)^2 / N_A \lambda_o^4$, n is the refractive index of the polymer solution at concentration c (in g/cm³) and $R_\theta = \frac{\langle I_\theta \rangle}{\langle I_{inc} \rangle} R_\theta^{Toluene}$ is the *Rayleigh ratio* of the sample, being $\langle I_{inc} \rangle$ the intensity of the incident beam, $\langle I_\theta \rangle$ the scattering intensity at angle θ and $R_\theta^{Toluene}$ the toluene *Rayleigh ratio* also at angle θ , which can be found tabulated at different temperatures (107).

Electrophoretic mobility of the polymers was carried out in the dilute regime, $c < c^*$. Although they are commercially presented as non-ionic polymers, the polarity of the water slightly ionizes the polymer giving rise to a certain charge (see comments of section 4.2 concerning the ion condensation giving to the monomer an effective charge). The electrophoretic mobility is $\mu_e = -1.1$ and $-0.9 \cdot 10^{-8}$

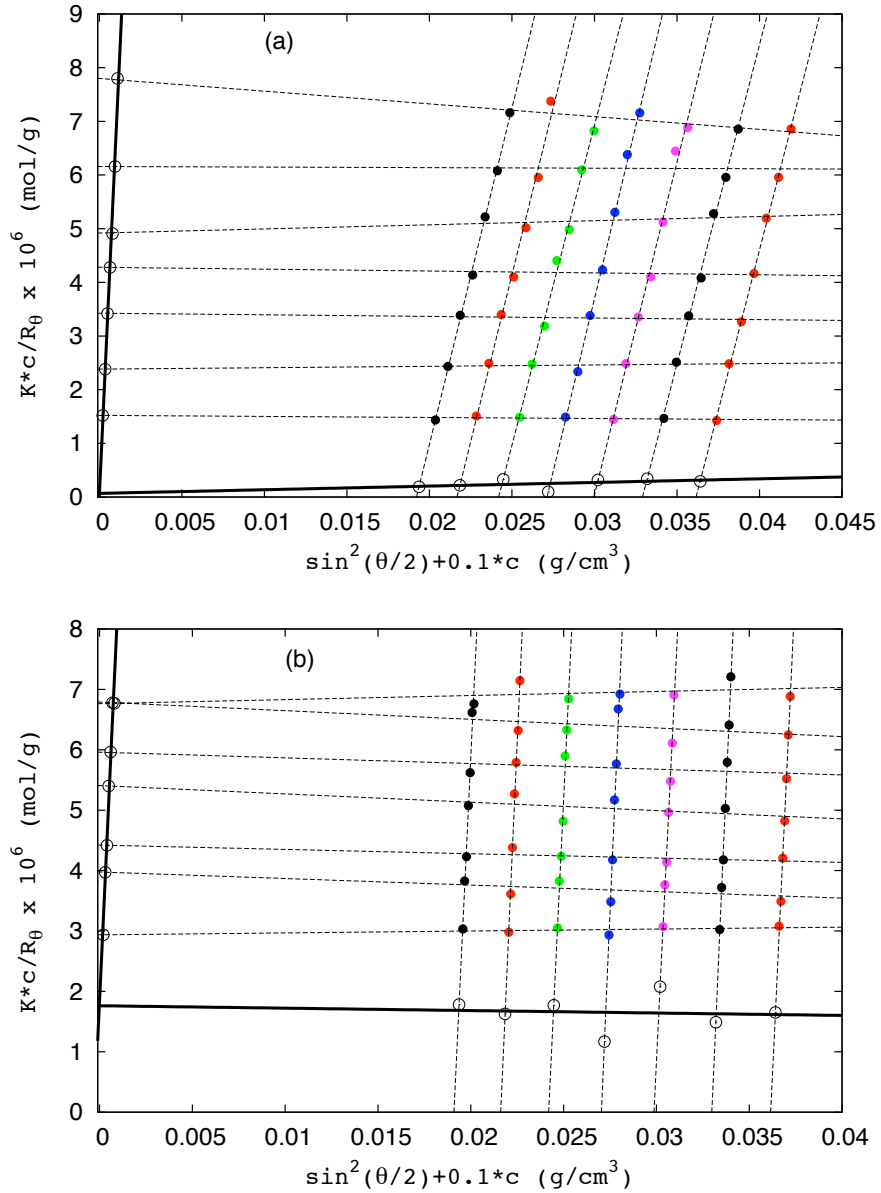


Figure 5.11: Zimm-plot for the short polymer, panel (a), and the long polymer, panel (b). Circles stand for the experimental data at different polymer concentrations c (g/cm³) and angular positions θ . Dashed lines represent the fits of the experimental data at constant c or θ . Hollow circles stand for extrapolation from the latter linear fits to $c = 0$ or $\theta = 0$. The two solid lines correspond with the lineal fit of the hollow circles following the procedure exposed in ref. (107).

5. EXPERIMENTAL DETAILS

$\text{m}^2\text{V}^{-1}\text{s}^{-1}$ for the small and long polymer, respectively. So that, both polymers present a negative charge in water. The prediction of the zeta-potential for polymers becomes a hard task, since the polymer is a conformational complex macromolecule. Therefore, the charge distribution and the resistance to flow in water are two subject hardly to model. In our case, the knowledge of the charge sign of both polymers in water was calculated by means of the Manning's expression for linear polyelectrolytes giving $Z_m^{eff} = 0.8$ (76).

Given the charge sign shown for colloids and polymer in water, the adsorption of the polymer in the colloidal surface can be discarded by electrostatic reasons, even more when the mixture remains in contact with Amberlite NRM-150 ion-exchanger resins that are responsible for enhancing the electrostatic repulsion. This ion-exchanger resin reduces the length of the ionic double layer, since it substitutes the big ions on suspension by protons (H^+) keeping fix the electroneutrality of the medium. Nevertheless, we have performed an additional test to confirm the non-adsorption. We have compared the viscosity η_{pol} of several polymer solutions with the viscosity of the bulk, $\eta_{col-pol}$, in a colloid-polymer mixture (*i.e.*, the viscosity depending on the solvent and the polymer suspended on it). The equivalency between η_{pol} and $\eta_{col-pol}$ was then studied. If $\eta_{pol} = \eta_{col-pol}$, the polymers mixed with the colloidal particles remains in the bulk. On contrary if $\frac{\eta_{pol}}{\eta_{col-pol}} > 1$, the polymer will be partially adsorbed to the colloidal surface. The bulk viscosity was indirectly measured by means of DLS. From the Stokes-Einstein equation, $\eta_{bulk}(= \eta_{col-pol}) = \frac{k_B T}{D_0 6\pi R_c}$, the bulk viscosity can be obtained knowing R_h and D_0 (which are measured in a DLS experiment). The η_{pol} was determined using a rheometer. The relative error was less than 1% in all the measurements performed. Additionally, the $\eta_{pol-col}$ measurements obtained via DLS were used to rescale the correlation time in paper III.

Finally, special care has been taken with the rate $\frac{\langle I_{col}(q) \rangle}{\langle I_{pol}(q) \rangle}$, where $\langle I_{col}(q) \rangle$ and $\langle I_{pol}(q) \rangle$ stand for the intensity scattered by colloids and polymers, respectively. We are interested in the study of the colloidal structure factor, $S_{cc}(q)$, and the effect of the polymer presence on that. In this respect, we should consider only single scattering from colloids. However, the light is also scattered from the polymers, in such a way that the collected information is analyzed together. To elude

5.3 Experimental systems

a sophisticated analysis separating both contributions, we have always worked in a scattering intensity rate $\frac{\langle I_{col}(q, \phi_c) \rangle}{\langle I_{pol}(q, c/c^*) \rangle} > 10^3$, in which it is totally justified to neglect the polymer contribution from the analysis, so $\langle I(q) \rangle \sim \langle I_{col}(q) \rangle$.

5. EXPERIMENTAL DETAILS

Chapter 6

Results

6. RESULTS

6.1 Paper I. *Nondiffusive Brownian motion of deformable particles:
Breakdownn of the “long-time tail”*

6.1 Paper I. *Nondiffusive Brownian motion of deformable
particles: Breakdownn of the “long-time tail”*

6. RESULTS

Nondiffusive Brownian motion of deformable particles: Breakdown of the “long-time tail”, Phys. Rev. E **80, 021403 (2009)**

S. Roldán-Vargas¹, M. Peláez-Fernández¹, R. Barnadas-Rodríguez^{2,3}, M. Quesada-Pérez⁴, J. Estelrich², and J. Callejas-Fernández¹

¹Grupo de Física de Fluidos y Biocoloides, Departamento de Física Aplicada, Universidad de Granada, E-18071 Granada, Spain.

²Departament de Fisicoquímica, Facultat de Farmàcia, Universitat de Barcelona, E-08028 Barcelona, Catalonia, Spain.

³Centre d’Estudis en Biofísica, Facultat de Medicina, Universitat Autònoma de Barcelona, Cerdanyola del Vallès Bellaterra, Barcelona, E-08193 Catalonia, Spain.

⁴Departamento de Física, Escuela Politécnica Superior de Linares, Universidad de Jaén, Linares, E-23700 Jaén, Spain.

6. RESULTS

Abstract

We study the nondiffusive Brownian motion of both rigid and deformable mesoscopic particles by cross-correlated dynamic light scattering with microsecond temporal resolution. Whereas rigid particles show the classical long-time tail prediction, the transition to diffusive motion of deformable particles presents a striking behavior not explained by the existing hydrodynamic treatments. This observation can be interpreted in terms of a damped oscillatory deformational motion on times cales of the order of the Brownian time. Finally, we show that the nondiffusive Brownian motion depends on the specific flexibility of the particles.

6.1 Paper I. *Nondiffusive Brownian motion of deformable particles: Breakdown of the “long-time tail”*

The dynamics of a Brownian particle can be formulated on different levels of description depending on the time scale of interest and the refinement of the hydrodynamic approach [1-3]. Thus, in Einstein’s classic investigation [4] no assumptions about the behavior of the particle velocity were made and the motion at long times of a “free” Brownian particle was shown to be diffusive. The initial attempt to incorporate velocity in the description of Brownian motion immediately came with the Langevin equation [5, 6]. Within this approximation, the interaction between the particle and the surrounding fluid was separated into two forces associated with a common origin, a systematic friction and a fluctuating noise, with no considerations of hydrodynamic memory effects. Despite its mathematical significance, this simple model predicts an extremely fast transition from ballistic to diffusive motion which is found to be nonrealistic.

The true character of the transition from ballistic to diffusive motion was successfully explored by Alder and Wainwright [7, 8] by means of molecular-dynamics simulations assuming a hard-sphere (HS) interaction. They found a “surprising persistence of the velocities” [8] through a “long-time tail” ($\propto \tau^{-3/2}$) in the velocity autocorrelation function, with the resultant delay in the emergence of the diffusive motion. In terms of macroscopic fluid dynamics, this observation was explained as a hydrodynamic memory effect due to the circulation of the fluid from the front of the particle, where the fluid is compressed, to the rear, where a rarefaction wave is developed. This vorticity effect pushes the particle resulting in a persistence of its motion. Soon, this finding was mathematically described by detailed hydrodynamics treatments [9-11] and the first real measurements of the long-time tail appeared for simple liquids [12, 13]. For rigid colloidal particles, experiments using dynamic light scattering (DLS) [14-16], diffusing-wave spectroscopy [17, 18], and optical trapping interferometry [19], have consolidated the existence of the long-time tail. Nevertheless, these studies have been based on the assumption of a HS-like interaction (computer simulations) or a fixed, rigid, geometrical shape of the tracer particles (experiments). However, despite their ubiquitous presence, a lack of these investigations devoted to deformable particles still persists.

In this paper, we use cross-correlated DLS to present experimental evidence against the validity of the classic long-time tail prediction in case of mesoscopic deformable particles suspended in a small-molecule solvent. Thus, as opposed to rigid particles, we document an original observation that can be interpreted in terms of the interplay between the translational and the deformational motion of our deformable particles on time

6. RESULTS

scales of the order of the Brownian time. These data demand a complete theoretical approach to account for the nondiffusive Brownian dynamics of mesoscopic deformable particles. In absence of a theoretical understanding, we show that two deformable particles with similar diffusivity can be distinguished by their specific flexibility through their nondiffusive Brownian motion. As a result, our investigation appears as especially stimulating to be applied to mesoscopic biological objects whose functionality depends on their elastic properties to a great extent [20].

An essential relation holds for the isotropic motion of a Brownian particle between any Cartesian component of its mean-square displacement, $\langle \Delta x^2(\tau) \rangle$, and its corresponding velocity autocorrelation function, $\langle v_x(0)v_x(\tau) \rangle$ [6]:

$$\langle \Delta x^2(\tau) \rangle = 2 \int_0^\tau (\tau - t) \langle v_x(0)v_x(\tau) \rangle dt, \quad (6.1.1)$$

The brackets denote ensemble averages. Equation (6.1.1) applied to the case of a Langevin's particle becomes [6]:

$$\langle \Delta x^2(\tau) \rangle = 2D_0[\tau - \tau_B + \tau_B \exp(-\tau/\tau_B)], \quad (6.1.2)$$

where D_0 is the particle's diffusion coefficient and $\tau_B = 2a^2\rho/9\eta$ the Brownian time. Here a and ρ represent the radius and density of a rigid mesoscopic spherical particle, whereas η is the shear viscosity of the fluid. In contrast, if we consider a complete hydrodynamic treatment including memory effects, Eq. (6.1.1) becomes [11, 15]:

$$\langle \Delta x^2(\tau) \rangle = 2D_0[\tau - 2(\frac{\tau_L}{\pi})^{1/2}\tau^{1/2} + \frac{\tau_L}{9}(8 - \frac{2\rho}{\rho'}) - \frac{\tau_L^{3/2}}{9\sqrt{\pi}}(7 - \frac{4\rho}{\rho'})\tau^{-1/2}]; (\tau > \tau_L), \quad (6.1.3)$$

where $\tau_L = (9/2)(\rho'/\rho)\tau_B$, ρ' being the fluid density. Although both results, Eq. (6.1.2) and (6.1.3), tend to a common diffusive regime, $\langle \Delta x^2\tau \rangle = 2D_0\tau$ ($\tau \gg \tau_B$), the latter presents a slower transition due to its second term ($\propto \tau^{1/2}$), which is associated to the presence of the long-time tail ($\propto \tau^{-3/2}$) in $\langle v_x(0)v_x(\tau) \rangle$, as can be deduced from Eq. (6.1.1).

To test these theoretical predictions via DLS, an experimental determination of the normalized autocorrelation function of the scattered field $g_1(q; \tau)$ (q being the magnitude of the scattering vector) can be performed. In case of noninteracting, identical, and rigid spherical particles $g_1(q; \tau) = \langle \exp(iq\Delta x(\tau)) \rangle$. If measurements of $g_1(q; \tau)$ are made at short times ($\tau \sim \tau_L$), non-Gaussian effects are hardly appreciable regardless of

**6.1 Paper I. Nondiffusive Brownian motion of deformable particles:
Breakdown of the “long-time tail”**

the statistics of v_x , as can be proved by Taylor’s expansion of $g_1(q; \tau)$ [15]. Accordingly [21]:

$$g_1(q; \tau) = \exp\left(-\frac{1}{2}q^2 \langle \Delta x^2(\tau) \rangle\right), \quad (6.1.4)$$

However, instead of using directly $g_1(q; \tau)$ to probe Eqs. (6.1.2) or (6.1.3), an experimental time-dependent “diffusion coefficient” $D_{exp}(\tau) \equiv (-1/q^2)d \ln g_1(q; \tau)/d\tau$ is frequently defined [15, 17]. As a result, the slopes of $\langle \Delta x^2(\tau) \rangle / 2$ obtained from Eqs. (6.1.2) and (6.1.3) are compared with $D_{exp}(\tau)$, which is determined by numerical differentiation. Nevertheless, we should note that whereas Eqs. (6.1.2) and (6.1.3) consider uniquely the theoretical translational motion, $D_{exp}(\tau)$ could also reflect the motion corresponding to nontranslational degrees of freedom. This will be a central point in our discussion.

To obtain $D_{exp}(\tau)$ for the suspensions investigated in this work, we used a three-dimensional DLS spectrometer (LS instruments, Fribourg, Switzerland) with two incident He-Ne laser beams ($\lambda = 632.8$ nm). Suspensions were contained in a cylindrical scattering cell which was immersed in a thermostated bath. A digital correlator (Flex03lq-OEM) computes the normalized cross-correlation function, $g_C^2(q; \tau)$ of the registered scattered intensities detected by two avalanche photodiodes (SPCM-AQRH) for which the time-dependent contributions of multiple scattered photons can be neglected. The experimental $g_1(q; \tau)$ were obtained through the relation $g_C^2(q; \tau) = 1 + \beta[g_1(q; \tau)]^2$ ($0 < \beta < 1$), with a similar protocol as that described in Ref. [22] for a two-color DLS scheme. The sample time resolved with our correlator is 12.5 ns, with 286 τ values along the interval $[1.25 \cdot 10^{-8}, 10^{-4}]$ s. For all the experiments, photon counting rates were kept within $[10^5, 5 \cdot 10^5]$ s⁻¹ to ensure a maximum dead time of 40 ns, being always under the saturation limit. A reliable statistical estimator of $g_1(q; \tau)$ resulted from the average of 25 independent measurements with 1000 s per measurement. Thus, spurious determinations due to electronic distortions, even at delay times as short as 0.2 μ s, are minimized. The magnitude of the scattering vector was fixed at $q_f = 0.026$ nm⁻¹.

For our experimental study, we used three different suspensions which were sufficiently diluted to avoid long-range interactions. First, an aqueous suspension of polystyrene microspheres, denoted as “sample R” (rigid), with mean radius $a_R = 650$ nm, relative standard deviation RSD= 0.04, and particle volume fraction $\phi_R = 0.002\%$. The second sample, “sample D” (deformable), was an aqueous suspension of liposomes made of soy-

6. RESULTS

bean phosphatidylcholine (SPC) from Lipoid, with mean external radius $a_D = 244$ nm, RSD= 0.15, and $\phi_D = 0.01\%$. The third sample, “sample RD” (rigid-deformable), was an aqueous suspension of liposomes made of dimyristoylphosphatidylcholine (DMPC) from Sigma-Aldrich Inc., with $a_{RD} = 242$ nm, RSD=0.15, and $\phi_{RD} = 0.01\%$. Due to the extrusion procedure, both SPC and DMPC liposomes show an unilamellar thickness of about 5 nm [23]. The twofold (rigid-deformable) behavior of sample RD comes from the composition of the lipid bilayers, since DMPC membranes exhibit two main phases separated by a threshold temperature (known as main transition temperature): a rigid gel phase and a deformable liquid crystalline phase. Below the main transition temperature, the DMPC membranes retain their rigidity. Above the main transition temperature, that is, in the liquid crystalline phase, it is considered that the majority of the single carbon-carbon bonds of the acyl chains of the lipid bilayers have free rotation [24]. This phenomenon evidences the conversion of the DMPC membrane from the gel to the liquid crystalline phase, where the membrane displays new properties such as an increased permeability and a fluidized state. Thus, we can treat sample RD as rigid or deformable by changing the temperature around its critical value. The main transition temperature of the DMPC bilayers was established at $23.0 \pm 0.1^\circ\text{C}$ by means of differential scanning calorimetry [24].

Using the described protocol, two examples of the classic long-time tail prediction at 13°C and 25°C are shown in Figs. 6.1.1(a) and 6.1.1(b) for sample R. While Langevins model does not predict the real evolution of $D_{exp}(\tau)$, the full hydrodynamic model (without fitting parameters) and $D_{exp}(\tau)$ show a good agreement. Thus, whereas at short times a significant contribution of the long-time tail term ($\propto \tau^{-1/2}$) is apparent, at moderate long times ($\tau \geq 40 \mu\text{s}$) the diffusive regime, $D(\tau)/D_0 = 1$, is nearly recovered. In addition, the time evolution of $D_{exp}(\tau)$ corresponding to sample D at 25°C is shown in Fig. 6.1.1(c): Neither Langevin’s model nor the full hydrodynamic treatment describe satisfactorily these new experimental results. Now $D_{exp}(\tau)$ shows a clear non-monotonic behavior with at least two marked maxima within our time window over the corresponding Langevin’s prediction. After reaching the second maximum ($\tau^* = 3.7 \mu\text{s}$), $D_{exp}(\tau)$ decreases smoothly and tends to its diffusive value, D_0 . Since their environments are similar, the distinct trends shown by $D_{exp}(\tau)$ for the polystyrene spheres and the SPC liposomes should be caused to the different structural properties of these particles. To support this statement, we present the results obtained for sample RD at different temperatures around the main transition temperature. Thus, the unique significant change in the dynamics of this suspension only involves the elastic properties

6.1 Paper I. *Nondiffusive Brownian motion of deformable particles: Breakdown of the “long-time tail”*

of the DMPC membranes.

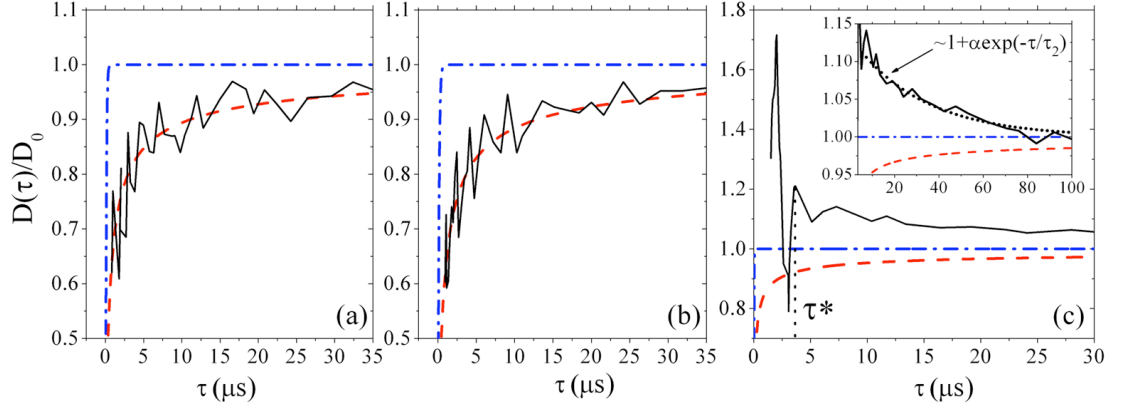


Figure 6.1.1: Normalized time-dependent diffusion coefficient $D(\tau)/D_0$ corresponding to sample *R* at (a) 13 and (b) 25° C, and sample *D* at 25° C (c). Blue dash-dotted line stands for Langevin’s model: $D(\tau)/D_0 = \langle d \Delta x^2(\tau) \rangle / 2d\tau / 2D_0$ [Eq. (6.1.2)]. Red dashed line corresponds to the full hydrodynamic model: $D(\tau)/D_0 = \langle d \Delta x^2(\tau) \rangle / 2d\tau / 2D_0$ [Eq. (6.1.3)]. Black solid line represents the experiment: $D(\tau) = D_{exp}(\tau)$. D_0 is the experimental free diffusion coefficient corresponding to each temperature. Inset in (c): dotted line represents the predicted exponential relaxation corresponding to $\tau = 32 \mu\text{s}$ and $\alpha = 0.1$.

$D_{exp}(\tau)$ corresponding to sample RD at 15°C, 23°C, and 34°C are shown in Figs. 6.1.2(a)- 6.1.2(c). In accord with our calorimetric determination, sample RD at 15°C is associated to the rigid gel phase of the DMPC membranes. In fact, the full hydrodynamic model and the experimental data show again a common tendency as in the case of sample *R* [Fig. 6.1.2(a)]. At 23°C, that is, at the main transition temperature, a moderated agreement between theory and experiment still persists although the fluctuations in $D_{exp}(\tau)$ appear more pronounced [Fig. 6.1.2(b)]. At 34°C the deformable crystalline phase of the lipid membranes is expected, and indeed a noticeable change in the trend shown by $D_{exp}(\tau)$ occurs [Fig. 6.1.2(c)]. As in the case of sample *D*, we observe a nonmonotonic behavior of $D_{exp}(\tau)$ with a clear maximum at very short times ($\tau^* \sim 0.6 \mu\text{s}$). However, sample RD presents a faster final relaxation than that associated to sample *D*, almost recovering its diffusive value around $\tau \sim 5 \mu\text{s}$.

In our opinion, the complex experimental patterns shown in Figs 6.1.1(c) and 6.1.2(c) reflect the intricate interplay between the translational and the deformational motion of

6. RESULTS

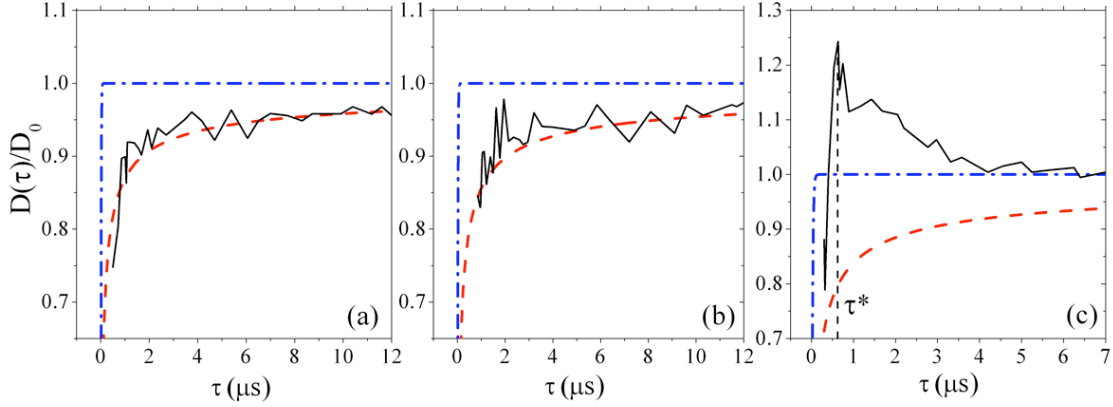


Figure 6.1.2: Normalized time-dependent diffusion coefficient $D(\tau)/D_0$ corresponding to sample RD at (a) 15, (b) 23, and (c) 34°C symbols as in Fig. (6.1.1).

our flexible particles. At short times, when the translational velocity has not yet been damped, $D_{exp}(\tau)$ would contain simultaneously the translational and the deformational displacements of the liposomes membrane. Thus, the strong fluid-membrane interaction due to the translational velocity would induce fast changes in the membrane's motion that would be elastically restored, being manifested through the sharp oscillations of $D_{exp}(\tau)$. In the absence of a dynamic model for $D_{exp}(\tau)$ in which both translational and deformational motions are considered simultaneously, the latter cannot be easily isolated to be described quantitatively. However, at long times, when the translational velocity is damped, the final relaxation of $D_{exp}(\tau)$ toward D_0 would reflect essentially the underlying overdamped deformations in the liposome's form.

Since we have chosen an adequate q -value for our experiments ($qfa_{liposome} \sim 6$), see for details Ref. [25], we are able to explore if this hypothetical deformational motion is present in $D_{exp}(\tau)$, attempting to reveal the internal modes of deformation of our flexible particles [26, 27]. Hence, we adopt the model proposed by Milner and Safran [26] to describe the small shape fluctuations of a single vesicle in thermal equilibrium, where the translational motion is not considered. Accordingly, the relative displacement of the membrane, $r(\tau, \Omega)$, is expanded into spherical harmonics, $Y_{lm}(\Omega)$, around a fixed radius a : $r(\tau, \Omega) = a(1 + \sum_{l>1,m} u_{lm}(\tau)Y_{lm}(\Omega))$, where Ω is the solid angle and $u_{lm}(\tau)$ the amplitude associated to a given mode. By appealing the fluctuation-dissipation theorem, the autocorrelation functions of the amplitudes present an exponential decay $\langle u_{lm}(\tau)u_{lm}(0) \rangle = \langle |u_{lm}(\tau)|^2 \rangle \exp(-\tau/\tau_l)$, where the relaxation time, τ_l , of a mode

**6.1 Paper I. Nondiffusive Brownian motion of deformable particles:
Breakdown of the “long-time tail”**

driven by bending forces (negligible surface tension [26, 27]) is

$$\tau_l = \frac{\eta^3(2l+1)(2l^2+2l+1)}{k_c l^2(l+1)^2(l+2)(l-1)}, \quad (6.1.5)$$

with k_c being the bending modulus of the membranes. According to Eq. (6.1.5), the slowest relaxation is expected for the second deformational mode. Restricting ourselves to the $l = 2$ contribution [25, 27], the final relaxation of $D_{exp}(\tau)$ would be in first approximation described by an overdamped exponential decay of the form $D(\tau) \sim D_0[1 + \alpha \exp(-\tau/\tau_2)]$, where the damping is mediated by τ_2 as in the case of $\langle u_2(\tau)u_2(0) \rangle$. Here we implicitly assume a small deformations regime $\langle |u|^2 \rangle^{1/2} \leq 0.1$, according to the theoretical prediction for standard k_c values of the lipid membranes [26, 28]. In particular, taking the bending modulus of the SPC membranes as $k_c = (1.5 \pm 0.5) \cdot 10^{-19}$ J [28], the relaxation time for a vesicle of $a = 244$ nm suspended in water at 25°C is $\tau_2 = 32 \mu\text{s}$ [Eq. (6.1.5)]. Using this value, our exponential approximation provides a good description of the final relaxation of $D_{exp}(\tau)$ even for amplitudes as big as $\alpha = 0.1$ [see inset, Fig. 6.1.1(c)]. This agreement is certainly encouraging, since it supports quantitatively our interpretation of the relaxation of $D_{exp}(\tau)$ in terms of an over-damped deformational motion. Regarding sample RD, due to their strong temperature and membrane composition dependence, values for k_c that typically range $(2 \cdot 10^{-19} - 6 \cdot 10^{-19})$ J have been documented for the DMPC membranes at the liquid crystalline phase [29]. Accordingly, the corresponding τ_2 -range for a vesicle of $a = 240$ nm suspended in water at 34°C results $\tau_2 \sim (6, 19) \mu\text{s}$. Although slightly overestimated, this prediction is also in reasonable accord with that observed for the final relaxation time of sample RD, which reaches the diffusive regime around $\tau \sim 5 \mu\text{s}$ [see Fig. 6.1.2(c)]. These results concerning our flexible particles are the quantitative observation of the damped deformational motion of a large vesicle under spontaneous nondiffusive Brownian motion. As a result, a powerful practical application emerges: Our methodology is useful to estimate and predict the elastic properties of a great variety of biological deformable particles.

In conclusion, we have revealed the complex scenario present in the nondiffusive motion of a deformable Brownian particle, which is mediated by the coupling between translational and deformational degrees of freedom. As opposed to rigid particles, a complete theoretical understanding of this motion, including its short times description, remains as a challenge.

The authors are grateful to MCINN (Projects No. MAT2006-12918-C05-01 -02, and

6. RESULTS

-05), ERDF Funds, and Junta de Andaluca (Project P07-FQM-02496) for financial support. We thank Walter Kob for valuable comments on our manuscript.

Reference List

- [1] P.N. Pusey, *Colloidal Suspensions*, Proceeding of the Les Houches Summer School of Theoretical Physics, L1, 1989 (North-Holland, Amsterdam, 1989).
- [2] G. Nägele, Phys. Rep. **272**, 215 (1996).
- [3] J. T. Padding and A.A. Louis, Phys. Rev E **74**, 031402 (2006).
- [4] A. Einstein, Ann. Phys. **322**, 549 (1905).
- [5] P. Langevin, C. R. Acad. Sci. Hebd Seances Acad Sci. D **146**, 549 (1908).
- [6] G. E. Uhlenbeck, and L. S. Ornstein, Phys. Rev. **36**, 823 (1930).
- [7] B. J. Alder and T.E. Wainwright, Phys. Rev. Lett. **18**, 988 (1967).
- [8] B. J. Alder and T.E. Wainwright, Phys. Rev. A **1**, 18 (1970).
- [9] R. Zwanzig and M. Bixon, Phys. Rev. A **2**, 2005 (1970).
- [10] A. Widom, Phys. Rev. A **3**, 1394 (1971).
- [11] E. J. Hinch, J. Fluid Mech. **72**, 499 (1975).
- [12] C.D. Andriessse, Phys. Lett. **33A**, 419 (1970).
- [13] K. Carneiro, Phys. Rev. A **14**, 517 (1976).
- [14] A. Boullier, J. P. Boon, and P. Deguent, J. Phys. **32**, 159 (1978).
- [15] G.L. Paul and P.N. Pusey, J. Phys. A **14**, 3301 (1981).
- [16] K. Ohbayashi, T. Kohno, and H. Utiyama, Phys. Rev. A **27**, 2632 (1983).
- [17] D.A. Weitz, D. J. Pine, P. N. Pusey, and R. J. A. Tough, Phys. Rev. Lett. **63**, 1747 (1989).
- [18] J.X. Zhu, D. J. Durian, J. Muller, D. A. Weitz, and D. J. Pine, Phys. Rev. Lett. **68**, 2559 (1992).
- [19] B. Lukić, S. Jeney, C. Tischer, A. J. Kulik, L. Forro, and E. L. Florin, Phys. Rev. Lett. **95**, 160601 (2005).
- [20] R. Lipowsky and E. Sackmann, *Structure and Dynamics of Membranes* (Elsevier, New York, 1995) Vol. 1.
- [21] W. D. Davenport and W. L. Root, *Random Signals and Noise* (New York, McGraw-Hill, 1958).
- [22] A. Moussaïd and P.N. Pusey, Phys. Rev. E **60**, 5670 (1999).
- [23] S. Roldán-Vargas, R. Barnadas-Rodríguez, M. Quesada-Pérez, J. Estelrich, and J. Callejas-Fernández, Phys. Rev. E **79**, 011905 (2009).
- [24] V. P. Torchillin and V. Weissing, *Liposomes, a Practical Approach*, (Oxford Uni-

**6.1 Paper I. *Nondiffusive Brownian motion of deformable particles:
Breakdownn of the “long-time tail”***

versity Press, New York, 2003).

[25] J. S. Huang, S. T. Milner, B. Farago, and D. Richter, Phys. Rev. Lett. **59**, 2600 (1987).

[26] S.T. Milner and S.A. Safran, Phys. Rev. A **36**, 4371 (1987)

[27] R. Joannic, L. Auvray, and D. D. Lasic, Phys. Rev. Lett. **78**, 3402 (1997).

[28] M. B. Schneider, J. T. Jenkins, and W. W. Webb, J. Phys. (Paris) **45**, 1457 (1984).

[29] P. Méléard et al., Biophys. J. **72**, 2616 (1997).

6. RESULTS

6.2 Paper II. *Structure of charged colloid-polymer mixtures*

6. RESULTS

Structure of charged colloid-polymer mixtures, EPL **90**, 46005
(2010)

M. Peláez-Fernández, A. Moncho-Jordá, and J. Callejas-Fernández

Departamento de Física Aplicada, Grupo de Física de Fluidos y Biocoloides, Universidad de Granada, E-18071 Granada, Spain.

6. RESULTS

Abstract

We use a light scattering technique to investigate the effect of adding non-adsorbing charged polymers to a very dilute electrostatically stabilized colloidal suspension at low electrolyte concentration. The experimental results show that, as the polymer concentration increases, the main peak of the colloid-colloid structure factor moves to higher q -values, which cannot be only due to the screening of the direct colloid-colloid electrostatic repulsion. We show that the colloid-polymer electrostatic repulsions lead to enhanced depletion forces that have a strong influence on the colloid structure, even for diluted suspensions. The experimental results are interpreted using the off-lattice Polymer Reference Interaction Site Model (PRISM), and very good agreement is found for all polymer concentrations.

Adding non-adsorbing polymers to an originally stabilized colloidal suspension in a good solvent leads to a new complex system with a very rich structural and phase behavior [1]. The stability of this kind of binary systems has motivated a growing attention of experimentalists and theoreticians during the last fifty years [2-9], as it is involved in many technological and industrial applications and in important biological processes [10]. Moreover, the colloid-polymer mixtures represents a model system where its properties can be easily tuned by varying, among others, the size ratio of the components, their concentrations, the quality of the solvent or the mutual interactions (controlling, for instance, the surface charge of the particles) [11, 12].

In general, it is known that the addition of a smaller component (polymers, colloids, . . .) to a sample of bigger colloidal particles leads to new small-small and small-big interactions that induce an effective interaction between the big particles. This interaction can be attractive (depletion) [2], repulsive (accumulation repulsion) [13] or even show other complex behaviours (haloing or bridging) [14], depending on whether the small and big particles attract or repel each other. Specifically, if the small component is a polymer chain, there are several theoretical models that try to explain the equilibrium properties of the mixture. In the seminal Asakura-Oosawa model [2] (where polymers are treated as interpenetrating spheres and colloids as hard spheres) the so-called effective depletion attraction between colloids emerges from purely entropic arguments. If this model is extended to consider that polymers are not ideal, but they interact through a soft excluded-volume repulsion [15-17], then the previous depletion attraction becomes reduced. More sophisticated models take into account the monomer-monomer correlations inside the polymer chain [18, 19]. Under the latter consideration, it is shown that the effective interaction induced by polymers is mainly controlled by its characteristic length, which depends on its concentration [20]. Finally, if the colloids bear certain amount of surface charge and the polymer coils are formed by ionizable monomers, there are extra colloid-colloid, colloid-polymer and polymer-polymer electrostatic interactions that have a strong influence on the stability and structure of the sample [21, 22]. Although one may find some theoretical works that study this situation [23-26], in literature there are scarce experiments focused on the microstructure of this kind of charged mixtures.

In this work, a light scattering technique is used to study the interplay between electrostatic repulsion and the attractive depletion interaction in mixtures of like-charged colloids and polymers in water. Initially, we start from a reference system consisting

6. RESULTS

of a strongly charged and highly structured diluted colloidal suspension at very low electrolyte concentration. Then, the effect of adding increasing amounts of a slightly charged non-adsorbing polymer on the colloid-colloid structure factor is studied. Using the Polymer Reference Interaction Site Model (PRISM), we are able to fit accurately the experimental structure factors and find a theoretical explanation in terms of the colloid-colloid effective potential.

The colloidal particles used in our experiments are polystyrene spheres synthesized using the procedures given in ref. [27], with a hydrodynamic diameter of $\sigma_c = 100 \pm 2$ nm measured by Dynamic Light Scattering (DLS) [28]. The particles bear a negative surface charge which is corroborated from the electrophoretic mobility measurements ($\mu_e = -3.5 \cdot 10^{-8}$ m²/Vs). The hydrosoluble polymer is polyacrylamide from Polysciences, Inc. Its molecular weight is $(1 - 0.6) \cdot 10^6$ g/mol and its radius of gyration in water is $R_g \approx 25$ nm determined again by DLS. Electrophoretic measurements reveal that polyacrylamide in water is slightly charged ($\mu_e = -0.9 \cdot 10^{-8}$ m²/Vs). Since colloids and polymer coils have the same charge sign, no adsorption of polymer on the colloidal surface is expected. The samples are prepared by mixing the binary colloid-polymer system in a bed of ion exchanger resin inside a cylindrical quartz cell two days before the light scattering measurement is performed. We found that this time is long enough to assure that the mixtures has reached equilibrium conditions. In all cases, the colloid volume fraction was $\phi_c = \pi \rho_c \sigma_c^3 / 6 = 0.0056$, where ρ_c is the colloidal number density. The different polymer volume fractions used in our study are shown in table (6.2.1).

The colloidal structure was captured via the structure factor $S(q)$ determination using the Static Light Scattering technique (SLS) [28]. The experimental setup comprises a three-dimensional light scattering spectrometer, 3D-DLS from LS Instruments (Fribourg, Switzerland), having two avalanche photodiode detectors (A and B) and digital correlator that computes the cross correlation function of the registered scattered intensities, for which the time-dependent contributions of multiple scattered photons is removed [29]. According to this design [30], the colloid-colloid structure factor of the sample is proportional to

$$S(q) \propto \sqrt{\frac{\langle I_A^m(q) \rangle \langle I_B^m(q) \rangle g_{AB}^m(q, \tau = 0) - 1}{\langle I_A^0(q) \rangle \langle I_B^0(q) \rangle g_{AB}^0(q, \tau = 0) - 1}} \quad (6.2.1)$$

where $\langle I_i^m(q) \rangle$ is the total time-averaged intensity registered by detector $i = A, B$ for the colloid-polymer mixture in a fixed q -value, whereas $\langle I_i^0(q) \rangle$ is the intensity corresponding to a dilute colloidal suspension. In our measures the time-averaged

6.2 Paper II. *Structure of charged colloid-polymer mixtures*

Table 6.2.1: The first column stands for the polymer volume fraction ϕ_p used on the experiments and theory. I_{ion} is the ionic strength that gives the best fit and it is the result of the sum of three contributions: a fixed colloidal contribution $Z_c\rho_c = 0.01$, a monomer contribution $Z_m\rho_m$ and a free electrolyte contribution $C_{electrolyte}$ which is the real fit parameter. The last two are represented together with their percentage on the value of I_{ion} .

ϕ_p (%)	I_{ion}	$Z_m\rho_m$	$C_{electrolyte}$
–	0.01	–	10^{-6}
0.00003	0.015	0.002(13.3%)	0.003(20.0%)
0.00015	0.029	0.007(24.1%)	0.012(41.4%)
0.00075	0.055	0.03(54.5%)	0.015(27.3%)
0.00100	0.08	0.04(50.0%)	0.03(37.5%)

intensity scattered by the polymers is negligible compared to the one by colloids $\langle I^p(q) \rangle < 10^{-3} \langle I^c(q) \rangle$. Therefore, the structure factor given in eq. (6.2.1) is indeed the colloid-colloid structure factor $S_{cc}(q)$. The ratio $(g_{AB}^m(q, \tau = 0) - 1) / (g_{AB}^0(q, \tau = 0) - 1)$ corrects the magnitude of the structure factor due to the disturbance of multiple scattering [30], where $g_{AB}(q, \tau) = \langle I_A(q, t) I_B(q, t + \tau) \rangle / \langle I_A(q) \rangle \langle I_B(q) \rangle$ is the *normalized cross-correlation function* of the registered intensities.

Fig. (6.2.1) shows the experimental colloid-colloid structure factor $S_{cc}(q)$ for mixtures with increasing polymer concentration (see table (6.2.1)). At zero polymer concentration (black hollow squares), $S_{cc}(q)$ shows a well-defined microstructure of a typical monocomponent colloidal fluid. The main peak at $q\sigma_c = 1.54$ reveals a centre-to-centre distance between particles of about $4.1\sigma_c$, obtained from the relationship $r_{cc} \sim 2\pi/q_{max}$. The peak height ($S_{cc}(q_{max}) = 2.64$) and the trend of $S_{cc}(q \rightarrow 0)$ to 0 for a diluted colloidal system are two signatures of a highly repulsive scenario. However, this peak is strongly affected by the polymer concentration, as can be seen in fig. (6.2.1). Three remarkable facts are observed with this increase in polymer concentration. Firstly, there is a noticeable increase of $S_{cc}(q)$ for $q \rightarrow 0$. Secondly, the height and width of the main peak decreases and broadens, respectively. Finally, the position of the peak moves to relatively high q -values.

The growth of $S_{cc}(0)$ when the polymer concentration increases is usually caused by

6. RESULTS

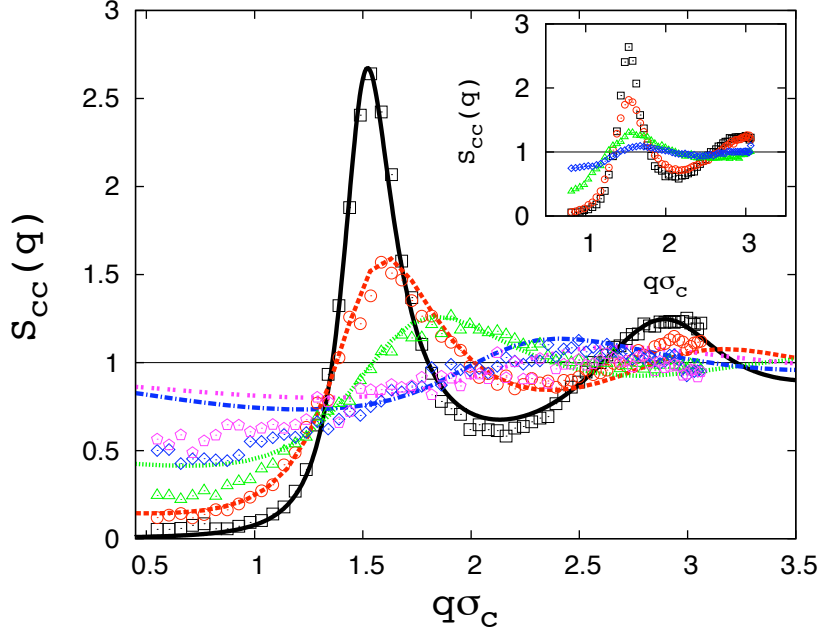


Figure 6.2.1: Colloid-colloid static structure factor $S_{cc}(q)$ corresponding to different colloid-polymer mixtures. Lines stand for the PRISM theoretical results and hollow symbols for light scattering experiments. The type of lines and symbols correspond to different polymer volume fractions as follow: 0 (black squares and solid line), 0.00003 (red circles and dashed line), 0.00015 (green triangles and dotted line), 0.00075 (blue diamonds and dot-dashed line) and 0.001 (pink pentagons and double-dashed line). The inset shows the colloid-colloid static structure factor at the same colloid volume fraction 0.0056 for different electrolyte concentrations without polymer: 0.6 (red circles), 1.2 (green triangles) and 2.4 mM (blue diamonds).

the existence of spatial inhomogeneities in the system [7]. Attractive interactions and polydispersity are the main reasons leading to heterogeneities in colloidal systems. Nevertheless, the excellent monodispersity of our colloidal particles points out to the conclusion that an attractive contribution in the effective interaction induced by the charged polymers appears as the most plausible explanation. However, this attraction is not strong enough to induce the fluid-fluid phase separation, as $S_{cc}(0)$ does not show any divergence for $q \rightarrow 0$. Moreover, we did not find any evidence of two phases emergence during the preparation and measurement process.

The decrease of the main peak shows that, as we increase the polymer concentration,

the liquid order becomes gradually lost. In principle, this effect could be attributed to the increase of the ionic strength I_{ion} induced by the inclusion of charged polymers in the sample, as entropic depletion effects should be insignificant at the small concentrations of colloids and polymers employed in our experiments [2, 7]. However, it should be stressed that the shift of the peak cannot be justified in this way.

In order to demonstrate that the ionic strength does not control all the structure behavior, we performed other experiments where the structure factor of colloidal suspensions at the same colloidal packing fraction was measured for different KBr concentrations without polymer (results are shown in the inset of fig. (6.2.1)). In these experiments, the conductivity of the sample was chosen identical to the one measured for the mixture with polymers. Indeed, as we increase the electrolyte concentration, the colloidal structure factor tends to 1.0 for all q -values (non-interacting particles). However, the shift of the peak is in all cases smaller than the one obtained by adding charged polymers. This can be appreciated in fig. (6.2.2), where the position of the peak is shown as a function of the polymer concentration (full circles). The experiments show that the presence of polymers induces an attractive effective interaction between colloids that leads to closer interparticle separations (going from $4.1\sigma_c$ to $2.3\sigma_c$) compared to the ones obtained by varying the KBr concentration (from $4.1\sigma_c$ to $3.8\sigma_c$).

Therefore, the observed shift in the colloid-polymer experiments is caused by a driving interaction counteracting the direct colloid-colloid electrostatic repulsion. This interaction is the enhanced depletion induced by the charged polymers around the colloids, provoked by the colloid-polymer electrostatic repulsion. In this sense, the physical origin of this depletion is more electrostatic than entropic. Nevertheless, the explanation of this behavior rests on the coupling of several effects that cannot be separated [26]. On the one hand, as we increase the polymer concentration in the mixture, depletion attraction becomes more important. On the other hand, increasing the polymer concentration also raises the ionic strength of the sample, which leads to the screening of all electrostatic interactions. While the screening of colloid-colloid electrostatic repulsion helps the particles to approach each other, the screening of the colloid-polymer repulsion weakens the electrostatic depletion induced by the polymers, so the shift of the peak is the result of the competition between these effects. However, in our opinion the experimental data clearly indicate that the combination of the screening of the colloid-colloid electrostatic repulsion plus the depletion induced by the added polymer dominate over the screening of the colloid-polymer electrostatic repulsion. This finally

6. RESULTS

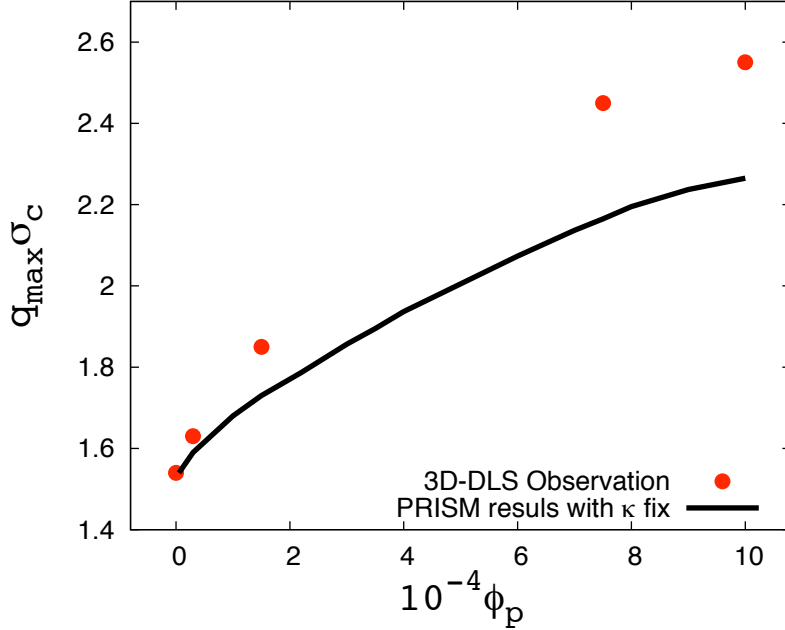


Figure 6.2.2: Position of the main peak of $S_{cc}(q)$, $q_{\max}\sigma_c$, as a function of the polymer volume fraction. Full circles are the experimental results, while the solid line is the PRISM prediction obtained under the assumption that the ionic strength of the sample does not grow with the polymer concentration.

leads to a net effective attractive well at intermediate distances that moves to smaller values as the polymer concentration (and so the ionic strength) increases. We will confirm this hypothesis later on in the paper.

So, although the underlying physics of the experiments appears to be understood, it would be desirable to contrast them with a suitable theoretical description. The selected model should consider the fact that polymers are not simple objects, but they are flexible chains formed by the bending of many smaller monomers (that hereafter will be considered as spherical). In other words, the correlations between monomers that belong to the same polymer chain must be included in order to obtain correct theoretical predictions for the structure of the polymers. This may be done by means of the PRISM theory, firstly proposed by Schweizer and Curro [19] for one-component polymer suspensions, and the excluded to colloid-polymer mixtures. The PRISM is based on the Ornstein-Zernike integral equation theory [31], where the correlation between monomers are taken into account explicitly. It states that, in a N-molecular system, the inter-

6.2 Paper II. *Structure of charged colloid-polymer mixtures*

monomer total correlation (between monomers belonging to different chains), $h(r)$, is related to the inter-monomer direct correlation $c(r)$ and the intra-correlation function for monomers on the same chain, $w(r)$. For a binary mixture, in the Fourier space, the PRISM is generalized to

$$h_{ij}(q) = w_{ij}(q)[c_{ji}(q)w_{ij}(q) + \sum_l c_{il}(q)\rho_l h_{lj}(q)] \quad (6.2.2)$$

where the first term in eq. (6.2.2) represents the direct correlation between species i and j , whereas the second term gives the correlation between i and j through the rest of particles. We will treat our colloid-polymer system as a mixture of colloids and monomers, while the solvent enters implicitly via an effective interaction-site potential as is the Debye-Hückel one,

$$\beta V_{ij}^{direct}(r) = \begin{cases} +\infty & r < \sigma_{ij} (= \frac{\sigma_i + \sigma_j}{2}) \\ \frac{L_B Z_i Z_j e^{-\kappa(r - \sigma_{ij})}}{r(1 + 0.5\kappa\sigma_i)(1 + 0.5\kappa\sigma_j)} & r \geq \sigma_{ij} \end{cases} \quad (6.2.3)$$

where subscripts i and j denote the colloid (c) and monomer (m) species. In the previous expression $\beta = 1/k_B T$, L_B is the Bjerrum length. σ_i is the diameter of the i -component, Z_i is its surface charge and κ is the inverse of the Debye length $\kappa = \sqrt{8\pi L_B I_{ion}}$. The ionic strength of the mixture, I_{ion} , is the sum of all possible ionic species present in the suspension: charged colloids, charged monomers and free electrolyte, $I_{ion} = Z_c \rho_c + Z_m \rho_m + C_{electrolyte}$.

In order to solve eq. (6.2.3) additional equations relating the interaction potentials to the correlations are required to close the algebraic system. We use the HNC closure equation for the colloid-colloid correlations and the PY closure for the colloid-monomer and monomer-monomer correlations [24-26]. The intra-monomer information stored in $w_{ij}(q)$ has been modeled as $w_{cc}(q) = 1$ (valid for spherical particles) and $w_{cm}(q) = w_{mc}(q) = 0$, while $w_{mm}(q)$ is given by the form factor of a single polymer chain. A suitable description for $w_{mm}(q)$ is provided by Koyama's model [32, 33], where an interpolation between two limit cases (Gaussian and rigid chain models) is performed through a semi-empirical parameter, the *persistence length* L_p . Intuitively, L_p is a measure of the intrinsic stiffness of the chain, and it controls the radius of gyration of the polymer [34].

Therefore, our mixtures have been modeled with the next parameters: for colloids $\sigma_c = 100$ nm, $Z_c = 600$ electrons per particle (calculated from the method explained

6. RESULTS

elsewhere [35]) and $\phi_c = 0.0056$. For polymers, the non-solution of the integral equations for large polymer chains demands an effective monomer size of $\sigma_m^{eff} = 15\sigma_m$, where ($\sigma_m = 0.8$ nm). This leads to $N_m^{eff} = 1000$ ($N_m = 14000$). The persistence length has been taken to be equal to this effective diameter, $L_p^{eff} = \sigma_m^{eff}$. The polymer charge, Z_m , has been chosen to be the one predicted by the Oosawa-Manning theory [31]. This model takes into account the electrostatic condensation of the counterions on the charged polymer coil. Although this model was derived for linear chains, it remains correct for the case of flexible ones [36] (according to this, $Z_m = 0.8$ for acrylamide monomer). The calculations were performed using the same experimental polymer volume fractions showed in table (6.2.1). The free electrolyte concentration is an uncontrolled parameter which can be substantially affected by external impurities coming from the polymer synthesization process or the external contamination during the protocol preparation. For these reasons, $C_{electrolyte}$ is selected as the only fitting parameter of our theoretical predictions. Table (6.2.1) shows the ionic strength that leads to the best fit. $Z_m\rho_m$ and $C_{electrolyte}$ have also been shown in order to confirm that they are increasing functions of the polymer concentration. Once these parameters have been chosen, the PRISM allows us to determine the theoretical colloid-colloid structure factor that will be compared to the experimental light scattering observations.

The results of these calculations are also shown in fig. (6.2.1) as different type of lines superimposed to the experimental data. In all cases, the theoretical predictions agree with the experimental $S_{cc}(q)$ for the five studied polymer concentrations. It must be emphasized that not only the height and width of the peaks is well captured, but also their positions. The PRISM is also able to predict the increase of the structure factor at low q -values, although the theory overestimates the light scattering observational evidence. In our opinion, this happens because the $w_{mm}(q)$ model employed is not exact and causes that PRISM calculations lose precision at large spatial scales in favor of an apparent fine accuracy at large q -values.

Since the PRISM capture quantitatively the experimental results, it is worth using this theory to deepen in the interplay between depletion attraction and electrostatic repulsion. Particularly, we are interested in understanding the previously mentioned shift of the peak of $S_{cc}(q)$. In fig. (6.2.2) we show the theoretical predicted peak position, assuming that κ does not increases with the polymer concentration. As can be observed, the peak displacement is also quite important, which is a confirmation that the almost unscreened polymer-colloid electrostatic repulsion induces a very strong de-

pletion attraction between colloids. However, the shift is still below the experimental data, showing that the screening of the colloidal charge enhances still more the depletion effect.

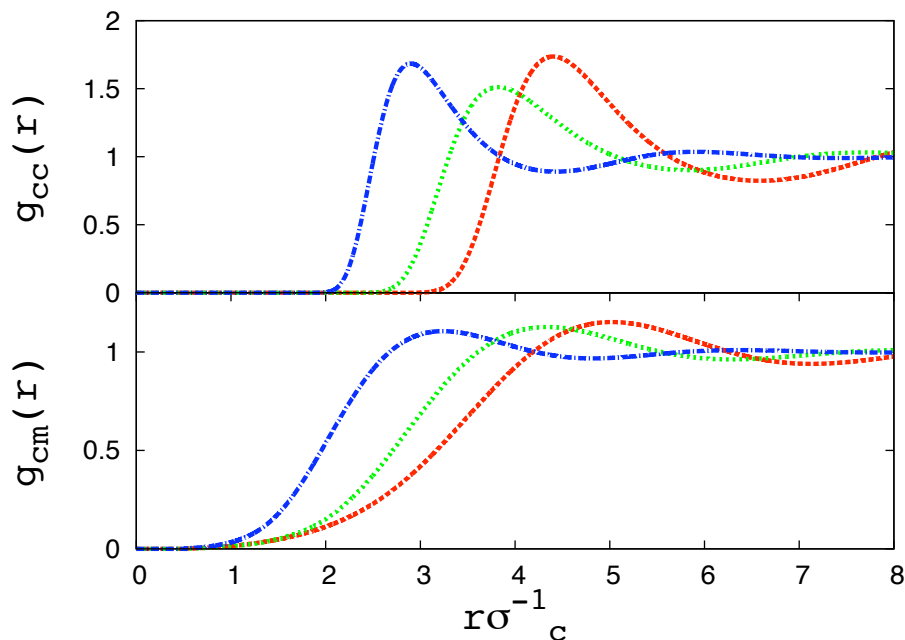


Figure 6.2.3: Colloid-colloid ($g_{cc}(r)$) and colloid-monomer ($g_{cm}(r)$) pair distribution functions obtained with the PRISM theory at the same experimental conditions. The type of lines stand for the polymer volume fractions studied in the experiment: 0.00003 (red dashed line), 0.00015 (green dotted line) and 0.00075 (blue do-dashed line).

An alternative way to quantify the importance of the depletion is comparing the colloid-colloid and colloid-monomer pair distribution functions ($g_{cc}(r)$ and $g_{cm}(r)$, respectively) predicted by the PRISM for the same experimental conditions. They are shown in fig. (6.2.3) for three different polymer concentrations. In all cases, the colloid-polymer electrostatic repulsion is strong enough so that the maximum of $g_{cm}(r)$ falls at larger distances than the maximum of $g_{cc}(r)$. That is, polymers are on average excluded from the region between two colloids, giving rise to an enhanced depletion attraction at such distances. These results agree with the conclusion given by a previous theoretical study performed for a similar situation [37].

Finally, we use the PRISM predictions to calculate the two-body total colloid-colloid

6. RESULTS

interaction potential as a function of the polymer packing fraction ϕ_p . To derive the latter potential we make use of the relationship $\beta V_{cc}^{Total}(r) = -\ln g_{cc}(r)$. This expression is exact by definition [38] only when the number of colloidal particles tends to zero. In other cases, the effective density pair potential must be properly interpreted taking into account the hypothesis used to derive it, as concluded in ref. [39]. Although the colloidal packing fraction used in our experiments is not diluted enough, the obtained potential is a suitable approximation to consider, in terms of interactions, a qualitative physical interpretation of our results.

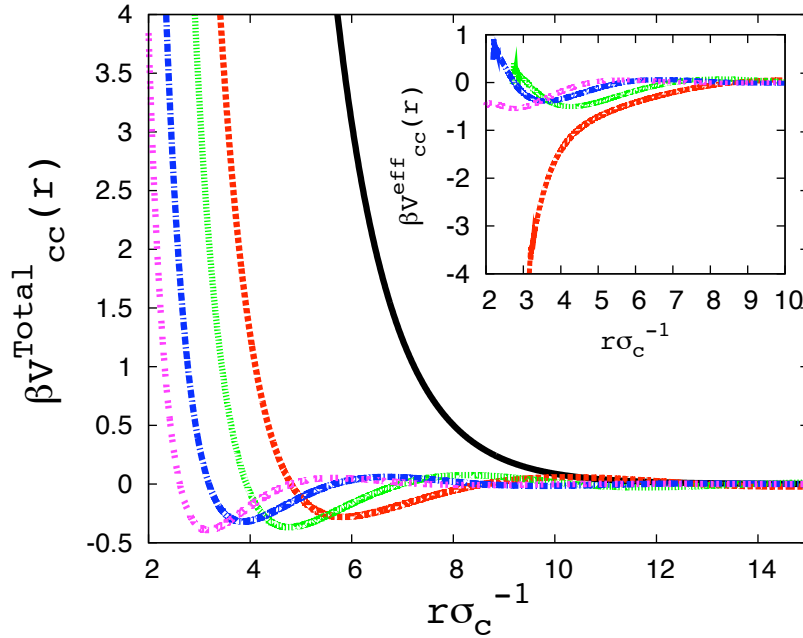


Figure 6.2.4: Dimensionless colloid-colloid total potential $\beta V_{cc}^{Total}(r)$ and colloid-colloid effective potential $\beta V_{cc}^{eff}(r)$ (shown in the inset). Curves were obtained from the PRISM predictions as is indicated in the text. The type of lines assigned in figs. (6.2.1) and (6.2.2) has been maintained.

Figure (6.2.4) shows $\beta V_{cc}^{Total}(r)$ in the limit $\phi_c \rightarrow 0$ for the five studied polymer concentrations. This interaction is in fact the sum of two contributions: the direct colloid-colloid electrostatic repulsion $V_{cc}^{direct}(r)$ and the polymer-induced effective potential $V_{cc}^{eff}(r)$, ($V_{cc}^{Total} = V_{cc}^{direct}(r) + V_{cc}^{eff}(r)$). The interaction potential picture helps us to separate all the effects responsible for the colloid structure. First of all, the plots show that as we increase the polymer concentration, $V_{cc}^{direct}(r)$ becomes gradually screened

by the extra ionic strength of the suspension. This causes the shift to shorter distances of the repulsive barrier of $V_{cc}^{Total}(r)$. At the same time, increasing of the ionic strength also induces the screening of the colloid-monomer repulsion, reducing the attractive effective depletion between colloids (see the inset of fig. (6.2.4)). However, if we add both contributions, the overall effect is attractive and a potential well appears at intermediate distances. Indeed, the polymer presence changes the shape of the curves from a purely repulsive pair interaction (black solid line) to a repulsive barrier with an attractive well (other lines). In fact, when the polymer concentration is increased, the attractive well moves to shorter centre-centre distances (from $r_{min} = 6\sigma_c$ to $r_{min} = 3\sigma_c$) and its width becomes narrower (from $4\sigma_c$ to $2\sigma_c$), while the depth remains almost constant ($\beta V_{cc}^{Total}(r) \sim -0.4$).

These theoretical results confirm that the depletion attraction induced by the colloid-polymer repulsion is playing the dominant role. Moreover, the effective potential picture gives another confirmation of the electrostatic origin of this depletion. Indeed, if we take a naive picture where polymer chains are treated as ideal [2], the range of the depletion attraction is given by $2R_g$. However, this framework must be automatically rejected since the range of the attractive wells shown in fig. (6.2.4) is always larger than $4R_g$. This results are in agreement with the shift of the main peak of $S_{cc}(q)$.

In conclusion, the experimental observations of the structure in charged colloid-polymer mixtures reveal a complex scenario, where different effects are coupled to yield important depletion attractive interactions, even at very low density of colloids. The results show that the addition of charged polymers induces an enhanced depletion attraction between the charged colloids that dominates over the electrostatic repulsion. This gives rise to an attractive potential well that moves to smaller interparticle distances as the polymer concentration increases. The PRISM theory is able to capture the interplay between repulsive and attractive interactions in the mixture, and represents a powerful tool to disentangle all the effects involved in this kind of systems.

The author are grateful to “MCINN” (Project No. MAT2009-13155-C04-02), ERDF Funds and “Junta de Andalucia” (projects P07-FQM-02496 and P07-FQM-02517) for financial support. MP-F would like to thank S. ROLDÁN-VARGAS for helpful discussions.

References

6. RESULTS

- [1] Tuinier R., Rieger J. and de Kruif C. G., *Adv. Colloid Interface Sci.* **103** (2003) 1.
- [2] Asakura S. and Oosawa F., *J. Chem. Phys.* **22** (1954) 1255.
- [3] Gast A. P., Hall C. K. and Russel W. B., *J. Colloid Interface Sci.* **96** (1983) 251.
- [4] Vrij A., *Pure Appl. Chem.* **48** (1976) 471.
- [5] Tuinier R., Smith P. A., Poon W. C. K., Egelhaaf S. U., Aarts D. G. A. L., Lekkerkerker H. N. W. and Fler G. J., *EPL* **82** (2008) 68002.
- [6] Eckert T. and Bartsch E., *Phys. Rev. Lett.* **89** (2002) 125701.
- [7] Pham K. N., Egelhaaf S. U., Pusey P. N. and Poon W. C. K., *Phys. Rev. E* **69** (2004) 011503.
- [8] Rosch T. W. and Errington J. R., *J. Chem. Phys.* **129** (2008) 164907.
- [9] Rotenberg B., Dzubiella J., Hansen J.-P. and Louis A. A., *Mol. Phys.* **102** (2004) 1.
- [10] Durbin S. D. and Feher G., *Annu. Rev. Phys. Chem.* **47** (1996) 171.
- [11] Soon-Chul K., Soong-Hyuck S. and Baek-Seok S., *J. Chem. Phys.* **127** (2007) 114903.
- [12] Fuch M. and Schweizer K. S., *J. Phys.: Condens. Matter* **14** (2002) R239; Fuch M. and Schweizer K. S., *Europhys. Lett.* **51** (2000) 621.
- [13] Rudhardt D., Bechinger C. and Leiderer P., *J. Phys.: Condens. Matter* **11** (1999) 10073.
- [14] Scheer E. N. and Schweizer K. S., *J. Chem. Phys.* **128** (2008) 164905.
- [15] Louis A. A., Bolhuis P. G., Meijer E. J. and Hansen J.-P., *J. Chem. Phys.* **117** (2002) 1893.
- [16] Moncho-Jord A., Louis A. A., Bolhuis P. G. and Roth R., *J. Phys.: Condens. Matter* **15** (2003) S3429.
- [17] Fortini A., Disjotra M. and Tuinier R., *J. Phys.: Condens. Matter* **17** (2005) 7783.
- [18] Chandler D. and Andersen H. D., *J. Chem. Phys.* **57** (1972) 1930.
- [19] Schweizer K. S. and Curro J. G., *Adv. Chem. Phys.* **98** (1997) 1.
- [20] Chatterjee A. P. and Schweizer K. S., *J. Chem. Phys.* **109** (1998) 10464.
- [21] Ggelein C. and Tuinier R., *Eur. Phys. J. E* **27** (2008) 171.
- [22] Ggelein C., Ngele G., Buitenhuis J., Tuinier R. and Dhont J. K. G., *J. Chem. Phys.* **130** (2009) 204905.
- [23] Denton A. R. and Schmidt M., *J. Chem. Phys.* **122** (2005) 2449111.
- [24] Ferreira P. G., Dymitrowska M. and Belloni L., *J. Chem. Phys.* **69** (1999) 9691.
- [25] Chen Y. L. and Schweizer K. S., *J. Chem. Phys.* **120** (2004) 7212.
- [26] Belloni L. and Ferrreira P. G., *Philos. Trans. R. Soc. London, Ser. A* **359** (2001)

867.

- [27] Búcsi A., Forcada J., Gibanel S., Héroguez V., Fontanille M. and Gnanou Y., *Macromolecules* **31** (1998) 2087.
- [28] Berne B. J. and Pecora R., *Dynamic Light Scattering* (New York: Wiley) 1976.
- [29] Phillies G., *J. Chem. Phys.* **74** (1980) 260.
- [30] Moussad A. and Pusey P. N., *Phys. Rev. E* **60** (1999) 5670.
- [31] Manning G. S., *J. Chem. Phys.* **51** (1969) 924.
- [32] Koyama R., *Macromolecules* **17** (1984) 194.
- [33] Honnell K. G., Schweizer K. S. and Curro J. G., *Macromolecules* **23** (1990) 3496.
- [34] Buhler E. and Boué, *Eur. Phys. J. E* **10** (2003) 89.
- [35] Gisler T., Shultz S. F., Borkovec M., Sticher H., Schurtenberger P., D'Aguanno B. and Klein R. 1994 *J. Chem. Phys.* **101** 9924.
- [36] Dymitrowska M. and Belloni L., *J. Chem. Phys.* **109** (1998) 4659.
- [37] Croze O. A. and Cates M. E., *Langmuir* **21** (2005) 5627.
- [38] Hansen J. P. and McDonald I. R., *Theory of Simple Liquids* (New York: Academic Press) 1976.
- [39] Louis A. A., *J. Phys.: Condens. Matter* **14** (2002) 9187.

6. RESULTS

6.3 Paper III. *Charged colloid-polymer mixtures: A study on electrostatic depletion attraction*

6.3 Paper III. *Charged colloid-polymer mixtures: A study on electrostatic depletion attraction*

6. RESULTS

6.3 Paper III. *Charged colloid-polymer mixtures: A study on electrostatic depletion attraction*

Charged colloid-polymer mixtures: A study on electrostatic depletion attraction, J. Chem. Phys. **134**, 054905 (2011)

M. Peláez-Fernández, A. Moncho-Jordá, and J. Callejas-Fernández

Departamento de Física Aplicada, Grupo de Física de Fluidos y Biocoloides, Universidad de Granada, E-18071 Granada, Spain.

6. RESULTS

Abstract

In this work, light scattering methods have been used to study the effect of adding charged polymer chains on the structural and dynamic properties of a charged colloidal system. The experimental measurements of the static structure factor $S_{cc}(q)$ show that as the polymer concentration increases, the main peak moves to higher q -values, which is interpreted in terms of the electrostatically enhanced depletion attraction induced by the polymer. Moreover, we found that the shift of the peak depends on the interplay between two relevant length scales, the polymer radius of gyration, R_g , and the Debye length, κ^{-1} . To reach these conclusions, the polymer reference interaction site model has been employed to explain the experimental results and to study how the effective depletion attraction depends on the polymer concentration, R_g and κ^{-1} . Additionally, the measurements of the dynamic structure factor $f(q, \tau)$ indicate that the colloidal diffusion increases with the polymer concentration. Both static and dynamic analysis point out that the repulsion between colloids becomes weaker as the charged polymer is added.

Introduction

In general, real colloidal suspensions are mixtures of particles with different properties. In these complex systems, one of the goals in colloidal physics is to know and manipulate the particle interactions (London van der Waals, electrostatic, magnetic, depletion, ...). One of the most studied systems in the literature is the polymer and colloid mixture (CPM) suspended in a solvent. At this respect, mixtures of hard neutral colloidal particles and nonadsorbing polymers have been well studied experimentally [1-6], theoretically [7-10] and by means of computer simulations [11-12]. In this particular case, the excluded volume repulsion between colloids and polymers induce an effective interaction between colloids, the so-called depletion attraction. This interaction is originated by entropic reasons, as the overlap of the depletion layers of two approaching colloids implies a larger free volume for the polymers, giving rise to the increase of the entropy of the mixture. The depth of this depletion interaction is mainly controlled by the polymer density, whereas its range is of the order of the polymer radius of gyration, R_g . For high enough polymer concentrations, this depletion attraction may lead to the destabilization of the solution towards phase separation between colloid-rich and polymer rich phases [3].

However, the above mentioned depletion attraction becomes strongly altered if both colloids and polymers are like-charged. Indeed, one of the more significant differences between charged and uncharged colloid-polymer mixtures is that the depletion attraction has an electrostatic origin instead of entropic, since it becomes dominated by the electrostatic repulsion between colloids and polymers. In the limit of small electrolyte concentration, this electrostatic depletion attraction can reach a relative large strength compared to the case of uncharged mixtures, and the range of the attraction may exceed the polymer radius of gyration, as it scales with the Debye length, κ^{-1} [13-15].

Recently, there has been a considerable interest focused on studying the electrostatic depletion mechanism manifested in binary charged colloidal systems. Waltz and Sharma [16] calculated numerically the depletion force between two charged spheres in a solution of charged spherical macromolecules. They reported results confirming that the long-range wall-particle electrostatic repulsion induces an enhancement of the depletion attraction between walls. Mondain-Monval *et al.* performed measurements of the force focus on charged droplets in the presence of smaller charged micelles and concluded that, apart from the electrostatic repulsion, an attractive depletion caused by

6. RESULTS

the charges of the micelles has to be considered too [17]. Helden *et al.* presented measurements of the depletion potential generated by charged rods using the total internal reflection microscopy technique, showing the important role that electrostatic depletion plays in this kind of charged colloid-polymer mixtures [18]. Campbell *et al.* studied gelation in suspensions of model colloidal particles with short-ranged attractive and long-ranged repulsive interactions by means of three-dimensional fluorescence confocal microscopy. They focused on the gel formation by increasing the packing fraction of particles [19, 20].

In this paper, we use experimental and theoretical methods to study the two component system formed by charged colloids and nonadsorbing like-charged polymers in water as solvent. We are particularly interested in the observation of the interplay between the electrostatic repulsion and this attractive depletion interaction. We will focus on mixtures at low colloid and electrolyte concentrations, where we expect to observe the above mentioned electrostatic enhancement of the depletion attraction. Then, we will explore the significant lengths involved in this electrostatic mechanism using two different chain lengths of the same polymer. The study is limited to the situation where the sample behaves as a stable fluid, so arrested states or aggregation phenomena are not present.

The experiments were performed applying light scattering techniques to measure the colloid-colloid structure factor $S_{cc}(q)$ and the dynamic structure factor $f(q, \tau)$. We started from a diluted colloidal suspension in water at very low electrolyte concentration, where electrostatic repulsion dominates. By adding increasing amounts of charged polymer the resulting structures were accordingly analyzed. Under these conditions of low salinity, the short-range excluded volume interaction between colloids and polymers are masked by the presence of long-range electrostatic interactions. The experimental results are compared to the theoretical predictions obtained using the polymer reference interaction site model (PRISM) [21, 22]. This model takes into account the fact that the monomers of the polymer are not free entities, but they are linked to form the polymer chain. Although the PRISM was originally applied to one-component polymer systems, it has been shown to be a very useful tool in the case of colloid-polymer mixtures. For instance, this model has been applied to show that the typical correlation length of uncharged polymer systems controls the behaviour of the induced interaction [23, 24]. Moreover, it has been also employed to predict the phase behaviour of a wide range of unexplored mixtures [25]. Recently, the PRISM has been used to describe the

6.3 Paper III. *Charged colloid-polymer mixtures: A study on electrostatic depletion attraction*

structural properties of mixtures of charged colloids and polyelectrolytes (polymer coils formed by ionizable monomers) [14]. However, there is a lack of experimental results to compare the previous theoretical predictions.

The paper is organized as follow. In Sec. II, we present the experimental techniques and protocols, the colloid-polymer systems employed, and the theoretical model. In Sec. III, we show the static light scattering experiments performed for different polymer concentrations and polymer chain lengths. The results are compared and discussed in terms of the theoretical predictions obtained with the PRISM. A dynamic analysis is inserted in the discussion in order to investigate the effects of the electrostatic depletion on the colloidal dynamics. Finally, in sec. IV we briefly show the conclusions.

Materials and Methods

Experimental System

We have employed a binary colloid-polymer system consisting on a mixture polystyrene colloids (latex) and polyacrylamide polymers (PAM), both characterized by light scattering. The polystyrene spheres were synthesized in distilled water using the polymerization procedures given in Ref. [26]. The colloidal characterization puts up an average diameter of $\sigma_c = 100 \pm 2$ nm and a negative surface (its electrophoretic mobility at $T = 25$ °C in distilled water is $\mu_e = -3.5 \times 10^{-8} \text{ m}^2\text{V}^{-1}\text{s}^{-1}$). The polymers used in this work are two different Polyacrylamide (Polysciences, Inc.) of molecular weights $(0.6 - 1) \cdot 10^6$ g/mol (catalog number 19901) and $5 \cdot 10^6$ g/mol (catalog number 21485), henceforth denoted by PAM1 and PAM2. The hydrodynamic radius measured by dynamic light scattering (DLS) for each polymer is 25 nm (PAM1) and 50 nm (PAM2), respectively. Although the manufacturer presents both products as nonionic polymers, they are slightly negatively charged in distilled water at low ionic strength due to the ion condensation around the monomers of acrylamide. This was experimentally confirmed by electrophoretic mobility measurements ($\mu_e \approx -0.9 \times 10^{-8} \text{ m}^2\text{V}^{-1}\text{s}^{-1}$ and $\mu_e \approx -1.1 \times 10^{-8} \text{ m}^2\text{V}^{-1}\text{s}^{-1}$ for PAM1 and PAM2, respectively). Given the repulsive character of the colloid-polymer interaction, the adsorption on the colloidal surface can be discarded. In any case, the nonadsorption of the polymer on the colloidal surface was also corroborated via shear viscosity measurements of the mixtures, as their values did not change significantly with respect to the free polymer system.

6. RESULTS

Experimental Procedure

The colloidal structure factor was determined using static light scattering (SLS) [27]. The experimental setup comprises a three-dimensional light scattering spectrometer 3D-DLS from LS Instruments (Fribourg, Switzerland), with two avalanche photodiodes (A and B) as detectors. A digital correlator computes the cross-correlation function of the registered scattered intensities, for which the time-dependent contributions of multiple scattered photons is attenuated [28]. According to this design [29], the colloid-colloid structure factor of the sample is proportional to

$$S(q) \propto \sqrt{\frac{\langle I_A^{cp}(q) \rangle \langle I_B^{cp}(q) \rangle g_{AB}^{cp}(q, 0) - 1}{\langle I_A^0(q) \rangle \langle I_B^0(q) \rangle g_{AB}^0(q, 0) - 1}} \quad (6.3.1)$$

where $\langle I_i^{cp}(q) \rangle$ is the total time-averaged intensity registered by detector $i = A, B$ of the colloid-polymer mixture as a function of the scattering vector, q , whereas $\langle I_i^0(q) \rangle$ is the time-averaged intensity corresponding to a dilute colloidal suspension. In our measurements the time-averaged intensity scattered by the polymers is negligible compared to the one for colloids ($\langle I^p(q) \rangle < 10^{-3} \langle I^c(q) \rangle$), so Eq. (6.3.1) corresponds to the colloid-colloid structure factor, $S_{cc}(q)$. The ratio $(g_{AB}^{cp}(q, \tau = 0) - 1)/(g_{AB}^0(q, \tau = 0) - 1)$ corrects the magnitude of the structure factor due to the disturbance of multiple scattering [29], where $g_{AB}(q, \tau) = \langle I_A(q, t) I_B(q, t + \tau) \rangle / \langle I_A(q) \rangle \langle I_B(q) \rangle$ is the so-called normalized cross-correlation function of the registered intensities.

The samples were prepared by mixing the binary colloid-polymer system in a bed of ion exchanger resin inside a cylindrical quartz cell. The use of the resin assures that all the electrolyte excess of the sample is removed, leading to electrostatically stabilized colloid-polymer mixtures [30]. The light scattering measurements were performed two days after the preparation of the samples. We checked that this time was in all cases long enough to guarantee that the mixtures have reached equilibrium conditions since no changes of the structure factors were observed. After equilibration, the samples were transferred to a thinner cylindrical quartz glass cells to minimize the attenuation caused by the non-illuminated remaining sample. The measurements were performed at temperature $T = 25$ °C, within a wide angular range going from 20° to 150° , where $\langle I(q) \rangle$ and $\langle I(q, t) I(q, t + \tau) \rangle$ were determined with an angular interval of $\Delta\theta = 2^\circ$ degrees. The average intensity $\langle I(q) \rangle$ was collected during 160 s to avoid spurious fluctuations.

6.3 Paper III. *Charged colloid-polymer mixtures: A study on electrostatic depletion attraction*

The colloidal dynamics was obtained by (DLS). For that, the normalized correlation of the registered intensities was measured from the stored scattered intensities in a wide interval of delayed times, τ . Under the assumption that this variable is ergodic, the so-called dynamic structure factor $f(q, \tau)$ can be extracted from the relationship [27]

$$f(q, \tau) = C\sqrt{g_{AB}(q, \tau) - 1} \quad (6.3.2)$$

where the factor C is the inherent correction from the cross-correlation technique mentioned above [29]. For a one-component system of interacting particles $f(q, \tau)$ is defined as

$$f(q, \tau) = \frac{1}{NS(q)} \sum_{i=1}^N \sum_{j=1}^N \langle \exp(i\vec{q} \cdot [\vec{r}_i(0) - \vec{r}_j(\tau)]) \rangle \quad (6.3.3)$$

where N is the number of colloidal particles. If the system is ergodic [31] then the displacement of the particles follows a Gaussian distribution and eq. (6.3.3) can be written as

$$f(q, \tau) = \exp\left(-q^2 \frac{\langle \Delta r^2(\tau) \rangle}{6}\right) \quad (6.3.4)$$

where $\langle \Delta r^2(\tau) \rangle$ is the mean square displacement of the particles at time τ . Eqs. (2) and (4) allow the determination of $\langle \Delta r^2(\tau) \rangle$ to be done by means of the DLS technique. In all cases, each measurement is the result of the average performed over three independent runs, collecting the experimental data during a long enough time interval ($t = 200$ s).

Theoretical Model

We consider a binary mixture formed by charged spheres (colloids) of diameter σ_c , and like-charged monomers of diameter σ_m , representing the units of the polymer chains. The water molecules and the electrolyte are treated as a background continuum, so that they only have an effect on the effective interactions between colloids and monomers. These interactions are assumed to have a hard core part plus an electrostatic repulsive tail given by the screened Debye-Hückel potential [32]. Therefore, considering the species i and j of diameters σ_i and σ_j , the dimensionless potential $\beta V_{ij}^{direct}(r)$ is written

6. RESULTS

as,

$$\beta V_{ij}^{direct}(r) = \begin{cases} +\infty & \text{if } r < \sigma_{ij} (= \frac{\sigma_i + \sigma_j}{2}) \\ \frac{L_B Z_i Z_j e^{-\kappa(r - \sigma_{ij})}}{r(1 + 0.5\kappa\sigma_i)(1 + 0.5\kappa\sigma_j)} & \text{if } r \geq \sigma_{ij} \end{cases} \quad (6.3.5)$$

where i and j indexes correspond to colloid (c) or monomer (m), r is the distance between particle centres, L_B is the Bjerrum length, and $\kappa = \sqrt{8\pi L_B I_{ion}}$ with $I_{ion} = Z_c \rho_c + Z_m \rho_m + C_{electrolyte}$ the ionic strength. Z_i and ρ_i stand for the effective surface charge and number density of the colloids (monomers), respectively, and $C_{electrolyte}$ denotes the electrolyte concentration in solution, which can have an important influence on the interaction range. This model for the site-site interactions neglects the structure of the electrolyte and the water molecules, and ignores the difference between the permittivities inside and outside the colloid, what may lead to a significant variation of its effective charge [33]. However, we believe that the exact details of the interaction potentials will not modify qualitatively the conclusions deduced in our work. At this respect, the simple Debye-Hückel potential is good enough to provide a fair theoretical justification of the experimentally observed electrostatic depletion mechanism, as will be shown latter on.

In order to study the effect of the polymer coils on the colloid-colloid structure factor, the chainlike structure of the polymers must be properly taken into account. The detailed treatment of the polymer structure at the monomer level description is in general a very complicated task as it needs the use of intensive calculations to determine the polymer configurations. At this point, an approximate theory for the intramolecular and intermolecular polymer correlations is required. An excellent candidate is the PRISM theory. This model takes into account the connectivity between the monomers that belong to the same polymer chain through the so-called intramolecular correlation $w_{ij}(r)$ (also known in the Fourier space as the form factor). PRISM establishes a relationship between $w_{ij}(r)$, the total intermolecular site-site correlation $h_{ij}(r)$ and the intermolecular direct correlation $c_{ij}(r)$ by means of a set of Ornstein-Zernike-like integral equations. In Fourier space, the PRISM equations take the following form,

$$h_{ij}(q) = w_{ij}(q) \left[c_{ij}(q) w_{ji}(q) + \sum_l c_{il}(q) \rho_l h_{lj}(q) \right] \quad (6.3.6)$$

The intermolecular structural factor $S_{ij}(q)$ is

$$S_{ij}(q) = w_i(q) \delta_{ij} + \sqrt{\rho_i \rho_j} h_{ij}(q) \quad (6.3.7)$$

6.3 Paper III. *Charged colloid-polymer mixtures: A study on electrostatic depletion attraction*

where δ_{ij} is the Kronecker delta. Since our colloidal particles are spherical, the colloidal form factor is simply given by $w_c(q) = 1$. For the polymers, we use the Koyama's form factor [34], which gives a good description of polyelectrolyte chains [13, 35]. It is an interpolation between two physical limits, attending to the stiffness of the chain: the Gaussian model and the rigid chain model. The parameter controlling the local stiffness is the persistence length, L_p . This model takes into account the fact that the positions of two monomers inside the polymer chain are strongly correlated at short monomer-monomer distances, whereas they are uncorrelated for large separations. The persistence length depends on the monomer-monomer electrostatic interactions and so it will be affected by the electrolyte concentration [36]. Neglecting end-effects and swelling, the form factor is given by

$$w_m(q) = 1 + \frac{2}{N_m} \sum_{|\alpha-\gamma|=1}^{N_m-1} (N_m - |\alpha - \gamma|) \hat{w}_{|\alpha-\gamma|}(q) \quad (6.3.8)$$

$$\hat{w}_{|\alpha-\gamma|}(q) = \frac{\sin(B_{|\alpha-\gamma|}q)}{B_{|\alpha-\gamma|}q} e^{-(A_{|\alpha-\gamma|}q)^2}$$

where N_m denotes the number of monomers per chain, $\hat{w}_{|\alpha-\gamma|}(q)$ represents the inter-correlation between monomers α and γ and the constants $A_{|\alpha-\gamma|}$ and $B_{|\alpha-\gamma|}$ are functions of the persistence length and the monomer size (explicit expressions can be found in [37]).

To solve Eq. (6.3.8), a set of three extra closure relations must be provided. We have employed the Hypernetted Chain (HNC) for the colloid-colloid correlation, and Percus-Yevick (PY) for the monomer-monomer and monomer-colloid correlations. This choice leads to a fair description of the structure of charge colloid-polymer mixtures, and avoids the spurious divergence obtained in other cases [14, 35].

$$\begin{aligned} c_{cc}(r) &= e^{(\gamma_{cc}(r) - \beta V_{cc}^{direct}(r))} - (\gamma_{cc}(r) + 1) && \text{HNC} \\ c_{im}(r) &= e^{(-\beta V_{im}^{direct}(r) - 1)} (1 + \gamma_{im}(r)) && \text{PY} \end{aligned} \quad (6.3.9)$$

Again, i denotes colloid (c) and monomer (m) and $\gamma_{ij}(r) = h_{ij}(r) - c_{ij}(r)$. The system of integral equations given by Eq. (6.3.6), together with Eqs. (6.3.8) and (6.3.9) can be solved using the standard iterative Picard method. Although the method used in this work is similar to the scheme presented in Ref. [25], we have also employed an additional density-loop to start in a dilute mixture and reach the convergence faster.

6. RESULTS

System Parameters

Before showing and discussing the results, it is convenient to carry out a careful argumentation of the parameters used to model our mixtures. Particularly, we need to know the colloid and monomer charge (Z_c and Z_m , respectively), the number of monomers per chain (N_m), the persistence length (L_p) and the Debye length, κ^{-1} . The latter two parameters depend on the electrolyte concentration of the suspension, I_{ion} . Unfortunately, I_{ion} can not be directly measured and, moreover, it can be substantially modified by external impurities from the polymer initial sample (e. g., due to the synthesis process and/or the external pollution, caused by the transference between cells). For these reasons, it must be considered as a fitting parameter of our model. A value of $Z_c = 600$ was obtained by fitting the colloidal structure factor for a pure colloidal system (black hollow symbols in Fig. 6.3.1 with the Ornstein-Zernike-HNC using the potential given by Eq. (6.3.5) (information about the fitting method may be found elsewhere [38]). To find the best fit it was not necessary to increase the value of $C_{electrolyte}$, so that it may be assumed that the suspension is totally deionized ($C_{electrolyte} \approx 10^{-6}$ M). Although Z_c may be determined using alternative routes, as electrophoretic mobility measurements [39], renormalization methods [40] or ion condensation theories [41], it is well known that the OZ-HNC procedure is particularly well suited in the case of highly charged colloidal suspension. Moreover, the HNC approximation is able to give an excellent fit of the experimental colloidal structure factor. The goodness of the HNC closure has been corroborated by comparing the results with the ones obtained with the more sophisticated Rogers-Young closure, finding a value of $Z_c = 635$.

In the case of polymers, the accessible experimental information has not a trivial interpretation. The number of monomers per chain can be extracted from the polymer molecular weight and from the molecular weight and mass density of acrylamide (all provided by Polysciences Inc.). For the two polymers employed in this work, N_m is 1.4×10^4 for PAM1 and 7×10^4 for PAM2. Then, the monomer diameter is obtained assuming that monomers are spherical entities, leading to $\sigma_m \approx 0.8$ nm. The monomer effective charge is $Z_m = 0.8$, calculated from the Manning's expression [42]. The total persistence length L_p may be estimated by following the model proposed by Odijk [43] for polyelectrolyte chains, where L_p is separated in two contributions $L_p = L_0 + L_e$. L_0 denotes the intrinsic chain local stiffness, and L_e corresponds to the contribution due to the electrostatic repulsion between neighbouring monomers. The value $L_0 = 12$ nm

6.3 Paper III. *Charged colloid-polymer mixtures: A study on electrostatic depletion attraction*

was estimated from the experimental R_g using the expression for the radius of gyration of a wormlike chain [36, 44],

$$\langle R_g^2 \rangle = \frac{L_c L_0}{3} - L_0^2 + \frac{2L_0^3}{L_c} - \frac{2L_0^4}{L_c^2} \left\{ 1 - \exp\left(\frac{-L_c}{L_0}\right) \right\} \quad (6.3.10)$$

where $L_c = \sigma_m N_m$ is the chain contour length. L_e may be calculated using an explicit expression found by Skolnick and Fixman [45] considering a Debye-Hückel interaction potential between monomers and assuming that ion condensation occurs. It is given by $L_e = \frac{\xi^2}{4\kappa^2 L_B}$ for $\xi < 1$ (with $\xi \equiv \frac{L_B}{\sigma_m}$) [36]. Since we don't have *a priori* information of the value of κ after mixing the polymer chains with the colloidal suspension, we performed a subsequent evaluation of this parameter after solving the integral equations. Notwithstanding, for the ionic strength values used to fit our results (shown in the Table (6.3.1)), L_e is always very small compared to L_0 .

An important inconvenience of PRISM is that it shows divergence problems when the number of monomers per polymer, N_m , is greater than $\approx 10^4$. Also the computing time greatly increases with N_m . To elude these problems we have chosen an optimum effective monomer radius 15 times larger, keeping the same contour length for the polymers, $N_m = 10^3$ for PAM1 and $N_m = 5 \times 10^3$ for PAM2. This mapping is performed by keeping constant the monomer charge Z_m derived previously by means of the Manning's equation. This approximation is indeed strong since the real monomer chain has been substituted by an effective chain with equivalent length but different width. This can affect the predictions at short distances, where the geometry of the polymer chain and its interaction is far away of the real one. Fortunately, the electrostatic repulsions between colloidal particles and polymers and the low concentrations employed in our experiments prevent the colloid-colloid and colloid-polymer approach, so that they are typically far away one from each other. For this reason, we expect that the theoretical predictions for the structure factor, the radial distribution function and the effective depletion potential obtained with our theoretical model are still valid in this framework.

Results and Discussion

Static Properties

Figs. 6.1.1(a) and 6.1.1(b) show a set of experimental colloid-colloid structure factors measured for binary mixtures of colloids at a volume fraction of 0.56% with the two kind of polymers PAM1 and PAM2, respectively (see Table (6.3.1)). In both plots we

6. RESULTS

Table 6.3.1: Experimental and theoretical relevant parameters. The second column stands for the monomer volume fraction ϕ_m used in both experiments and theoretical predictions. $\kappa\sigma_c$ is the one that gives the best fit between the experiments and theory. The latter depends on three ionic contributions: the colloidal $Z_c\rho_c$, the monomer $Z_m\rho_m$, and the free electrolyte contributions $C_{electrolyte}$, which is treated as the only fitting parameter. In all cases the colloidal volume fraction is $\phi_c = 0.56\%$.

Polymer	$\phi_m \times 10^4$	$\kappa\sigma_c$	$Z_m\rho_m$ (mM)	$C_{electrolyte}$ (mM)
PAM1	0.3	0.32	2.0	3.0
PAM1	1.5	0.44	7.0	12.0
PAM1	7.5	0.53	30.0	15.0
PAM2	1.5	0.29	2.0	1.0
PAM2	2.3	0.33	4.0	3.1
PAM2	7.3	0.50	20.0	5.4

include the structure factor for a pure colloidal system as a reference. At zero polymer concentration (black hollow squares), $S_{cc}(q)$ shows a very large and narrow peak of height $S_{cc}(q_{max}) = 2.67$ located at $q\sigma_c = 1.56$. This maximum clearly reveals the existence of a highly repulsive interaction between colloids, with a typical interparticle distance of about $4.03\sigma_c$. This result is consistent with the fact that the electrolyte concentration is very low as the ion exchanger resins have removed most of the ions from the suspension. In the limit $q \rightarrow 0$, the structure factor tends to 0, which indicates that the system is far from the fluid-solid binodal.

However, all the previous liquid-order properties become strongly affected by the presence of the polymer chains. As we increase the polymer concentration, the height and width of the main peak decreases and broadens, respectively, while the position of the peak shifts to relatively high q -values for both polymers, PAM1 and PAM2. It can be also appreciated a noticeable increase of $S_{cc}(q)$ for $q \rightarrow 0$, what can be interpreted as a consequence of interparticle attractions. A similar behaviour has been reported in other binary systems, such as mixtures of casein micelles and exocelular polysaccharide [46], and mixtures of PMMA particles and linear polystyrene polymer chains with short-range attractive interactions [47].

These results reveal that the liquid order becomes gradually lost and the colloidal particles approach each other to closer distances as we increase the polymer density. This

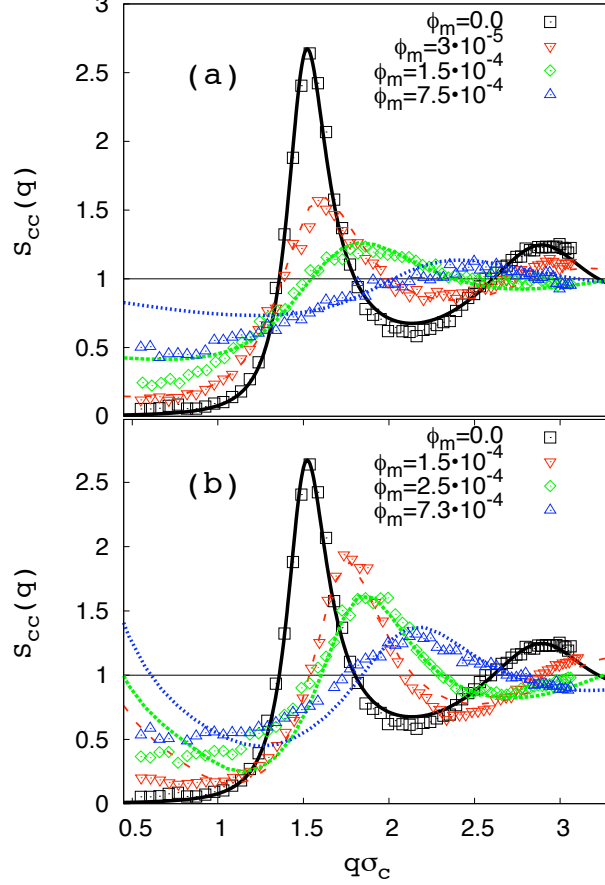


Figure 6.3.1: Colloid-colloid structure factor of colloid-polymer mixtures at different polymer concentrations for (a) PAM1 and (b) PAM2. The experimental results are represented with different types of symbols (see the legend) while the theoretical predictions are plotted with different type of lines.

behaviour can not be only attributed to the increase of the ionic strength induced by the presence of charged polymers in the solution. Indeed, as it was stressed in our previous work [13], the shift of the main peak due to the addition of KNO_3 is much smaller than the one obtained adding polymers. Therefore, this clearly indicates the existence of a polymer-induced depletion attraction between colloids. However, it must be emphasized that such depletion can not be caused by the excluded volume interactions between colloids and polymers, given the small colloidal density employed in our experiments [13]. On the contrary, the strength and long-range character of the

6. RESULTS

depletion effects observed in our experiments must be interpreted as a consequence of the colloid-polymer electrostatic repulsion. In other words, we are treating with an electrostatic depletion instead of an entropic one.

Keeping this fact in mind, it is obvious that adding charged polymers also increases the total ionic strength of the sample, which in turns leads to a more efficient screening of the electrostatic interactions. On the one hand, this screening reduces the colloid-colloid repulsion, leading to a particle approach. On the other hand, it also reduces the colloid-polymer repulsion, which plays the opposite role as it causes the decrease of the electrostatic depletion attraction. In real experiments, both effects can not be separated one from another and always come together. Therefore, the final colloidal structure is the result of the competition between them.

In order to separate these crossed effects and help us to understand the underlying physics behind the observed structure factors, we have fitted the experimental data using the PRISM. This integral equation theory comes out as a suitable model to disentangle the structure and determine the contribution of the polymer-induced effective potential to the total colloid-colloid interaction. We have fitted the experimental data using the parameters given in Table (6.3.1), leaving $C_{electrolyte}$ as the only free parameter of the model. The value of $C_{electrolyte}$ employed to fit the experimental curves grows with the polymer concentration, as expected (see Table (6.3.1)). The results are shown again in Fig. 6.3.1 as different line types. In all cases, the theoretical predictions agree with the experimental $S_{cc}(q)$ for the four studied polymer concentrations. It must be emphasized that not only the height and width of the peaks is well captured, but also their positions. The PRISM predictions are also able to capture the rising of the structure factor at low q -values, although the model overestimate the experimental results. In particular, a large disagreement is observed for the longer polymer [Fig. 6.3.1(b)] at low q -values [48-51]. These discrepancies could be caused by the approximations performed in our theoretical model, since only pair correlations are considered [52]. In fact, the contribution of higher level correlations for long polymer chains could have a great relevance in the final average polymer conformation. In this sense, future theoretical works employing better models are necessary.

Next, we study the effect of the chain length on the colloidal structure. Fig. 6.3.2 compares the position of the main peak of the structure factor q_{max} as a function of the polymer volume fraction for the two studied polymer lengths. As it may be

6.3 Paper III. Charged colloid-polymer mixtures: A study on electrostatic depletion attraction

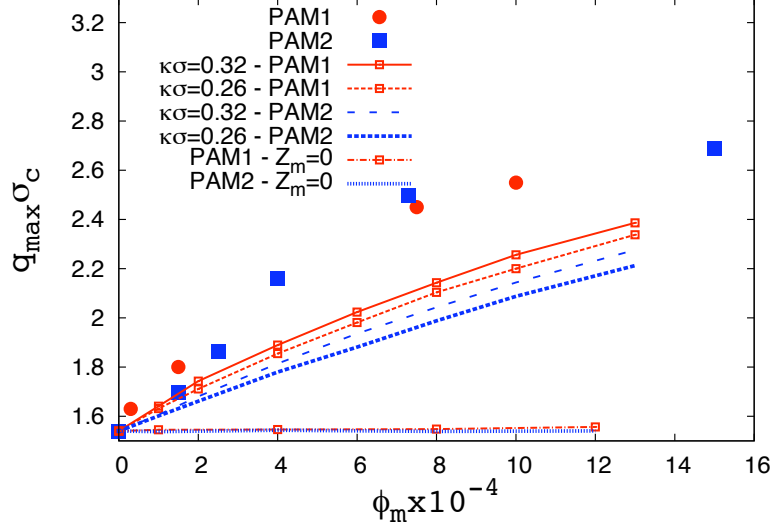


Figure 6.3.2: Position of the main peak of $S_{cc}(q)$ vs the monomer volume fraction (ϕ_m) for the two polymers studied in this work (full circles for PAM1, and full square for PAM2). The PRISM predictions for the peak position have been calculated for two $\kappa\sigma_c$ values (see the legend) and for the two polymer lengths. The figure also shows $q_{max}\sigma_c$ as a function of ϕ_m for the particular case of uncharged polymers, $Z_m = 0$.

observed, the experimental data for both polymer lengths fall approximately into a common curve. Similar results are obtained for other packing fractions of colloids. Nevertheless, the fact that the displacement of the main peak is roughly the same for both polymers does not necessary mean that the depletion effect is independent on the polymer size, as the ionic strength of the sample is different for each case. In fact, there are two relevant length scales involved in the depletion attraction arising in charged colloid-polymer mixtures: the polymer radius of gyration R_g , and the reach of the electrostatic double layer κ^{-1} . The relative importance of these length scales will depend on the ionic strength of the sample. At low electrolyte concentrations the range of the depletion interactions will be of the order of κ^{-1} . On the contrary, at high salt concentration, the electrostatic repulsions between colloids and polymers will be screened and only excluded volume interactions will be important, leading to a range of the depletion attraction around $2R_g$.

Again, the PRISM can help us on separating these coupled effects involved in the experimental results, as κ^{-1} , R_g and ϕ_m can be independently tuned. In Fig. 6.3.2 we

6. RESULTS

plot q_{max} for the two polymer lengths and for two electrolyte concentrations. Also the theoretical predictions for uncharged polymers ($Z_m = 0$) are included. As observed, the shift depends on both, κ^{-1} and R_g . Although increasing the electrolyte concentration weakens the depletion attraction, the screening of the colloid-colloid electrostatic repulsive barrier dominates. This finally enhances the approach between colloids and so, leads to larger q_{max} values. On the other hand, increasing the polymer length induces a smaller peak shift. The reason why longer polymers are less efficient depletants may be attributed to the fact that the depletion attraction has longer range but smaller depth. Therefore, the attraction induced by long polymers is not strong enough to compensate the electrostatic repulsive barrier between colloids. It is important to emphasize again that these depletion effects are mainly electrostatic. Indeed, if we plot q_{max} for uncharged polymers, we find that it is practically insensitive to the increase on polymer concentration.

In order to confirm these results, we have also calculated the two-body total colloid-colloid interaction potential. The total potential was derived from the relationship $\beta V_{cc}^{Total}(r) = -\ln g_{cc}(r)$, where $g_{cc}(r)$ was obtained from PRISM. The latter expression is exact in the so-called colloidal limit, when the number of colloidal particles tends to zero [53, 54]. In our case, although ϕ_c is not zero, it is small enough to consider the latter expression as a valid approximation. Fig. 6.3.3(a) shows $\beta V_{cc}^{Total}(r)$ in the limit $\phi_c \rightarrow 0$ for the two polymer lengths and for different electrolyte concentration at a constant monomer packing fraction given by $\phi_m = 0.001$. For both polymers there is a clear attractive well at small ionic strength. By increasing the salt concentration the range of the repulsive barrier shortens and the position of this minimum moves to smaller interparticle distances, at the time that its depth becomes reduced. For the longer polymers, the minimum disappears completely, so the depletion attraction is overcome by the repulsive electrostatic barrier at any distance.

We can have a more clear picture of these effects by plotting the effective depletion colloid-colloid interaction (see Fig. 6.3.3(b)), defined as $V_{cc}^{eff}(r) = V_{cc}^{Total}(r) - V_{cc}^{direct}(r)$, where $V_{cc}^{direct}(r)$ is the direct colloid-colloid repulsion (Eq. (6.3.5)). The effective potential shows a pronounce attractive well at low ionic strength, what is a clear indication that the colloid-polymer electrostatic repulsion greatly enhances the depletion attraction between colloids, even for small values of the polymer concentration. Also the range of the depletion is larger than the one expected for uncharged polymers. Although the range of the depletion induced in charged colloid-polymer mixtures is

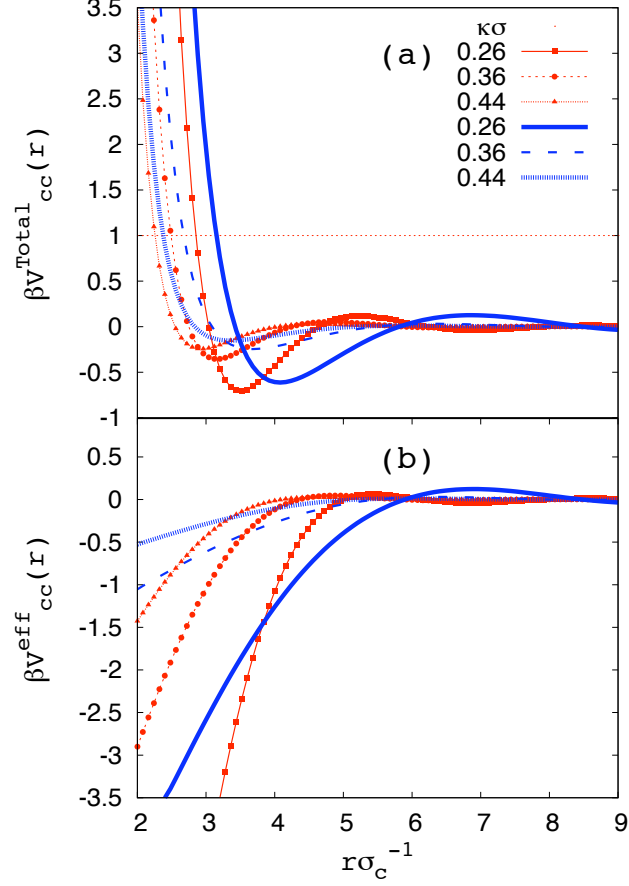


Figure 6.3.3: The plot shows (a) the total interaction potential between colloids, predicted by the PRISM in the colloidal limit and (b) the effective interaction potential. All the calculations are performed at the same monomer volume fraction ($\phi_m = 0.001$). The figure shows the results at three different $\kappa\sigma_c$ for two polymer lengths (PAM1, line-points and PAM2, lines).

mainly controlled by κ^{-1} , the results reveal that the length of the polymer chains plays also an important role. This can be easily checked by comparing the effective interactions at the lowest studied salt concentration. Indeed, long polymers induce a less deep depletion attraction with longer range, what corroborates the explanation given above for the shift of q_{max} . Increasing the salt concentration induces the screening of the colloid-polymer repulsion, and so reduces dramatically the depletion attraction.

6. RESULTS

Table 6.3.2: Relevant parameters in the discussion of the dynamic analysis (Fig. 6.3.4) and comparison with the static ones. The first column shows the four studied PAM1 concentrations. Second column is the effective diffusion coefficient obtained from the short-time slope of the $f_{exp}(q, \tau)$. Third column is the mean square force used to fit the experimental data with Eq. (6.3.11). Fourth column stands for the effective diffusion coefficient derived from the static light scattering experiments. Finally, fifth column represents the mean square force, but calculated with Eq. (6.3.12) using data from the static analysis.

Samples	DYNAMIC ANALYSIS		STATIC ANALYSIS	
	$\phi_m \times 10^4$	$\frac{D_{eff}(q^*)}{D_0}$ Eq. (6.3.11)	$\frac{D_{eff}(q^*)}{D_0} (= 1/S_{cc}(q^*))$ Eq. (6.3.12)	
0.0	0.38	68801	0.38	55819
0.3	0.51	2009	0.50	6346
1.5	0.63	1394	0.62	3640
7.5	0.72	1080	0.71	2780

Dynamics Properties

In Sec. III A, we have shown that the addition of charged polymers to an originally stabilized like-charged colloidal suspensions has a deep impact on the colloidal structure factor. Using the PRISM model we were able to conclude that these changes on the colloidal microstructure are induced by the existence of an electrostatically enhanced depletion attraction. However, we still don't know how this depletion can affect the dynamic of the colloidal particles. In principle, we expect that the electrostatic depletion will also have an important influence on the dynamics, since the particle diffusion strongly depends on the particle-particle interactions [55, 56]. It is well known that the long-range repulsive interparticle interactions arising in colloidal suspensions at low electrolyte concentration reduces the particle mobility. At extremely low salinity conditions, this reduction finally leads to the loss of ergodicity (caging) [49]. However, in our experiments the electrostatic repulsion is not strong enough to induce caging [47], since in all cases the samples showed liquid behavior. As we include polymer chains in the sample, we expect that the electrostatic-enhanced depletion attraction and the subsequent increase of the electrolyte concentration will lead to an increase of the particle mobility.

In order to quantify the effect of the polymer on the colloidal dynamic, we have mea-

6.3 Paper III. Charged colloid-polymer mixtures: A study on electrostatic depletion attraction

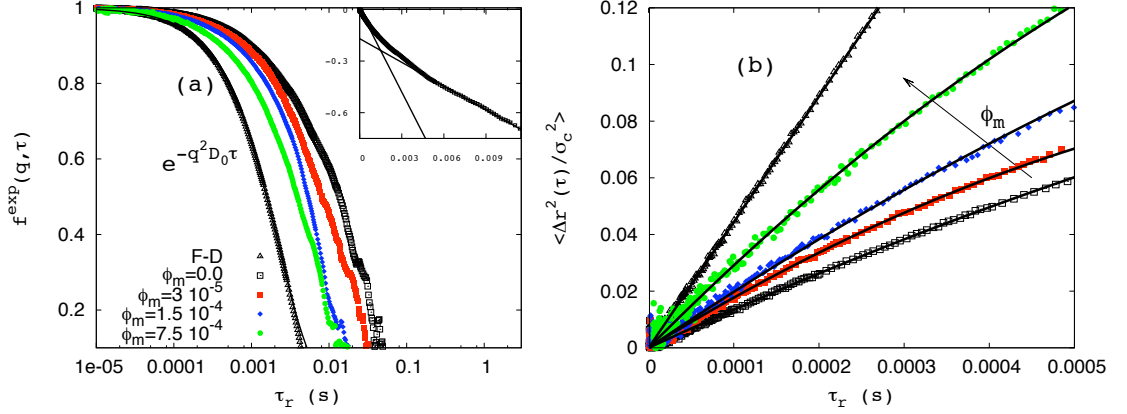


Figure 6.3.4: (a) Dynamic structure factor for two samples without polymer, diluted ($\phi_c = 0.002\%$, hollow triangles), and concentrated at $\phi_c = 0.56\%$ (hollow squares), and for three colloid-polymer mixtures using PAM1 (full symbols). All the results are shown in a common rescaled time, $\tau_r = (\sigma_c q)^2 \tau / \eta_r$. The plot shows in a semi-log scale the experimental dynamic structure factor $f^{exp}(q, \tau)$ and the fit of the diluted sample to the exponential decay $e^{-q^2 D_0 \tau}$ (solid line). The inset shows, in lineal-lineal scale, $\ln(f(q, \tau))$ for the concentrated sample (hollow square) to highlight the different diffusive regimes found for interacting particles at short (solid line) and long times (dashed line). (b) Dimensionless mean square displacement for the same samples shown in plot (a). The results are plotted in lineal-lineal scale to highlight the lineal or parabolic shapes of the curves. The fitting performed with Eq. (6.3.12) is also shown as solid lines.

sured the normalized cross-correlation function, $g_{AB}(q, \tau)$, of the mixtures at the main peak q_{max} . Then, the dynamic structure factor, $f(q_{max}, \tau)$, is obtained appealing to Eq. (6.3.2). These results are shown in Fig. 6.3.4(a) for some of the samples studied in the last section (PAM1 mixtures). Before discussing the results, it is important to emphasize that the shear-viscosity of each sample varies slightly with the polymer concentration. Also the position of the main peak of the structure factor q_{max} is different for each sample (Fig. 6.3.4). To discuss these results using a common time, we have employed a rescaled time given by $\tau_r = \frac{(\sigma_c q_{max})^2}{\eta_r} \tau$, where $\eta_r = \eta / \eta_{H_2O}$ is the relative shear-viscosity between the polymer sample, η , and water, η_{H_2O} .

Firstly, we discuss the results obtained for the two samples without polymer, one diluted ($\phi_c = 0.002\%$) with added salt (2 mM) to screen the surface charge, and another concentrated ($\phi_c = 0.56\%$) without salt, which corresponds with the reference case studied in Sec. III A. As it may be observed in Fig. 6.3.4(a), the experimental dynamic

6. RESULTS

structure factor obtained for the diluted sample (hollow triangles) is well described by the exponential decay $e^{-D_0 q^2 \tau}$, theoretically predicted for non-interacting particles [57], where $D_0 = 4.9 \times 10^{-12}$ m²/s is the Stokes-Einstein diffusion coefficient for our particles within the free-diffusion regimen (F-D). This agreement confirms that the surface charge has been screened so colloidal particles diffuse freely. On the contrary, long-range electrostatic interactions are present in the second sample without polymer (hollow squares) so that $f^{exp}(q_{max}, \tau)$ deviates notably from the single exponential decay. In fact, there are two well separated diffusive regimes at short and slightly long times, as is usually found in systems with strong repulsive interactions [see inset of Fig. 6.3.4(a)].

Fig. 6.3.4(a) also shows $f^{exp}(q_{max}, \tau)$ for the colloid-polymer mixtures with PAM1 at exactly the same experimental conditions that the ones employed in Sec. III A (see Table (6.3.1)) (similar results have been found for PAM2). The comparison between these curves provides a qualitative estimation of how the colloidal diffusivity increases as the colloid-colloid interaction is tuned by addition of polymer. As we have shown in the static section, the addition of charged polymer leads to the screening of the original long-range repulsion. From a dynamical point of view, long-range repulsion implies slower relaxation of any correlation function. Consequently, the screening of the long-range repulsion means a faster relaxation. This may be clearly appreciated in Fig. 6.3.4(b), where the mean square displacement of the particles is plotted against the rescaled time τ_r . As observed, increasing the polymer concentration leads to a larger mean square displacement, so that particles diffuse more during the same given time. The mean square displacement for the dilute sample can be fitted by a straight line, as expected for diffusion in the absence of interparticle interactions. However, as soon as colloidal interactions become important, we observe a progressive deviation from the linear behavior. According to Langevin theory [58], the first short-time correction to this linear dependence is given by the expression

$$\langle \Delta r_i^2(\tau) \rangle = 6D_0\tau \left(1 - \frac{\tau}{2f} \langle \left(\frac{\partial U}{\partial r_i} \right)^2 \rangle \right) + O(\tau^2) \quad (6.3.11)$$

where $f = 3\pi\eta\sigma_c$ is the colloidal friction coefficient and $\langle \left(\frac{\partial U}{\partial r_i} \right)^2 \rangle$ is the average square force on a i -colloid exerted by the surrounding ones. We have applied this equation to reproduce the experimental results in the short-time regime, using $\langle \left(\frac{\partial U}{\partial r_i} \right)^2 \rangle$ as fitting parameter. This expression provides a rough estimation of the mean strength on the colloidal particle. The obtained curves are shown in Fig. 6.3.4(b) as solid lines and the resulting average square forces are given in Table (6.3.2). As can be seen, this

6.3 Paper III. *Charged colloid-polymer mixtures: A study on electrostatic depletion attraction*

theoretical approach is able to capture the first-order deviation from the linear trend. The results indicate that the average square force becomes smaller as the polymer concentration increases. This agrees with the fact that the colloidal repulsion becomes weaker as we add polymer, caused by the screening of the repulsive double layers and the existence of the electrostatic-enhanced depletion attraction.

The numerical results obtained in the dynamic analysis (shown in Table (6.3.2)) have been compared with those derived from the static data. Within the static route, the average square force is given by the following integral

$$\langle (\frac{\partial(\beta U)}{\partial r})^2 \rangle = 4\pi\rho_c \int_0^\infty r^2 g_{cc}(r) (\frac{\partial(\beta V_{cc}(r))}{\partial r})^2 dr \quad (6.3.12)$$

where $g_{cc}(r)$ is the radial distribution function derived from the fitting of the experimental structure factor using the PRISM integral equations (Fig. (6.3.1)), and $\beta V_{cc}(r)$ is the pair interaction potential obtained with the PRISM in the colloidal limit, $\rho_c \rightarrow 0$. The results are shown in Table (6.3.2) together with those obtained from the dynamic analysis. As observed, the average square force predicted by the static route also decreases with the polymer concentration. However, the static route leads to different values than the ones calculated by dynamics. These discrepancies are the consequence of the strong hypothesis used in the static case. Moreover, the PRISM theory overestimates the structure factor in the limit of $q \rightarrow 0$, inducing a wrong prediction of $g_{cc}(r)$ for large r . Despite this problem, the numerical values obtained with both routes are consistent with the fact that the depletion forces arising in charged colloid-polymer mixtures have an strong effect on the colloidal dynamics.

Finally, it is well-known that the dynamic of the colloidal particles could be also affected by the solvent-induced hydrodynamic interactions (HI). However, this is not our case given the low particle concentration employed in our experiments. To corroborate this fact, we studied the dynamics at very short times, where the mean square displacement grows linearly with time. In that case, when interaction between particles is not negligible, the proportionality constant is not longer D_0 but the effective diffusion coefficient $D_{eff}(q)$, which describes the initial decay of $f(q, \tau)$. This coefficient is expected to follow the relationship $D_{eff}(q) = \frac{D_0}{S(q)}$ [57], when HI are negligible. In Table (6.3.2) we compare the $D_{eff}(q_{max})$ derived from the short-time slope of the experimental data shown in Fig. 6.3.4(b) with the ones obtained from the latter relationship using the corresponding experimental $S(q_{max})$ shown in Fig. (6.3.1). Indeed, we find that there is always good agreement between both routes within an error of $< 5\%$ which suggests

6. RESULTS

that hydrodynamics interactions do not play an important role here.

Conclusions

We show that adding small amounts of charged polymers to a charge-stabilized colloidal dispersion provokes a shift of the structure factor that can not simply explained by the screening of the electrostatic interactions neither by the standard entropic depletion interaction arising for uncharged polymer chains. With the help of the PRISM theory, we are able to conclude that this shift is the consequence of the polymer charge, as the colloid-polymer electrostatic repulsion greatly enhances the depletion attraction between colloids.

At very low electrolyte concentrations, the range of this depletion is mainly controlled by the range of the electrostatic colloid-polymer repulsion, which is given by the inverse of the Debye length. However, for larger ionic strength the polymer length also plays an important role, as larger polymers induce depletion potentials of longer range and smaller depth.

Although the addition of polymers also leads to the increase of the ionic strength of the sample and the subsequent screening of the electrostatic interactions, we observe that the enhanced depletion attraction is still strong enough to induce an attractive well at intermediate distances in the colloid-colloid interaction potential.

We also study the dynamic properties of the colloidal suspensions in the limit of very short times, and show that the addition of charged polymer coils enhances the colloidal diffusivity. At intermediate times, the deviation of the mean square displacement from the linear time-dependence is interpreted in terms of the average square force acting on the colloids. The results show that the average square force, and so the overall colloid-colloid repulsive strength, decreases with the polymer concentration. Qualitative agreement of the latter is found determining the average of the square force with Eq. (6.3.12). Nevertheless, more sophisticated theoretical models for improving the PRISM are necessary in order to find quantitative agreement between the static and dynamic predictions.

Finally, it would be very interesting to investigate the effect of the electrostatic depletion attraction on the long-time behavior of the dynamic structure factor ($\tau \gg \frac{\sigma_c^2}{D_0}$).

6.3 Paper III. *Charged colloid-polymer mixtures: A study on electrostatic depletion attraction*

New experiments are planned to address this question and to study the dependence of the long-time diffusion coefficient as a function of the polymer concentration.

Acknowledgments

The authors are grateful to “MICINN” (Project No. MAT2009-13155-C04-02) ERDF Funds and “Junta de Andalucía” (Excellency Project P07-FQM-02517 and P07-FQM-02496) for financial support. The authors would like to thank J. Forcada for the latex samples, J. J. Iruin for discussions on polymers and J. de Vicente for the viscosities measurements. M. P.-F. would also like to thank S. Roldán-Vargas for helpful discussions.

References

- [1] P. N. Pusey, A. D. Pirie, and W. C. K. Poon, *Physica A* **201**, 322 (1993).
- [2] T. Eckert and E. Bartsch, *Phys. Rev. Lett.* **89**, 125701 (2002).
- [3] A. P. Gast, W. B. Russell, and C. K. Hall, *J. Colloid Interface Sci.* **96**, 1977 (1983).
- [4] R. Mezzenga, P. Schurtenberger, A. Burbidge, and M. Michael, *Nature (London)* **4**, 729 (2005).
- [5] P. J. Lu, J. C. Conrad, H. M. Wyss, A. B. Schofield, and D. A. Weitz, *Phys. Rev. Lett.* **96**, 028306 (2006).
- [6] P. J. Lu, E. Zaccarelli, F. Ciulla, A. B. Schofield, F. Sciortino, and D. Weitz, *Nature (London)* **453**, 499 (2008).
- [7] S. Asakura and F. Oosawa, *J. Chem. Phys.* **22**, 1255 (1954);, *J. Polym. Sci.* **33**, 183 (1958).
- [8] H. N.W. Lekkerkerker, W. C. Poon, P. N. Pusey, A. Stroobants, and P. B. Warren, *Europhys. Lett.* **20**, 559 (1992).
- [9] M. Fuchs and K. S. Schweizer, *J. Phys.: Condens. Matter* **14**, R239 (2002).
- [10] V. Krakoviack, J. P. Hansen, and A. A. Louis, *Europhys. Lett.* **58**, 53 (2002).
- [11] A. A. Louis, P. G. Bolhuis, E. J. Meijer, and J. P. Hansen, *J. Chem. Phys.* **117**, 1893 (2002).
- [12] A. R. Denton and M. Schmidt, *J. Chem. Phys.* **122**, 2449111 (2005).
- [13] M. Peláez-Fernández, A. Moncho-Jordá, and J. Callejas-Fernández, *Europhys. Lett.* **90**, 46005 (2010).
- [14] L. Belloni and P. G. Ferreira, *Phil. Trans. R. Soc. Lond. A* **359**, 867 (2001).
- [15] S. Buzzaccaro, R. Piazza, J. Colombo, and A. Parola, *J. Chem. Phys.* **132**, 124902

6. RESULTS

(2010).

- [16] J. Y. Walz and A. Sharma, *J. Colloid Interface Sci.* **168**, 485 (1994).
- [17] O. Mondain-Monval, F. Leal-Calderon, J. Phillip, and J. Bibette, *Phys. Rev. Lett.* **75**, 3364 (1995).
- [18] L. Helden, G. H. Koenderink, P. Leiderer, and C. Bechinger, *Langmuir* **20**, 5662 (2004).
- [19] A. I. Campbell, V. J. Anderson, J. S. van Duijneveldt, and P. Bartlett, *Phys. Rev. Lett.* **94**, 208301 (2005).
- [20] G. Petekidis, L. A. Galloway, S. U. Egelhaaf, M. E. Cates, and W. C. K. Poon, *Langmuir* **18**, 4248 (2002).
- [21] D. Chandler and H. D. Andersen, *J. Chem. Phys.* **57**, 1930 (1972).
- [22] K. S. Schweizer and J. G. Curro, *Adv. Chem. Phys.* **98**, 1 (1997).
- [23] A. P. Chatterjee and K. S. Schweizer, *Macromolecules* **31**, 2353 (1998).
- [24] Y. L. Chen and K. S. Schweizer, *J. Chem. Phys.* **120**, 7212 (2004).
- [25] M. Dymitrowska and L. Belloni, *J. Chem. Phys.* **109** 4659 (1998); *J. Chem. Phys.* **111**, 6633 (1999).
- [26] A. Búcsi, J. Forcada, S. Gibanel, V. Héroguez, M. Fontanille, and Y. Gnanou, *Macromolecules* **31**, 2087 (1998).
- [27] B. J. Berne and R. Pecora, *Dynamic Light Scattering* (Wiley, New York, 1976).
- [28] G. Phillies, *J. Chem. Phys.* **74**, 260 (1980).
- [29] A. Moussad and P. N. Pusey, *Phys. Rev. E* **60**, 5670 (1999).
- [30] . Palberg, W. Hrtl, U. Witting, H. Versmold, M. Würth, and E. Simnacher, *J. Phys. Chem.* **96**, 8180 (1992).
- [31] P. N. Pusey and W. Van Megen, *Physica A* **157**, 705 (1989).
- [32] P. Debye and E. Hückel, *Phys. Z.* **24**, 185 (1923).
- [33] P. González-Mozuelos and M. Olvera de la Cruz, *Phys. Rev. E* **79**, 031901 (2009).
- [34] R. Koyama, *Macromolecules* **17**, 1594 (1984); **19**, 178 (1986).
- [35] P. G. Ferreira, M. Dymitrowska, and L. Belloni, *J. Chem. Phys.* **113**, 9849 (2000).
- [36] E. Buhler and F. Boué, *Euro. Phys. J. E* **10**, 89 (2003).
- [37] K. G. Honnell, K. S. Schweizer, and J. G. Curro, *Macromolecules* **23**, 3496 (1990).
- [38] T. Gisler, S. F. Schultz, M. Borkovec, H. Sticher, P. Schurtenberger, B. D’Aguanno, and R. Klein, *J. Chem. Phys.* **101**, 9924 (1994).
- [39] N. Garbow, M. Evers, T. Palberg, and T. Okubo, *J. Phys.: Condens. Matter* **16**, 3835 (2004).
- [40] M. Quesada-Pérez, J. Callejas-Fernández, and R. Hidalgo-Álvarez, *Adv. Colloid Interface Sci.* **95**, 295 (2002).

6.3 Paper III. *Charged colloid-polymer mixtures: A study on electrostatic depletion attraction*

- [41] M. Quesada-Pérez, J. Callejas-Fernández, and R. Hidalgo-Álvarez, *Phys. Rev. E* **61**, 574 (2001).
- [42] G. S. Manning, *J. Chem. Phys.* **51**, 924 (1969).
- [43] T. Odjik, *Physica A* **278**, 347 (2000).
- [44] H. Benoit and P. Doty, *J. Phys. Chem.* **57**, 958 (1953).
- [45] J. Skolnick and M. Fixman, *Macromolecules* **10**, 944 (1977).
- [46] R. Tuinier, E. ten Grotenhuis, C. Holt, P. A. Timmins, and C. G. de Kruif, *Phys. Rev. E* **60**, 848 (1999).
- [47] K. N. Pham, S. U. Egelhaaf, P. N. Pusey, and W. C. K. Poon, *Phys. Rev. E* **69**, 011503 (2004).
- [48] X. Ye, T. Narayanan, P. Tong, J. S. Huand, M. Y. Lin, B. L. Carvalho, and L. J. Fetters, *Phys. Rev. E* **54**, 6500 (1996).
- [49] M. Laurati, G. Petekidis, N. Koumakis, F. Cardinaux, A. B. Schofield, J. M. Brader, M. Fuchs, and S. U. Egelhaaf, *J. Chem. Phys.* **130**, 134907 (2009).
- [50] S. A. Shah, S. Ramakrishnan, Y. L. Chen, K. S. Schweizer, and C. F. Zukoski, *Langmuir* **19**, 5128 (2003).
- [51] S. A. Shah, Y. L. Chen, K. S. Schweizer, and C. F. Zukoski, *J. Chem. Phys.* **118**, 3350 (2003);, **119**, 8747 (2003).
- [52] M. Fuchs and K. S. Schweizer, *Phys. Rev. E* **64**, 021514 (2001).
- [53] J. P. Hansen and I. R. McDonald, *Theory of Simple Liquids* (Academic, New York, 1976).
- [54] A. A. Louis, *J. Phys.: Condens. Matter* **14**, 9187 (2002).
- [55] G. Nägele, *Phys. Rep.* **272**, 215 (1996).
- [56] J. L. Arauz-Lara and M. Medina-Noyola, *Physica A* **122**, 547 (1983).
- [57] P. N. Pusey, *Liquids, Freezing and the Glass Transition*, Les Houches Summer School Proceedings Session S1, edited by D. Levesque, J. P. Hansen, and J. Zinn-Justin (North-Holland, Amsterdam, 1981).
- [58] R. J. A. Tough, P. N. Pusey, H. N. W. Lekkerkerker, and C. van den Broeck, *Mol. Phys.* **59**, 595 (1986).
- [59] X. Cao, R. Bansil, D. Gantz, E. W. Moore, N. Niu, and N. H. Afdhal, *Biophys. J.* **73**, 1932 (1997).

6. RESULTS

6.4 Paper IV. *The structure of charged colloid-polymer binary mixtures:
From like Wigner glass systems to fluid of clusters*

6.4 Paper IV. *The structure of charged colloid-polymer
binary mixtures: From like Wigner glass systems to
fluid of clusters*

6. RESULTS

**6.4 Paper IV. *The structure of charged colloid-polymer binary mixtures:
From like Wigner glass systems to fluid of clusters***

**The structure of charged colloid-polymer binary mixtures:
From like Wigner glass systems to fluid of clusters, Phys.
Rev. E (under revision)**

¹M. Peláez-Fernández, ²S. García-Jimeno, ¹A. Moncho-Jordá, ²J. Estelrich and ¹J. Callejas-Fernández

¹Departamento de Física Aplicada, Grupo de Física de Fluidos y Biocoloides, Universidad de Granada, E-18071 Granada, Spain.

²Departament de Fisicoquímica, Facultat de Farmàcia, Universitat de Barcelona, E-08028 Barcelona, Catalonia, Spain.

6. RESULTS

Abstract

The effect of adding charged non-adsorbing polymers to electrostatically structured suspensions of charged liposomes has been experimentally studied by light scattering techniques. The static structure factor of the mixtures is explored using two polymers of different sizes. As the polymer concentration increases, the main peak of structure factor decreases and shows an important shift to larger values of the scattering vector. Such displacement is the consequence of the entropic and mainly electrostatic-enhanced depletion attraction induced by the polymers that counteract the electrostatic repulsion. For the shorter polymer, the system remains stable for all studied polymer concentrations. However, for the larger polymer chains the effective attraction is strong enough to induce the aggregation of the liposomes, in such a way that clusters and particles coexist during several days in the sample. In general, the clusters have a low fractal dimension, which corresponds to linear and ramified structures.

Introduction

Complex fluids are usually found in technological products, biological fluids, foods, etc. They are formed by mixtures of different types of colloids (synthetic particles, proteins, polymers, ...). The characterization and knowledge of binary mixtures, i.e., two components immersed in a solvent, represents a first step in a further comprehension of those more complex systems. One of the most studied binary mixture is the formed by neutral sterically stabilized colloids and non-adsorbing polymers [1-3]. Simulation and experimental results show that the presence of neutral polymers in a colloidal sample has a deep impact on the structural and dynamical properties. This leads to a very rich phenomenology, including the formation of gels, glasses or fluids of clusters [4-9], where the driven mechanism is mainly the so-called entropic depletion attraction [10, 11]. For mixtures of charged colloidal particles and uncharged polymer coils, there is a competition between the long-range electrostatic repulsion and the short-range entropic depletion attraction. For these systems the colloidal structure goes from electrostatically stabilized colloidal clusters to the formation of attractive gels [5, 12-19].

Recently, the attention has been drawn to colloid-polymer mixtures where both species are like-charged. Here, the electrostatic repulsion between colloids and polymers enhances the effective depletion attraction between colloids. The existence of such long-range electrostatic depletion has been confirmed theoretically [20], by means of computer simulations [21] and experiments [22-27]. The resulting depletion attraction arising in this kind of systems is very strong even at small polymer concentrations, where the entropic depletion is negligible. Moreover, its range can be tuned by changing the electrolyte concentration in the suspension and the polymer radius of gyration, R_g . In spite of these studies, more efforts are required to understand the colloidal microstructure, dynamic, phase separation and gel formation.

In this article, we perform an experimental study on the structure of mixtures formed by a charged colloids (liposome) and like-charged non-adsorbing polymers immersed in water. Reviewing the literature, most of the experimental works regarding charged colloid-polymer mixtures employ weakly charged colloids, so that the repulsive electrostatic interaction are easily overcome by the depletion attraction induced by the polymer [4, 17]. Under this situation, the colloidal particles can be arrested into an attractive gel, that arises as the consequence of the attractive bonds between colloids. However, our experimental studies strongly differs from this procedure. Here, we start

6. RESULTS

from a quasi-arrested colloidal systems (a low-density Wigner glass [28-30]), in such a way that the addition of polymer coils of different lengths causes an increase of the particle mobility and a weakening of the colloidal microstructure, that can be explained in terms of the competition between electrostatic and depletion interactions.

This interplay between long-range electrostatic repulsion and short-range depletion attractive interactions points out a noticeable phenomenology [31]. In particular, it has been observed that the electrostatic repulsion between the colloidal double layers is counteracted by the entropic and mainly electrostatically-enhanced depletion attraction induced by the charged polymer. We find that the addition of short polymer coils causes a weak screening of the electrostatic repulsion. However, for long polymers the depletion attraction is strong enough to induce the formation of clusters and finally the phase separation of the mixture. Static (SLS) and dynamic light scattering (DLS) techniques are used to follow the structure of the mixtures.

This paper is organized as follows. In Section II we briefly describe the experimental setup and the characteristics of the liposome and polymer samples employed in this work. The results and discussions are shown in Section III, and the main conclusions are summarized in Section IV.

Materials and methods

In the experiments, different concentrations of phosphatidylserine (PS) liposomes dispersed in purified water are used. Via the measure and fit of their form factor $P(q)$ in dilute suspensions, a mean liposome radius of $R_c = 120$ nm and polydispersity (relative standard deviation) of about 0.3 are obtained. As a consequence of the extrusion procedure [32], the liposomes showed a lipid bilayer with thickness of about 4.5 nm. The liposome dispersions have a refractive index only slightly different to 1.33 (water), allowing the preparation of nearly transparent suspensions at relatively high volume fractions [33]. Consequently, these colloidal systems allow us to explore the structure and dynamic of concentrated suspensions reducing the multiple scattering effects. Due to the specific ionization of the PS molecule in water, the liposomes are negatively charged, having an electrophoretic mobility of about $-2.1 \times 10^{-8} \text{m}^2 \text{V}^{-1} \text{s}^{-1}$. The polymers are two different Polyacrylamide (Polysciences, Inc.) of molecular weights $(0.6 - 1) \cdot 10^6$ g/mol (catalog number 19901) and $5 \cdot 10^6$ g/mol (catalog number 21485), henceforth denoted by PAM-short and PAM-long, respectively. Their radius of gyration obtained

**6.4 Paper IV. *The structure of charged colloid-polymer binary mixtures:
From like Wigner glass systems to fluid of clusters***

via Zimm-Plot diagrams are 25 nm (PAM-short) and 50 nm (PAM-long). Although the manufacturer presents both products as non-ionic polymers, they are slightly negative-charged when immersed in distilled water at low ionic strength, due to the dissociation of the acrylamide monomers. This was experimentally confirmed by electrophoretic mobility measurements ($\mu_e \approx -0.9 \times 10^{-8} \text{ m}^2\text{V}^{-1}\text{s}^{-1}$ and $\mu_e \approx -1.1 \times 10^{-8} \text{ m}^2\text{V}^{-1}\text{s}^{-1}$ for PAM-short and PAM-long, respectively).

The light scattering experiments were performed using a three-dimensional DLS spectrometer (LS instruments, Fribourg-Switzerland) [34]. The scattered light was collected using two avalanche photodiodes and the corresponding cross-correlation function was calculated within a digital correlator. According to this design, the time-dependent contributions of multiple scattered photons can be neglected [35]. Omitting multiplicative factors, the experimental structure factor of the samples may be determined using the following equation [36]

$$S(q) \propto \sqrt{\frac{\langle I_A^{cp}(q) \rangle \langle I_B^{cp}(q) \rangle g_{AB}^{cp}(q, \tau = 0) - 1}{\langle I_A^0(q) \rangle \langle I_B^0(q) \rangle g_{AB}^0(q, \tau = 0) - 1}} \quad (6.4.1)$$

where $\langle I_i^{cp}(q) \rangle$ is the total time-averaged intensity registered by the detectors $i = A$ and B , whereas $\langle I_i^0(q) \rangle$ corresponds to the intensity of a dilute liposome suspension. The ratio $\frac{g_{AB}^{cp}(q, \tau = 0) - 1}{g_{AB}^0(q, \tau = 0) - 1}$ corrects the magnitude of the structure factor due to the q -dependent disturbance of the multiple scattering [35, 37] in a cross-correlation experiment, where $g_{AB}^i(q, \tau) = \frac{\langle I_A^i(q, t + \tau) I_B^i(q, t) \rangle}{\langle I_A^i(q) I_B^i(q) \rangle}$ is the normalized cross-correlation function of the registered intensities. In our colloid-polymer mixtures, the intensity scattered by the polymers was always very small compared to the one by liposomes, so that the experimental structure factor obtained is directly the liposome-liposome structure factor $S_{cc}(q)$.

Using both polymers, two kinds of mixtures were prepared. In the first one, liposomes and polymers were mixed without adding ion-exchanger resins. Under these conditions, all samples with PAM-short formed stable dispersions and did not show any noticeable change during weeks. On the contrary, with PAM-long the initially homogeneous suspensions became unstable in a time scale of one week, after that a rich colloid zone was observed in the bottom of the cell, indicating a phase separation between liposomes and polymers. These results clearly indicate that long polymers induce a stronger depletion attraction than the short ones.

6. RESULTS

In the second kind of samples, the mixtures were prepared with a fixed amount of ion-exchanger resins in order to remove all the ionic impurities of the sample, so that the electrostatic interactions were reinforced. The samples were tumbled during a couple of hours after the preparation of the mixture to assure the low ionic strength condition in the systems. After one day, the mixtures were transferred to a thinner cylindrical quartz glass cell. This allows as to minimize the attenuation caused by the non-illuminated remaining sample and to remove the possible angular distortion of the resin in the light scattering pattern. Then, the light scattering experiments were carried out. The measurements were performed at a temperature of $T = 25^\circ\text{C}$, within a wide angular range going from 20° to 150° , with a resolution of 2° . For PAM-short, the mixtures showed a homogeneous aspect that persisted during very long time. Quite differently is the behaviour found with PAM-long. Now, the mixtures were apparently homogeneous within the first 2 days after preparation. However, after the third day, the system undergoes a visible phase separation into a concentrated and a diluted colloidal phase. Therefore, the measurements with PAM-long were performed in a metastable state where the system is under phase separation. This means that our measurements contain information about the process that finally leads to a phase separation, but they are collected during an initial period where the system is evolving slowly but still in a single phase.

Results and discussion

Figure 6.4.1(a) depicts the experimental static structure factor $S_{cc}(q)$ calculated via eq. (6.4.1) for different liposome volume fractions ($\phi_c = 0.1, 0.12, 0.14$ and 0.17 , respectively) without added polymer. As may be observed, a well defined peak is obtained as a consequence of the interparticle electrostatic repulsion. By increasing the liposome concentration, the peak height grows and its position, q^* , shifts to higher q -values, what agrees with the expected trend observed for fluid-like structures formed in the presence of repulsive interactions. The position and height of the main peak have been fitted using a Yukawa interaction potential and the Ornstein-Zernike integral equation within the HNC approximation. According to this, the effective charge of the liposomes is given by $180 e^-$ for an electrolyte concentration of 10^{-6}M . The large value of the peak width is reminiscent of the polydispersity of the liposome sample. The height of the peak reaches a value of 2.5 for the larger particle concentrations. This is close to the critical value 2.8 predicted by the Hansen-Verlett criterion for a monodisperse repulsive

6.4 Paper IV. *The structure of charged colloid-polymer binary mixtures: From like Wigner glass systems to fluid of clusters*

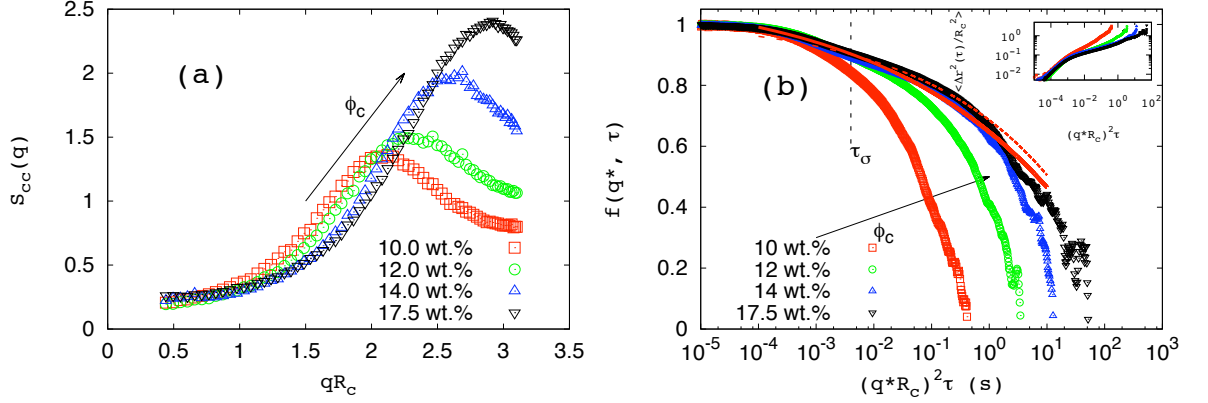


Figure 6.4.1: Panel (a) shows the liposome-liposome structure factor, $S_{cc}(q)$, for increasing liposome concentrations ϕ_c as a function of the dimensionless scattering vector qR_c . The normalized dynamic structure factor, measured at the peak q^* , is shown in panel (b) versus a rescaled correlation time. The lines in panel (b) correspond with the best fit according to the MCT theory. The inset in panel (b) represents the liposome mean-square displacement $\langle \Delta r^2(\tau) \rangle / R_c^2$ derived from $f(q^*, \tau)$.

glass. This means that although the colloidal particles are in the fluid state, they are almost arrested by the repulsive interactions [39].

By measuring the normalized intensity cross-correlation, $f(q^*, t)$ was obtained appealing to the Stiegert relationship $f(q, \tau) = \frac{1}{A} \sqrt{g_{AB}(q, \tau) - 1}$, where A is a parameter mainly dependent on the experimental conditions. Figure 6.4.1(b) shows $f(q^*, \tau)$ obtained at the main peak of $S_{cc}(q)$ for the same liposome samples. The measurements were performed during 3500 s that is a long enough time to guarantee good statistics and to capture the full decay of the dynamic structure factor. In all cases, $f(q^*, t)$ deviates notably from the single exponential decay of free liposomes, what is a straightforward consequence of the long-range electrostatic repulsive interactions. This repulsion is able to induce a highly structured system, but is not strong enough to induce the total caging of the particles. Indeed, $f(q^*, t)$ always decays to zero, with a relaxation time that increases with the liposome concentration. Although the liposome dispersion behave as a non-arrested colloidal fluid, the shape of the curves clearly resembles the one obtained for an arrested Wigner glass [28]. In particular, they show multistep relaxations (specially at the largest particle concentration), typically observed in concentrated colloidal dispersions close to the glass transition [40]. Figure 6.4.1(b) also depicts the

6. RESULTS

two β -decays, indicating the bounded motion of the liposomes inside their cages. Both decays are followed by the cage break-up (α -decay) which is hardly captured even during a long-time DLS experiment. As it is well known, Mode Coupling Theory (MCT) is able to describe these dynamical behaviour [40, 42, 43]. From the fit of $f(q^*, \tau)$, both the a parameter corresponding to the first β -decay ($f(q^*, \tau) - f(q^*, \infty) \propto (\tau)^{-a}$) and b parameter, the second β -decay, ($f(q^*, \tau) - f(q^*, \infty) \propto -(\tau)^b$) can be calculated. For this task, τ_D is defined as the time when $f(q^*, \tau)$ shows the inflection points. Figure 6.4.1(b) includes the corresponding fits for $\phi_c = 0.17$ to obtain a (solid line) and b (dashed line). They are given by $a = 0.135$ and $b = 0.20$, that satisfy the relation $\frac{\Gamma(1-a)^2}{\Gamma(1-2a)} = \frac{\Gamma(1+b)^2}{\Gamma(1+2b)}$, where Γ is the Euler function. Also, the inset of Figure 6.4.1(b) plots the mean square displacement of the liposomes calculated through $\langle \Delta r^2(\tau) \rangle = -\frac{6}{q^2} \ln(f(q^*, \tau))$. The decrease of the slope at intermediate times, as much as ϕ_c increases, clearly supports the idea that liposomes are confined into their electrostatic-origin cages.

Figures (6.4.2) and (6.4.3) depict the experimental $S_{cc}(q)$ for liposome-polymer mixtures using three different liposome volume fractions for PAM-short and PAM-long, respectively. The curves without added polymer are also included for comparison. First, we analyze the effect of adding PAM-short. As may be observed in fig. (6.4.2), the position of the main peak of the structure factor moves to high q -values while their height and width decreases and broadens, respectively. For the lowest liposome concentration (fig. 6.4.2(a)) the shift of the main peak is indeed very important even at the small polymer concentrations employed in the experiments, implying that the liposomes are approaching each other. This effect is caused by a driving interaction counteracting the colloid-colloid electrostatic repulsion. However, it should be emphasized that such displacement is very large compared to the one obtained assuming only the double layer screening induced by the presence of charged polymers in the solution. This means that attractive depletion interactions will play a key role in the equilibrium structure factor as is demonstrated on [25].

In order to understand this effect, we need to account for all the effective interactions arising in the liposome-polymer mixture. In fact, including charged polymers implies three different effects to the liposome-liposome interaction. Firstly, the extra charge of the polymer (and the corresponding electrolyte concentration necessary for the electroneutrality of the mixture) induces the above commented screening of the repulsive electrostatic double layers. Secondly, the electrostatic repulsion between liposomes and

6.4 Paper IV. *The structure of charged colloid-polymer binary mixtures:
From like Wigner glass systems to fluid of clusters*

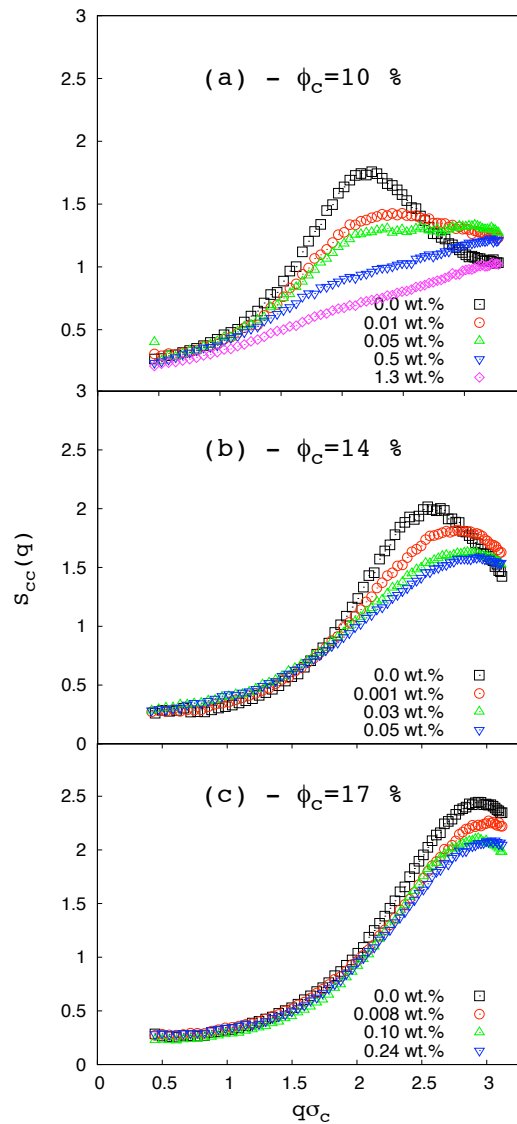


Figure 6.4.2: Liposome-liposome structure factor for liposome-polymer mixtures with PAM-short, at different liposome packing fractions: $\phi_c = 0.1$ (a), 0.14 (b) and 0.17 (c). Polymer concentrations are given using different type of symbols (see the legends).

6. RESULTS

polymers causes a depletion region around the liposomes. For small polymer concentration, the size of this region is very large compared to the polymer length, and the result is an important enhanced and long-ranged depletion attraction between liposomes. The origin of this depletion is mainly electrostatic. For large polymer concentrations, the screening of the double layers also reduces the range and magnitude of this electrostatic depletion. The third effect of adding polymer is caused by the excluded volume interactions between polymers and liposomes, which induces an entropic depletion attraction between liposomes. The range of this depletion is roughly equal to $2R_g$ and its strength is nearly proportional to the polymer density. The competition between these effects has been discussed in previous papers working on dilute suspensions of charged latex particles [25-26]. In the current case, the large liposome packing fraction employed in the experiments suggests that both entropic and electrostatic depletion will both contribute to the final microstructure of the binary mixtures.

At higher liposome packing fractions (fig. 6.4.2 (b)-(c)) the shift of $S_{cc}(q^*)$ becomes smaller. However, it does not mean that the polymer-induced effective depletion attraction is less important here, as the depletion interaction only depends on the solvent and polymer properties. For higher liposome packing fraction, the particles are closer to each other and so they feel a stronger and sharper repulsive electrostatic barrier. Under this situation, the effect of adding an attractive contribution to the total interparticle interaction is only to slightly reduce this repulsive barrier, leading to a small approach between liposomes.

We have tried to fit these experimental results, without success, with a theoretical model (PRISM [41]). Although it was corroborated that PRISM is a suitable description for charged colloid-polymer mixtures [25, 26], we have to note that it is not accurate for the description of our polydisperse suspensions [44].

Next, we discuss the results with PAM-long, figure (6.4.3). By increasing its concentration, similar trends are found, i.e., a weakening and displacement of the main peak of the structure factor to larger q -values. However, there are important differences comparing with the structure factor measured with PAM-short. Now, a larger peak displacement is observed. Moreover, increasing the concentration of PAM-long leads to a noticeable upturn of $S_{cc}(q)$ at low q -values. Although our observation window is not wide enough, the trends shown by $S_{cc}(q)$ are consistent with the evidence of a second peak at low q . This results points out the existence of an aggregation process between

6.4 Paper IV. *The structure of charged colloid-polymer binary mixtures:
From like Wigner glass systems to fluid of clusters*

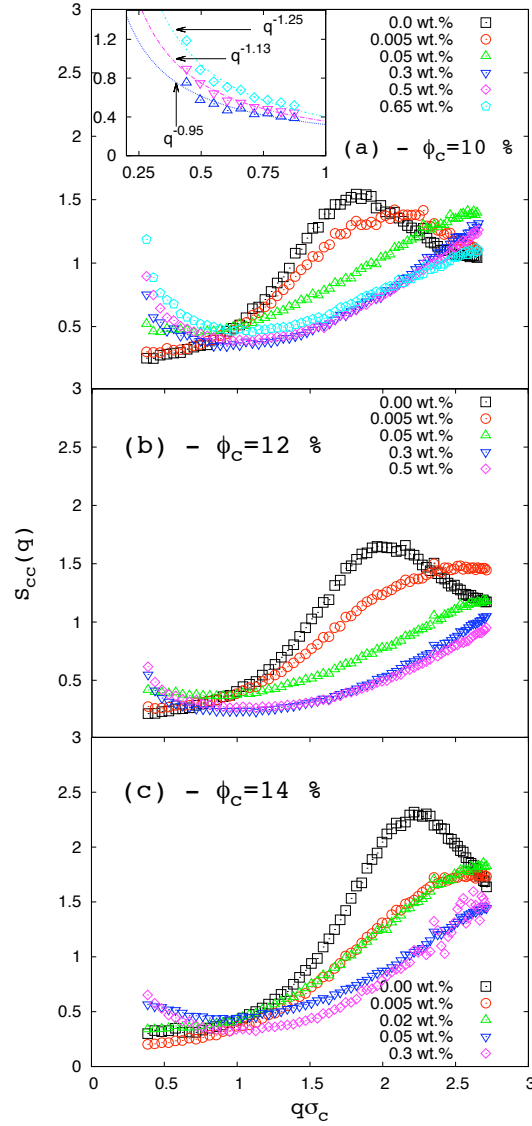


Figure 6.4.3: Liposome-liposome structure factor for liposome-polymer mixtures with PAM-long, at different liposome packing fractions: $\phi_c = 0.1$ (a), 0.12 (b) and 0.14 (c). Polymer concentrations are shown using different type of symbols (see the legends). The inset in panel (a) shows the $S_{cc}(q)$ at short q -values for the three higher polymer concentrations: 0.3 , 0.5 and 0.65 wt.%. Lines stand for the best fit using the power law $S_{cc}(q) \propto q^{-d_f}$.

6. RESULTS

liposomes resulting from the competition between long-range electrostatic repulsions and the depletion attraction induced by the charged polymers. PAM-long can induce a stronger and longer-range depletion forces than the ones created by the PAM-short. Indeed, this behavior resembles the one obtained in the formation of clusters in neutral and charged binary mixtures, as has been reported experimentally [6-8]) and by computer simulation [12, 28]. In this framework, the aggregation process induced by depletion attractions and the different routes leading to gelation are still controversial subjects [12, 14]. There is a wide literature focused on mixtures of hard-sphere colloids and non-adsorbing uncharged polymers where the entropic depletion is the only mechanism causing the phase separation [6-8, 19]. However, less is known about the aggregation process arising in binary mixtures when both colloids and polymers are charged, or when the polymer-colloid size ratio is high [19].

For small amounts of PAM-long, the liposomes still repel each other strongly and they persist in a nearly Wigner glass. This structure is the origin of the peak of the structure factor located at high q . For larger amounts of polymer, the screening of the double layers plus the polymer-induced depletion attraction are able to break the repulsive cages and allow the liposomes to approach each other. The experiments suggest that the depletion is strong enough to counterbalance the electrostatic repulsion and induce the aggregation of the liposomes that stick together by short-range London-van der Waals attractions. Therefore, the peak at low q -value corresponds with clusters separated by several particles diameters, although our q -range does not allow to determine the exact location of this peak. Under these conditions, the system is composed by a mixture of particles and clusters.

In our opinion, the stronger attraction induced by PAM-long can be related with a larger entropic contribution to the depletion due to the size. As an example, at $\phi_c = 10\%$ and 0.05 wt. %, i.e., using the same colloid and polymer concentrations, (see figs. 6.4.2(a) and 6.4.3(a)), the aggregation is only observed with PAM-long. In this case, the typical surface-surface liposome distance is about 80 – 90 nm, so the PAM-short can get inside the inter-liposome space the PAM-long cannot. Consequently, entropic depletion would be only expected for the mixtures with PAM-long. For higher ϕ_c the typical surface-surface distance diminishes and the entropic depletion would be stronger for PAM-long and even would appear for PAM-short at the higher liposome concentrations. Nevertheless, this pure entropic analysis is disturbed by the presence of charge on colloids and polymers. Although both contributions (entropic and electrostatic) cannot be sep-

6.4 Paper IV. *The structure of charged colloid-polymer binary mixtures: From like Wigner glass systems to fluid of clusters*

arated from each other, entropic depletion represents an additional effect that explain the aggregation observed only in the PAM-long case.

Here, we also provide experimental evidences of the aggregation process in charged liposome-polymer mixtures, using PAM-long. As usually, the cluster morphology is characterized by means of its fractal dimension d_f . It has been calculated from the fitting of the $S_{cc}(q)$ using the power law $S(q) \sim q^{-d_f}$ (see inset of Figure 6.4.3(a)), in the corresponding q range ($R_{agg}^{-1} \leq q \leq R_c^{-1}$, where R_{agg} is the hydrodynamic aggregate radius).

The low fractal dimensions obtained (see inset in fig. 6.4.3(a)) suggests that liposomes coagulate into linear clusters. In this sense, our experimental results agree with the observations of Campbell [14], who obtains chain-like aggregates, and Sedgwick [15], where mixtures of particles and chain-like clusters are found. On the contrary, our results disagree with other experimental evidences in fluid of clusters induced by depletion attractions [7], where the clusters are compact structures with larger fractal dimensions, 2.4 – 2.6. The reason for this discrepancy can be attributed to two effects. First, the reminiscent electrostatic repulsions between liposomes that favour the aggregation at the tips of the cluster. Secondly, due to the very strong short-range of van der Waals attractions, the bonds between liposomes forming the cluster are almost irreversible, impeding the particle reorganization inside the aggregate. It can be observed that the fractal dimension slightly grows with the polymer concentration, see inset in fig. 6.4.3(a), which can be also understood in terms of the competition between electrostatic repulsion and depletion attraction. Indeed, a higher polymer concentration implies the screening of the Coulombic forces and an increase of the entropic depletion attraction and in some cases also the electrostatic one [25]. Therefore, with weaker repulsive interactions the aggregation takes place in more internal regions of the clusters leading to the slightly increase of d_f . In principle, these clusters will grow until they reach a critical total charge that is large enough to compensate the depletion attraction. However, in our case the clusters formed by addition of PAM-long are not stable, as they keep slowly growing during several days, and finally the system phase-separate after 3 days into two phase.

Conclusions

It has been shown that the addition of charged polymers to charged stabilized lipo-

6. RESULTS

some suspensions at low electrolyte concentration leads to significant changes on the structure of liposome suspensions. The displacement of the main peak of the structure factor can be only explained in terms of an induced long-range attraction. This is mainly explained by the electrostatic depletion attraction, arising by the fact that charged polymers are depleted from the surrounding region around the liposomes as a consequence of the electrostatic liposome-polymer repulsion. However, a stronger induced attraction for the larger polymer has been documented which support the fact that entropic depletion is also relevant in our experiments.

What is more, the polymer length has an important effect on the stability of the mixture. For the shorter polymer chain the suspensions remain stables while the addition of the longer one destabilizes the suspensions, inducing the aggregation of the liposomes. This fact has been experimentally confirmed by the evidence of two peaks in the liposome structure factor, the first one at large q -values (particle-particle) and the second at very low q (cluster-cluster). For small polymer concentrations, the liposome-liposome electrostatic repulsion is not totally counteracted and the aggregation occurs in the external regions of the clusters, leading to almost linear fractal objects. For larger polymer concentrations, the screening of the double layer repulsion allows the free diffusion of particles and clusters, more branched structures are formed and, for that reason, we have obtained an increase of the measured fractal dimension that approaching the value predicted by DLCA.

Acknowledgments

The authors are grateful to “MICINN” (Project No. MAT2009-13155-C04-02 and MAT2009-13155-C04-03) ERDF Funds and “Junta de Andalucía” (Excellency Project P07-FQM-02517 and P07-FQM-02496) for financial support. We would also like to thank S. Roldán-Vargas for helpful discussions and R. Barnadas for advises in the synthesizing of PS liposomes.

References

- [1] W. C. K. Poon, *J. Phys.: Condens. Matter*, **14**, R859-R880 (2002).
- [2] A. P. Gast, W. B. Rüssell and C. K. Hall, *J. Colloid Interface Sci.* **96**, 1977 (1983).
- [3] H. N. W. Lekkerkerker, W. C. Poon, P. N. Pusey, A. Stroobants and P. B. Warren, *Europhys. Lett.* **20**, 559 (1992).

**6.4 Paper IV. *The structure of charged colloid-polymer binary mixtures:
From like Wigner glass systems to fluid of clusters***

- [4] P. N. Segre, V. Prasad, A.B. Schofield and D.A. Weitz, *Phys. Rev. Lett.* **86**, 6042 (2001).
- [5] H. Sedgwick, S. U. Egelhaaf and W.C. K. Poon, *J. Phys.: Condens. Matter* **16**, S4913 (2004).
- [6] S. Manley, H. M. Wyss, K. Miyazaki, J. C. Conrad, V. Trappe, L. J. Kaufman, D. R. Reichman and D.A. Weitz, *Phys. Rev. Lett.* **95**, 238302 (2005).
- [7] P. J. Lu, J. C. Conrad, H. M. Wyss, A. B. Schofield, and D. A. Weitz, *Phys. Rev. Lett.* **96**, 028306 (2006).
- [8] P. J. Lu, E. Zaccarelli, F. Ciulla, A. B. Schofield, F. Sciortino and D. Weitz, *Nature* **453**, 499 (2008).
- [9] M. Laurati, G. Petekidis, N. Koumakis, F. Cardinaux, A. B. Schofield, J. M. Brader, M. Fuchs and S. U. Egelhaaf, *J. Chem. Phys.* **130**, 134907 (2009).
- [10] S. Asakura and F. Oosawa, *J. Chem. Phys.* **22**, 1255 (1954). *idem J. Polymer Sci.* **33** 183 (1958).
- [11] A. Vrij, *Pure. Appl. Chem.* **48** 471 (1976).
- [12] F. Sciortino, S. Mossa, E. Zaccarelli and P. Tartaglia, *Phys. Rev. Lett.* **93**, 055701 (2004).
- [13] S. A. Shah, S. Ramakrishnan, Y. L. Chen, K. S. Schweizer and C. F. Zukoski, *Langmuir* **19**, 5128 (2003).
- [14] A. I. Campbell, V. J. Anderson, J. S. van Duijneveldt, and P. Bartlett, *Phys. Rev. Lett.* **94**, 208301 (2005).
- [15] A. Stradner, H. Sedgwick, F. Cardinaux, W. C. K. Poon, S. Egelhaaf and P. Shurtenberger, *Nature* **432**, 492 (2004).
- [16] C. P. Royall, D. G. A. L. Aarts and H. Tanaka, *J. Phys.: Condens. Matter* **17**, S3401 (2005).
- [17] T. H. Zhang, J. Groenewold and W. K. Kegels, *Phys. Chem. Chem. Phys.* **11**, 10827 (2009).
- [18] C. L. Klix, C. P. Royall and H. Tanaka, *Phys. Rev. Lett.* **104**, 165702 (2010).
- [19] C. Gögelein, G. Nägele, J. Buitenhuis, R. Tuinier and J. K. Dhont, *J. Chem. Phys.* **130**, 204905 (2009).
- [20] L. Belloni and P. G. Ferreira, *Phil. Trans. R. Soc. Lond. A* **359**, 867 (2001).
- [21] A. R. Denton and M. Schmidt, *J. Chem. Phys.* **122**, 2449111 (2005).
- [22] J. Y. Walz, and A. Sharma, *J. Colloid Interface Sci.* **168**, 485 (1994).
- [23] O. Mondain-Monval, F. Leal-Calderón, J. Philip, and J. Bibette, *Phys. Rev. Lett.* **75**, 3364 (1995).
- [24] L. Helden, G. H. Koenderink, P. Leiderer, and C. Bechinger, *Langmuir* **20**, 5662

6. RESULTS

(2004).

[25] M. Peláez-Fernández, A. Moncho-Jordá and J. Callejas-Fernández, *Europhys. Lett.* **90**, 46005 (2010).

[26] M. Peláez-Fernández, A. Moncho-Jordá and J. Callejas-Fernández, *J. Chem. Phys.* **134**, 46005 (2011).

[27] S. Buzzaccaro, R. Piazza, J. Colombo and A. Parola, *J. Chem. Phys.* **132**, 124902 (2010).

[28] E. Zaccarelli, S. Andreev, F. Sciortino and D. R. Reichman, *Phys. Rev. Lett.* **100**, 195701 (2008).

[29] H. M. Lindsay and P. M. Chaikin, *J. Chem. Phys.* **76**, 3774 (1982).

[30] D. Bonn, H. Tanaka, G. Wegdam, H. Kellay and J. Meunier, *Europhys. Lett.* **45**, 52 (1998).

[31] M. Peláez-Fernández, A. Moncho-Jordá and J. Callejas-Fernández, (2011) (In preparation).

[32] C. Haro-Peréz, *Nanoestructuras Tridimensionales Formadas con Liposomas: Propiedades Estáticas y Dinámicas*, (PhD Thesis, University of Granada 2005).

[33] C. Haro-Pérez, L.F. Rojas-Ochoa, V. Trappe, R. Castañeda-Priego, J. Estelrich, M. Quesada-Pérez and J. Callejas-Fernández, R. Hidalgo-Álvarez, *Structure and Functional Properties of Colloidal Systems. Chapter 4. volume 146*, 77 (2010).

[34] C. Urban, *J. Coll. Interface Sci.* **207**, 150 (1998).

[35] G. D. J. Phillies, *J. Chem. Phys.* **74**, 260 (1980); *ibid Phys. Rev. A* **24**, 1939 (1981).

[36] A. Moussaïd and P. N. Pusey, *Phys. Rev. E* **60**, 5670 (1999).

[37] K. Schätzel, *J. Modern Optics* **38**, 1849 (1991).

[38] S. Roldán-Vargas, J. de Vicente, R. Barnadas-Rodríguez, M. Quesada-Pérez, J. Estelrich, J. Callejas-Fernández, *Phys. Rev. E* **82**, 021406 (2010).

[39] E.B. Sirota, H.D. Ou-Yang, S. K. Sinha, P.M. Chaikin, J. D. Axe and Y. Fujii, *Phys. Rev. Lett.* **62**, 1524 (1989).

[40] W. Gotze and L. Sjogrem, *Rep. Prog. Phys.* **55**, 241 (1992).

[41] K. S. Schweizer and J. G. Curro, *Adv. Chem. Phys.* **98**, 1 (1997).

[42] F. Sciortino and P. Tartaglia, *Adv. Phys.* **54**, 471 (2005).

[43] L. Cipelletti and L. Ramos, *J. Phys.: Condens. Matter*, **17**, R253-R285 (2005).

[44] An optional route to reach a solution is to solve OZ as a three component suspension (equivalently PRISM should be solved for four components) weighted in such way that the average diameter and polydispersity match the real suspension. However, PRISM leads to a system of 10 coupled equations, which complicates the calculation.

**6.4 Paper IV. *The structure of charged colloid-polymer binary mixtures:
From like Wigner glass systems to fluid of clusters***

Previous studies [38] have shown that, although one can solve OZ with polydispersity, the improve in the fit is not good enough to make the effort (the width of the structure factor still remains far, too narrow from the observed experimentally).

6. RESULTS

6.5 Paper V. *Study on the effective potential of an asymmetric charged binary mixture: the non-monotonic behaviour with the big colloid charge*

6.5 Paper V. *Study on the effective potential of an asymmetric charged binary mixture: the non-monotonic behaviour with the big colloid charge*

6. RESULTS

6.5 Paper V. Study on the effective potential of an asymmetric charged binary mixture: the non-monotonic behaviour with the big colloid charge

Study on the effective potential of an asymmetric charged binary mixture: the non-monotonic behaviour with the big colloid charge, J. Chem. Phys. (under revision)

M. Peláez-Fernández, J. Callejas-Fernández and A. Moncho-Jordá

Departamento de Física Aplicada, Grupo de Física de Fluidos y Biocoloides, Universidad de Granada, E-18071 Granada, Spain.

6. RESULTS

Abstract

In this work we study the effective force between charged spherical colloids induced by the presence of smaller charged spheres using Monte Carlo simulations. The analysis is performed for a broad spectrum: two size ratios, $q = R_s/R_b$, two screened direct repulsions, κ , and two small particle packing fractions, ϕ_s . We specially focus on the effect charge of the big colloids (Z_b), and observe that the repulsion between big particles shows a non-monotonic behaviour: for sufficiently small charge, we find an anomalous regime where the total repulsion weakens by increasing the big colloid charge. For large charges the system recovers the usual behaviour and the big-big repulsion grows with Z_b . This effect is linked to the existence of strong attractive depletion interactions caused by the small-big electrostatic repulsion. We have also calculated the effective force using the Ornstein-Zernike equation with the HNC closure. We find this theory is able to capture the mechanism leading to this non-monotonic behaviour and provide theoretical results that agree with the simulations for small Z_b , but strongly underestimates the depletion forces for large Z_b .

Introduction

One of the most studied topics in Colloidal Physics is the stability of colloidal suspensions. The stability is commonly associated to the repulsive interaction between colloids that avoids the colloidal coagulation [1]. A clear example may be found for charged colloidal suspensions, where the long-range electrostatic repulsion between colloids prevents the approach of the particles at distances where the London-van der Waal's attraction is manifested. Notwithstanding, there is a great debate on the conditions for which two charged colloids suspended in a medium formed by anions and cations are repelled. It has been proved that under some specific conditions, *e.g.*, taking into account the size of the ions, the effective interaction between charged colloids of the same sign could be attractive driving even to the destabilization of the system [2-5].

The research on the stability of asymmetric binary mixtures of colloids, *i.e.*, a mixture of two kind of colloidal sizes, is fully justified due to the ubiquitous presence of systems with more than one component in many technological and biological applications [6-8]. The presence of the second component introduces additional thermodynamic degrees of freedom leading to a much richer phase diagram than for an one-component system. It is usual to describe a binary mixture as the one-component system (big colloids), where the second component (small colloids) is substituted by an effective interaction between the big colloids [9-12]. For mixtures of (big) hard spheres and smaller interpenetrable spheres, the excluded volume interactions between big and small particles create a depletion layer around the big particles. When two big particles overlap their depletion layers, the total volume accessible for the small particles increases, enhancing the entropy. The result is an entropically induced effective attraction between big colloids [13]. The stability of an asymmetric binary mixture will depend on the strength of this effective attraction, which increases with the concentration of small particles, ρ_s [14,15]. For large ρ_s , these depletion attraction can be strong enough to induce the fluid-fluid phase separation of the system.

A more complex system arises when we consider mixtures of charged spheres of different size and charge [16-18]. In principle, for particles with the same charge sign we expect that the system will become electrostatically stabilized by increasing the charge of the big particles, as is usually observed for one-component systems. However, in binary systems there are also effective interactions induced by the presence of the second smaller component that can have a strong influence on the structure, thermodynamic properties

6. RESULTS

and stability of the mixture. At this point, two aspects must be highlighted: on the one hand, the phase separation of these kind of mixtures is not only entropically-driven [19], since the long-range electrostatic repulsive interactions plays also an important role. In fact, the competition between both entropic-origin and electrostatic interactions has devoted very much interest in recent years, mostly in colloid-polymer mixtures [20, 21]. On the other hand, the presence of long-range repulsions, or even attractions, between big-small and small-small colloids give rise to new physical phenomena, as the formation of repulsive-halos [11] or the bridging [22] representing alternative ways of stabilization.

The effective attraction between two charged colloids induced by the presence of the charged small colloids has been intensively studied in the last decade. Using computer simulations and theory, A. A. Louis *et al.* systematically investigated the latter problem. They focus on the effect of a hardcore pair potential with either repulsive or attractive Yukawa tails for the direct interactions. The arbitrary combination of both repulsive and attractive interactions, for big-small and small-small, enhances the rich variety of mechanisms present in such mixtures leading to either depletion attraction emerged by repulsion or accumulation repulsion mediated by attraction [11]. E. Allahyarow *et al.* studied the second virial coefficient, B_2 , as a function of the added salt for a globular protein solutions (two big colloids with discrete charge in a sea of finite microions). Their study proofs that the existence of a discrete charge pattern on the protein surface profoundly influences the effective interactions leading to a non-monotonic behaviour of B_2 , which in last term is due to the finite microion distribution around the protein [23]. G. Cinacchi *et al.* calculated the interaction between two colloids mediated by a fluid of small spheres with theory and simulation considering soft repulsive spherical particles (Lennard-Jones). Their results indicate that even a modest degree of softness in the pair potential governing the direct pair interactions may lead to a significantly more attractive total potential between big particles than in the hard-sphere case. This attraction showed an important impact on the phase diagram, leading to stable fluid-fluid coexistence respect to the fluid-solid one [24]. Trying to shed light in more complex systems, A. Jamnik *et al.* studied the effective interaction between two large hardcore colloids immersed in a bidisperse suspension of short-ranged attractive colloids mimicking a lyophobic suspension. Using theory and simulations, they have shown that the induced attraction between big colloids reaches a longer range as much as the stickiness between small colloids is increased [25]. The non-additivity of the repulsion between particles was also studied by E. Allahyarow *et al.* for binary charged colloidal suspensions using computer simulations. They have

6.5 Paper V. Study on the effective potential of an asymmetric charged binary mixture: the non-monotonic behaviour with the big colloid charge

shown that a realistic model of charged suspensions based on the effective pairwise Yukawa model should incorporate a non-vanishing additivity either for repulsive or attractive big-small interactions [26].

Despite of the interest aroused in charged colloidal binary mixtures, there is a lack of a systematic study on the effect of the big and small charges, range of the interactions, size ratio and the particle concentrations on the effective interaction between big particles. In this paper, we study like-charged asymmetric binary mixtures, with equal charge sign (direct repulsion), of two motionless big spherical particles immersed in a sea of small charged particles. The induced force between the two big particles is calculated by Monte-Carlo simulation. We find that the coupling between the direct big-small and small-small long-range repulsion has a strong influence on the big-big total force, which corroborates results for relatively similar systems [11, 23-25]. As we increase the charge of the big colloids, we observe a non-monotonic behaviour of the induced potential, which becomes less repulsive until a critical value of the charge is reached. Above this value, the repulsion between the big particles grows with the charge, as is usually found in one component charged colloidal samples. From our knowledge, this non-intuitive phenomenon has not been studied for like-charged asymmetric binary mixtures either in simulations, theories or experiments before. The study of this phenomenon under different size ratios, small particle concentrations and electrostatic repulsive ranges is performed to capture the conditions where the non-monotonic behavior is enhanced. We also compare our simulations results with the Ornstein-Zernike predictions together with the HNC closure equation [27] looking for a suitable theoretical description capturing the latter behaviour. Our simulation results represent an experimental challenge to be corroborated and exploited as a useful stabilizing/destabilizing tool.

The paper is organized as follows. In Section II, we explain the simulation details used to calculate the big-big total force calculation; Section III presents the theoretical model used to compare with the simulation results; In Section IV, the simulation results are presented and discussed. Moreover, we compare with the theoretical results in terms of the effective force between big colloids and the second virial coefficient; Finally in Section V, we highlight the relevant points stated in this paper.

Simulation details

We have used Monte-Carlo (M-C) simulations to obtain the interaction force between

6. RESULTS

a pair of big particles immersed in a sea of small ones [28]. Each simulation has been performed in a box of dimensions $L_x \times L_y \times L_z$, where the volume V and temperature T remain constant. The simulation box contains two motionless big particles of diameter σ_b separated a center-to-center distance R , located at the coordinates $(0.5(L_x - \frac{R}{2}), 0.5L_y, 0.5L_z)$ and $(0.5(L_x + \frac{R}{2}), 0.5L_y, 0.5L_z)$, respectively. The rest are N_s moving small particles of diameter σ_s , which are randomly placed at the beginning of each simulation. The dimensions of the simulation box are determined from N_s , the size ratio $q = \frac{\sigma_s}{\sigma_b}$ and the packing fraction of small spheres ϕ_s using the following set equations:

$$\begin{aligned} \phi_s &= \frac{v_s N_s}{L_x L_y L_z - 2v_b} = \frac{\frac{\pi}{6} \sigma_s^3 N_s}{L_x L_y L_z - \frac{\pi}{3} \sigma_b^3} \\ L_y &= L_z \\ L_x &= L_y + \sigma_b + R, \end{aligned} \quad (6.5.1)$$

where ϕ_s really represents the packing fraction of small spheres in the reservoir.

The suspension is considered as a continuous solvent of relative dielectric permittivity given by $\epsilon_r = 80$ and temperature $T = 300\text{K}$, mimicking water at room temperature. Both big and small colloids bear effective negative charges given by Z_b and Z_s , respectively. We also assume the existence of certain concentration of monovalent cations n_+ and anions n_- , such that the electroneutrality condition is satisfied. To model the direct interaction between any pair of particles suspended under the latter conditions, we employ the simple Debye-Hückel (D-H) interaction potential [29],

$$\beta V_{ij}(r) = \begin{cases} +\infty & , r < \sigma_{ij} (= \frac{\sigma_i + \sigma_j}{2}) \\ \frac{L_B Z_i Z_j e^{-\kappa(r - \sigma_{ij})}}{r(1 + 0.5\kappa\sigma_i)(1 + 0.5\kappa\sigma_j)} & , r \geq \sigma_{ij} \end{cases} \quad (6.5.2)$$

where r is the center-to-center distance between any pair of particles, $\beta = 1/k_B T$ with k_B the Boltzmann constant, $L_B = \frac{e^2}{4\pi\epsilon_0\epsilon_r k_B T}$ is the Bjerrum length (in our simulations $L_B = 6.97 \text{ \AA}$) with ϵ_0 the vacuum permittivity, κ is the inverse of the Debye length and the subscripts denote the different kind of particles. As can be seen in eq. (6.5.2), the Debye length controls the range of the repulsive tail. In our study, we have assumed that κ depends only on the ionic concentration of the medium, $\kappa = \sqrt{8\pi N_A L_B (|n_+| + |n_-|)}$, being N_A the Avogadro's number. Such assumption simplify the discussion of our results being $n_+ \gg n_-$ to work with a neutral system, since the charge of the colloids

6.5 Paper V. Study on the effective potential of an asymmetric charged binary mixture: the non-monotonic behaviour with the big colloid charge

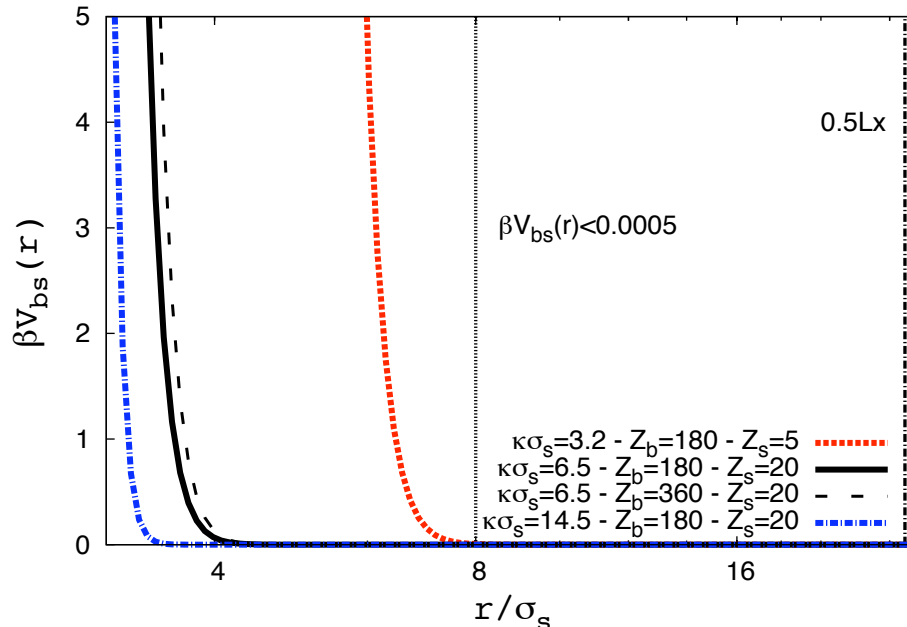


Figure 6.5.1: Normalized pair interaction between big and small spherical colloids as a function of the interparticle distance for some of the particular cases studied in this work (see table (6.5.1)). The vertical dashed-dotted line indicates the simulation box size from the center of a big colloid, while the vertical dotted line represents the cut-off distance r^{trunc} for the longer ranged big-small repulsive potential.

has been selected negative.

For each simulation, the D-H potential is truncated at r^{trunc} , where $\beta V_{ij}(r^{trunc}) = 0.0005$. As is shown in fig. (6.5.1), the big-small cut-off distance is in all cases smaller than the simulation box dimensions. In fact, the distance between the cut-off and the end of the simulation box is long enough allowing the separation of big colloids up to distances of $\sim 17\sigma_s$. Periodic boundary condition have been applied in the three directions as usual.

In the course of each simulation, we systematically compute the small particles bulk density, defined as $\rho^{bulk}(\mathbf{r}) = \langle \sum_j \delta(\mathbf{r}_j - \mathbf{r}) \rangle$, where \mathbf{r}_j is the position of the centre of the j th-particle, and the angular bracket $\langle \dots \rangle$ denotes a canonical average over a large enough number of configurations. For that, the simulation box was divided in $100 \times 100 \times 100$ cells, which were continuously updated during the simulation with the

6. RESULTS

average number of small particles contained inside. In order to determine the density of small particles in contact with the surface of the big colloids, we define a thin slice of thickness Δ and compute the density of small particles close to the surface using spherical coordinates, $\rho^{shell}(r', \theta, \phi)$, where $r' \in [\frac{\sigma_b}{2}, \frac{\sigma_b}{2} + \Delta]$ and the spherical coordinates θ and ϕ are taken respect to the center of each big particle. The spherical shells around the big colloids are divided into 360×360 equal elements and the small particle average density for each element is also updated during the simulation run.

By means of an accurate estimation of the latter magnitudes, we are able to calculate the total force acting on the big colloids at all directions, \vec{F} , taking into account that it involves three different contributions:

$$\vec{F}(R) = \vec{f}^{(1)}(R) + \vec{f}^{(2)}(R) + \vec{f}^{(3)}(R). \quad (6.5.3)$$

$\vec{f}^{(1)}(R)$ is the direct force that the particle 1 exerts on particle 2 at a centre-to-centre distance of R , given by eq. (6.5.2). $\vec{f}^{(2)}(R)$ is the electrostatic force induced by the small charged particles, which is calculated using the bulk density of small particles as follows,

$$\vec{f}^{(2)}(R) = - \int \rho^{bulk}(\mathbf{r}'; R) \frac{\partial}{\partial \mathbf{r}'} V_{bs}(r') d\mathbf{r}' \quad (6.5.4)$$

Here R notes the dependence of the bulk density on the pre-fixed distance between the two big colloids, in such a way that $\vec{f}^{(2)}$ is explicitly a function of the relative distance between the big colloids. Finally, $\vec{f}^{(3)}(R)$ stands for the force that may be traced back from the imbalance of the small particles at the contact of the big colloid surface. Fig. (6.5.2) shows a color map of the small particle density in a central slice along the z-axis. As can be appreciated, near to each big particle an important high density halo of small particles emerges. Therefore, the imbalance of pressure at the contact when the big colloids approach must be taking into account in the total force calculation, specially to modest big-small repulsions. In a M-C simulation, the force between particles is not calculated in the course of the simulation as in the Molecular Dynamic one, so that a special routine for the small particle pressure at the contact was developed. The explicit expression for the force calculation at the contact is derived from eq. (6.5.4) taking the limit $r' \rightarrow \frac{\sigma_b^+}{2}$,

$$f_x^{(3)}(\theta, \phi; R) = \lim_{\Delta \rightarrow 0} \frac{\rho^{shell}(\frac{\sigma_b^+}{2} = \frac{\sigma_b}{2} + \Delta, \theta, \phi; R)}{\Delta} \sin(\theta) \cos(\phi). \quad (6.5.5)$$

6.5 Paper V. Study on the effective potential of an asymmetric charged binary mixture: the non-monotonic behaviour with the big colloid charge

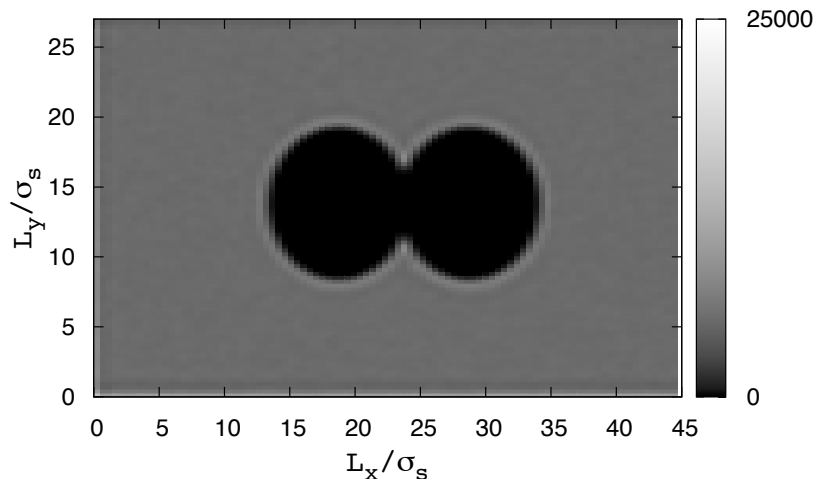


Figure 6.5.2: Color map of the small particle density in the simulation box with the two big colloids placed in the x-axis. The average corresponds with a central slice along the z-axis.

In our simulations, we have found that the optimal thickness value for the calculation of eq. (6.5.5) is $\Delta^{opt} = 0.06\sigma_s$. To reach this value, we have looked for the best compromise between computing time and accuracy. On the one hand, if $\Delta > \Delta^{opt}$ we get a quickly average value for ρ^{shell} , however the thickness of the shell is too large, so that many particles far to the contact area are considered for the calculation of the contact density. Thus, the absolute error of the calculated pressure is unacceptable. On the other hand, if $\Delta < \Delta^{opt}$, we get a more reliable average at the contact. Against this, the calculation of the ensemble average takes longer computing time than the necessary for the other calculated magnitudes, as ρ^{bulk} . We consider that our technique to compute $f_x^{(3)}(R)$ does not employ much more computer time than other more sophisticated options [30].

Starting from a random configuration of $N_s = 7000$ small particles, 2×10^4 M-C cycles were run to thermalize the system (each cycle consists of N_s trials of randomly chosen small particles). The maximum displacement of the random trials is adapted in such a way that the ratio of accepted trials is 50%. After the thermalization, 10^6 additional M-C cycles were performed to compute the average densities and forces. During the

6. RESULTS

Table 6.5.1: The table shows the different cases studied in this work. ϕ_s is the small particles packing fraction in the reservoir, $\kappa\sigma_s$ is the normalized inverse of the Debye length, q stands for the small-big size ratio and Z_s corresponds with the small particle charge.

SET	ϕ_s	$\kappa\sigma_s$	$q(= \frac{\sigma_s}{\sigma_b})$	Z_s
(a)	0.10	3.2	0.1	5.0
(b)	0.10	6.5	0.2	20.0
(c)	0.10	14.5	0.2	20.0
(d)	0.25	6.5	0.2	20.0

production stage, the average total force applied to one of the big colloids is calculated. Here, we will only consider the x -component of this force, since the y and z components are zero after performing their corresponding averages.

Theoretical details

A detailed theoretical description of a binary mixture of colloidal particles can be found under the framework of the Ornstein-Zernike equation [27]. For a system of two spherical components the equations which describes the pair correlations are

$$h_{ij}(\mathbf{r}) = c_{ij}(\mathbf{r}) + \sum_k^2 \rho_k \int d^3\mathbf{r}' c_{ik}(\mathbf{r}') \cdot h_{kj}(\mathbf{r} - \mathbf{r}') \quad (6.5.6)$$

where $c(\mathbf{r})$ is the direct correlation function, $h(\mathbf{r}) + 1$ is the radial distribution function, ρ_i is the density number of particles and the subscripts i , j and k run for each species of particles. Besides these integral equations, three extra closure equations that relate these three functions are necessary. We have employed the Hippednetted Chain closure equation (HNC), which is commonly used for long-range repulsive interactions.

$$c_{ij}(\mathbf{r}) = -\beta V_{ij}(\mathbf{r}) + h_{ij}(\mathbf{r}) - \ln [h_{ij}(\mathbf{r}) + 1]. \quad (6.5.7)$$

We have numerically solved the system formed by eqs. (6.5.6) and (6.5.7) using the iterative Picard's method. In order to compare with the simulations, the equations must be solved in the so-called colloidal limit, where the concentration of big particles tends to zero, $\rho_b \rightarrow 0$. In this case, the total potential between two big colloids is given by the exact relationship, $\beta V_{bb}^{Total}(\mathbf{r}) = -\ln [h_{bb}(\mathbf{r}) + 1]$ [27].

6.5 Paper V. Study on the effective potential of an asymmetric charged binary mixture: the non-monotonic behaviour with the big colloid charge

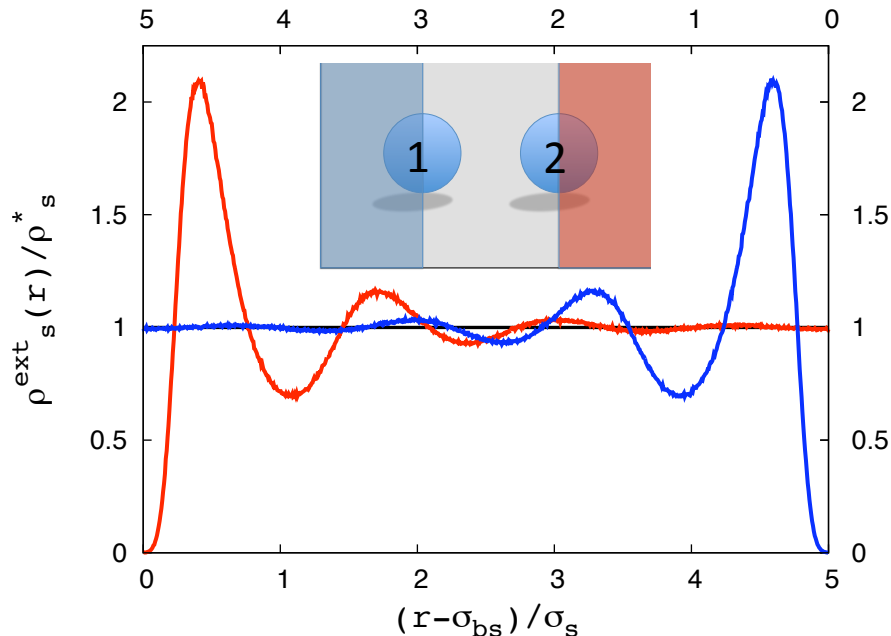


Figure 6.5.3: External density profile of small particles in the outer face of each big particle (colored regions in the scheme) normalized to the unity. The red and blue lines stand for the external density profile of small particles at the right hand of the particle 2 and the left hand of the particle 1, respectively. The latter can be expressed as a function of r (distance in spherical coordinates) given the spherical symmetry in the consider regions. This result corresponds with the set (d) for $Z_b = 280$ and was taken for a centre-to-centre big separation of $R = 10\sigma_s$.

Results and Discussion

The properties of an asymmetric binary mixture of hard spheres in the colloidal limit depend on ϕ_s , and q . Including the electrostatic interaction between any pair of particles, we get three new parameters to account for: Z_b , Z_s and κ . Therefore, the phenomenology presented in such systems is hidden among a large number of possible combinations between the set of parameters. In this study, we mainly focus on the effect of Z_b on the big-big induced effective potential. For that reason, we have explored the increase of Z_b keeping fixed Z_s with the intention of assessing the charge effect under certain conditions of q (set (a) front set (b)), κ (set (b) front set (c)) and ϕ_s (set (b) front set (d)) (see table (6.5.1)). In a charged binary mixture, the big-big effective

6. RESULTS

potential, $V_{bb}^{eff}(r)$ ($= V_{bb}^{Total}(r) - V_{bb}(r)$), is a complex function of both big-small and small-small direct interactions. Therefore, our systematic study deeps into $V_{bb}^{eff}(r)$ as a function of $V_{bs}(r)$, since $V_{ss}(r)$ remains equal for any studied case (Z_s is constant).

The big-small repulsion goes from HS-like ($Z_b = 0$) to a strong repulsive tail (maximum Z_b value). Before to show the computed effective forces, we should mention that even for the most repulsive case, the rearrangement of small particles around the big one is completely captured within the simulation box dimensions. To confirm this, we show in fig. (6.5.3) the external density profile of small particles around the big ones, $\rho_s^{ext}(r)/\rho_s$, where ρ_s is the number density of small particles far from the surface of the big particles. By external density profile, we mean the average density of small particles in the outer face of each big particle (colored region in the scheme presented in fig. (6.5.3)). Fig. (6.5.3) shows an extremely charged case (set (d), $Z_b = 280$, $R = 10\sigma_s$ and $N_s = 7000$), where the dimensions of the simulation box are $L_x \sim 40\sigma_s$ and $L_y = L_z \sim 20\sigma_s$. As observed, the oscillations of the density profile in the outer regions becomes negligible before reaching the border.

Fig. (6.5.4) shows the simulation results divided in a set of four panels, each one related with one of the studied cases (the relevant parameters for each case are given in table (6.5.1)). In each panel, the big-big normalized effective force, $\beta\sigma_b\vec{F}^{eff}(R)$ ($= \beta\sigma_b(\vec{f}^{(2)}(R) + \vec{f}^{(3)}(R))$), is plotted as a function of the interparticle distance, R , for six different Z_b values.

In general, we observe that the effective force shows a similar qualitative behaviour as we increase Z_b . It is attractive near to the big-big contact ($R \geq \sigma_b$). This is a direct consequence of the depletion region appearing in the region between the big colloids, that generates an unbalanced pressure exerted by the small particles at the outer faces of the colloids. For small Z_b values, the attractive well is mainly originated by the concentration of small particles at the contact, and the range of the attraction is roughly given by σ_s . Moreover, the effective force shows a repulsive barrier at $R^{bar} = (\sigma_b + \sigma_s)$. This repulsion is provoked by the accumulation of small particles around the big colloids. Indeed, at such big-big distance, the space between the surfaces of the big colloids is large enough to allow the small particle to fit inside. Since the repulsion between the small charged particles is larger than the repulsion with the big colloids, the result is the accumulation of small particles in the internal region that overcomes the pressure originated in the outer faces of the big colloids. As Z_b increases, there is a progressive

6.5 Paper V. Study on the effective potential of an asymmetric charged binary mixture: the non-monotonic behaviour with the big colloid charge

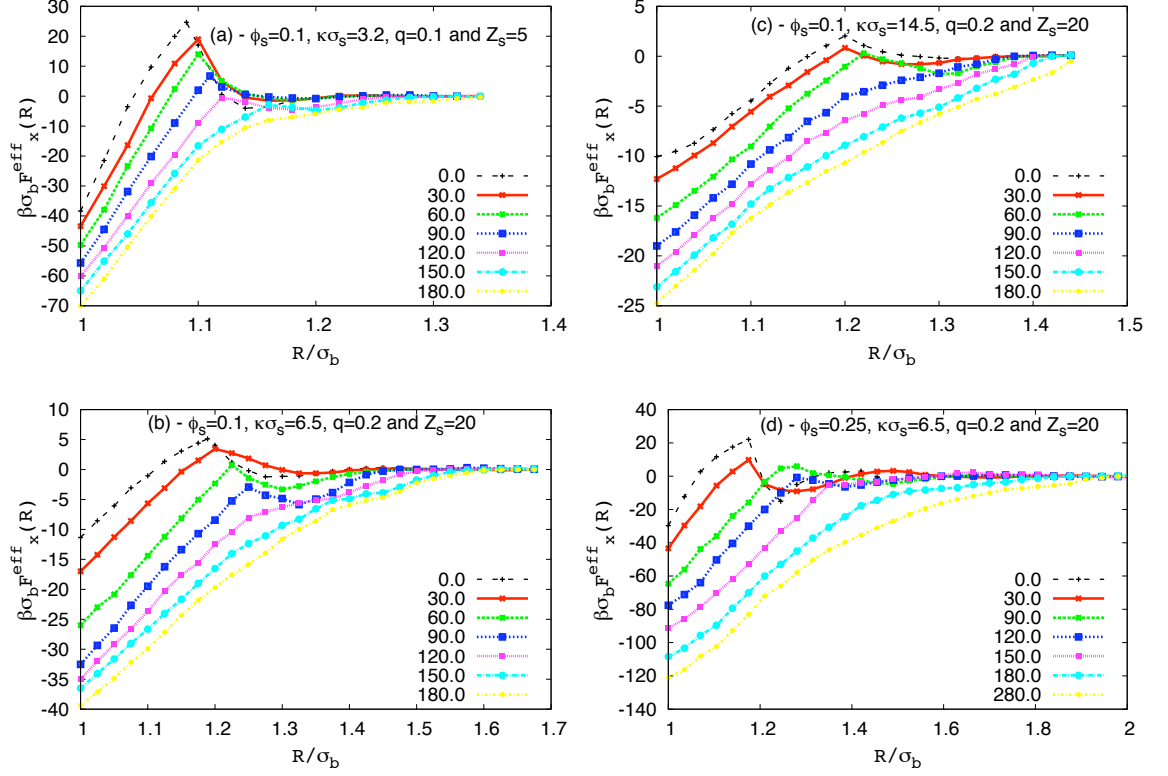


Figure 6.5.4: Effective force between big colloids induced by the small charged particles obtained by simulation (eqs. (6.5.4) and (6.5.5)) for different values of Z_b . The four plots corresponds to the four cases shown in table (6.5.1).

enhancement of the big-small direct repulsion leading to a more efficient depletion of small particles. Since the big-small repulsion becomes more and more dominated by the electrostatic contribution, the range of the attraction slightly increases to reach the value $\sigma_b + \sigma_s + \kappa^{-1}$. For large enough Z_b , the big-small repulsion is so strong that the small particles are not able to diffuse inside the region between the big colloids for $R \approx R^{bar}$, and the repulsive barrier disappears, leading to an attractive effective force that tends monotonically to zero as a function of R .

Although we have observed the same behaviour with Z_b for different values of q , κ and ϕ_s , it should be emphasized that there are important differences between the four cases studied. First, we compare plot 6.5.4(a) with (b). Both sets have the same packing fraction of small spheres, but with twice larger radius (N_s , Z_s and $\kappa\sigma_s$ have been con-

6. RESULTS

veniently modified in order to keep constant ϕ_s , the surface charge of the small colloids and the inverse Debye length, κ^{-1}). Increasing σ_s leads to weaker but longer-range depletion forces, which is consistent with the fact that the size of the small particles is larger but the number density is smaller.

Comparing plot (b) with (c) we observe that reducing the range of the electrostatic interactions (that is, increasing κ) has a strong impact on the effective force. For small Z_b , increasing κ has an almost negligible effect on the big-small repulsion, that is mainly controlled by the hard-sphere contribution. However, the repulsion between the small charged particles is decreased and shortened, and so there is a weaker accumulation of small particles on the surface of the big colloids. It leads to a smaller attractive depletion force for $R < \sigma_b + \sigma_s$ with a smaller repulsive barrier. For large Z_b , the increase of κ also screens the repulsion between big and small particles. This reduces the pressure over the outer faces of the big colloids, resulting in a weaker effective depletion forces.

The effect of the packing fraction of small particles is deduced from the comparison between plots (b) and (d). Increasing the packing fraction to $\phi_s = 0.2$ leads to an enhancement of the attraction at short distances, which again may be explained in terms of the largest concentration of small particles near the big colloids. For small Z_b , this enhancement is nearly proportional to the packing fraction. Moreover, the effective force has a higher repulsive barrier and shows oscillations at larger interparticle distances, the reason being that the equilibrium distribution of small particles around one big colloid has several coordination layers where particles have a larger local density, typically observed in dense hard-sphere systems. For large Z_b the depth of the attractive forces grows with ϕ_s even faster than the linear behaviour. For $\phi_s = 0.2$, the repulsive barrier remains for greater Z_b values, due to the fact that small particles are now strongly pushed in the region between the big colloids.

Following the same scheme that in fig. (6.5.4), fig. (6.5.5) shows the big-big effective forces calculated by simulation and theory. Due to the number of Z_b values studied, we have presented just 4 cases to clarify the comparison between theory (lines) and simulation (symbols) ($Z_b = 0, 30, 150$ and 180). In general, for small Z_b , the agreement between theory and simulation is acceptable, specially at small ϕ_s values. As Z_b increase, the theory leads to less attractive and shorter-range forces respect to the M-C simulations. Moreover, the OZ-HNC model predicts the appearance of the repulsive barrier at intermediate distances, even for the larger studied Z_b cases, where the M-C

6.5 Paper V. Study on the effective potential of an asymmetric charged binary mixture: the non-monotonic behaviour with the big colloid charge

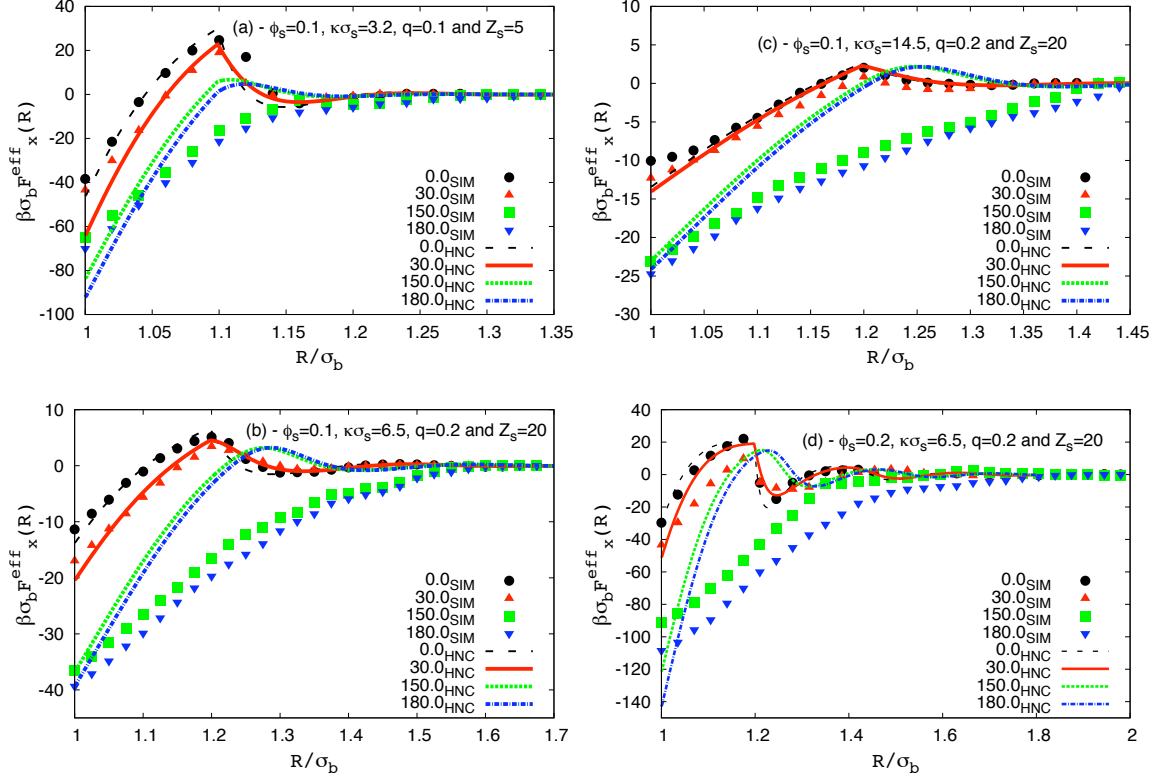


Figure 6.5.5: Effective force between big colloids induced by the small charged particles obtained by simulation (eqs. (6.5.4) and (6.5.5)) for different values of Z_b . Here, we keep the same panel structure that in fig. (6.5.4). Symbol stand for some of the studied cases by simulation, while lines stand for the OZ-HNC predictions.

simulation indicates that this repulsive barrier disappears from the effective depletion potential being attractive and monotone. At the big-big contact ($R \sim \sigma_b$), the theory agrees with simulation overall for set (b) and (c), which correspond with the biggest q and κ studied for the smallest ϕ_s . As the size ratio diminishes (set (a)) or the small packing fraction increases (set (d)) the theory overestimates the attraction at the contact. It also coincides with the cases where the induced attraction is stronger. So, we can conclude that the OZ-HNC equation predicts effective interactions less attractive than the calculated by simulation and becomes worst as much as the repulsion and the induced attraction are enhanced.

The previous results show that the effective forces between big colloids is in general at-

6. RESULTS

tractive. However, in order to know exactly the role of this attractive interaction in the stability of the mixture, we need to calculate the total force, defined as the sum of the effective force (induced by the small particles) and the direct Yukawa repulsion between big particle, $F = F^{eff} + F^{Yuk}$. By increasing Z_b , the direct repulsion grows, but at the same time the effective forces become more attractive. This leads to a competition between opposite effects where it is not clear which effect is the dominant. To express clearly the final results, we have calculated the normalized big-big second virial coefficient as a function of Z_b , $B_2^*(Z_b) = \frac{B_2(Z_b)}{B_2^{HS}}$. To calculate B_2^* , we have interpolated and integrated the effective forces of fig. (6.5.4) and added the corresponding direct big-big Yukawa potential (eq. (6.5.2)) to obtain $V_{bb}^{Total}(R)$. Then, the normalized second virial coefficient is obtained as follows,

$$B_2^*(Z_b) = 1 + 3\sigma_b^2 \int R^2 (1 - \exp(-\beta V_{bb}^{Total}(R; Z_b))) dR. \quad (6.5.8)$$

The simulation results of B_2^* are plotted in fig. (6.5.6) with different symbol-lines (see the legend). As observed, the second virial coefficient is always positive, which indicates that the repulsion always dominates over the effective induced attraction. However, it clearly shows a non-monotonic behaviour as a function of Z_b . The origin of this effect can be attributed to the interplay between the big-big direct interaction (eq. (6.5.2)) and the effective induced potential (mainly attractive as is shown in fig. (6.5.4)). Indeed, the big-big repulsive amplitude grows as Z_b^2 , but the big-small direct repulsion depends on $Z_b Z_s$. For small Z_b values (compared with Z_s) the electrostatically-enhanced depletion attraction is larger than the direct electrostatic repulsion between big colloids, and so B_2^* drops by increasing Z_b . For larger Z_b values, the direct repulsion dominates and becomes the main interaction governing the stability of the mixture, so the second virial coefficient grows again.

The critical charge Z_b^c at which this crossover occurs depend on ϕ_s , Z_s and κ^{-1} . On the one hand, for strongly screened electrostatic interactions (see set (c), which corresponds to the smaller value of κ^{-1} studied in this work), all interactions are mainly dominated by the hard-sphere contributions, so the results become less sensitive to changes in Z_b . In fact, the crossover is not reached for the studied values of Z_b . On the other hand, by increasing the concentration of small particles (set (d)) we observe a significant enhancement of this non-monotonic behaviour. Also the critical charge Z_b^c increases, as a consequence that the direct big-big repulsion must overcome the strong

6.5 Paper V. *Study on the effective potential of an asymmetric charged binary mixture: the non-monotonic behaviour with the big colloid charge*

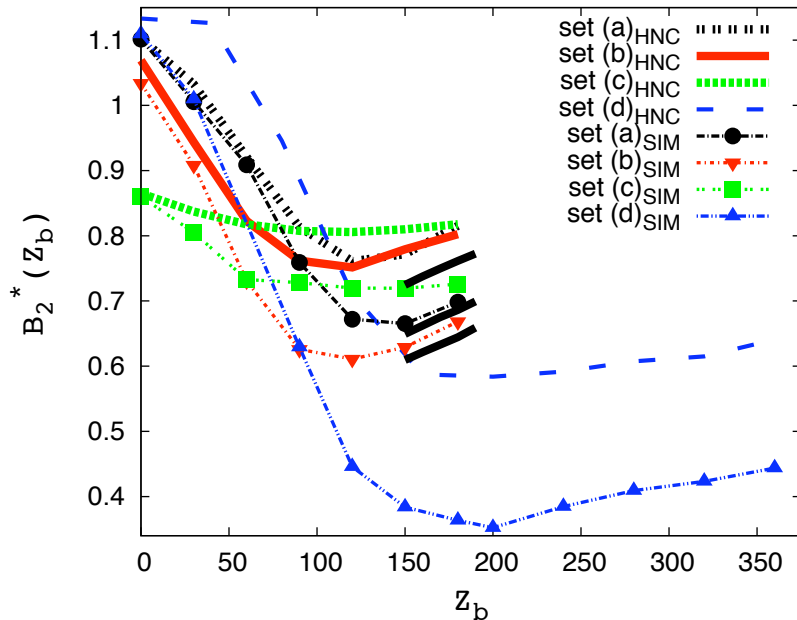


Figure 6.5.6: Normalized second virial coefficient, $B_2^* = B_2/B_2^{HS}$ as a function of the charge of the big colloids, Z_b . Symbol-lines stand for the simulation results while lines correspond with the OZ-HNC predictions. Several black solid lines have been included to guide the eye with the expected behaviour for a total potential given by eq. (6.5.2).

depletion exerted by the small particles in order to be the dominant contribution. As expected from fig. (6.5.5), the theoretical predicted values of B_2^* are quite similar to the simulation ones for small Z_b , but become larger when we increase Z_b due to the fact that the theory underestimates the effective attraction. Nevertheless, the OZ-HNC is still able to capture the non-monotonic behaviour, as is shown in fig. (6.5.6) with lines.

Conclusions

The effect of the charge in the effective force for a binary mixture of asymmetric charged colloids is studied by Monte-Carlo simulation. The increase of the big colloid charge, Z_b , is analysed for several cases: two size ratios, q , two screened repulsions, κ and two small particle packing fractions, ϕ_s . The simulation results show that the effective force becomes more attractive as Z_b increase keeping fix Z_s and the rest of parameters. Comparing the results for different set of parameters, we have observed that for smaller particles and larger packing fractions (ϕ_s) the induced force is more attractive, while

6. RESULTS

as the direct repulsions are screened (increase of κ) the effect of Z_b on the induced attraction is decreasing.

The competition between big-big and big-small direct repulsions induce a non-monotonic behaviour of the second virial coefficient. This phenomenon is enhanced for smaller q and κ values and larger ϕ_s . The latter emerges as an experimental challenge to prove that under the suitable conditions the use of more charged colloids in a binary mixture not necessarily implies an increase of the interparticle repulsion. It has been also shown that the OZ-HNC theoretical approach is able to capture the competition between direct interactions leading to this non-monotonic behaviour. However, the quantitative agreement between theory and simulation is only reached for small Z_b values, so that an accuracy theoretical description for more repulsive mixtures is demanded.

Acknowledgments

The authors are grateful to “MCINN” (Project No. MAT2009-13155-C04-02) ERDF Funds and “Junta de Andalucía” (Excellency Project P07-FQM-02517 and P07-FQM-02496) for financial support.

References

- [1] J. Lyklema, *Fundamentals of Interface and Colloid Science* **2**, 3208 (1995).
- [2] E. Allahyarov, H. Löwen and S. Trigger, *Phys. Rev. E* **57**, 5818 (1998).
- [3] E. Allahyarov, I. D’Amico and H. Löwen, *Phys. Rev. Lett.* **81**, 1334 (1998).
- [4] E. Allahyarov and H. Löwen, *Phys. Rev. E* **63**, 041403 (2001).
- [5] A. Cuetos, J. A. Anta and A. M. Puertas, *J. Chem. Phys.* **133**, 154906 (2010).
- [6] K. P. Velikov, C. G. Christora, R. P. A. Dullens and A. van Blaaderen, *Science* **296**, 106 (2002).
- [7] A. Y.-G. Fuh, J. G. Chen, S.-Y. Huang and K.-T. Cheng, *Applied Physics Letters* **96**, 051103 (2010).
- [8] T. H. Windhom and C. A. Cain, *Transactions on biomedical engineering* **148**, BME.26 3, (1979).
- [9] M. Bier, R. van Roij, M. Dijkstra, *J. Chem. Phys.* **133**, 124501 (2010).
- [10] M. Dijkstra, R. van Roij and R. Evans, *Phys. Rev. E* **59**, 5744 (1999).
- [11] A. A. Louis, E. Allahyarov, H. Löwen, and R. Roth, *Phys. Rev. E* **65**, 061407 (2002).

6.5 Paper V. Study on the effective potential of an asymmetric charged binary mixture: the non-monotonic behaviour with the big colloid charge

- [12] H. N. W. Lekkerkerker and A. Stroobants, *Physica A* **195**, 387 (1993).
- [13] S. Asakura and F. Oosawa, *J. Chem. Phys.* **22** 1255 (1954); *J. Polym. Sci.* **33**, 183 (1958).
- [14] A. P. Gast C. K. Hall and W. B. Russel, *J. Colloid Interface Sci.* **109**, 161 (1986).
- [15] A. P. Gast, C. K. Hall and W. B. Russell, *J. Colloid Interface Sci.* **96**, 251 (1983).
- [16] N. J. Lorenz, J- Lin, T. Palberg, *Colloids and Surfaces A: Physicochem. Eng. Aspects* **319**, 109-115 (2008).
- [17] N. J. Lorenz, H.-J. Schöpe, H. Reiber, T. Palberg, P. Wette, I. Klasseu, D. Holland-Montz, D. Hertach and T. Okubo, *J. Phys.: Condens. Matter* **21**, 464116 (2009).
- [19] A. Vrij, *Pure. Appl. Chem.* **48**, 471 (1976).
- [20] M. Peláez-Fernández, A. Moncho-Jordá, J. Callejas-Fernández, *Europhys. Lett* **90**, 46005 (2010); *idem*, *J. Chem. Phys.* **134**, 054905 (2011).
- [21] S. Buzzaccaro, R. Piazza, J. Colombo, and A. Parola, *J. Chem. Phys.* **132**, 124902 (2010).
- [22] S. Karanikas, J. Dzubeuella, A. Moncho-Jordá and A. A. Louis, *J. Chem. Phys.* **128**, 204704 (2008).
- [23] E. Allahyarov, H. Löwen, J. P. Hansen, and A. A. Louis, *Phys. Rev. E* **67**, 051494 (2003).
- [24] G. Cinacchi, Y. Martínez-Ratón, L. Mederos, G. Navascués, A. Tani and E. Velasco, *J. Chem. Phys.* **127**, 214501 (2007).
- [25] A. Jamnik, *J. Chem. Phys.* **131**, 164111 (2009); A. Lajovic, M. Tomsic and A. Jamnik, *ibid* **130**, 104101 (2009).
- [26] E. Allahyarov and H. Löwen, *J. Phys.: Condens. Matter* **21**, 424117 (2009).
- [27] J. P. Hansen and I. R. McDonald, *Theory of Simple Liquids* (Academic, New York, 1976).
- [28] D. Frenkel, B. Smit, *Understanding of Molecular Simulation: from algorithms to applications* (Academic Press, San Diego, 1996).
- [29] P. Debye and E. Hückel, *Phys. Z.* **24**, 185 (1923).
- [30] J. Z. Wu, D. Bratko, H. W. Blanch, and J. M. Prausnitz, *J. Chem. Phys.* **111**, 7084 (1999).

6. RESULTS

6.6 Project in progress. *Deformation of the polymer close to the colloidal surface: beyond the “thread limit”.*

6.6 Project in progress. *Deformation of the polymer close to the colloidal surface: beyond the “thread limit”.*

6. RESULTS

6.6 Project in progress. *Deformation of the polymer close to the colloidal surface: beyond the “thread limit”.*

Here, we present the advances in the theoretical project performed during a short stay in the Soft Matter Theory Group at the University of Konstanz (Germany). It is been carried out in collaboration with Prof. Matthias Fuchs. Although this project is not concluded, we have already found some relevant results that will be exposed on the next.

Until now, the PRISM formalism has been applied to charged colloid-polymer mixtures with good results (paper II and III). Indeed, this model represents an useful tool to describe the structural properties of these mixtures. However it is limited in the sense that the model does not considers the polymer deformation near the colloidal surface induced by entropic or electric effects (see section 4.3). Therefore, the application of the m-PY closure equation to charged colloid-polymer mixtures is fully justified with the aim to improve our theoretical description.

For highly repulsive mixtures (*e.g.*, paper II, III and IV), it is expected that the electrostatic interactions govern all the structural behavior. However, the polymer deformation effects (*e.g.*, the one captured with the m-PY closure) should be evaluated to establish the conditions where they can be relevant. The numerical resolution of PRISM m-PY with thermodynamic consistency allows us also to deep into the structure and phase behavior of mixtures where the polymer is constituted by finite-size monomers. It represents an important step forward to the description of more real polymers, which has not been carried out until now, even for uncharged colloid-polymer mixtures.

Thermodynamic consistency applied to neutral mixtures of colloids and polymers with finite-size monomers

The PRISM m-PY theory is here applied to neutral mixtures of colloids and polymers with finite-size monomers. It can be considered as the first step before studying charged colloid-polymer mixtures. We have to note that in the literature this problem has been only treated in the “thread limit”¹, where the theory becomes analytic (63). Since the PRISM m-PY analytical solution cannot be applied to finite-size monomers, the first stage of this subproject represents an original work in itself. The finite-size monomer limitation is easily solved by mean of the numerical resolution of the PRISM equations using the m-PY as the colloid-monomer closure relation. Nevertheless, it should be noted that the use of the m-PY closure is not defined as usual (compare with eqs. (3.15) and (3.16)), since it cannot be trivially introduced in the standard

¹A brief description of the “thread limit” is given in section 4.2.

6. RESULTS

numerical scheme of resolution (62, 68). It demands a special care, since the m-PY closure is defined from the previous knowledge of the PY direct correlation function. Therefore, this is an unusual closure equation that require a calculation in accord with its definition.

In order to study the validity of the numerical solution reached from the PRISM m-PY theory under the new algorithm, we have followed the same procedure that the one given in section 4.2, looking for the convergence of our numerical prediction to the analytical one (by increasing the number of monomers per chain, N_m). Indeed, we have not yet applied the *thermodynamic consistency* (the reason will be given some paragraphs later). Instead of this, the convergence is studied using the λ provided for neutral colloid-polymer mixtures in the “thread limit”, which satisfies the *thermodynamic consistency* of the analytical solution (see ref. (63)):

$$\lambda^{-1} = \xi^{-1} + \frac{1 + 2\phi_c \lambda_1}{1 - \phi_c \sigma_c} \quad (6.6.1)$$

where $\xi = \frac{R_g}{\sqrt{2}}$ is the polymer correlation length and $\lambda_1 = 1 + \sqrt{5}$. A set of g_{ij} PRISM m-PY predictions are shown in fig. (6.6.1) using $c/c^* = 0.001$, $\phi_c = 0.05$ and $\xi = 0.5$ (hereinafter, $\sigma_c = 1$). For this test, a gaussian polymer chain and HS-like interactions are selected to mimic the analytical conditions. In fig. (6.6.1), solid lines stand for the analytical solution in the “thread limit”, while dashed lines represent the numerical one. The most important finding is that the numerical solution of PRISM m-PY converges to the analytical one for $N_m = 10^6$. Comparing with the results in fig. (4.3) (the convergence was found for $N_m = 8000$), we have to note that the m-PY closure is more sensitive to the finite-size monomer than the PY one. The small disagreement in g_{mm} (the logarithmic scale is applied to enhance it) comes from a numerical precision problem in the calculation of the analytical g_{mm} at short distances. It leads to $g_{mm}(r) < 0$ for very short distances. The latter unphysical result is slightly transmitted along the g_{mm} function and leads to a small general disagreement. Despite the satisfactory agreement found for g_{cc} and g_{cm} (even g_{mm} , if the accuracy of the analytical prediction is improved), we have to point out that the special sensitivity of m-PY to the finite-size monomer has strong consequences in the applicability of the thermodynamic consistency.

Regardless the application of the thermodynamic consistency, some relevant results of

6.6 Project in progress. *Deformation of the polymer close to the colloidal surface: beyond the “thread limit”.*

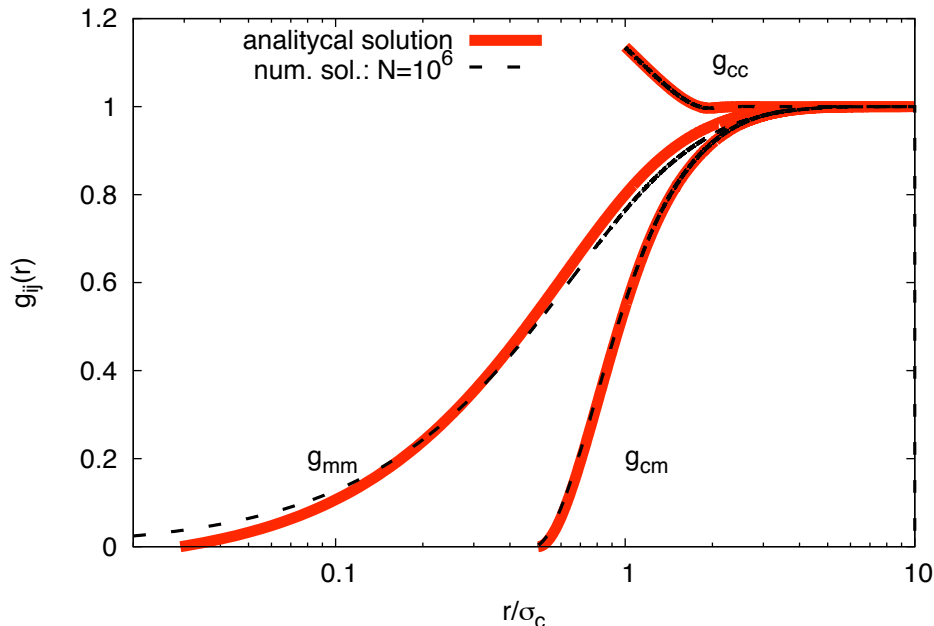


Figure 6.6.1: PRISM m-PY prediction of the radial distribution functions for a neutral colloid-polymer mixture close to the “thread limit” in semi-log scale. Solid lines stand for the analytical solutions in the “thread limit” (courtesy of Prof. M. Fuchs), while dashed lines correspond with the numerical solutions for $N_m = 10^6$, HS-like interactions and a gaussian polymer chain. The rest of used parameters are as follows: $c/c^* = 0.001$, $\phi_c = 0.05$ and $\xi = 0.5$.

the g_{cm} dependence with λ have been illustrated in fig. (6.6.2) for a gaussian polymer with $N_m = 10^6$ and $\xi = 0.5$, while $\phi_c = 0.05$ and $c/c^* = 0.01$. The increase of λ from 0.0 (PY) to 0.2 generates strong changes in the monomer distribution around a colloidal particle: the polymer is depleted from the colloidal surface and, at the contact, the linear dependence of $g_{cm}(r)$ is lost becoming quadratic. Both results agree with the analytical predictions given in ref. (86). It is important to highlight that the colloid-monomer redistribution for $\lambda > 0$ implies a more depleted polymer, which is transformed into a stronger attraction between colloids. This supports the original idea that PY ($\lambda = 0$) underestimates the induced depletion attraction.

In order to discuss the new features derived from the finite-size monomer, the inset (a) of fig. (6.6.2) shows a zoom around the colloid-monomer contact, $r \sim \sigma_{cm}$. The results suggest that $g_{cm}(\sigma_{cm})$ tends to 0 as λ is increased. Although this result is congruent

6. RESULTS

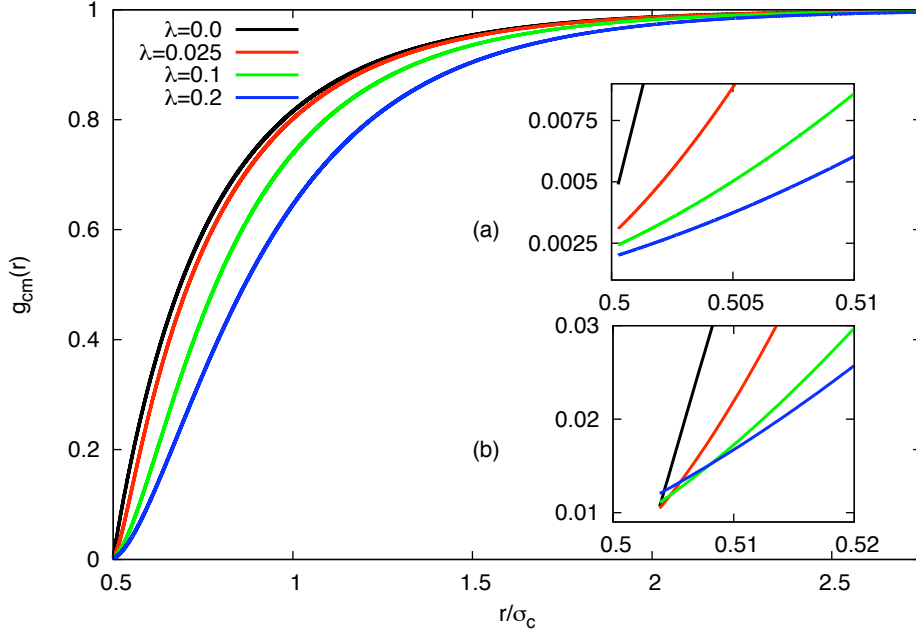


Figure 6.6.2: PRISM m-PY predictions for g_{cm} and several λ values. $N_m = 10^6$, $\phi_c = 0.05$, $c/c^* = 0.01$ and $\xi = 0.5$ remain equal in all calculations. Inset (a) shows a zoom around the contact of the before g_{cm} curves. Inset (b) presents a zoom around the contact for a smaller polymerization degree, $N_m = 5 \cdot 10^4$. In inset (b), the rest of parameters and λ values have been kept equal to the ones given in the legend of the main window.

with the behavior predicted by Fuchs *et al.* in the “thread limit”, there are differences of several order of magnitude between the numerical and the analytical results at the contact (compare with eq. (29) of ref. (63)). For this reason, the numerical application of the thermodynamic consistency looking for the convergence to the analytical solution becomes unappropriated. Only in the limit $N \rightarrow \infty$ (numerically unreachable), the numerical solution seems to converge.

The other inconvenient that avoids the application of the thermodynamic consistency is shown in the inset (b) of fig. (6.6.2). Here, the zoom around σ_{cm} is again represented for a gaussian polymer chain, now with $N_m = 5 \cdot 10^4$ or, equivalently a larger monomer size (see that the new contact value is greater in the inset (b) than in the inset (a)). For a larger monomer, the numerical solution of the PRISM m-PY theory predicts now that g_{cm} at the contact increases with λ . The physical meaning of this result is opposite to the general idea that a monomer becomes more depleted from the colloidal surface

6.6 Project in progress. *Deformation of the polymer close to the colloidal surface: beyond the “thread limit”.*

by increasing the interaction length λ . Although far to the contact g_{cm} behaves as is expected with λ , this new behavior at the contact has also a strong influence on the thermodynamic consistency. On the one hand, the compressibility route predicts that to the excess polymer chemical potential, $\delta\mu^{(1)}$, increases with λ (63). On the other hand, inset (b) shows that from certain monomer size, $g_{cm}(\sigma_{cm})$ also increases with λ , which in turn induces an upturn on $\delta\mu^{(2)}$ (eq. (4.11)) leading to a situation where the convergence of both routes is unreachable.

Here, it should be reminded that fig. (6.6.1) proofs the accurate convergence of our numerical solutions using the λ value predicted for eq. (6.6.1) and, therefore these surprising results (shown in the inset of fig. (6.6.2)) are just a consequence to the finite-size monomer. The understanding of what happens demands more effort and it will be treated in the future with the intention to find the right λ value able to predict the phase diagram of neutral colloid-polymer mixtures under thermodynamic consistency.

Thermodynamic consistency applied to charged mixtures of colloids and polymers with finite-size monomers

The main interest to apply the m-PY closure to charged colloid-polymer mixtures comes from the fact that the theory accounts for the conformational changes on the polymer, even when the system is mainly governed by electrostatic repulsive interactions. Since this memory treats to shed light into charged colloid-polymer mixtures, a theoretical description where both entropic and electrostatic effects are captured would respond to the desire of a complete theoretical description. Therefore, we have initiated this task by extending the PRISM m-PY theory to charged systems.

The main point consists in developing a new local packing route (eq. (4.12)) considering the long-range interaction between sites. By means of the local packing route ($\delta\mu^{(2)}$), the polymer excess chemical potential is calculated for a process where the colloid goes from geometric points to σ_c . In this respect, the latter excess chemical potential depends only on the $g_{cm}(\sigma_{cm})$ and $g_{cc}(\sigma_c)$ for neutral colloids and polymers. However, when both components interact at long distances, the excess chemical potential calculated by the local packing route will also depend on the colloid-monomer and colloid-colloid spatial distribution for all the distances, *i.e.* $g_{cm}(r)$ and $g_{cc}(r)$. Following the Chandler’s formalism (56) for functional integration procedures in polyatomic systems, we have

6. RESULTS

generalized eq. (4.12) to charged colloid-polymer mixtures,

$$\begin{aligned} \beta\delta\mu_p^{(2)}|_{\rho_m \rightarrow 0} = & 2\pi\rho_c\sigma_c \int_0^1 d\zeta \int_{|r| \geq 0.5(\sigma_m + \zeta\sigma_c)}^\infty r^2 g_{cm}^{(\zeta)}(r)|_{\rho_m \rightarrow 0} \frac{\partial\beta\phi_{cm}^{(\zeta)}(r)}{\partial\zeta} dr \\ & + 2\pi\rho_c^2\sigma_c^3 \int_0^1 d\zeta \int_{|r| \geq \zeta\sigma_c}^\infty r^2 \frac{\partial g_{cc}^{(\zeta)}(r)}{\partial\rho_m}|_{\rho_m \rightarrow 0} \frac{\partial\beta\phi_{cc}^{(\zeta)}(r)}{\partial\zeta} dr \end{aligned} \quad (6.6.2)$$

where $g_{ij}^{(\zeta)}(r)$ and $\phi_{ij}^{(\zeta)}(r)$ stand for the site-site radial distribution and the site-site direct interaction, respectively, for a mixture where the effective colloidal diameter is given by $\sigma_c^{(\zeta)} = \zeta\sigma_c$. Thus, $\phi_{ij}^{(\zeta)}(r)$ is a parameterized long-range pair potential. It is easy to proof that for HS-like colloids and monomers, eq. (6.6.2) leads directly to eq. (4.12).

At this point, it should be mentioned that for charged colloid-polymer mixtures, the behavior shown in the insets (a)-(b) of fig. (6.6.1), concerning the dependency at the contact value of g_{cm} with λ , still persists. In eq. (6.6.2), the excess chemical potential has two different contributions, namely HS-like and repulsive long-range tail contributions. The first one can be important for charged colloid-polymer mixtures, so it must be taken into account for the local packing calculation. Therefore, the thermodynamic consistency applicability to charged colloid-polymer mixtures again requires more work.

Although we are not able to apply the thermodynamic consistency, we still can explore the structure of charged colloid-polymer mixtures as a function of λ , while a well conditioned solution with the thermodynamic consistency problems is developed. The number of relevant parameters in an uncharged colloid-polymer mixture is four: σ_m , R_g , ϕ_c and c/c^* (assuming that $\sigma_c = 1$). In charged colloid-polymer mixtures, we must include four additional parameters: Z_c , Z_m , κ^{-1} and l_p (if we consider a semiflexible polyelectrolyte, the Koyama's form factor is recommended). Following the decomposition of l_p explained in section 4.2 for charged polymers, the set of 8 parameters can be reduced to 7 in case of $l_e \gg l_o$, under a strong electrostatic repulsion. Since a charged colloid-polymer mixture depends on more parameters as usual, we have only focused on some of them to show how the polymer deformation is presented in a mixture governed by electrostatic repulsion.

The results are shown in fig. (6.6.3), where 4 panels represent g_{cm} for two different κ^{-1} values and two c/c^* (both parameters are contained in the legend of each panel).

6.6 Project in progress. *Deformation of the polymer close to the colloidal surface: beyond the “thread limit”.*

The rest of parameters are fixed: $N_m = 500$, $l_p = 10\sigma_m$ (Koyama’s model), $Z_c = 50$, $Z_m = 0.347$, $\sigma_c = 40\sigma_m$ (Debye-Hückel potential) and $\phi_c = 0.05$. In each panel, we have presented results for several λ values covering a wide range of the relevant polymer lengths (from $\lambda = 0$ to $\lambda = l_p$). To simplify, the discussion of the results shown in fig. (6.6.3) are divided in two points: the first one concerning charged colloid-polymer mixtures with a strong electrostatic repulsion ($\kappa^{-1} = 6\sigma_m$), panels (a) and (b), and the second one, with a weaker electrostatic repulsion ($\kappa^{-1} = \sigma_m$), panels (c) and (d).

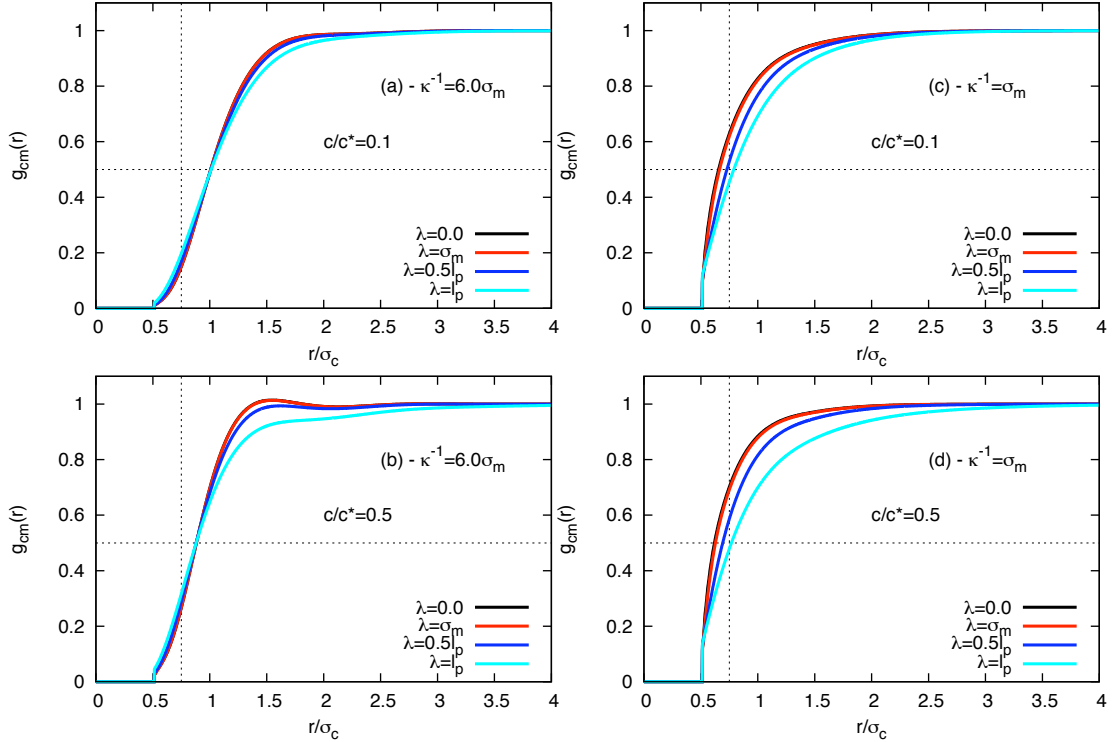


Figure 6.6.3: PRISM m-PY prediction for the colloid-monomer radial distribution functions of a charged colloid-polymer mixture. The results are divided in 4 panels: in (a) and (b) $\kappa^{-1} = 6\sigma_m$ and $c/c^* = 0.1$ and 0.5 , respectively, while in (c) and (d) $\kappa^{-1} = \sigma_m$ for the same concentrations. The rest of parameters are pre-fixed: $N_m = 500$ and $l_p = 10\sigma_m$ leading to $R_g = 40\sigma_m$ (Koyama’s model) and $Z_c = 50$, $Z_m = 0.347$ and $\sigma_c = 40\sigma_m$ (Debye-Hückel potential), while $\phi_c = 0.05$. Within each panel the prediction for several λ values is given.

6. RESULTS

- In panel (a), no relevant changes on the colloid-monomer radial distribution are appreciated, even when λ is similar to the polymer persistence length. However, as the polymer concentration increases (see panel (b)) the polymer deformation becomes relatively important for the largest λ values ($\lambda = l_p$). This confirms that the colloid-monomer arrangement is mainly controlled by the electrostatic repulsion and the polymer deformation effect only can be appreciable when the polymer is enforced to be close to the colloidal surface by increasing c/c^* . Consequently, in panel (a) and (b), the so-called *depletion layer* (defined as the length ω that satisfy $g_{cm}(\sigma_{cm} + \omega) = 0.5$ (63)) remains constant for all the λ -values (follow the horizontal dashed line plotted *ad hoc*). The dashed vertical line indicates that the range, where the polymer deformation effects may be important (the largest λ value is presented), is smaller than the range of the *depletion layer* for $\lambda = 0$. So that, due to the strong electrostatic repulsion, the polymer depletion caused by entropic effects is negligible.
- In panels (c) and (d) the range of the electrostatic repulsion is smaller respect to the panels (a) and (b). Therefore, the entropic effects are more important for the same set of λ values. The weaker electrostatic repulsion allows monomer/polymer to approach the colloidal surface (for $\lambda = 0$ the depletion layer is smaller than some of the studied λ values). The theory predicts that the polymer feels the presence of the colloid adapting its conformation and so, the monomer distribution around the colloids. In this situation, the increase of the depletion layer with λ is recovered (fig. (6.6.2)). From these results, we can confirm that when the system is less charged, the deformation of the polymer becomes important. It must be remarked that the prediction for the thermodynamic consistency λ will be related also with the intensity of the repulsion, giving smaller λ values as the electrostatic repulsion increases. Notwithstanding, it will always be greater than the monomer diameter, σ_m , so that the polymer deformation cannot be discarded *a priori*.

Two assumptions have been imposed in the latter example to make clear the discussion: κ^{-1} is constant respect to the increase of c/c^* (from 0.1 to 0.5) and $l_p \sim l_o$, so that the changes in l_e when κ^{-1} increase does not overcome the value of the intrinsic rigidity of the polymer, l_o . If we want to compare with experimental results, both coupled effects must be incorporated in the theory. In this respect, it should be said that the complete description of an experimental system (including the coupling between κ^{-1} with c/c^* , ...) can be in principle carried out with PRISM m-PY theory. Anyway, as fig. (6.6.3) illustrates, the extension of m-PY to charged colloid-polymer mixtures

6.6 Project in progress. *Deformation of the polymer close to the colloidal surface: beyond the “thread limit”.*

makes sense, since details of the polymer deformation by the action of the colloid can be non-negligible. In summary, this theory represents a very promising tool providing more accuracy results to compare with experiments and simulations.

6. RESULTS

Chapter 7

Conclusions

7.1 English

Paper I:

In this first work, the non-diffusive motion of rigid and deformable Brownian particles was experimentally studied using dynamic light scattering.

- The non-diffusive motion of deformable Brownian particles is quite different to the rigid ones as a consequence of the coupling between translational and rotational degrees of freedom.
- Our results with deformable liposomes represent a theoretical challenge, since the hydrodynamic theory that describe with accuracy the non-diffusive motion of rigid particles fails in its prediction for the deformable ones.
- The deformable particles reach the diffusive regime at time-scales where the translation and rotation are decoupled. It strongly depends on the elastic characteristic of each particle. This conclusion will be useful on future works to disentangle the time-resolution where the effects of the particle deformability are present in its diffusive motion.

Paper II:

The behavior of the colloidal structure factor on a mixture of charged colloid and non-adsorbing charged polymer was experimentally analyzed for increasing polymer concentrations. The experiments were performed using static light scattering. The experimental results were compared with a theoretical model considering colloid-colloid, colloid-monomer and monomer-monomer interactions, as well as the connectivity of monomers along the polymer chain.

7. CONCLUSIONS

- The presence of charged polymer in a structured suspension of charged colloids induces a strong effect on its structure: the colloids are forced to be at closer distances with the increase of the polymer concentration. The origin of this behavior is explained in terms of the coupling of two effects: the colloid-monomer electrostatic repulsion inducing an effective attraction between colloids and the screening of any electrostatic interactions, which is provoked by the increase of the charged polymer concentration. In turns, the screened colloid-colloid repulsion allows to the colloids approach each other, while the screened colloid-monomer repulsion weakens the polymer-induced attraction. Therefore, we find that the mechanism controlling the equilibrium of the system is more electrostatic than entropic.
- The theoretical model (PRISM) that we have used is able to describe with high accuracy the experimental results using just one fit parameter: the ionic strength. Moreover, PRISM allows us to deep into the structure features of each component of the mixture more than light scattering techniques.

Paper III:

From the conclusions derived in paper II, we carried out in this paper a second study of the effect that the polymer size has on the colloidal structure factor of charged colloid-polymer mixtures. The experimental results obtained by means of static light scattering were correlated with the dynamic analysis in the main peak of the structure factor.

- The effective force induced by the charged polymer does not only depend on the polymer radius of gyration, R_g , as occurs in neutral mixtures. From the performed experiments at two different polymer sizes and the help of the PRISM, it is proved that the range of the electrostatic repulsion, κ^{-1} , also plays an important role controlling the induced attraction for mixtures.
- The experimental data obtained with static light scattering (SLS) are consistent with the ones measured with dynamic light scattering (DLS). In both cases, the results show that the colloid-colloid total interaction becomes more attractive, or less repulsive, as much as the charged polymer concentration is increased.

Paper IV:

The work developed in the two previous papers was extrapolated to charged colloid-polymer mixtures using liposomes as biocompatible colloids. Another relevant property

to employ this colloidal particles was the transparency of such system, allowing us to work with mixtures at high colloidal concentrations.

- At the studied liposome packing fractions, the short polymer chain is smaller than the typical distance between colloids. Therefore, the colloidal structure changes in accord with the electrostatic mechanisms documented in paper II.
- For larger polymer chains and using the same liposome packing fractions as before, the experimental structure factor shows an upturn at low q values (large spatial scales). This evidence, is explained in terms of the aggregation of the liposomes due to the polymer-induced attraction. In our opinion, the extra-attraction activating the colloidal aggregation must be related with the entropic depletion, since in this case the polymer size is greater than the colloidal interspace (entropic depletion is favored).

Paper V:

A study of the effective force between two charged particles (big colloids) induced by a system of smaller charged particles was performed using Monte-Carlo simulations. The dependence of the effective force on the big colloid charge was systematically studied. The simulation results were compared with the Ornstein-Zernike equation with the HNC closure.

- As much as the big colloid charge is increased, the induced attraction is stronger. Such behavior is mainly controlled by the big-small repulsion giving rise to an imbalance of electrostatic pressure on the two big colloids, which leads to an effective attraction.
- The big-big total interaction, sum of the big-big electrostatic and the induced interaction, behaves non-monotonically with the big colloid charge. The non-monotonicity behavior controls the total interaction in such a way that it is more attractive with the increase of the charge of the big colloids. From a certain value of the big colloid charge this behavior is reversed being more repulsive with the big colloid charge.
- The comparison between simulation and theory shows an intriguing qualitative agreement, since the theory also captures the non-monotonic dependence of the total potential. In this respect, the theory is far to describe quantitatively the simulation results for relatively charged big colloids.

7. CONCLUSIONS

7.2 Español

Artículo I:

En este primer trabajo, se estudia experimentalmente el movimiento no difusivo de partículas Brownianas rígidas y deformables, mediante la técnica de dispersión de luz dinámica.

- El movimiento no difusivo de partículas Brownianas deformables presenta grandes diferencias con el de partículas rígidas. Esto es consecuencia del acoplamiento entre los grados de libertad de traslación y rotación de cada tipo de partículas.
- Estos resultados con partículas deformables representan un reto teórico, ya que la teoría hidrodinámica que describe con bastante precisión el movimiento no difusivo de partículas rígidas falla en sus predicciones para el caso de partículas deformables.
- Las partículas deformables alcanzan el régimen difusivo como consecuencia del desacoplamiento entre la traslación y la rotación en el movimiento. Dicho desacoplamiento depende fuertemente de las características elásticas de cada partícula. En trabajos futuros, este resultado será útil para distinguir la escala temporal donde los efectos de la deformabilidad de la partícula están presentes en su movimiento Browniano.

Artículo II:

El comportamiento del factor de estructura coloidal de mezclas de coloide y polímero, ambos cargados con el mismo signo, se ha estudiado experimentalmente para cantidades crecientes de polímero. Los experimentos se llevaron a cabo mediante dispersión de luz estática. Los resultados experimentales se han comparado también con un modelo teórico el cual considera las interacciones coloide-coloide, coloide-monómero y monómero-monómero, además de la correlación entre los monómeros de una misma cadena polimérica.

- La presencia de polímero cargado en una suspensión coloidal estructurada por repulsión electrostática induce un fuerte efecto sobre su estructura: los coloides son forzados a estar típicamente más cerca debido al aumento de concentración de polímero. El origen de este comportamiento es explicado en términos del acoplamiento de dos efectos: la repulsión directa coloide-monómero, que induce una atracción efectiva entre los coloides, y el apantallamiento de cualquier repulsión electrostática, el cual es provocado por el aumento en la concentración

de polímero cargado. A su vez, el apantallamiento de la repulsión entre coloides permite a estos aproximarse entre sí con más facilidad, mientras que el apantallamiento en la repulsión coloide-monomero debilita la atracción inducida por el polímero. Por lo tanto, el mecanismo que gobierna el equilibrio del sistema es más electrostático que entrópico.

- El modelo teórico empleado (PRISM) es capaz de describir los resultados experimentales con tan solo un parámetro de ajuste: la fuerza iónica del medio. Además, PRISM nos permite obtener más información, sobre el ordenamiento espacial de ambos componentes de la mezcla, que la meramente accesible a través de un experimento de dispersión de luz.

Artículo III:

Partiendo de la base establecida con los resultados del artículo II, el efecto del tamaño del polímero sobre el factor de estructura del coloide se ha estudiado en mezclas cargadas de coloides y polímeros. Los resultados obtenidos mediante dispersión de luz estática se han correlacionado con los de la dinámica de las partículas en el pico del factor de estructura coloidal.

- La fuerza efectiva inducida sobre los coloides cargados no solo depende del radio de giro del polímero, R_g , como ocurre en mezclas neutras. A partir de la información experimental recopilada para dos tamaños diferentes de cadena y la ayuda del modelo PRISM, se ha demostrado que el alcance de la repulsión electrostática, κ^{-1} , juega un papel fundamental en esa atracción. El alcance de dicha interacción llega a ser controlado por κ^{-1} en sistemas experimentales con una fuerza iónica muy baja.
- Los datos experimentales obtenidos con la dispersión de luz estática son consistentes con los medidos mediante dispersión de luz dinámica. En ambos casos, los resultados muestran que la interacción total entre coloides llega a ser más atractiva, o menos repulsiva, a medida que la concentración de polímero aumenta.

Artículo IV:

El trabajo presentado en los dos artículos anteriores se extrapoló a una mezcla coloide polímero cargada utilizando liposomas como coloides biocompatibles. Otra propiedad importante que sugiere su uso, reside en sus propiedades ópticas, ya que tales partículas son transparentes incluso para altas concentraciones.

7. CONCLUSIONS

- Para las concentraciones de liposoma estudiadas, el polímero corto es más pequeño que la distancia típica entre coloides. Por lo tanto, la estructura coloidal cambia de acuerdo con el mecanismo electrostático descrito en el artículo II.
- Para el polímero más largo, usando las mismas concentraciones de liposoma que antes, el factor de estructura coloidal muestra un alzamiento a bajo q (escalas espaciales grandes). Esta nueva observación, es explicada en términos de la agregación de los liposomas debido a la atracción inducida por el polímero. En nuestra opinión la atracción extra que activa el proceso de agregación debe estar relacionada con la depleción entrópica, ya que en este caso el polímero está excluido de la zona intercoloidal debido a su tamaño.

Artículo V:

Un estudio de la fuerza efectiva entre dos partículas coloidales cargadas (coloides grandes) inducida por un sistema de partículas de menor tamaño y también cargadas (coloides pequeños) se llevó a cabo utilizando simulaciones Monte-Carlo. Se estudió sistemáticamente el efecto del aumento de la carga de los coloides grandes en dicha fuerza efectiva para distintos casos. Los resultados obtenidos mediante simulación fueron comparados con la ecuación de Ornstein-Zernike para el cierre HNC.

- A medida que se va aumentando la carga de las partículas grandes se ha encontrado que la atracción inducida por las partículas pequeñas sobre las grandes es cada vez mayor. Dicho comportamiento de la atracción inducida es principalmente controlado por la repulsión grande-pequeña, la cual genera un desequilibrio en la presión electrostática sobre los coloides grandes dando origen a una atracción efectiva.
- Al estudiar el potencial total grande-grande, suma de la interacción electrostática directa grande-grande y la interacción inducida, se ha observado un comportamiento no monótono de la parte efectiva respecto a la carga de las partículas grandes. El comportamiento no monótono llega a controlar la interacción total de manera que es más atractiva con el aumento de la carga de las partículas grandes cuando dicha carga no es muy alta. A partir de un cierto valor, la dependencia de la interacción total con la carga se invierte siendo más repulsivo con el aumento de la misma.
- La comparación de las simulaciones con las predicciones teóricas de Ornstein-Zernike para el cierre HNC muestra un acuerdo cualitativo interesante entre

ambas, ya que la teoría captura el comportamiento no monótono anterior. No obstante, la teoría está lejos de describir cuantitativamente los resultados de simulación para coloides grandes relativamente cargados.

7. CONCLUSIONS

References

- [1] <http://www.purestcolloids.com/> 1
- [2] <http://www.repsol.com/> 1
- [3] C. J. Hernandez and T. G. Mason, *J. Phys. Chem. C* **111**, 4477 (2007) or <http://www.chem.ucla.edu/dept/Faculty/Mason/> 1
- [4] D. Qiu, T. Cosgrove, and A. M. Howe, *Langmuir* **23**, 475 (2007) 2
- [5] U. S. PATENT DOCUMENT 4,775,541 A * 10/1988 Brown *et al.* 426/271
(Ion exchange method of treating liquid fermentation products to reduce the content of coloring matter therein) 3
- [6] U. S. PATENT DOCUMENT 7,022,366 B2 4/2006 Ferrarini 426/592
(Method for tartaric stabilization of wine) 3
- [7] J. Y. Walz, and A. Sharma, *J. Colloid Interface Sci.* **168**, 485 (1994). 3
- [8] O. Mondain-Monval, F. Leal-Calderon, J. Phillip, and J. Bibette, *Phys. Rev. Lett.* **75**, 3364 (1995). 4
- [9] L. Helden, G. H. Koenderink, P. Leiderer, and C. Bechinger, *Langmuir* **20**, 5662 (2004). 4
- [10] A. I. Campbell, V. J. Anderson, J. S. van Duijneveldt, and P. Bartlett, *Phys. Rev. Lett.* **94**, 208301 (2005). 4
- [11] G. Petekidis, L. A. Galloway, S. U. Egelhaaf, M. E. Cates, and W. C. K. Poon, *Langmuir* **18**, 4248 (2002). 4
- [12] L. Belloni and P. G. Ferreira, *Phil. Trans. R. Soc. Lond. A* **359**, 867 (2001). 4, 36, 39, 45

REFERENCES

- [13] R. Brown, *Phil. Mag.* **4**, 161 (1828). 8
- [14] A. Einstein, *Annalen der Physik* **17**, 549 (1905). 8
- [15] J. Perrin, *Annales de Chimie et de Physique* **18**, 5 (1909). 8
- [16] G. E. Uhlenbeck and L. S. Ornstein, *Phys. Rev.* **36**, 823 (1930). 8, 9
- [17] M. von Smoluchowski, *Annalen der Physik* **21**, 756 (1906). 8
- [18] P. Langevin, *C.r. hebdomadaire des seances Acad. Sci.* **146**, 549 (1908). 8
- [19] J. Alder and T. E. Wainwright, *Phys. Rev. Lett.* **18**, 988 (1967); *idem* *Phys. Rev. A* **1**, 18 (1969). 9, 10
- [20] A. Boullier, J. P. Boon and P. Deguent, *J. Physique* **32**, 159 (1978). 10
- [21] G. L. Paul and P. N. Pusey, *J. Phys. A* **14**, 3301 (1981). 10
- [22] D. A. Weitz, D. J. Pine, P. N. Pusey and R. J. A. Tough, *Phys. Rev. Lett.* **27**, 2632 (1982). 10
- [23] B. Lukić, S. Jeney, C. Tischer, A. J. Kulik, L. Forró and E.-L. Florin, *Phys. Rev. Lett.* **95**, 160601 (2005). 10
- [24] A. E. Bailey, et al., *Phys. Rev. Lett.* **99**, 205701 (2007). 11
- [25] P. N. Pusey, *Colloidal Suspensions*, Lecture Notes for Les Houches 1989, Session L1 (Amsterdam: North-Holland, 1989). 11, 58
- [26] B. J. Ackerson, *J. Chem. Phys.* **69**, 684 (1978). 12
- [27] W. Gotze and L. Sjogren, *Rep. Prog. Phys.* **55**, 241 (1992). 12
- [28] J. N. Israelachvili, *Intermolecular and Surface Forces*, Academic Press, London (1991). 12
- [29] D. L. Chapman, *Phil. Mag.* **6**, 475 (1913). 12, 13
- [30] P. N. Pusey, *Liquids, Freezing and Glass Transition, Lecture Notes for Les Houches, Session L1, Part 2, Course 10: Colloidal Suspensions*, Amsterdam, North-Holland (1989). 13
- [31] P. Debye and E. Hückel, *Phys. Z* **24**, 185 (1923). 13

REFERENCES

- [32] S. Asakura and F. Oosawa, *J. Chem. Phys.* **22**, 1255 (1954). *idem* *J. Polymer Sci.* **33**, 183 (1958). 15, 16, 29
- [33] D. Aussere, H. Hervet and F. Rondelez, *Macromolecules* **149**, 85 (1982). 15
- [34] A. P. Gast, C. K. Hall and W. B. Russel, *J. Colloid Interface Sci.* **96**, 251 (1983). 15
- [35] W. B. Russell, D. A. Saville and W. R. Schowalter, *Colloidal Dispersions*, Cambridge University Press (1989). 15
- [36] A. Vrij, *Pure. Appl. Chem.* **48**, 471 (1976). 15, 16
- [37] H. N. W. Lekkerkerker, W. C. Poon, P. N. Pusey, A. Stroobants and P. B. Warren, *Eurpophys. Lett.* **20**, 559 (1992). 15
- [38] W. C. K. Poon, J. S. Selfe, M. B. Robertson, S. M. Ilett, A. D. Pirie and P. N. Pusey, *J. Phys. II (France)* **3**, 1075 (1993). 16
- [39] Weisstein, Eric W. "Sphere-Sphere Intersection." From MathWorld—A Wolfram Web Resource. <http://mathworld.wolfram.com/Sphere-SphereIntersection.html> 17
- [40] K. S. Schweizer and J. G. Curro, *Adv. Pol. Sci.* **116**, 319 (1994), *idem* *Adv. Chem. Phys.* **98**, 1 (1997). 17, 30, 36
- [41] R. Roth and R. Evans, *Eurpophys. Lett.* **53**, 271 (2001). 18
- [42] R. Roth, *J. Phys.: Condens. Matter* **22**, 063102 (2010). 18
- [43] L. D. Landau and E. M. Lifshitz, *Física Estadística Volumen 5* Editorial Reverté (1969). 20
- [44] J. W. Gibbs, *Elementary Principles in Statistical Mechanics* Yale Unimpressed New Heaven (1902). 20
- [45] J. P. Hansen and I. R. Mc Donald, *Theory of Simple Liquids* London (1986). 20, 26, 47
- [46] N. W. Ashcroft and N. D. Mermin, *Solid State Physics* Holt, Rinehart and Winston (1976). 25
- [47] J. B. Pawley, *Handbook of Biological Confocal Microscopy*, New York: Plenum Press (1995). 24

REFERENCES

- [48] A. Mc Quarrie. *Statistical Mechanics* Harper and Row, New York (1976). 25, 36
- [49] D. Frenkel and B. Smit, *Understanding Molecular Simulation: From Algorithm to Applications* Academic Press (1996). 26
- [50] A. A. Louis, E. Allahyarov, H. Lowen and R. Roth, Phys. Rev. E **65**, 061407 (2002). 28
- [51] M. Dijkstra, R. van Roij and R. Evans, Phys. Rev. E **59**, 5744 (1999). 28, 29
- [52] R. Roth, R. Evans and A. A. Louis, Phys. Rev. E **64**, 051202 (2001). 29
- [53] J. M. Méndez-Alcaraz, B. D'Aguanno and R. Klein, Phys. A **178**, 421 (1991). 31
- [54] D. S. Wilson and L. L. Lee, J. Chem. Phys. **123**, 044512 (2005). 31
- [55] M. Peláez-Fernández, *Efecto de la Carga en la Estabilidad de Mezclas Binarias Coloide-Coloide y Coloide-Polímero*, Diplomas de Estudios Avanzados, Universidad de Granada (2008). 31
- [56] D. Chandler, *Studies in Statistical Mechanics*, edited by Montroll E. and Lebowitz J. L., Vol. **VIII** (North Holland, Amsterdam) 1982, p. 274. 33, 34, 35, 47, 189
- [57] J. G. Curro and K. S. Schweizer, Macromol. **20**, 1928 (1987). 36
- [58] K. S. Schweizer and J. G. Curro, Phys. Rev. Lett. **58**, 246 (1987). 36
- [59] J. G. Curro and K. S. Schweizer, J. Chem. Phys., **87**, 1842 (1987). 36
- [60] D. Chandler and H. C. Andersen, J. Chem. Phys. **57**, 1930 (1972). 36
- [61] L. Belloni, M. Olvera de la Cruz, M. Delsanti, J. P. Dalbiez, O. Spalla and M. Drifford, Il Nuovo Cimento, **16**, 727 (1994). 36
- [62] P. G. Ferreira, M. Dymitrowska and L. Belloni, J. Chem. Phys. **69**, 9691 (1999). 38, 42, 186
- [63] M. Fuchs and K. S. Schweizer, Phys. Rev. E **64**, 021514 (2001). 38, 45, 46, 47, 185, 186, 188, 189, 192
- [64] A. Yethiraj, C. K. Hall and R. Dickman, J. Col. Interface Sci. **131**, 102 (1992). 38
- [65] P. G. Khalatur, L. V. Zherenkova and A. R. Khokhlov, Phys. A **247**, 205 (1997). 38

-
- [66] X. Ye, T. Narayanan, P. Tong and J. S. Huang, Phys. Rev. Lett. **76**, 4640 (1996). 39
- [67] D. G. Gromov and J. J. de Pablo, J. Chem. Phys. **103**, 8247 (1995). 39
- [68] M. Quesada-Pérez, *Estructuras en Líquidos Coloidales: Interacción entre Partículas y Carga Efectiva.*, PhD Thesis, Universidad de Granada (1999). 39, 67, 72, 186
- [69] M. Fuchs, Z. Phys. B **103**, 521 (1997). 40
- [70] R. Koyama, Macromolec. **1986**, 178 (2002). 41
- [71] O. Kratky and G. Porod, G. Recl. Trav. Chim. **68**, 1106 (1949). 41
- [72] S. Lifson, A. Katchalsky, K. Polym. Sci. **13**, 43 (1954). 41, 42
- [73] K. G. Honnell, J. G. Curro and K. S. Schweizer, Macromol. **23**, 3496 (1990). 41
- [74] P. J. Flory, J. Chem. Phys. **9**, 660 (1941). 42
- [75] T. Odijk, J. Polym. Sci., Polym. Phys. **15**, 477 (1977), *idem*, Phys. A **278**, 347 (2000). 42
- [76] G. S. Manning, *J. Chem. Phys.* **51**, 924 (1969). 42, 76
- [77] M. Fixman, *J. Chem. Phys.* **76**, 6346 (1982). 42
- [78] J. Skolnick and M. Fixman, Macromol. **10**, 944 (1977). 42
- [79] E. Buhler and F. Bou, *Eur. Phys. J. E* **10**, 89 (2003). 42
- [80] A. Denton, M. Schmidt, J. Chem. Phys. **122**, 2449111 (2005). 45
- [81] O. A. Croze and M. E. Cates, Langmuir **21**, 5627 (2005). 45
- [82] E. J. Meijer and D. Frenkel, Phys. Rev. Lett. **67** 1110 (1991); *idem* J. Chem. Phys. **100**, 6873 (1994). 45
- [83] X. Ye, T. Narayanan, P. Tong and J. S. Huang, Phys. Rev. Lett. **76**, 4640 (1996). 45
- [84] X. Ye, T. Narayanan, P. Tong, J. S. Huang, M. Y. Lin, B. J. Carvalho and L. J. Fetters, Phys. Rev. E **54**, 6500 (1999). 45

REFERENCES

- [85] M. Fuchs and K. S. Schweizer, *Europhys. Lett.*, **51**, 621 (2000). 45
- [86] M. Fuchs and K. S. Schweizer, *J. Phys.: Condens. Matter* **14**, R239 (2002). 45, 187
- [87] J. Bergenholtz, N. J. Wagner and B. D'Aguzzo, *Phys. Rev. E* **53**, 2968 (1996). 47
- [88] B. J. Berne and R. Pecora, *Dynamic Light Scattering*, New York, Wiley (1976). 52, 54
- [89] K. Pham, S. Egelhaaf, A. Moussiad and P. N. Pusey, *Rev. Sci. Instrum.* **75**, 2419 (2004). 54, 60
- [90] P. N. Pusey and W. van Meegen, *Physica A* **157**, 705 (1989). 54, 60
- [91] B. Fultz and J. Howe, *Transmission Electron Microscopy and Diffractometry of Materials*, Springer (2007). 55
- [92] S. Roldán-Vargas, M. Quesada-Pérez, J. Callejas-Fernández, *J. Chem. Phys.* **131**, 034509 (2009). 57
- [93] G. Nägele, *Physics Reports* **272**, 215 (1996). 58
- [94] G. Phillies, *J. Chem. Phys.* **74**, 260 (1980); *ibid* *Phys. Rev. A* **24**, 1939 (1981). 61
- [95] K. Schätzel, *J. Modern Optics* **38**, 1849 (1991). 61, 63
- [96] C. Urban and P. Schurtenberger, *J. Colloid Interface Sci.* **207**, 150 (1998). 62
- [97] P. N. Segre, W. van Meegen, P. N. Pusey, K. Schätzel and W. Peters, *J. Modern Optics* **42**, 1929 (1995). 62, 64
- [98] A. Moussaïd and P. N. Pusey, *Phys. Rev. E* **60**, 5670 (1999). 65
- [99] Y. Li and S. M. Lindsay, *Rev. Sci. Instrum.* **63**, 2630 (1991). 67
- [100] A. Búcsi, J. Forcada, S. Gibanel, V. Héroguez, M. Fontanille and Y. Gnanou, *Macromolecules* **31**, 2087 (1998). 67
- [101] S. Roldán-Vargas, R. Barnadas-Rodríguez, M. Quesada-Pérez, J. Estelrich, and J. Callejas-Fernández, *Phys. Rev. E* **79**, 011905 (2009). 69
- [102] V. P. Torchillin and V. Weissing, *Liposomes, a Practical Approach* (Oxford University Press, New York, 2003). 72

REFERENCES

- [103] L. Helmholtz, *Ann. Phys. Chem.* **7**, 337 (1879) 73
- [104] T. Gisler, S. F. Schultz, M. Borkovec, H. Sticher, P. Schurtenberger, B. D'Aguanno and R. Klein, *J. Chem. Phys.* **101**, 9924 (1994). 73
- [105] T. Palberg, W. Härtl, U. Witting, H. Versmold, M. Wüsth, E. Simnacher, *J. Phys. Chem.* **96**, 8181 (1992). 73
- [106] T. Palberg, W. Mönch, F. Bitzer, R. Piazza, T. Bellini, *Phys. Rev. Lett.* **74**, 4555 (1995). 73
- [107] P. C. Heimenz and R. Rajagopalan, *Principles of Colloid and Surface Chemistry* Marcer Dekker, Inc. (New YorkBasel, 1997). 74, 75